

JSCSEN 78(10)1461–1632(2013)

ISSN 1820-7421(Online)

Journal of the Serbian Chemical Society

ersion
lectronic

VOLUME 78

No 10

BELGRADE 2013

Available on line at



www.shd.org.rs/JSCS/

The full search of JSCS
is available through

DOAJ DIRECTORY OF
OPEN ACCESS
JOURNALS
www.doaj.org

CONTENTS

L. V. Rajaković, Ž. N. Todorović, V. N. Rajaković-Ognjanović and A. E. Onjia: Analytical methods for arsenic speciation analysis (Review) 1461

Organic Chemistry

S. J. Saghanezhad and H. R. Safaei: B(HSO₄)₃: An efficient and recyclable catalyst for the Friedländer synthesis of substituted quinolines 1481

Biochemistry and Biotechnology

N. Ž. Prlainović, D. I. Bezbradica, Z. D. Knežević-Jugović, D. V. Veličković and D. Ž. Mijin: Enzymatic synthesis of a vitamin B₆ precursor 1491

D. Dekanski, T. Todorović, D. Mitić, N. Filipović, N. Polović and K. Anđelković: High antioxidative potential and low toxic effects of selenosemicarbazone metal complexes 1503

Inorganic Chemistry

I. A. Dereven'kov, S. S. Ivanova, E. V. Kudrik, S. V. Makarov, A. S. Makarova and P. A. Suzhin: Comparative study of reactions between μ-nitrido- or μ-oxo-bridged iron tetrasulfophthalocyanines and sulfur-containing reductants 1513

D. P. Dimitrijević, S. B. Novaković, G. R. Radić, V. V. Jevtić, L. Menéndez-Taboada, S. García-Granda and S. R. Trifunović: Synthesis, characterization and crystal structure of butyl *N*-(3-chloropropyl)-(2*S*)-alaninate hydrochloride (Short communication) 1531

Theoretical Chemistry

I. Gutman, S. Radenković, M. Antić and J. Durđević: A test of Clar aromatic sextet theory .. 1539

Physical Chemistry

K. Majlesi, S. Rezaiejad, N. D. Sarabi, M. Fahmi and F. Tahamtan: Calculation of the stability constants for complex formation of dioxovanadium(V) with methylimino-diacetic acid in various H₂O + CH₃OH solutions using the Kamlet–Abboud–Taft equation 1547

A. Farajtabar, F. Naderi and F. Gharib: Autoprotolysis in water/methanol/NaCl ternary systems 1561

Electrochemistry

M. Bučko, U. Lačnjevac and J. Bajat: The influence of substituted aromatic aldehydes on the electrodeposition of Zn–Mn alloy 1569

M. M. Rajčić-Vujanović, V. J. Grekulović, Z. M. Stević, S. D. Nestorović, I. I. Marković and S. B. Šimov: Comparison of the electrochemical behavior of cast and sintered CuAg 4 at. % alloy during thermomechanical treatment 1583

S. Mohammadzadeh and M. Fouladgar: Electrocatalytic oxidation and determination of homocysteine at nanotubes-modified carbon paste electrode using dopamine as a mediator 1595

Materials

R. Omidirad, F. H. Rajabi and B. V. Farahani: Preparation and *in vitro* drug delivery response of doxorubicin-loaded poly(acrylic acid)-coated magnetite nanoparticles... 1609

Environmental

M. Vukčević, A. Kalijadis, B. Babić, Z. Laušević and M. Laušević: Influence of different carbon monolith preparation parameters on pesticide adsorption 1617



J. Serb. Chem. Soc. 78 (10) 1461–1479 (2013)
JSCS–4510

REVIEW

Analytical methods for arsenic speciation analysis

LJUBINKA V. RAJAKOVIĆ^{1*#}, ŽAKLINA N. TODOROVIĆ²,
VLADANA N. RAJAKOVIĆ-OGNJANOVIĆ³ and ANTONIJE E. ONJIA²

¹Faculty of Technology and Metallurgy, University of Belgrade, Karnegijeva 4, 11000 Belgrade, Serbia, ²Vinča Institute of Nuclear Sciences, University of Belgrade, P. O. Box 522, 11001 Belgrade, Serbia and ³Faculty of Civil Engineering, University of Belgrade, Bulevar kralja Aleksandra 73, Belgrade, Serbia

(Received 15 March, revised 29 May 2013)

Abstract: Arsenic exists in the form of various chemical species differing in their physicochemical behaviour, toxicity, bioavailability and biotransformation. The determination of arsenic species is an important issue for environmental, clinical and food chemistry. However, differentiation of these species is a quite complex analytical task. Numerous speciation procedures have been studied that include electrochemical, chromatographic, spectrometric and hyphenated techniques. This review presents the relevant research in the field of arsenic speciation analysis with novel applications and significant advances. Stability of arsenic species and each of the analytical steps (sample collection, storage, preservation, extraction) of the arsenic speciation methods is particularly evaluated. Analytical validation and performance of these methods are also reviewed.

Keywords: arsenic speciation; adsorption; extractions; water, soil; biological sample.

CONTENTS

1. INTRODUCTION
2. ARSENIC CHEMISTRY AND ARSENIC SPECIATION – PREVIOUS REVIEWS
3. ANALYTICAL METHODS FOR SPECIATION ANALYSIS
4. STABILITY OF ARSENIC SPECIES: SAMPLE COLLECTION, STORAGE AND PRESERVATION
5. SAMPLE EXTRACTION
6. SEPARATION AND DETERMINATION OF ARSENIC SPECIES IN WATER
7. CONCLUSIONS

* Corresponding author. E-mail: ljubinka@tmf.bg.ac.rs

Serbian Chemical Society member.

doi: 10.2298/JSC130315064R

1. INTRODUCTION

Arsenic research is opening up new scientific topics, especially in speciation analysis. Methods for determining traces of total arsenic and different chemical forms of arsenic have become increasingly important due to the different toxicity and chemical behaviour of the various forms of arsenic. Consequently, various speciation procedures have been proposed and reviewed.¹ For the routine determination of a large number of arsenic samples, well-established methods that involve the coupling of separation techniques, such as ion chromatography (IC)² and high performance liquid chromatography (HPLC)³, with a sensitive detection system, such as inductively-coupled plasma-mass spectrometry (ICP-MS), atomic fluorescence spectrometry-hydride generation (AFS-HG) and atomic absorption spectrometry-hydride generation (AAS-HG)⁴ are the methods of choice. Procedures for the separation of arsenic species on various sorbents and exchange resins have also been developed and proposed.⁵⁻⁹ The most important aspect in non-chromatographic and chromatographic methods is the selective separation of the arsenic species. Recently, our research group was involved in finding a procedure and material that are efficient for the selective separation of arsenic species⁶⁻⁸ and arsenic removal from water.^{10,11}

The maximum permissible concentration (*MPC*) of total arsenic in drinking water is set at 10 $\mu\text{g L}^{-1}$, while the limit values for arsenic species have not been established.^{12,13} For this toxic element and its species, highly sophisticated equipment and sensitive methods should be applied. An adequate method for the estimation of the limits would facilitate the necessity and relevant progress in determining arsenic and its species. Numerous methods for total arsenic concentration and speciation are reported in the literature.¹⁴ The ICP-MS method is highly sophisticated technique that enabled a decrease in the limit of detection (*LoD*) from 5 or even 25 $\mu\text{g L}^{-1}$ established at the end of the 20th century¹⁵ to values below 1 $\mu\text{g L}^{-1}$ for arsenic determination.

This review considers primarily the remarkable developments in speciation analysis of arsenic in the last decade.

The chemical species are specific forms of an element defined though its: 1) isotopic composition, 2) electronic or oxidation state, 3) inorganic and organic compounds and their complexes, 4) organometallic species and 5) macromolecular compounds and complexes.¹⁶ Speciation analysis involves analytical activities for identifying and measuring the quantities of individual chemical species in a sample.¹⁷ Determination of total element concentration does not provide adequate information to understand the effects observed in the environment and in living systems.

The toxicity, bioavailability, physiological and metabolic processes and mobility are greatly dependant on the specific chemical form of the element. Potentially, toxic arsenic compounds are found in every aspect of the environ-

ment. Inorganic arsenic occurs on earth naturally in small amounts. Humans may be exposed to arsenic through food, water and air. Exposure may also occur through skin contact with soil or water that contains arsenic. Arsenic exists in different inorganic and organic chemical forms and different arsenic species exhibit different toxicities.¹⁸ Inorganic arsenic compounds are more toxic than organic compounds and the acute toxicity generally decreases with increasing degree of methylation.¹⁹ Depending on the source, a metal or metalloid can enter the environment, where it might be converted into another compound. Therefore, in order to obtain information on the activity and toxicity of a specific element it is necessary to know its specific chemical and physical forms.²⁰

2. ARSENIC CHEMISTRY AND ARSENIC SPECIATION – PREVIOUS REVIEWS

Arsenic has more than fifty identified different naturally occurring arsenic containing chemical species.²¹ The names, abbreviations and structure of the most widespread arsenic species in the environment are presented in Table I. Arsenic occurs in the environment in four oxidation states (As^{3+} , As^{5+} , As^0 and As^{3-}) in inorganic as well as in organic forms.^{1,21,22} Inorganic arsenic comprises two oxyanions, arsenite As(III) and arsenate As(V). Different organoarsenic compounds exist but the most common in the environment are monomethylarsenic acid (MMA) and dimethylarsinic acid (DMA). In addition, simple methylated arsenic species are trimethylarsine oxide (TMAO) and the tetramethylarsonium ion (TETRA). A number of organoarsenic compounds are present in biological samples: arsenobetaine (AB) as a dominant species in fish, arsenocholine (AC) and trimethylarsoniopropionate (TMAP). Other forms of As, such

TABLE I. Names, abbreviation and structure of the most common arsenic species

Name of arsenic species	Abbreviation	Structure
Arsenous acid, arsenite	As(III)	H_3AsO_3 , H_2AsO_3^- , HASO_3^{2-} , AsO_3^{3-}
Arsenic acid, arsenate	As(V)	H_3AsO_4 , H_2AsO_4^- , HASO_4^{2-} , AsO_4^{3-}
Monomethylarsenic acid	MMA	$\text{CH}_3\text{AsO}(\text{OH})_2$
Dimethylarsinic acid	DMA	$(\text{CH}_3)_2\text{AsO}(\text{OH})$
Trimethylarsine oxide	TMAO	$(\text{CH}_3)_3\text{AsO}$
Trimethylarsoniopropionate	TMAP	$(\text{CH}_3)_3\text{As}^+\text{CH}_2\text{CH}_2\text{COO}^-$
Tetramethylarsonium ion	TETRA, TMA	$(\text{CH}_3)_4\text{As}^+$
Arsenobetaine	AB	$(\text{CH}_3)_3\text{As}^+\text{CH}_2\text{COOH}$
Arsenocholine	AC	$(\text{CH}_3)_3\text{As}^+\text{CH}_2\text{CH}_2\text{OH}$
Dimethylarsinyolacetic acid	DMAA	$(\text{CH}_3)_2\text{AsOCH}_2\text{COOH}$
Phenylarsine oxide	PAO	$\text{C}_6\text{H}_5\text{AsO}$
Phenylarsonic acid	PAA	$\text{C}_6\text{H}_5\text{AsO}(\text{OH})_2$
Arsenosugars $\text{C}_7\text{H}_{14}\text{AsO}_3\text{CH}_2\text{CH}(\text{OH})\text{CH}_2\text{R}$		
Arsenosugar 1 (glycerol sugar)	–	$\text{R}=\text{OH}$
Arsenosugar 2 (phosphate sugar)	–	$\text{R}=\text{OP}(\text{O})(\text{O}^-)\text{OCH}_2\text{CH}(\text{OH})\text{CH}_2\text{OH}$
Arsenosugar 3 (sulphonate sugar)	–	$\text{R}=\text{SO}_3^-$
Arsenosugar 4 (sulphate sugar)	–	$\text{R}=\text{OSO}_3^-$

as arsenosugars, occur mainly in water organisms. Extensive toxicity studies of As showed that different forms exhibit different toxicities. Inorganic arsenic species are about 100 times more toxic than organic arsenic compounds.²² Trivalent arsenic is about 60 times more toxic than the oxidized pentavalent state.²³ Methylation of inorganic arsenic in the body is a detoxification process, which reduces the affinity of the compound for tissue as an adsorbent.²³

In natural waters, arsenic appears most often in inorganic forms and to a lesser extent in organic form such as MMA and DMA. As(V), MMA and DMA are stable in oxidized systems, while As(III) is unstable under oxidizing conditions and is readily oxidized.²⁴ In natural water, As(III) occurs at much lower concentrations compared to As(V), which makes its direct detection difficult and inevitably pre-concentration steps are required.²⁵

Recent complementary reviews on specific aspects of arsenic speciation analysis are listed in Table S-I of the Supplementary material to this review. The review starts from Francesconi¹⁴, who gives the base on how to understand the complexity of arsenic environmental and biological chemistry and it ends with Komorowicz,¹ a paper devoted to HPLC–ICP-MS techniques for arsenic and its speciation in water samples.

During the last decade, a significant number of scientific papers reporting the development in arsenic speciation have been published. The focus of research was the development and improvement of methods for arsenic extraction, separation and detection. The selection of an appropriate method for the extraction of arsenic species from different matrices without changing the oxidation state or with minimal loss by volatilisation or adsorption is still a challenging topic for research.

Liquid separation techniques, such as high-performance liquid chromatography (HPLC) and less popular capillary electrophoresis (CE) are the most frequently used techniques for the separation of soluble forms of arsenic species. The advantage of HPLC is the extended range of separation mechanisms by different mobile and stationary phases. The most applied detection technique is ICP-MS, especially after HPLC separation. This technique was applied in many studies for different sample types (environmental, biological and food samples). Application of ICP-MS has great capabilities since it can be used as a highly sensitive and element specific detector. Hydride generation atomic absorption spectrometry (HG-AAS) is a relatively simple and inexpensive technique but suitable only for hydride active As species. Electrochemical methods are suitable only for direct measurements in simple solutions.

The number of publications on arsenic speciation analysis has increased steadily since 2003. The number of publications, as shown in Fig. 1 from Science Direct, has increased from 32 articles per year (published in 2003), up to 125

articles per year (published in 2012). As presented, the interest for arsenic species is permanently growing.

3. ANALYTICAL METHODS FOR SPECIATION ANALYSIS

The ideal solution for direct measurement of species would be *in situ* analysis. However, very few techniques provide the necessary selectivity and sensitivity required for trace element speciation analysis. Those are: nuclear magnetic resonance (NMR), X-ray photoelectron spectroscopy (XPS), electron spectroscopy for chemical analysis (ESCA), X-ray absorption fine structure spectroscopy (XAFS), electron spin resonance (ESR), tandem mass spectroscopy (TMS) and Mössbauer spectroscopy.

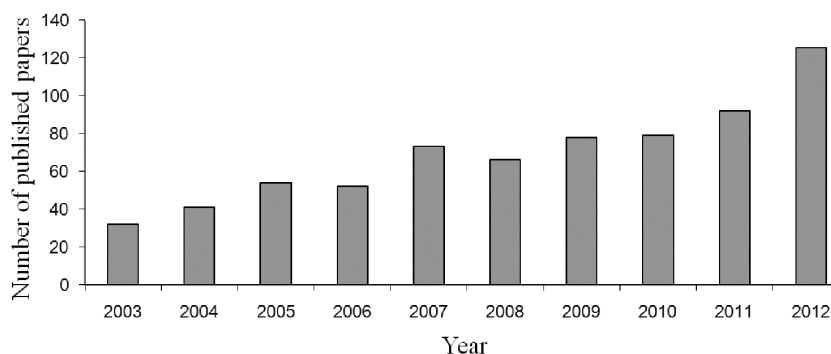


Fig. 1. Evolution of the number of published papers on arsenic speciation since 2003.

However, for species determination in practice at least two steps are usually applied: separation and detection. The most commonly used detection methods in speciation analysis are atomic absorption spectrometry (AAS), atomic fluorescence spectrometry (AFS), atomic emission spectrometry (AES) and inductively coupled plasma mass spectrometry (ICP-MS). Furthermore, electrochemical methods are also powerful tools for speciation analysis.³⁹

Coupled techniques combining the separation power of a chromatographic or equivalent separation technique with the detection power of the most sensitive atomic spectroscopic techniques are the most applicable hyphenated techniques. Nowadays, hyphenated techniques couple the separation technique on-line with the detection technique. The advantages of such hyphenated techniques are manifold: a high degree of automation, a high sample throughput and a good reproducibility, a short analysis time, reduced risk for species transformation during analysis, a reduction in contamination due to a closed system and a high degree of information due to enhanced combined selectivity of the involved techniques. Different separation techniques that could be successfully coupled with sensitive detection techniques are presented in Fig. 2.⁴⁰

Analytical methods for determining different arsenic species have become increasingly important due to the different toxicity and chemical behaviour of the various arsenic forms. Well-established methods that involve the coupling of separation techniques, such as ion chromatography (IC)^{41,42} and high performance liquid chromatography (HPLC)^{43,44} with a sensitive detection system, such as inductively coupled plasma-mass spectrometry (ICP-MS),⁶ hydride generation-atomic fluorescence spectrometry (HG-AFS), hydride generation-atomic absorption spectrometry (HG-AAS)⁴⁵ and graphite furnace-atomic absorption spectrometry (GF-AAS)⁴⁶ are the methods of choice for the routine determination of a large number of water samples.

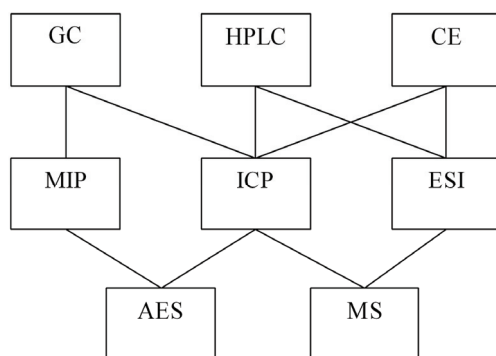


Fig. 2. Actual techniques for speciation analysis.⁴⁰ Legend: GC – gas chromatography; HPLC – high performance liquid chromatography; MIP – microwave-induced plasma; ICP – inductively coupled plasma; CE – capillary electrophoresis; ESI – electrospray ionization; AES – atomic emission spectrometry; MS – mass spectrometry.

A compilation of the developed methods commonly employed in speciation analyses is provided in Table S-II of the Supplementary material. The HPLC–ICP-MS method was applied in many studies with all types of sampled and this was the main step in improving arsenic speciation analysis. The only other technique that had application for all sample types is HG-AAS, usually after on-line HPLC separation. X-ray spectroscopic methods dominate in solid sample analyses. This is not surprising since all the coupled techniques require the arsenic species to be in solution, and suitable extraction procedures have not yet been developed for sediments and soils. Indeed, sample extraction is becoming one of the key issues in arsenic speciation analysis.

The analytical performance of an analytical method must be evaluated through validation protocols. Besides specificity and/or selectivity, linearity of calibration, repeatability and accuracy, the most important parameters are *LoD* (limit of detection) and *LoQ* (limit of quantification). All of the limits are related and have distinct definitions. Through the limits, it is possible to define the lowest concentration of an analyte that can be reliably detected and quantified. In this part of the review, the focus is analytical limits in the determination of arsenic species.

The obtained values for *LoD* and *LoQ* (Tables S-II and S-III of the Supplementary material) depend not only on the different matrices, extraction techniques and instruments for the measurements, but also on the different approaches for calculation. It could be noticed that several protocols are commonly used for *LoD* estimation: traditionally the 3σ method, method detection limit (MDL) according to US EPA and method of calculating signal to noise ratio based on manual measurements of peak heights on chromatogram printout. These methods are popular due to their simplicity, but at the same time characterized as not valid. Once again, the proper use of basic Currie definitions should be emphasized. The procedure for *LoD* determination should include testing whether the analytical measurement system is homoscedastic (standard deviation of measurement error is constant) or heteroscedastic (standard deviation of measurement error changes with concentration), and subsequently the adequate formulae for both the critical value and *LoD* should be used. Incorporating a blank subtraction factor and taking heteroscedasticity into account leads to unbiased and efficient estimates of the limits.⁸³

Some recent articles dealing with arsenic speciation are reviewed concerning limit of detection, *LoD* and limit of quantification, *LoQ*, determined by different analytical techniques and different sample preparation procedure, are listed in Table S-III of the Supplementary material. The precision, most often determined as a value of relative standard deviation, is also analyzed and presented in Tables S-II and S-III of the Supplementary material. The obtained values of precision do not exceed 20 %. The recovery of the methods is usually calculated from spiking of the samples or from standard reference materials (SRM). The values for the recovery were also studied and the obtained values, which were greater than 70 %, are listed in Tables S-II and S-III of the Supplementary material.

4. STABILITY OF ARSENIC SPECIES: SAMPLE COLLECTION, STORAGE AND PRESERVATION

Sampling problems such as loss of analyte or contamination have long plagued trace element analyses, but they are nowadays reasonably well understood and controlled. The situation with arsenic speciation analysis is much more complex, and for many types of samples/species, there is still a long way to go before the problems can be adequately addressed.¹⁴ Sampling and storage procedures could be considered as a key requirement in order to preserve the species information during the whole analytical process. Two main strategies could be distinguished for achieving this goal. Firstly, species preservation should keep the chemical species of interest unchanged during all steps of analysis to avoid changes in the oxidation state, changes induced by microbial activity and losses by volatilization or adsorption. Secondly, the species could be quantitatively

transformed into suitable derivatives for further separation, accumulation and quantification.⁸⁹

The most reliable method for preserving natural water samples is, therefore, acidification to pH 2, refrigeration and deoxygenation.⁹⁰ According to Segura *et al.*⁴³, arsenic species in water are stable under neutral conditions for a period of 4 months if they are placed in polypropylene bottles in a refrigerator. Using phosphoric acid as a preservation agent, samples remain stable for 3 months, even if they show evidence of high concentrations of iron or manganese.⁹¹ Phosphoric acid at a final concentration of 10 mM is recommended as a preservation agent, combined with keeping the samples cool (6 °C) and in the dark.

McCleskey *et al.*⁹² investigated the influence of preservation of water samples for As(III) and As(V) determinations. To stabilize dissolved As redox species, it is imperative for the samples to be filtered, preserved with HCl, H₂SO₄, or ethylenediaminetetraacetic acid (EDTA) to stabilize Fe, and to be stored in the dark. Filtering the sample removes most of the colloidal material and micro-organisms that can affect the dissolved As(III/V) ratio. Acidification prevents oxidation and precipitation of Fe and Mn hydroxides that could co-precipitate or adsorb As. EDTA sequesters Fe and the formation of precipitates is inhibited. Arsenic has never been shown to be photochemically reactive, but oxidation of As(III) in conjunction with the photoreduction of Fe(III) could occur unless light is excluded. Excluding light prevents photochemical reactions that could affect the As redox distribution. Preservation of As depends on the analytical technique and the need to stabilize other redox species, especially Fe(II/III). Hydrochloric acid works well as a preservative for As, Fe and Se redox species for a wide range of natural water samples when the samples are properly filtered and stored in the dark and is preferred when using HG-AAS for determining hydride-forming elements. For HPLC–ICP-MS applications, EDTA is the preferred preservative.

There is no general agreement on stability procedures and reports are sometimes even contradictory. This is especially true for complex solid matrices, such as soils, sediments and biological tissues. Dahl *et al.*⁹³ showed that processing or storage by freezing did not change the total arsenic content in seafood samples, or alter the speciation pattern greatly. According to Pizarro *et al.*,⁹⁴ arsenic species in rice extracts remained stable during a three-month test period, whereas in fish and chicken tissue extracts, AB was transformed into DMA over time. As species from chicken and fish (higher protein content than rice and/or soil) became more stable as the methanol content in the employed extractant mixture increased.

Salgado *et al.*⁹⁵ investigated the stability of total arsenic and arsenic species in alga samples (*Sargassum fulvellum* and *Hizikia fusiformis*), as well as in their aqueous extracts, which were stored in amber glass and polystyrene containers at

different temperatures. The results obtained for solid alga samples showed that total arsenic (for *Hizikia* alga) and arsenic species present (As(V) for *Hizikia* and NIES No. 9 – reference material of a lyophilised *Sargasso* material, *Sargassum fulvellum*, National Institute for Environmental Studies (Japan)) were stable for at least 12 months when samples are stored in polystyrene containers at 20 °C. On the other hand, different behaviours in the stability of total arsenic and As(V) species in aqueous extracts were observed for both samples. The best storage conditions for the *Sargassum* extracts were in polystyrene containers at temperature of –18 °C, when they were stable for at least 15 days, while *Hizikia* extracts had to be stored in polystyrene containers at 4 °C in order to ensure stability for 10 days.

5. SAMPLE EXTRACTION

Extraction is the selective separation of target species from their matrix (water, soil, sediment, biological tissue or fluid). Table III summarises recent application and research papers dealing with arsenic speciation, and the different methods applied for sample preparation for different matrices. The most commonly used extraction methods are: solvent extraction, enzymatic hydrolysis, solid phase extraction (SPE), solid phase micro-extraction (SPME) and microwave extraction.

However, there is no universal extraction procedure for different species and different matrices, which means that for each application and target analyte, a specific sample treatment method has to be developed. This has been realized for arsenic speciation from biological samples, coal and ash, plant, water and soil samples.

Solvent extraction. The solvent extraction technique is commonly used for the determination of organic arsenic compounds, especially in biological samples. Methanol/water mixtures are widely used for extracting less polar species. Ciardullo *et al.*⁹⁶ used a 1/1 (v/v) methanol/water mixture for the quantification of water-soluble As compounds in the muscle tissues of freshwater fish. In addition, extraction with water, or extraction with methanol/water followed by centrifugation and filtration,³⁵ or extraction with chloroform/methanol/water and sonication⁹⁷ are very powerful extraction media and often used extraction procedures. The total arsenic in different samples is usually extracted using the microwave extraction procedure.⁹⁸ In order to avoid species losses or transformation, parameters such as extraction medium, applied microwave power and exposure time have to be carefully optimized.

On the other hand, it has been repeatedly proven that a simple, inexpensive reagent, such as tetramethylammonium hydroxide (TMAH) in alkaline medium, is useful as a solubilising agent for a wide variety of biological matrices. Speciation analysis of arsenic in fish-based baby foods by electrothermal atomic

absorption spectrometry (ET-AAS) using suspensions prepared in a 0.01 mol L⁻¹ tetramethylammonium hydroxide (TMAH) solution has limits of detection for the determination of AB, DMA and inorganic arsenic 15, 25 and 50 ng g⁻¹ expressed as arsenic, respectively.⁹⁹

Methods such as these in which methanol/water is used have the feature of extracting only a small percentage of the arsenic in soil and sediment samples. Accordingly, methods for soils and sediments and other abiotic samples are often based on those used in classical fractionation studies, using aqueous solutions of varying ionic strengths/pH/redox potential to release arsenic bound to the various mineral phases in the samples. Speciation information on the solid fraction is more difficult to acquire. For some time, a series of sequential extractions has been employed to acquire the information required to understand the cycling of As in sediments (on water-soluble, phosphate-exchangeable, organically bound and residual phases in such media).^{100,101} Digestion using the mixture of acids: nitric and sulphuric in presence of vanadium pentoxide as catalyst is a powerful technique for the separation and determination of arsenic in coal and coal ash.^{46,102}

Giacomino *et al.*¹⁰³ investigated the fractionation and speciation of As in contaminated soil. Regarding speciation, they found that As(V) prevailed over As(III), while more than 40 % of total arsenic was in an organic form. The fractionation of As was investigated with two sequential extraction methods: with concentrated hydrochloric acid and using the solvent extraction technique. The concentration of organic arsenic was determined by the difference between the total concentration of arsenic determined by acid digestion and total inorganic arsenic. Determination was realized by ICP-AES and GF-AAS. The extraction percentages for As ranged from 30 to 65 %.

Enzymatic hydrolysis. The use of enzymes, mainly those of a proteolytic nature, is another approach for speciation studies.¹⁰⁴ Enzymes are able to break down specific bonds of the substrate (biomolecules hydrolysis) under neutral pH and room temperature, and they allow a selective analyte release from the sample matrix without chemical species changes. However, enzymatic hydrolysis methods offer as a disadvantage the long time required for completing the substrate hydrolysis (several hours), which strongly conditions the applicability of the methods. To overcome this problem, pioneering developments based on the use of ultrasound energy (sonication probes) to assist the hydrolysis process have been proposed for extracting arsenic species.¹⁰⁵ The reduction of the hydrolysis time when using ultrasound could be attributed to fast cell membrane disruption, which allows a direct contact of cytosolic structures and the enzymes. Enzymatic hydrolysis procedures can also be assisted by microwave irradiation. In this case, improvements on enzymatic hydrolysis efficiency under microwaves are attributed to pressure effects on the enzyme and/or the substrate–enzyme interaction

and conformational changes in the protein. Moreda-Pineiro *et al.*¹⁰⁶ proposed enzymatic hydrolysis of seafood materials for isolating arsenic species (As(III), As(V), DMA and AB) by assisting the procedure with ultrasound energy supplied by an ultrasound water bath. The use of pepsin, as a proteolytic enzyme, under optimized operating conditions (pH 3.0, temperature 40 °C, enzyme to sample ratio of 0.3) led to an efficient assistance of the enzymatic process in a short period (from 4.0 to 30 min). The method was successfully applied to different seafood samples (molluscs, white fish and cold-water fish).

Microwave-assisted extraction. Microwave extraction is a frequently used technique for the extraction of biological and environmental matrices, considerably faster than conventional Soxhlet extraction procedure. Parameters such as extraction medium, applied microwave power and exposure time have to be carefully optimized in order to avoid species losses or transformation. Sample preparation for speciation analysis can be improved using a focused-microwave oven owing to a better control of the energy delivered to the sample. Extraction procedures using dilute acid or organic solvents at low temperature can be easily realized in focused-microwave ovens.

Microwave-based strategies for speciation analysis of arsenic, mercury, tin and selenium from matrices such as urine, fruit juices, fish, mussel, sediments and diatomea were reviewed by Nobrega *et al.*,¹⁰⁷ emphasising both its suitability for the leaching of labile species and to support derivatisation reactions. Raber *et al.*¹⁰⁸ used microwave extraction for the determination of inorganic arsenic in food. The method was based on sample extraction with trifluoroacetic acid/H₂O₂, and measurement of arsenate by anion-exchange HPLC–ICP-MS using aqueous malonic acid as the mobile phase. The method showed good extraction efficiencies (generally >90 %) for samples of rice, tuna fish and wheat.

Solid phase extraction. Solid phase extraction (SPE) is a frequently used method for pre-concentration and/or separation. The principle of SPE is partitioning between a liquid (sample matrix) and a solid (sorbent) phase. The mechanism of retention depends on the nature of the sorbent, and may include simple adsorption, chelation, ion-exchange or ion-pair solid phase extraction. SPE offers the advantages of high sensitivity due to the possibility of performing a simultaneous enrichment step, and versatility, since different substrates interact with different metal species. SPE is a popular technique because of its ability to work in combination with different detection techniques: on-line and off-line. In on-line techniques, there is no sample manipulation between pre-concentration and analysis, so the risks of loss and contamination are avoided and reproducibility is better. Likewise, all species are analyzed, so the volume of the sample can be smaller than the off-line procedure, the consumption of organic solvents is less and the potential for automation is greater. Nevertheless, the off-line SPE approach remains useful for analyzing complex samples due to its greater flexi-

bility and its ability to analyze the same extract using various techniques.¹⁰⁹ Various sorbents (*e.g.*, activated alumina, zirconium-loaded polymeric resin, Fe(III)-loaded resin, metal-loaded active charcoal and lanthanum hydroxide) have been reported for the separation of oxo-species of arsenic but a metal leaching problem and their poor stability in alkaline or acidic medium restrict their use. The application of chelating resins became extremely popular with the successful introduction of chelating groups (*e.g.*, imidazole, benzimidazole, 6-mercaptopurine, 2-naphthol-3,6-disulphonic acid, thiosalicylic acid, and bis(2-aminophenyl) disulphide) into a resin matrix, and has been reported for arsenic speciation.¹⁰⁹

For the development of an extraction method, it is necessary to bear in mind that various arsenic species have different physical and chemical properties. The same extraction procedure applied to different samples can result in various extraction recoveries. Sometimes sequential extraction with a combination of different solvents and different extraction techniques should be developed.

6. SEPARATION AND DETERMINATION OF ARSENIC SPECIES IN WATER

Determination of arsenic is of the cardinal importance for water quality analysis. Arsenic has been reported as a groundwater pollutant in India, Bangladesh, Vietnam and Cambodia. It has also been detected in the south-eastern European Pannonian Basin region, where increased arsenic concentrations were found in the groundwater of Hungary, Romania and Serbia. The concentration of arsenic in the Banat region of Serbia ranges from 50 to 250 $\mu\text{g L}^{-1}$.¹¹⁰ This was the reason for scientific investigations in Serbia of arsenic compounds and the possibilities of their removal from water.¹¹¹ Conventional and non-conventional treatment technologies for aqueous arsenic remediation were the subject of many studies. Adsorption is considered a relatively simple, efficient and low cost removal technique, especially convenient for application in rural areas. A wide range of sorbent materials for aqueous arsenic removal is available nowadays: biological materials, mineral oxides, different soils, activated carbons and polymer resins. Nevertheless, finding inexpensive and effective sorbent for arsenic removal from water is still highly desirable.

Chemisorption filters (activated with Ag^+ , Mg^{2+} , Cu^{2+} , Al^{3+} and Fe^{3+}) made by the paper manufacture method and consisting of cellulose, cationic and anionic ion exchangers, activated carbon and a corresponding chemical agent were used as adsorbents for the removal of arsenic from water.¹¹² Cu^{2+} ions exhibited the most efficient removal. The mechanisms of total arsenic removal were determined based on measurements of active Cu^{2+} ion propagation inside the filter structure. A decrease in the arsenic concentration was determined using a continuous chromatographic system with multifunctional filters combining the effects of adsorption, ion exchange and filtration; for an active layer of 8 mm and

a contact time of 2 s, the decrease was more than 1000-fold. Investigations have shown that arsenic removal is valence dependent (the removal of pentavalent arsenic was more effective). The initial concentration, pH value of the water and the concentration of anionic pollutants, which affected the selectivity, were important for all the investigated processes.

Activated carbon impregnated with metallic silver and copper is also a very powerful adsorbent for the removal of arsenic from water.¹¹³ The ability of activated carbon to adsorb arsenic depends on the arsenic oxidation state, the pH of water and the activity of the metal used for impregnation of the activated carbon. Physical adsorption is effective only for As(V) species in water. Activated carbon adsorbs As(V) with a saturation adsorption capacity of 0.27 mmol g⁻¹. The chemisorption process is effective for both As species. When active carbon is impregnated with copper, the sorption process for As(III) species was significantly improved, with saturation adsorption capacities of 0.41 and 0.23 mmol g⁻¹ for As(III) and As(V) species, respectively. The pH value of the water is important for the adsorption of both As species because of the change in the ionic forms of arsenic. The optimal pH range is between 4 and 9, which is a consequence of the affinity between the carbon surface and H₃AsO₃ and H₂AsO₄⁻ that are the predominant As species at this range of pH values.

Arsenic sorption onto hydrated iron(III) oxide (HFO)-coated materials, at neutral pH values, when As occurs in both molecular and ionic forms, is a multi-stage process consisting of both macropore and intraparticle diffusion.¹⁰ Higher sorption values were obtained for As(III), which was attributed to the beneficial features of HFO.

Natural materials (zeolite, bentonite, sepiolite, pyrolusite and limonite) and industrial by-products (steel-mill waste, waste filter sand as water treatment residuals and blast furnace slag from steel production)^{11,114} are low-cost adsorbents for inorganic arsenic removal from water. The natural zeolite and the industrial by-products were found to be good and inexpensive sorbents for arsenic while bentonite and sepiolite clays showed little affinity towards arsenic. The sorption capacities for As(V) compared to As(III) were significantly higher when natural zeolite and blast furnace slag were investigated, while the waste filter sand exhibited similar removal efficiencies for both As species. In equilibrium studies, the efficiency of As removal was found to be valence dependent, suggesting that the molecular forms of As bond less efficiently compared to its ionic forms.

Future research should involve the analysis of the desorption mechanisms for the examined waste materials and investigations of fixed-bed sorption systems, as well as the economic aspect of iron waste slag modification in terms of the possible application of this material in real water treatment systems.

A simple method for the preparation, separation of As(III) and As(V) species and pre-concentration of the total As on fixed bed columns in natural and drink-

ing water was developed by ben Issa *et al.*⁶ Two resins, a strong base anion exchange (SBAE) resin and a hybrid (HY) resin were utilized. The inductively-coupled plasma-mass spectrometry method was applied for the determination of the arsenic concentration in water. The governing factors for the ion exchange/sorption of arsenic on resins in a batch and a fixed bed flow system were compared. Acidity of the water, which plays an important role in the control of the ionic or molecular forms of arsenic species, was beneficial for the separation; by adjusting the pH values to less than 8.00, the SBAE resin separated As(V) from As(III) in water by retaining As(V) and allowing As(III) to pass through. The sorption activity of the hydrated iron oxide particles integrated into the HY resin was beneficial for the bonding of all inorganic As species over a wide range of pH values from 5.00 to 11.00. In other papers,^{7,8} a simple and efficient method for the separation and determination of inorganic arsenic and organic arsenic in drinking, natural and wastewater was proposed. A procedure for the separation and determination of arsenic species in water is presented in Fig. 3. Three types of resins: a strong base anion exchange (SBAE) and two hybrid (HY) resins: HY-Fe and HY-AgCl based on the activity of hydrated iron oxides and silver chloride, respectively, were investigated. The procedures showed that they were accurate, precise and time efficient, and that just a very simple sample treatment is required.

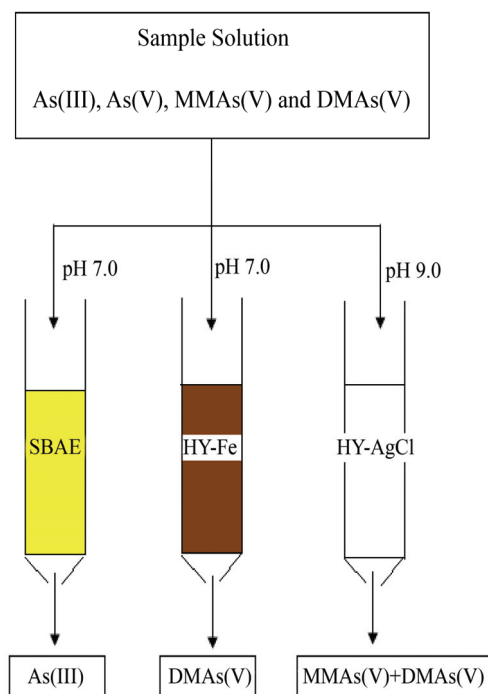


Fig. 3. Scheme for the selective separation of the arsenic species in water using SBAE, HY-Fe and HY-AgCl resins.⁷

7. CONCLUSIONS

The speciation analysis of arsenic is of great importance for human health, but it is challenging for analysts and is still a challenge for analytical chemistry. Complete characterization of arsenic compounds is necessary due to the different toxicological effects demonstrated by particular arsenic species. The chemical nature of arsenic compounds, in particular their tendency to change valence states or chemical form under a wide range of pH and redox conditions, makes it difficult to assess their fate and mobility in the environment.

There are a large number of papers on arsenic speciation in various matrices including a number of different extraction techniques. It is not possible to set an universal extraction procedure for different species and different matrices.

The most commonly used method for arsenic speciation involves liquid chromatographic separation followed by element detection (ICP-MS, AAS, and HG-AFS). Selecting the most appropriate method for the determination in arsenic species can be of vital importance in the achievement of reliable and accurate results.

SUPPLEMENTARY MATERIAL

Tables S-I–S-III are available electronically at <http://www.shd.org.rs/JSCS/>, or from the corresponding author on request.

Acknowledgements. This work was financially supported by the Ministry of Education, Science and Technological Development of the Republic of Serbia through the Research Project III 43009.

ИЗВОД

АНАЛИТИЧКЕ МЕТОДЕ ЗА АНАЛИЗУ АРСЕНОВИХ ЈЕДИЊЕЊА

ЉУБИНКА В. РАЈАКОВИЋ¹, ЖАКЛИНА Н. ТОДОРОВИЋ², ВЛАДАНА Н. РАЈАКОВИЋ-ОГЊАНОВИЋ³
и АНТОНИЈЕ Е. ОЊИЋ²

¹Технолошко–металуршки факултет, Универзитет у Београду, Карнегијева 4, п.пр. 494, 11120 Београд, ²Институт за нуклеарне науке „Винча“, Универзитет у Београду, п.пр. 522, 11001 Београд и ³Грађевински факултет, Универзитет у Београду, Булевар Краља Александра 73, Београд

Арсен се налази у многобројним хемијским врстама које се разликују по физичко–хемијском понашању, токсичности, биодоступности и биотрансформацији. Одређивање појединих арсенових једињења је неопходно у хемији животне средине, клиничкој хемији и хемији хране. Међутим, диференцијација ових врста је врло сложен аналитички задатак. За анализу арсенових врста развијен је велики број метода и поступака које укључују хроматографске, спектрометријске и електрохемијске технике и њихове комбинације. У овом прегледном раду обухваћена су релевантна истраживања у области специјационе анализе арсена са нагласком на најзначајнија достигнућа и примену. Одржавање непроменљивог, оригиналног састава арсенових специја у току појединачних аналитичких корака (прикупљање узорака, чување, конзервација, екстракција) посебно су разматрани. Извојене су методе за директно и индиректно одређивање арсенових врста. Побројане су спрегнуте технике које се најчешће примењују у пракси применом методологије која подразумева прелиминарну сепарацију једињења, а затим поједи-

начно одређивање. Дат је преглед аналитичких својстава, предности и недостатака најпримеренијих аналитичких метода, развијених управо за анализу трагова арсенових врста од неорганских до органских у различитим матрицама. Издвојене су и детаљније презентоване најзначајније студије о арсеновим једињењима у води.

(Примљено 15. марта, ревидирано 29 маја 2013)

REFERENCES

1. I. Komorowicz, D. Baralkiewicz, *Talanta* **84** (2011) 247
2. A. G Gault, D. A. Polya, P. R Lythgoe, M. L. Farquhar, J. M Charnock, R. A Wogelius, *Appl. Geochem.* **18** (2003) 1387
3. S. N. Ronkart, V. Laurent, P. Carbonnelle, N. Mabon, A. Copin, J. P. Barthélemy, *Chemosphere* **66** (2007) 738
4. K. F. Akter, Z. Chen, L. Smith, D. Davey, R. Naidu, *Talanta* **68** (2005) 406
5. D. Chen, C. Huang, M. He, B. Hu, *J. Hazard. Mater.* **164** (2009) 1146
6. N. Ben Issa, V. N. Rajaković-Ognjanović, B. M. Jovanović, Lj. V. Rajaković, *Anal. Chim. Acta* **673** (2010) 185
7. N. Ben Issa, V. N. Rajaković-Ognjanović, A. D. Marinković, Lj. V. Rajaković, *Anal. Chim. Acta* **706** (2011) 191
8. N. B. Issa, A. D. Marinković, Lj. V. Rajaković, *J. Serb. Chem. Soc.* **77** (2012) 775
9. B. Daus, J. Mattusch, R. Wennrich, H. Weiss, *Talanta* **75** (2008) 376
10. B. Jovanović, V. L. Vukašinović-Pešić, Lj. V. Rajaković, *Water Environ. Res.* **83** (2011) 498
11. B. M. Jovanović, V. L. Vukašinović-Pešić, Đ. N. Veljović, Lj. V. Rajaković, *J. Serb. Chem. Soc.* **76** (2011) 1437
12. US EPA: United States Environmental Protection Agency, *National primary drinking water regulations: arsenic and clarifications to compliance and new source contaminants monitoring*, in: *Final Rule, Code of Federal Regulations*, title 40, parts 141 and 142, USA, 2001.
13. WHO: World Health Organization, *Arsenic in Drinking Water*, Geneva, 2001
14. K. A. Francesconi, D. Kuehnelt, *Analyst* **129** (2004) 373
15. P. Thomas, K. Sniatecki, *Fresenius J. Anal. Chem.* **351** (1995) 410
16. C. B. Hymer, J. A. Caruso, *J. Chromatogr., A* **1045** (2004) 1
17. A. Kot, J. Namiesnik, *Trends Anal. Chem.* **19** (2000) 69
18. D. Q. Hung, O. Nekrassova, R. G. Compton, *Talanta* **64** (2004) 269
19. E. Munoz, S. Palmero, *Talanta* **65** (2005) 613
20. P. Rodriguez-Gonzalez, J. M. Marchante-Gayon, J. I. Garcia Alonso, A. Sanz-Medel, *Spectrochim. Acta, B* **60** (2005) 151
21. R. V. Hedegaard, J. J. Slouth, *Biotechnol. Agron. Soc. Environ.* **15** (2011) 45
22. M. Leermakers, W. Baeyens, M. De Gieter, B. Smedts, C. Meert, H. C. De Bisschop, R. Morabito, Ph. Quevauviller, *Trends Anal. Chem.* **25** (2006) 1
23. C. K. Jain, I. Ali, *Water Res.* **17** (2000) 4304
24. V. K. Sharma, M. Sohn, *Environ. Int.* **35** (2009) 743
25. P. I. Smedley, D. G. Kinniburgh, *Appl. Geochem.* **17** (2002) 517
26. C. Dietz, J. Sanz, E. Sanz, R. Munoz-Olivas, C. Camara, *J. Chromatogr., A* **1153** (2007) 114
27. V. Devesa, D. Velez, R. Montoro, *Food Chem. Toxicol.* **46** (2008) 1
28. S. Wang, C. N. Mulligan, *Environ. Int.* **34** (2008) 867
29. V. K. Sharma, M. Sohn, *Environ. Int.* **35** (2009) 743

30. D. E. Mays, A. Hussam, *Anal. Chim. Acta* **646** (2009) 6
31. Y. W. Chen, N. Belzile, *Anal. Chim. Acta* **671** (2010) 9
32. C. Niegel, F. M. Matysik, *Anal. Chim. Acta* **657** (2010) 83
33. M. Popp, S. Hann, G. Koellensperger, *Anal. Chim. Acta* **668** (2010) 114
34. A. R. Kumar, P. Riyazuddin, *Trends Anal. Chem.* **29** (2010) 10
35. R. Rubio, M. J. Ruiz-Chancho, J. F. Lopez-Sanchez, *Trends Anal. Chem.* **29** (2010) 1
36. K. C. Hsu, C. C. Sun, Y. L. Huang, *Kaohsiung J. Med. Sci.* **27** (2011) 382
37. V. L. Dressler, F. G. Antes, C. M. Moreira, D. Pozebon, F. A. Duarte, *Int. J. Mass Spectrom.* **307** (2011) 149
38. H. Md Anawar, *Talanta* **88** (2012) 30
39. M. A. Ferreira, A. A. Barros, *Anal. Chim. Acta* **459** (2002) 151
40. EVISA: European Virtual Institute for Speciation Analysis, <http://www.speciation.net/Public/Document/2003/09/11/503.html> (accessed October, 2013)
41. F. A. Duarte, J. S. Fagundes Pereira, M. F. Mescos, F. Goldschmidt, E. M. de Moraes Flores, V. L. Dressler, *Spectrochim. Acta, B* **62** (2007) 978
42. P. Pohl, B. Pruisisz, *Trends Anal. Chem.* **23** (2004) 63
43. M. Segura, J. Munoz, Y. Madrid, C. Camara, *Anal. Bioanal. Chem.* **374** (2002) 513
44. A. J. Bednar, J. R. Garbarino, M. R. Burkhardt, J. F. Ranville, T. R. Wildeman, *Water Res.* **38** (2004) 355
45. K. Jitmanee, M. Oshima, S. Motomizu, *Talanta* **66** (2005) 529
46. V. L. Vukašinović, N. Z. Blagojević, Lj. V. Rajaković, *Instrum. Sci. Technol.* **37** (2009) 482
47. K. Ito, C. D. Palmer, A. J. Steuerwald, P. J. Parsons, *J. Anal. At. Spectrom.* **25** (2010) 1334
48. R. Xie, W. Johnson, S. Spayd, G. S. Hall, B. Buckley, *Anal. Chim. Acta* **578** (2006) 186
49. P. Heitland, H. D. Koster, *Int. J. Hyg. Environ. Health* **212** (2009) 432
50. R. Sur, L. Dunemann, *J. Chromatogr., B* **807** (2004) 169
51. P. K. Petrov, I. Serafimovski, T. Stafilov, D. L. Tsalev, *Talanta* **69** (2006) 1112
52. Y. C. Sun, Y. J. Chen, Y. N. Tsai, *Microchem. J.* **86** (2007) 140
53. R. A. Assis, I. L. Kuchler, N. Miekeley, M. B. Tozzi, *Anal. Bioanal. Chem.* **390** (2008) 2107
54. C. Yeh, S. Jiang, *Electrophoresis* **26** (2005) 1615
55. P. Cava-Montesinos, K. Nilles, M. L. Cervera, M. de la Guardia, *Talanta* **66** (2005) 895
56. I. B. Rodriguez, G. Raber, W. Goessler, *Food Chem.* **112** (2009) 1084
57. N. M. M. Coelho, L. M. Coelho, E. S. de Lima, A. Pastor, M. de la Guardia, *Talanta* **66** (2005) 818
58. M. N. Matos-Reyes, M. L. Cervera, R. C. Campos, M. de la Guardia, *Spectrochim. Acta, B* **62** (2007) 1078
59. I. B. Karadjova, L. Lampugnani, M. Onorb, A. D'Ulivob, D. L. Tsaleva, *Spectrochim. Acta, B* **60** (2005) 816
60. M. N. Matos-Reyes, M. L. Cervera, R. C. Campos, M. de la Guardia, *Talanta* **75** (2008) 811
61. P. Cava-Montesinos, A. de la Guardia, C. Teutsch, M. L. Cervera, M. de la Guardia, *Anal. Chim. Acta* **493** (2003) 195
62. J. M. Bundaleska, T. Stafilov, S. Arpadjan, *Int. J. Environ. Anal. Chem.* **85** (2005) 199
63. R. Xie, W. Johnson, S. Spayd, G. S. Hall, B. Buckley, *J. Anal. At. Spectrom.* **22** (2007) 553
64. A. N. Anthemidis, G. A. Zachariadis, J. A. Stratis, *Anal. Chim. Acta* **547** (2005) 237

65. P. Niedzielski, M. Siepak, *Cent. Eur. J. Chem.* **3** (2005) 82
66. E. A. Cordos, T. Frentiu, M. Ponta, B. Abraham, *Chem. Spec. Bioavailab.* **18** (2006) 1
67. P. Niedzielski, M. Siepak, *Chem. Ecol.* **21** (2005) 241
68. Z. Gong, X. Lu, C. Watt, B. Wen, B. He, J. Mumford, Z. Ning, Y. Xia, X. C. Le, *Anal. Chim. Acta* **555** (2006) 181
69. C. I. S. Narcise, L. dlC. Coo, F. R. del Mundo, *Talanta* **68** (2005) 298
70. A. Castillo, A. F. Roig-Navarro, O. J. Pozo, *J. Chromatogr., A* **1202** (2008) 132
71. G. G. Bortoleto, S. Cadore, *Talanta* **67** (2005) 169
72. P. Herbello-Hermelo, M. C. Barciela-Alonso, A. Bermejo-Barrera, P. Bermejo-Barerra, *J. Anal. At. Spectrom.* **20** (2005) 662
73. J. Narvaez, P. Richter, M. I. Toral, *Anal. Bioanal. Chem.* **381** (2005) 1483
74. L. M. Coelho, N. M. M. Coelho, M. A. Z. Arruda, M. de la Guardia, *Talanta* **71** (2007) 353
75. B. Daus, M. Hempel, R. Wennrich, H. Weiss, *Environ. Pollut.* **158** (2010) 3439
76. P. Niedzielski, *Anal. Chim. Acta* **551** (2005) 199
77. Y. Morita, T. Kobayashi, T. Kuroiwa, T. Narukawa, *Talanta* **73** (2007) 81
78. X. Li, J. Jia, Z. Wang, *Anal. Chim. Acta* **560** (2006) 153
79. J. C. Gonzalez, I. Lavilla, C. Bendicho, *Talanta* **59** (2003) 525
80. M. Ponthieu, P. Pinel-Raffaitin, I. Le Hecho, L. Mazeasb, D. Amouroux, O. F. X. Donard, M. Potin-Gautier, *Water Res.* **41** (2007) 3177
81. Y. Li, G. K. C. Low, J. A. Scott, R. Amal, *Chemosphere* **79** (2010) 794
82. J. Szakova, P. Tlustoš, W. Goessler, Z. Frkova, J. Najmanova, *J. Hazard. Mater.* **172** (2009) 1244
83. Lj. V. Rajaković, D. D. Marković, V. N. Rajaković-Ognjanović, D. Z. Antanasijević, *Talanta* **102** (2012) 79
84. T. Sakai, S. Wilbur, *Routine Analysis of Toxic Arsenic Species in Urine Using HPLC with ICP-MS, Application note*, Agilent Technologies, Inc. USA, 2006, Publication No. 5989-5505EN
85. P. Heitland, H. D. Köster, *J. Anal. Toxicol.* **32** (2008) 308
86. S. Hirata, H. Toshimitsu, M. Aihara, *Anal. Sci.* **22** (2006) 39
87. A. H. E. Petursdottir, *Determination of toxic and non-toxic arsenic species in Icelandic fish meal*, Master Thesis, Faculty of Physical Sciences, University of Iceland, 2010
88. K. Sathrugnan, S. Hirata, *Talanta* **64** (2004) 237
89. M. F. Mescos, C. A. Hartwig, C. A. Bizzi, J. S. F. Pereira, P. A. Mello, E. M. M. Flores, *Int. J. Mass Spectrom.* **307** (2011) 123
90. J. Aggett, M. R. Kriegman, *Analyst* **112** (1987) 153
91. B. Daus, H. Weiss, J. Mattusch, R. Wennrich, *Talanta* **69** (2006) 430
92. R. B. McCleskey, D. K. Nordstrom, A. S. Maest, *Appl. Geochem.* **19** (2004) 995
93. L. Dahl, M. Molin, H. Amlund, H. M. Meltzer, K. Julshamn, J. Alexander, J. J. Sloth, *Food Chem.* **123** (2010) 720
94. I. Pizarro, M. Gómez, C. Cámara, M. A. Palacios, *Anal. Chim. Acta* **495** (2003) 85
95. S. G. Salgado, M. A. Quijano Nieto, M. M. Bonilla Simon, *Talanta* **75** (2008) 897
96. S. Ciardullo, F. Aureli, A. Raggi, F. Cubadda, *Talanta* **81** (2010) 213
97. V. L. Dresslera, F. G. Antes, C. M. Moreira, D. Pozebon, F. A. Duarte, *Int. J. Mass Spectrom.* **307** (2011) 149
98. C. M. Moreira, F. A. Duarte, J. Leberherz, D. Pozebon, E. M. M. Flores, V. L. Dressler, *Food Chem.* **126** (2011) 1406
99. I. Lopez-Garcia, M. Briceno, M. Hernandez-Cordoba, *Anal. Chim. Acta* **699** (2011) 11

100. A. S. Kinsela, R. N. Collins, T. D. Waite, *Chemosphere* **82** (2011) 879
101. D. M. Crnković, N. S. Crnković, A. J. Filipović, Lj. V. Rajaković, A. A. Perić-Grujić, M. Ristić, *J. Environ. Sci. Health, A* **43** (2008) 1353
102. V. L. Vukašinović-Pešić, Lj. V. Rajaković, *Energy Sources, A* **31** (2009) 1583
103. A. Giacomino, M. Malandrino, O. Abollino, M. Velayutham, T. Chinnathangavel, E. Mentasti, *Environ. Pollut.* **158** (2010) 416
104. L. Yehiayan, N. Membreno, S. Matulis, L. H. Boise, Y. Cai, *Anal. Chim. Acta* **699** (2011) 187
105. E. Sanz, R. Munoz-Olivas, C. Dietz, J. Sanz, C. Camara, *J. Anal. At. Spectrom.* **22** (2007) 131
106. A. Moreda-Pineiro, J. Moreda-Pineiro, P. Herbello-Hermelo, P. Bermejo-Barrera, S. Muniategui-Lorenzo, P. Lopez-Mahia, D. Prada-Rodriguez, *J. Chromatogr., A* **1218** (2011) 6970
107. J. A. Nobrega, L. C. Trevizan, G. C. L. Araujo, A. R. A. Nogueira, *Spectrochim. Acta, B* **57** (2002) 1855
108. G. Raber, N. Stock, P. Hanel, M. Murko, J. Navratilova, K. A. Francesconi, *Food Chem.* **134** (2012) 524
109. D. Das, U. Gupta, A. K. Das, *Trends Anal. Chem.* **38** (2012) 163
110. V. L. Vukašinović-Pešić, M. Đikanović, N. Z. Blagojević, Lj. V. Rajaković, *Chem. Ind. Chem. Eng. Q.* **11** (2005) 44
111. Lj. V. Rajaković, M. Mitrović, S. Stevanović, S. Dimitrijević, *J. Serb. Chem. Soc.* **58** (1993) 131
112. Lj. V. Rajaković, M. Mitrović, *Environ. Pollut.* **75** (1992) 279
113. Lj. V. Rajaković, *Sep. Sci. Technol.* **27** (1992) 1423
114. B. Jovanović, Lj. V. Rajaković, *J. Environ. Eng.* **136** (2010) 1277.



J. Serb. Chem. Soc. 78 (10) S117–S126 (2013)

SUPPLEMENTARY MATERIAL TO
Analytical methods for arsenic speciation analysis

LJUBINKA V. RAJAKOVIĆ^{1*}, ŽAKLINA N. TODOROVIĆ²,
VLADANA N. RAJAKOVIĆ-OGNJANOVIĆ³ and ANTONIJE E. ONJIA²

¹Faculty of Technology and Metallurgy, University of Belgrade, Karnegijeva 4, 11000 Belgrade, Serbia, ²Vinča Institute of Nuclear Sciences, University of Belgrade, P. O. Box 522, 11001 Belgrade, Serbia and ³Faculty of Civil Engineering, University of Belgrade, Bulevar kralja Aleksandra 73, Belgrade, Serbia

J. Serb. Chem. Soc. 78 (10) (2013) 1461–1479

TABLE S-I. Some review articles from 2003 to 2011 dealing with aspects of arsenic speciations relevant and complementary to this review (for the reference number refer to the Reference list in the paper)

Title of the review	Comments	Ref.
Determination of arsenic species: A critical review of methods and applications, 2000–2003	A detailed review of more than 400 published papers on the speciation of arsenic in the period from 2000–2003. Different methods of extraction and stability of arsenic species and advances in separation and detection techniques are analysed.	14
Arsenic and its speciation analysis using HPLC and ICP-MS	Applications and work using only HPLC and ICP-MS for arsenic speciation of environmental and biological samples are presented in this review.	17
Analytical methods for inorganic arsenic in water	Reports an overview of more than 100 papers, regarding existing methods for analysis of As(III) and As(V) in water, including various spectroscopic, ICP and electrochemical techniques. Recent field portable analytical applications are also reviewed.	18
Analysis and speciation of arsenic by stripping potentiometry	Summarized several examples of the literature from 1980 to 2003, to illustrate the applications of stripping potentiometry for the determination and speciation of arsenic in several samples.	19
Isotope dilution analysis for elemental speciation	Describes the application of isotope dilution analysis to quantitative elemental speciation.	20
Current perspectives in analyte extraction strategies for tin and arsenic speciation	Summarises different extraction techniques for arsenic and tin speciation as one of the most important error sources in modern analytical methods.	26

* Corresponding author. E-mail: ljubinka@tmf.bg.ac.rs

TABLE S-I. Continued

Title of the review	Comments	Ref.
Effect of thermal treatments on the contents of arsenic species in food	This article summarizes and discusses the published papers on the effect of thermal treatment used in the cooking or processing of food, including sterilization and preservation stages, on total arsenic and arsenic species content. It also reviews possible transformations of arsenic species.	27
Speciation and surface structure of inorganic arsenic in solid phases	The objective of this paper was to examine advancement in the speciation and surface structure identification of inorganic arsenic species in solid phases. An analysis of related methodological, analytical and surface structure modelling aspects is made.	28
A review of non-chromatographic methods for speciation analysis	Describes the relevant scientific literature concerning speciation of trace elements using non-chromatographic methods.	16
Aquatic arsenic: Toxicity, speciation, transformations, and remediation	Describes the toxicity, speciation and biogeochemistry of arsenic in aquatic environmental systems.	29
Voltammetric methods for determination and speciation of inorganic arsenic in the environment	Reports recent work on the separation and detection of arsenic compounds using voltammetric methods.	30
HPLC coupled to AFS for the speciation of the hydride and chemical vapour-forming elements As, Se, Sb and Hg	The review focuses on sample preparation, post-column treatments and on the applications of HPLC hyphenated to hydride generation or chemical vapour generation and atomic fluorescence spectrometry (HG/CVG-AFS) to various liquid and solid samples for the determination and speciation of the selected hydride-forming elements As, Se and Sb and the chemical vapour-forming metal Hg.	31
Analytical methods for the determination of arsenosugars – A review of recent trends and developments	Describes the typical experimental approaches for sample pre-treatment, extraction, separation and detection.	32
Environmental application of elemental speciation analysis based on HPLC or GC hyphenated to ICP-MS	This review summarizes developments in environmental applications of elemental speciation analysis using ICP-MS coupled with HPLC and GC.	33
Preservation of inorganic arsenic species in environmental water samples for reliable speciation analysis	Describes stability of inorganic arsenic species in water samples as a key item in the speciation analysis.	34
Sample pre-treatment and extraction methods that are crucial to arsenic speciation in algae and aquatic plants	Using information covering the period since 2000, summarized and discussed sample handling, cleaning, drying and powdering of fresh samples and the later extraction of As species.	35

TABLE S-I. Continued

Title of the review	Comments	Ref.
As speciation in biomedical sciences: Recent advances and applications	Deals with recent advances and applications of methods for arsenic speciation in biomedical sciences, with emphasis on the specimens commonly encountered in biomedical laboratories.	36
As, Hg, I, Sb, Se and Sn speciation in body fluids and biological tissues using hyphenated-ICP-MS techniques	Focuses on different technique for speciation of As, Hg, I, Sb, Se and Sn in biological tissues. The focus is on ICP-MS as a powerful analytical tool for elemental speciation analysis.	37
As speciation in environmental samples by hydride generation and electrothermal atomic absorption spectrometry	Overview of analytical methods, pre-concentration and separation techniques using hydride generation and electrothermal atomic absorption spectrometry for the determination of inorganic As and organoarsenic species in environmental samples.	38
As and its speciation in water samples by HPLC and ICP-MS	Covers last decade research in speciations of arsenic compounds in water samples by high performance liquid chromatography inductively coupled plasma mass spectrometry.	1

TABLE S-II. Sample preparation methods, separation and detection for arsenic species in different matrices; LC/ESI-MS/MS – liquid chromatography/electrospray ionisation tandem mass spectrometry; DRC – dynamic reaction cell; CE/UV – capillary electrophoresis/ultraviolet detector (for the reference number refer to the Reference list in the paper)

Matrix	Species	Sample pre-treatment	Separation/detection technique	Analytical features	Ref.
Whole blood and urine	As(III), As(V), MMA, AB	Dilution with HgCl ₂ and ultrafiltration	LC/ICP-MS	<i>LoD</i> / $\mu\text{g L}^{-1}$: <0.3	47
Urine	As(III), As(V), MMA, DMA	Dilution with deionised water and filtration	IC/ICP-MS	<i>LoD</i> / $\mu\text{g L}^{-1}$: 0.11 As(III), 0.25 As(V), 0.18 MMA, 0.17 DMA, 0.75 AB; Repeatability, %: 1.9 As(III), 2.7 As(V), 2.1 MMA, 1.9 DMA, 2.8 AB	48
Urine	As(III), As(V), MMA, AB	Dilution with deionised water and filtration	HPLC/ICP-MS	Recovery: 85 to 100 %	49
Urine	As(III), As(V), MMA, DMA, TMAO	Dilution with mobile phase and filtration	HPLC/HG-AAS	From 1.1 $\mu\text{g L}^{-1}$ for TMAO to 2.6 $\mu\text{g L}^{-1}$ for As(V)	50

TABLE S-II. Continued

Matrix	Species	Sample pre-treatment	Separation/detection technique	Analytical features	Ref.
Urine	As(III), As(V), MMA, DMA	Dilution HCl and L-cysteine	HPLC/electro- thermal -AAS	<i>LoD</i> / $\mu\text{g L}^{-1}$: 0.038	51
Urine	As(III), As(V), MMA, DMA	Dilution with deionised water and filtration	HPLC/HG-ICP-MS	<i>LoD</i> / $\mu\text{g L}^{-1}$: 0.37 As(III), 0.22 As(V), 0.18 MMA, 0.17 DMA; Precision, %: 4.1 As(III), 5.4 As(V), 6.0 MMA, 6.6 DMA	52
Whole blood	MMA, DMA	Centrifuge	CE/ICP-MS	<i>LoD</i> / $\mu\text{g L}^{-1}$: 1; <i>LoQ</i> / $\mu\text{g L}^{-1}$: 0.8 As(III), 1.0 As(V), 1.0 MMA, 0.9 DMA	53
Fish and oyster tissues	As(III), As(V), MMA, DMA	Lyophilisation / microwave digestion	CE/ICP-MS	–	54
Fish	As(III), As(V), MMA, DMA	Ultrasonic extraction and 4 different experimental conditions	HG-AFS	<i>LoD</i> / $\mu\text{g kg}^{-1}$: 0.62 As(III), 2.1 As(V), 1.8 MMA, 5.4 DMA; <i>RSD</i> : 6.8 % As(III), 10.3 % As(V), 8.5 % MMA, 7.4 % DMA; Recovery > 93%	55
Fish sauce	AB, AC, TMAO	Extraction with water/ /methanol (1+1,v/v)/ /shaking/cen- trifugation	HPLC/ICP-MS	<i>LoD</i> / mg kg^{-1} : 0.01	56
Beverages (soft drinks, lemon juice, beer)	As(III), As(V), MMA, DMA	Sample were passed through a C18 sep-pack and filtered	HPLC/ICP-MS	<i>LoD</i> / mg kg^{-1} : 0.2, 0.2, 0.3 and 0.5 for As(III), DMA, MMA and As(V), respectively; <i>RSD</i> of As(III), DMA, MMA and As(V) were 1.2, 2.1, 2.5 and 3.0 %, respectively	57
Cereals	As(III), As(V), MMA, DMA	Ultrasonic extraction with H_3PO_4 and Triton XT-114	HG-AFS	<i>LoD</i> / mg kg^{-1} : 1.3, 0.9, 1.5 and 0.6 for As(III), As(V), DMA and MMA, respectively; Recoveries: > 90 %; Repeatability, %: As(III), 3; DMA, 5; As(V) and MMA, 6	58

TABLE S-II. Continued

Matrix	Species	Sample pre-treatment	Separation/detection technique	Analytical features	Ref.
Wines	As(III), As(V), MMA, DMA	Treatment with cysteine in HCl for total As; dilution with citrate buffer or acetic acid for As species	HG-AFS	<i>LoD</i> / $\mu\text{g L}^{-1}$: 0.12, 0.27, 0.15 and 0.13 (as As); <i>RSD</i> / %: 2–6, 5–9, 3–7 and 2–5 for As(III), As(V), MMA and DMA, respectively	59
Vegetables	As(III), As(V), MMA, DMA	Ultrasonic extraction with H_3PO_4 and Triton XT-114	HG-AFS	<i>LoD</i> / mg kg^{-1} : 3.1 As(III), 3.0 As(V), 1.5 DMA, 1.9 MMA; Recovery / %: > 91%	60
Milk	As(III), As(V)	Ultrasonic extraction with/without KI	HG-AFS	<i>LoD</i> / mg L^{-1} : 8.1 and 10.3 for As(III) and As(V); <i>RSD</i> / %: 5.7 and 5.5 for As(III) and As(V)	61
Water	As(III), As(V), MMA, DMA	Pre-treatment with KI and HCl or acetic acid or tartaric acid	HG-AAS	–	62
Water	As(III), As(V), DMA	Treatment with cysteine, KI, urea or acids	HG-AAS, CE/UV, LC/ICP-MS	<i>LoD</i> / mg L^{-1} : 0.10 As(III), As(V), 0.19 (DMA) for HG-AAS, 100 (As(III), DMA) to 500 (As(V)) for CE/UV and 0.1 (DMA, MMA) to 0.2 (As(III), As(V)) for LC/ICP-MS; Precision (<i>RSD</i> / %): < 5; Recovery, %: 80–110 except CE/UV only 50	4
Water and urine sample	Inorganic, organic As	Treatment with/without cysteine	HG-ICP-MS	<i>LoD</i> / ng L^{-1} : 6	63
Water and reference materials	As(III), As(V)	Treatment with HCl and NaBH_4	HG-AAS	<i>LoD</i> / $\mu\text{g L}^{-1}$: 0.1 for As(III) and 0.06 for total As. Precision (<i>RSD</i> / %) is 2.9 for As(III) and 3.1 for total As	64

TABLE S-II. Continued

Matrix	Species	Sample pre-treatment	Separation/detection technique	Analytical features	Ref.
Water	As(III), As(V)	None	HG-AAS	<i>LoD</i> / $\mu\text{g L}^{-1}$: 0.019 total As, 0.031 As(III)	65
Water	As(III), As(V)	Reaction with cysteine, NaBH_4	HG-AAS	<i>LoD</i> / $\mu\text{g L}^{-1}$: 0.1	66
Water	As(III), As(V)	Reaction with cysteine	HG-ETAAS	–	67
Water	As(III), As(V)	None	HG-AFS	–	68
Water	As(III), As(V)	pH adjustment	HG-AAS	<i>LoD</i> / $\mu\text{g L}^{-1}$: 0.07–0.4 As(V) and 0.1–0.5 As(III + V); Recovery, %: 90–102	69
Water	As(III), As(V)	Treatment with KMnO_4	ICP-AES	<i>LoD</i> / $\mu\text{g L}^{-1}$: 0.1–0.6	9
Water	As(III), As(V), MMA, DMA	None	HPLC/ICP-MS	<i>LoD</i> / $\mu\text{g L}^{-1}$: 0.33 As(III), 0.69 As(V); <i>LoQ</i> / $\mu\text{g L}^{-1}$: 50	70
Water	Inorganic As	Pre-reduction of As(V) with cysteine	HG-AAS	<i>LoD</i> / $\mu\text{g L}^{-1}$: 0.15; <i>LoQ</i> / $\mu\text{g L}^{-1}$: 0.5; <i>RSD</i> ($n = 10$): <8 %	71
Seawater	As(III)	Complexation with pyrrolidine dithiocarbamate	ET-AAS	<i>LoD</i> / $\mu\text{g L}^{-1}$: 0.008; <i>RSD</i> ($n = 11$): 4.5 %	72
Water	As(III), As(V), MMA, DMA	None	HG-ICP-AES	Recovery, %: As(V) 97.6, As(III) 100, MMA 99.8, DMA 99.9	73
Water	As(III), As(V)	Treatment with KMnO_4	ET-AAS	<i>LoD</i> / $\mu\text{g L}^{-1}$: 0.35; Recovery, %: 93.5–106.4; <i>RSD</i> / %: 3–7	74
Water	As(III), As(V), MMA, DMA, AB	None	HPLC/ICP-MS	<i>LoD</i> / $\mu\text{g L}^{-1}$: 0.017 As(III), 0.026 As(V), 0.026 MMA, 0.023 DMA, 0.024 AB; <i>LoQ</i> / $\mu\text{g L}^{-1}$: 0.056 As(III), 0.085 As(V), 0.088 MMA, 0.076 DMA, 0.080 AB	3
Ground-water	As(III), As(V), MMA, TMAO, PAA and PAO	None	HPLC/ICP-MS	<i>LoQ</i> / $\mu\text{g L}^{-1}$: 0.2–0.8	9

TABLE S-II. Continued

Matrix	Species	Sample pre-treatment	Separation/detection technique	Analytical features	Ref.
Groundwater	As(III), As(V), PAA, diphenylarsinic acid (DPAA) and PAO	None	HPLC/ICP-MS	–	75
Groundwater	As(III), As(V)	None	HPLC/HG-AAS	<i>LoD</i> / $\mu\text{g L}^{-1}$: 7.8 As(III), 12.0 As(V); Precision (<i>RSD</i> / %): 10.5 As(III), 12.1 As(V)	76
Hot spring water	As(III), As(V), MMA, DMA, TMAO, TMA, AC and AB	None	HPLC/ICP-MS	<i>LoD</i> ($\mu\text{g L}^{-1}$): 0.2; <i>RSD</i> / % ($n = 6$): < 2	77
Human hair	As(III), As(V)	Reduction of As(V) to As(III)	HG-AAS	<i>LoD</i> / $\mu\text{g L}^{-1}$: 0.2 As(III), 0.5 As(V); <i>RSD</i> / %: 2.1 As(III), 2.5 As(V)	78
Sediment and fly ash	Water soluble and phosphate-exchangeable As(III) and As(V)	Extraction with water and phosphate buffer	HG-AAS	<i>LoD</i> / $\mu\text{g L}^{-1}$: 0.06–0.10; <i>LoQ</i> / $\mu\text{g L}^{-1}$: 0.20–0.31. Repeatability expressed as <i>RSD</i> : <1 %	79
Landfill leachate	As(III), As(V), MMA, DMA, TMAO, AB	Filtration	HPLC/ICP-MS	<i>LoD</i> / ng L^{-1} between 11 for DMA to 27 for As(V). <i>LoQ</i> / ng L^{-1} between 36 and 90	80
Municipal landfill leachates	As(III), As(V), MMA and DMA	Filtration	LC/ESI-MS/MS and HPLC/DRC-ICP-MS	Recovery, %: 68–94	81
Soil	Total As	Extraction with HNO_3 , acetic acid, EDTA and Mehlich III	HG-AAS	–	82

TABLE S-III. The most important analytical performance parameters in arsenic speciation analysis (for the reference number refer to the Reference list in the paper)

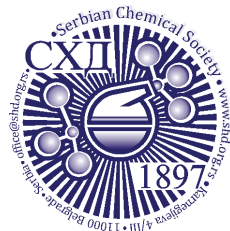
Author(s)	Title	LOD/DL Method	Ref.
Sakai and Wilbur, 2006	Routine Analysis of Toxic Arsenic Species in Urine Using HPLC with ICP-MS	Detection limits (<i>DL</i>) for each arsenic species were calculated as three times the chromatographic peak-to-peak signal to noise. All species met the goal of $\approx 0.1 \mu\text{g L}^{-1}$, <i>RSD</i> ranged from 1.3 to 2.8 % and recoveries from 93 to 101 %	84
K. Ito <i>et al.</i> , 2010	Determination of Five Arsenic Species in Whole Blood by LC Coupled with ICP-MS	The method <i>LoD</i> $< 0.3 \mu\text{g L}^{-1}$ for each arsenic species, range from 2 to $200 \mu\text{g L}^{-1}$ for urine, and 2 to $12 \mu\text{g L}^{-1}$ for blood. Method detection limits (<i>MDL</i>) were estimated from concentrations at which the peak intensities were 3 standard deviation (<i>SD</i>) of the blank background signal for each of the five arsenic species, <i>LOQ</i> as 1 mg L^{-1} based on 10 <i>SD</i> . Recovery $> 80 \%$.	47
Xie <i>et al.</i> , 2006	Arsenic Speciation Analysis of Human Urine Using Ion Exchange Chromatography Coupled to ICP-MS	For this study, the detection limits of speciation were defined as three times the standard deviation of seven replicate measurements of a standard solution with the lowest concentration of species whose peaks could be distinguished from the baseline in the speciation chromatogram. Obtained values ($\mu\text{g L}^{-1}$) were: 0.11 As(III), 0.25 As(V), 0.18 MMA, 0.17 DMA, 0.75 AB, repeatability $< 5 \%$.	48
Heitland and Köster, 2008	Fast Determination of Arsenic Species and Total Arsenic in Urine by HPLC-ICP-MS: Concentration Ranges for Unexposed German Inhabitants and Clinical Case Studies	<i>LOQ</i> ($0.1 \mu\text{g L}^{-1}$) were defined as the analyte concentration corresponding to 10 times the <i>SD</i> of 5 measurements of a spiked sample. This sample was urine. Recoveries estimated from the standard reference materials (SRM) only for total As and <i>RSD</i> of the average concentrations were in the range 6.3–8.7 %.	85
Hirata <i>et al.</i> , 2006	Determination of Arsenic Species in Marine Samples by HPLC-ICP-MS	<i>DL</i> were calculated based on 3 <i>SD</i> of baseline noise at the peaks retention time ($n=9$). The <i>DL</i> ranged from 0.02 to $0.10 \mu\text{g L}^{-1}$. The precision (<i>RSD</i>) were 3.1–7.3 % for all eight species.	86

TABLE S-III. Continued

Author(s)	Title	LOD/DL Method	Ref.
Ronkart <i>et al.</i> , 2007	Speciation of Five Arsenic Species (Arsenite, Arsenate, MMA, DMA and AB) in Different Kinds of Water by HPLC-ICP-MS	<p><i>LoD</i> and <i>LoQ</i> were evaluated by analysing ten samples containing an arsenical concentration close to the expected <i>LoD</i> and <i>LoQ</i> under repeatability conditions and using Eqs. (below), where <i>y</i> signal is the medium value and <i>S</i> signal is the standard deviation.</p> $LoD = y_{\text{signal}} + 5S_{\text{signal}} \quad (1)$ $LoQ = y_{\text{signal}} + 10S_{\text{signal}} \quad (2)$ <p><i>LoQ</i> values were confirmed by analysing ten replicates of a solution containing all arsenic species at the <i>LoQ</i>. Variation coefficient of 9.87, 8.38, 8.33, 12.3 and 8.84 % were obtained for respectively AB, DMA, As(III), MMA and As(V). Recoveries were calculated through analysis of three spiked real samples and ranging from 95–108 %.</p>	3
A. H. E. Petursdottir, 2010	Determination of Toxic and Non-Toxic Arsenic Species in Icelandic Fish Meal	<p><i>LoD</i> was taken to be three times the noise (3σ) and the <i>LoQ</i> was evaluated as the area of the smallest standard analysed and was 0.04 mg kg⁻¹. Recovery ranged from 82–111 %.</p>	87
Komorowicz and Baralkiewicz, 2011	Arsenic and Its Speciation in Water Samples by High Performance Liquid Chromatography Inductively Coupled Plasma Mass Spectrometry – Last Decade Review	<p><i>DL</i> was mainly calculated as three times the <i>SD</i> of the background signal or replicate analyses of spiked deionised water samples. <i>RSD</i> values did not exceed 20 % and the recoveries were between 80 and 120 % in all reviewed water samples.</p>	1
Sathrugnan and Hirata, 2004	Determination of Inorganic Oxyanions of As and Se by HPLC-ICP-MS	<p><i>DL</i> was calculated based on 3σ of the blank intensities at respective retention time and were less than 80 and 0.77 g L⁻¹ for As and Se, respectively. The standard addition in the order of 6 s (<i>LoQ</i>) into sample extracts produced significant peaks from baseline. The <i>RSD</i> of the proposed method for As was less than 4.8 % and recovery were in the range of 98–102 %</p>	88
Ponthieu <i>et al.</i> , 2007	Speciation Analysis of Arsenic in Landfill Leachate	<p>Detection limits were calculated for the HPLC-ICP-MS system using the IUPAC (International Union of Pure and Applied Chemistry) definition as three times the <i>SD</i> of noise level. Relative detection limits varied between 11 ng L⁻¹ for DMA to 27 ng L⁻¹ for As(V). The <i>LoQ</i> ranged between 36 and 90 ng L⁻¹</p>	80

TABLE S-III. Continued

Author(s)	Title	LOD/DL Method	Ref.
Rajaković <i>et al.</i> , 2012	Review: The Approaches for Estimation of Limit of Detection for ICP-MS Trace Analysis of Arsenic	<p>Detection limits were reviewed and calculated for the ICP-MS system using different approaches:</p> <ul style="list-style-type: none"> – <i>LoD</i> values calculated according to the traditional approaches (Currie, IUPAC, US EPA 200.8), $n = 26$ – <i>LoD</i> values calculated according to the prediction interval approaches (Hubaux–Vos, ISO), $n = 8$ <p>The most appropriate values were obtained according to Currie's variation of the traditional method; the critical value was 0.011 mg L^{-1} and the <i>LoD</i> was 0.022 mg L^{-1}.</p>	83



J. Serb. Chem. Soc. 78 (10) 1481–1489 (2013)
JSCS–4511

Journal of
the Serbian
Chemical Society

JSCS-info@shd.org.rs • www.shd.org.rs/JSCS

UDC 547.368+546.27:547.831+542.9

Original scientific paper

B(HSO₄)₃: An efficient and recyclable catalyst for the Friedländer synthesis of substituted quinolines

SEYYED JAFAR SAGHANEZHAD¹ and HAMID REZA SAFAEI^{2*}

¹Young Researchers Club, Shiraz Branch, Islamic Azad University, Shiraz, Iran and

²Department of Applied Chemistry, College of Science, Shiraz Branch, Islamic Azad University, P. O. Box 71993-5, Shiraz, Iran

(Received 17 October 2012, revised 26 May 2013)

Abstract: Substituted quinolines have been synthesized in the presence of catalytic amounts of boron hydrogen sulfate (BHS) under solvent-free conditions. This methodology offers some advantages, including high yield, short reaction time, low cost of the catalyst, green conditions by avoiding toxic solvents and recoverable catalyst.

Keywords: boron hydrogen sulfate; substituted quinolines; solvent-free conditions; Friedländer reaction.

INTRODUCTION

The presence of quinoline moiety core in several natural compounds, such as cinchona alkaloids, and pharmacologically active substances¹ with a broad range of biological activities, including anti-asthmatic,² antibacterial,³ anti-inflammatory⁴ and antihypertensive⁵ properties, has raised the interest of organic chemists for finding straightforward routes for the synthesis of these compounds.

Considering the above reports, and due to great importance of quinolines, it is not surprising that many synthetic procedures, such as the Skraup, Doebner von Miller, Conrad–Limpach–Knorr, Pfitzinger, Friedländer and Combes reactions, were developed for the preparation of these compounds.^{6,7} Nevertheless, the development of novel synthetic approaches for the synthesis of quinolones remain an active area of research.

Amongst various methodologies reported for the preparation of quinolines, the Friedländer reaction is still one of the simplest and most straightforward protocols. Friedländer synthesis involves a condensation followed by a cyclodehydration between an aromatic 2-aminoaldehyde or ketone and an aldehyde or ketone possessing α -active methylene groups.⁸ While different catalysts have

* Corresponding author. E-mail: hrs@iaushiraz.net
doi: 10.2298/JSC121017061S

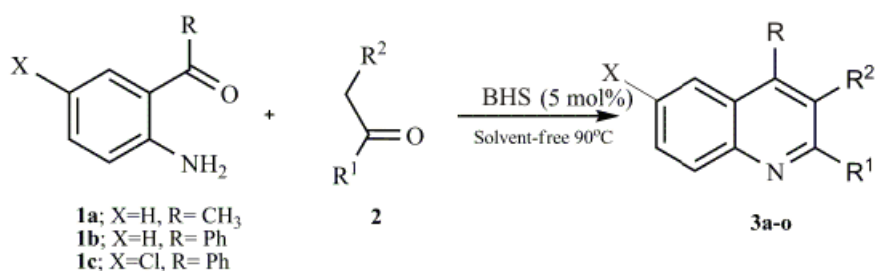


been proposed for Friedländer annulations, it has been shown that acidic catalysts are superior to basic ones.⁹ Other than different acidic catalysts, such as Brønsted acids^{10–14} and Lewis acids,^{15–17} ionic liquids,¹⁸ and other catalysts^{19,20} have also been employed to promote this reaction. Friedländer reaction has recently been reviewed.²¹

Uncatalyzed Friedländer syntheses require drastic reaction conditions, with temperatures in the range 150–220 °C. Most of the synthetic protocols for quinolines reported so far suffer from harsh conditions, low yields, prolonged reaction time and the use of hazardous and often expensive catalysts. Moreover, the syntheses of these heterocycles have usually been performed in polar solvents, such as acetonitrile, THF, DMF and DMSO, leading to complex isolation and recovery procedures. These processes also generate waste-containing solvent and catalyst, which have to be recovered, treated and disposed of.

Solid acids have many advantages both in industry and the laboratory, such as simplicity in handling, reduced reactor and plant corrosion problems, and more environmentally safe disposal in chemical processes.²² Solid acids are employed under heterogeneous conditions and hence can be conveniently handled and removed from the reaction mixture by simple filtration and recovered for reuse. Boron hydrogen sulfate has recently been successfully used as an efficient solid acid catalyst for the preparation of thiocyanohydrins under solvent-free conditions.²³

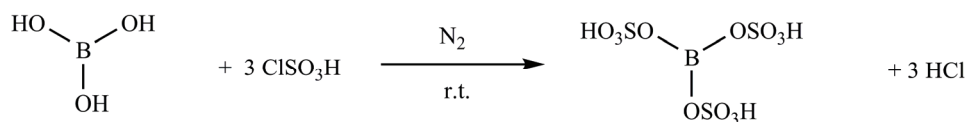
In continuation of efforts in the synthesis of new solid acid catalysts, and their application in organic synthesis,^{23–25} boron hydrogen sulfate was utilized in the present study as an efficient solid acid catalyst for the preparation of substituted quinolines by Friedländer annulation (Scheme 1).



Scheme 1. Preparation of substituted quinolines in the presence of BHS.

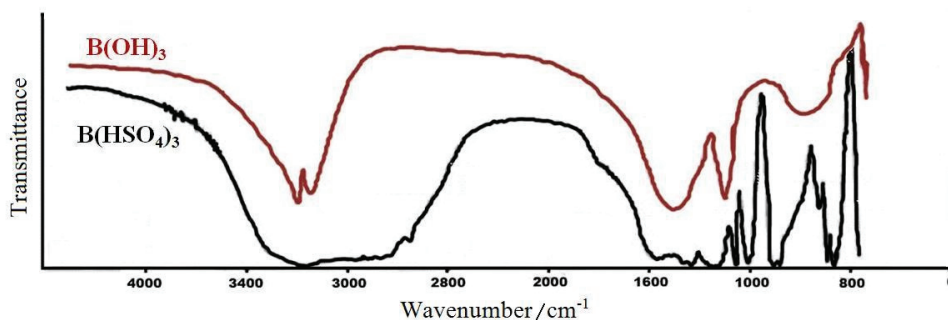
RESULTS AND DISCUSSION

Boron hydrogen sulfate, BHS, was easily prepared by simply mixing boric acid and chlorosulfonic acid in CH₂Cl₂ at room temperature (Scheme 2). This reaction is easy and clean, because the evolved HCl gas leaves the reaction vessel immediately.

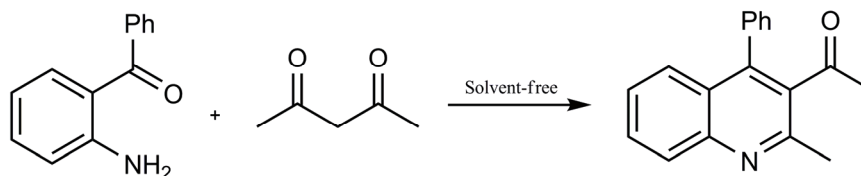


Scheme 2. Preparation of the catalyst.

One of the informative techniques for an investigation of catalyst formation is FT-IR spectroscopy. Thus, the structure of the catalyst was characterized by FT-IR spectroscopy (Fig. 1). As seen in Fig. 1, the spectrum of $\text{B}(\text{HSO}_4)_3$ was different from that of boric acid. The FT-IR spectrum of $\text{B}(\text{HSO}_4)_3$ showed absorption bands at 1400 ($\nu(\text{S}=\text{O})$ asymmetric stretching), 1200 ($\nu(\text{S}=\text{O})$ symmetric stretching) and at 650 cm^{-1} corresponding to $\nu(\text{S}-\text{O})$. Moreover, a broad band from $2700\text{--}3400 \text{ cm}^{-1}$ corresponds to acidic O–H stretching.

Figure 1. IR spectra of $\text{B}(\text{HSO}_4)_3$ and $\text{B}(\text{OH})_3$.

To evaluate the catalytic activity of BHS in the preparation of substituted quinolines, a model reaction of 2-aminobenzophenone (1 mmol), and acetylacetone (1.2 mmol) under solvent-free conditions at different temperatures and in the presence of variable catalyst loadings was examined (Scheme 3). It was found that in the absence of the solid acid catalyst, only a trace amount of the desired product was observed on the TLC plate even after heating for 2 h. (Table I, Entry 1). When the reaction was performed in the presence of BHS, it proceeded rapidly to give the desired product.



Scheme 3. Optimization of the reaction conditions for 2-aminobenzophenone and acetylacetone as a model reaction.

In order to evaluate the appropriate catalyst loading, the model reaction was performed using 3.5 to 9.5 mol % at different temperatures in the absence of solvent (Table I). It was found that 5 mol % catalyst gave the maximum yield in the minimum time. A higher percentage of loading of the catalyst (7–9.5 mol %) neither increases the yield nor lowers the conversion time substantially. In the next step, the effect of temperature was evaluated for the model reaction. It was observed that the reaction did not proceed at room temperature. Elevating the reaction temperature proved helpful, and the yield of desired product increased considerably. To our satisfaction, the reaction was found to proceed smoothly, and almost complete conversion of product was observed at 90 °C, affording 1-(2-methyl-4-phenylquinolin-3-yl)ethanone (**3f**) in 91 % yield within a short time.

TABLE I. Optimization of the reaction conditions for 2-aminobenzophenone and acetylacetone as a model reaction under thermal solvent-free conditions

Entry	Catalyst amount, mol %	Temperature, °C	Time, min	Yield, %
1	–	r.t.	120	10
2	3.5	r.t.	120	45
3	5	r.t.	120	52
4	5	60	60	65
5	3.5	90	60	68
6	5	90	35	91
7	7	90	34	92
8	9.5	90	45	88

Subsequently, with the optimal conditions in hand, using 1:1.2 molar ratio of a 2-aminoaryl ketone, a carbonyl compound and 5 mol % of BHS at 90 °C under solvent-free conditions, the generality and synthetic scope of this coupling protocol were demonstrated by synthesizing a series of substituted quinolines (Table II). Gratifyingly, a wide range of aromatic aldehydes was well tolerated under the optimized reaction conditions. The time taken for complete conversion (monitored by TLC) and the isolated yields are presented in Table II. All the new compounds were characterized by their satisfactory microanalytical (C, H, N) and spectral (IR, ¹H-NMR, ¹³C-NMR and MS) studies, and known compounds by comparison of their physical and spectral data with those of the authentic samples.

As shown in Table II, the different carbonyl compounds, including ethyl acetoacetate, acetylacetone, cyclohexanone, cyclohexane-1,3-dione and dione, were uniformly transformed into the corresponding quinolines in good to excellent yields within 25–62 min.

The reusability of the catalyst in the reaction of 2-aminobenzophenone, and acetylacetone, under solvent-free conditions at 90 °C was evaluated. In this procedure, after completion of each reaction, hot ethanol was added and the catalyst was filtered off. The recovered catalyst was washed with ethanol, dried

and reused six times. A small decrease in the catalytic activity of the catalyst was observed after the 6th time of reuse (Table III).

TABLE II. Preparation of substituted quinolines promoted by BHS under solvent-free conditions at 90 °C

Product	1	2	3	Time, min	Yield, %
3a	1a			62	65
3b	1a			45	68
3c	1a			48	67
3d	1a			50	62
3e	1a			50	72
3f	1b			41	91
3g	1b			49	92
3h	1b			46	80

TABLE II. Continued

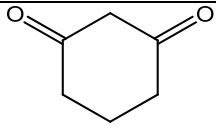
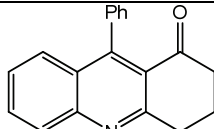
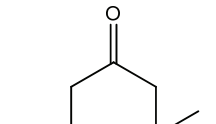
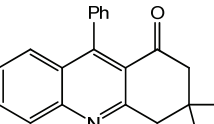
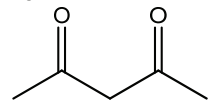
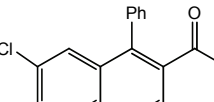
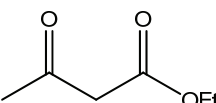
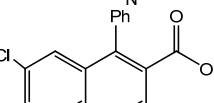
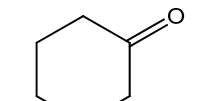
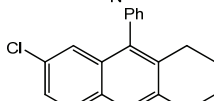
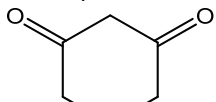
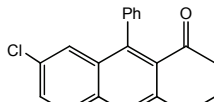
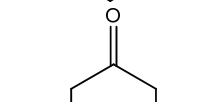
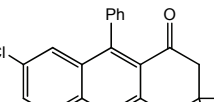
Product	1	2	3	Time, min	Yield, %
3i	1b			35	95
3j	1b			28	98
3k	1c			38	94
3l	1c			41	92
3m	1c			45	88
3n	1c			32	82
3o	1c			25	96

TABLE III. The reusability of the catalyst in six cycles for the reaction of 2-aminobenzophenone and acetylacetone under solvent-free conditions at 90 °C

Run	Time, min	Yield, %
1	41	91
2	42	90
3	44	88
4	46	85
5	48	82
6	52	78

To compare the advantage of the use of BHS over other reported catalysts, the model reaction of 2-aminobenzophenone and acetylacetone was considered as a representative example (Table IV). While in most of these cases, comparative yields of the desired product were obtained following the BHS-catalyzed procedure, the reported procedures required high catalyst loading (entry 2 and 4), or long reaction times (entry 1 and 2). These results clearly demonstrate that BHS is an equally or more efficient catalyst for this three-component reaction.

TABLE IV. Comparison of BHS with reported catalysts in the reaction of 2-aminobenzophenone and acetylacetone

Entry	Catalyst/temp., °C	Catalyst loading, mol %	Time, min	Yield, %	Ref.
1	NaAuCl ₄ ·2H ₂ O/80	3	1440	46	19
2	[Hbim]BF ₄ /100	100	198	94	18
3	Oxalic acid/80	10	120	90	13
4	HClO ₄ -SiO ₂ /60	0.2 g	150	92	12
5	Sulfamic acid/70	5	45	89	10
6	BHS/90	5	41	91	This work

EXPERIMENTAL

Chemicals and apparatus

All chemicals were purchased from Merck or Fluka. All the synthesized compounds are known and were identified by comparison of their melting points, elemental analyses, mass spectra, IR, ¹H- and ¹³C-NMR data with those of authentic samples. Monitoring of the reactions was accomplished by TLC on silica gel Polygram SIL G/UV 254 plates.

Preparation of boron hydrogen sulfate

A 50 mL suction flask was equipped with a constant pressure, dropping funnel. The gas outlet was connected to a vacuum system through an adsorbing solution (water) and an alkali trap. Boric acid (1.55 g, 25 mmol) was charged into the flask and chlorosulfonic acid (8.74 g, *ca.* 5 mL, 75 mmol) was added dropwise over a period of 1 h at room temperature. HCl was evolved immediately. After completion of the addition, the mixture was shaken for 1 h, while the residual HCl was eliminated by suction. Then the mixture was washed with diethyl ether to remove the unreacted chlorosulfonic acid. Finally, a grayish solid material was obtained in 85 % yield (6.4 g).²³

Typical procedure for the preparation of substituted quinolines

A mixture of 2-aminoaryl ketone (1 mmol), a carbonyl compound (1.1 mmol), and BHS (5 mol %) was heated at 90 °C for 10 min. Completion of the reaction was indicated by TLC (*n*-hexane/ethyl acetate, 4:1). After completion of the reaction, the insoluble crude product was dissolved in hot ethanol and boron hydrogen sulfate was filtered. The crude product was purified by recrystallization in ethanol to afford the pure product.

CONCLUSION

In summary, a simple and facile protocol was proposed for the synthesis of substituted quinolines by Friedländer quinoline synthesis using boron hydrogen sulfate as a novel environmentally safe heterogeneous solid acid catalyst under

solvent-free conditions. The method offers several advantages, including high yields, application of an inexpensive catalyst, short reaction times, easy workup and performing the reaction under solvent-free conditions that is considered relatively environmentally benign.

Acknowledgements. We appreciate the Islamic Azad University (Shiraz Branch) Research Councils, Iran, for the financial support of this work.

ИЗВОД

В(HSO₄)₃: ЕФИКАСАН И РЕЦИКЛАБИЛАН КАТАЛИЗАТОР ЗА ФРИЛЕНДЕРОВУ СИНТЕЗУ ХИНОЛИНАSEYYED JAFAR SAGHANEZHAD¹ и HAMID REZA SAFAEI²

¹Young Researchers Club, Shiraz Branch, Islamic Azad University, Shiraz, Iran и ²Department of Applied Chemistry, College of Science, Shiraz Branch, Islamic Azad University, P. O. Box 71993-5, Shiraz, Iran

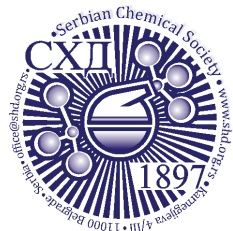
Извршена је синтеза супституисаних хинолина употребом каталитичких количина бор-хидроген сулфата (BHS), без присутног растварача. У поређењу са другим методама, описани поступак нуди предности, као што су висок принос, кратко реакционо време, ниска цена катализатора, еколошки прихватљиви реакциони услови, избегавање токсичних растварача и катализатор који може да се рециклира.

(Примљено 17. октобра 2012, ревидирано 26. маја 2013)

REFERENCES

1. M. Balasubramanian, J. G. Keay, *Pyridines and their Benzo Derivatives: Applications*, In *Comprehensive Heterocyclic Chemistry II*, A. R. Katritzky, C. W. Rees, E. F. V. Scriven, Eds., Pergamon Press, New York, 1996, Vol. 5, p. 245
2. A. von Sprecher, M. Gerspacher, A. Beck, S. Kimmel, H. Wiestner, G. P. Anderson, U. Niederhauser, N. Subramanian, M. A. Bray, *Bioorg. Med. Chem. Lett.* **8** (1998) 965
3. Y. L. Chen, K. C. Fang, J. Y. Sheu, S. L. Hsu, C. C. Tzeng, *J. Med. Chem.* **44** (2001) 2374
4. G. Roma, M. D. Braccio, G. Grossi, F. Mattioli, M. Ghia, *Eur. J. Med. Chem.* **35** (2000) 1021
5. P. L. Ferrarini, C. Mori, M. Badawneh, V. Calderone, R. Greco, C. Manera, A. Martinelli, P. Nieri, G. Saccomanni, *Eur. J. Chem.* **35** (2000) 815
6. G. Jones, *Pyridines and their Benzo Derivatives: Synthesis*, in *Comprehensive Heterocyclic Chemistry II*, A. R. Katritzky, C. W. Rees, E. F. V. Scriven, Eds., Pergamon, New York, 1996, Vol. 5, p. 167
7. M. E. Theoclitou, L. A. Robinson, *Tetrahedron Lett.* **43** (2002) 3907
8. P. Friedländer, *Chem. Ber.* **15** (1882) 2572
9. E. A. Fehnel, *J. Org. Chem.* **31** (1966) 2899
10. J. S. Yadav, P. P. Rao, D. Sreenu, R. S. Rao, V. N. Kumar, K. Nagaiah, A. R. Prasad, *Tetrahedron Lett.* **46** (2005) 7249
11. G. W. Wang, C. S. Jia, Y. W. Dong, *Tetrahedron Lett.* **47** (2006) 1059
12. M. Narasimhulu, T. Srikanth Reddy, K. Chinni Mahesh, P. Prabhakar, C. Bhujanga Rao, Y. Venkateswarlu, *J. Mol. Catal., A* **266** (2007) 114
13. M. Dabiri, M. Baghbanzadeh, M. S. Nikcheh, *Monatsh. Chem.* **138** (2007) 1249
14. S. Ghassamipour, A. R. Sardarian, *Tetrahedron Lett.* **50** (2009) 514

15. M. Barbero, S. Bazzi, S. Cadamuro, S. Dughera, *Tetrahedron Lett.* **51** (2010) 2342
16. M. A. Zolfigol, P. Salehi, A. Ghaderi, M. Shiri, *Catal. Commun.* **8** (2007) 1214
17. S. Genovese, F. Epifano, M. C. Marcotullio, C. Pelucchini, M. Curini, *Tetrahedron Lett.* **52** (2011) 3474
18. S. S. Palimkar, S. A. Siddiqui, T. Daniel, R. J. Lahoti, K. V. Srinivasan, *J. Org. Chem.* **68** (2003) 9371.
19. S. Atechian, N. Nock, R. D. Norcross, H. Ratni, A. W. Thomas, J. Verron, R. Masciadri, *Tetrahedron* **63** (2007) 2811
20. B. Das, K. Damodar, N. Chowdhury, R. A. Kumar, *J. Mol. Catal., A* **274** (2007) 148
21. J. Marco-Contelles, E. Perez-Mayoral, A. Samadi, M. do Carmo Carreiras, E. Soriano, *Chem. Rev.* **109** (2009) 2652
22. J. H. Clark, *Acc. Chem. Res.* **35** (2002) 791
23. A. R. Kiasat, M. Fallah-Mehrjardi, *J. Braz. Chem. Soc.* **19** (2008) 1595
24. A. R. Kiasat, M. Fallah-Mehrjardi, *Synth. Commun.* **40** (2010) 1551
25. A. R. Kiasat, A. Mouradezadegan, S. J. Saghanezhad, *J. Serb. Chem. Soc.* **78** (2013) 469.



J. Serb. Chem. Soc. 78 (10) 1491–1501 (2013)
JSCS–4512

Enzymatic synthesis of a vitamin B₆ precursor

NEVENA Ž. PRLAINOVIĆ^{1*#}, DEJAN I. BEZBRADICA², ZORICA D. KNEŽEVIĆ-
JUGOVIĆ^{2#}, DUŠAN V. VELIČKOVIĆ³ and DUŠAN Ž. MIJIN^{2#}

¹Innovation Center of Faculty of Technology and Metallurgy, University of Belgrade, Karnegijeva 4, 11000 Belgrade, Serbia, ²Faculty of Technology and Metallurgy, University of Belgrade, Karnegijeva 4, 11000 Belgrade, Serbia and ³Faculty of Chemistry, University of Belgrade, Studentski trg 12, 11000 Belgrade, Serbia

(Received 22 March, revised 10 May 2013)

Abstract: 3-Cyano-4-(ethoxymethyl)-6-methyl-2-pyridone, an important precursor in the synthesis of vitamin B₆, is obtained in the addition reaction between 2-cyanoacetamide and 1-ethoxy-2,4-pentanedione catalyzed by lipase from *Candida rugosa* (triacylglycerol acylhydrolases, EC 3.1.1.3). This work shows new experimental data and mathematical modeling of the lipase-catalyzed synthesis of 3-cyano-4-(ethoxymethyl)-6-methyl-2-pyridone. Kinetic measurements were performed at 50 °C with an enzyme concentration of 1.2 % w/v. The experimental results were fitted with two kinetic models: the ordered bi-ter and ping-pong bi-ter model, and the initial rates of the reaction were found to correlate best with the ping-pong bi-ter mechanism with inhibition by 2-cyanoacetamide. The obtained specificity constants indicated that lipase from *C. rugosa* had a higher affinity towards 1-ethoxy-2,4-pentanedione compared to 2-cyanoacetamide.

Keywords: *Candida rugosa* lipase; ping-pong kinetics; pyridone; 1-ethoxy-2,4-pentanedione.

INTRODUCTION

A large number of natural and synthetic compounds that possess interesting pharmacological activity contain a 2-pyridone ring in their structure. 3-Cyano-2-pyridones, especially their substituted analogs, were the subject of many studies in recent years.¹ They were found to be associated with a wide range of therapeutic activities, *i.e.*, antimicrobial,^{2,3} and antiviral.¹ They can also possess anti-HIV,⁴ anticancer,^{5,6} and cardiotoxic activities,^{7,8} and can serve as a basis for the synthesis of more complex systems⁹ and precursors for the synthesis of biologically active compounds.¹⁰

* Corresponding author. E-mail: nprlainovic@tmf.bg.ac.rs

Serbian Chemical Society member.

doi: 10.2298/JSC130322050P

3-Cyano-4-(ethoxymethyl)-6-methyl-2-pyridone is the first in a series of intermediates in the synthesis of vitamin B₆ according to the Harris and Folkers method.^{10–12} The reaction between 2-cyanoacetamide and 1-ethoxy-2,4-pentanedione gives this product *via* Michael addition. Very few reports are available on the chemical synthesis of this intermediate,¹³ and they all include organic catalysts and polar solvents. In addition, a few investigations of enzyme-catalyzed carbon–carbon bond formation *via* Michael addition are reported,^{14–16} and to the best of our knowledge, there are no reports on the synthesis of 3-cyano-4-(ethoxymethyl)-6-methyl-2-pyridone using an enzyme as catalyst.

Enzyme-mediated reactions are attractive alternatives to tedious and expensive chemical methods. Chemical methods have problems such as high reaction temperatures, toxic catalysts and solvents, larger amounts of raw materials due to the non-selectiveness of the process and high waste generation.¹⁷ Enzymes, also known as “green” catalysts, can be used to overcome these shortcomings. The use of enzymes in water, instead of toxic catalysts in polar organic solvents, offers less extreme conditions of temperature and pressure and minimizes energy consumption. Moreover, the production of waste is lowered, because the high specificity of an enzyme leads to fewer unwanted side effects and by-products.¹⁸ It is very important to mention that there is an increasing need for industries to nurse environmental protection and to find more environmentally friendly materials and conditions to perform syntheses.

Lipases (triacylglycerol acylhydrolases, EC 3.1.1.3) are ubiquitous enzymes that catalyze the hydrolysis of fats and oils.^{19,20} Lipases are powerful catalysts and the most commonly used enzymes in synthetic organic chemistry. Due to their ability to utilize a variety of substrates, lipases are very important and increasingly employed enzymes in a large number of fields, such as in the food, textile, dairy, cosmetics, and pharmaceutical industries. They have been extensively used in the synthesis of many biologically active compounds and natural products.^{21–23} Moreover, their high enantio- and regio-selectivity are extremely important in the production of key intermediates for organic and medicinal chemistry.²⁴

It has been shown^{25–28} that the cyclization reaction of 2-cyanoacetamide and 1,3-diketones can be catalyzed by the lipase from *Candida rugosa*. In a previous work,²⁹ the condensation of 2-cyanoacetamide and 2,4-pentanedione was optimized using the response surface methodology (RSM). In addition, a mechanism for the enzyme-catalyzed reaction was proposed.

In continuation of this work, herein, a study of the enzyme-catalyzed synthesis of 3-cyano-4-(ethoxymethyl)-6-methyl-2-pyridone is presented in which the kinetics of the lipase-catalyzed condensation of 2-cyanoacetamide (CAA) and 1-ethoxy-2,4-pentanedione (EPD), Fig. 1, was investigated. A kinetic mechanism

is proposed, and the inhibition effect of the substrates was investigated, since this phenomenon is quite often found in lipase-catalyzed reactions.

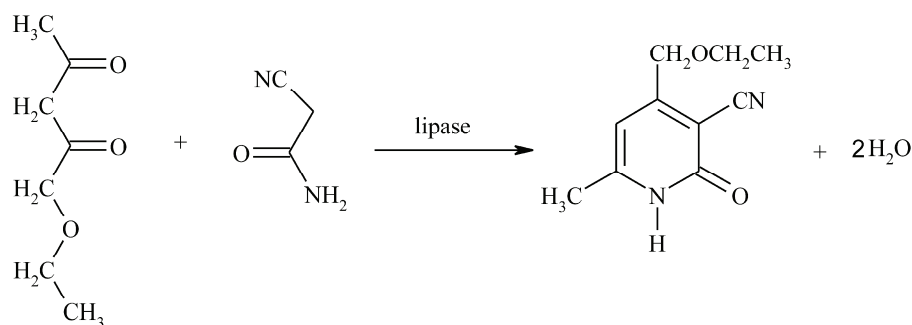


Fig. 1. Enzymatic synthesis of 3-cyano-4-(ethoxymethyl)-6-methyl-2-pyridone.

EXPERIMENTAL

Reagents

Candida rugosa lipase (3.1.1.3), Type VII, activity 1410 unit mg^{-1} of solid was purchased from Sigma (St. Louis, USA). 2-Cyanoacetamide was purchased from Fluka (Buchs, Switzerland) while 1,3-diketone (1-ethoxy-2,4-pentanedione) was prepared by the method described by Bruce *et al.*³⁰ All other chemicals were of analytical grade.

Methods

The synthesis of 3-cyano-4-(ethoxymethyl)-6-methyl-2-pyridone was performed in a 50 cm^3 flask with a working volume of 5 cm^3 of deionized water containing appropriate amounts of 2-cyanoacetamide and 1-ethoxy-2,4-pentanedione. The enzyme (1.2 % w/v) was added to the freshly prepared reaction mixture and incubated on a shaker at 150 rpm at 50 °C. Aliquots of the reaction mixture were periodically withdrawn (0.5, 1, 2, 3 and 24 h) and analyzed using UV spectroscopy (UV Shimadzu 1700, Shimadzu Corporation, Kyoto, Japan) at 328 nm (maximum absorption of 3-cyano-4-(ethoxymethyl)-6-methyl-2-pyridone). Blanks were also run. All experiments were conducted in duplicate. All results present the difference between enzyme catalyzed and spontaneous chemical reaction. The initial reaction rates were determined as described previously.²⁹

3-Cyano-4-(ethoxymethyl)-6-methyl-2-pyridone was isolated by filtration and purified using Akta Purifier HPLC equipped with a fraction collector. Chromatography was carried out on a semi-preparative reversed-phase C18 column (Hypersil Gold 5 μm ODS, 10 $\text{mm} \times 250$ mm) using the mobile phases A (water + 0.1 % v/v formic acid) and B (acetonitrile + 0.1 % v/v, formic acid), at a flow rate of 6 $\text{cm}^3 \text{min}^{-1}$. A linear concentration gradient, increasing from 20 to 100 % B, was applied. The length of the gradient was one column volume, and after that, the length of isocratic elution with 100 % B was one column volume. The detection wavelengths were 210 and 320 nm. Fractions containing the product were combined, evaporated and analyzed.

3-Cyano-4-(ethoxymethyl)-6-methyl-2-pyridone. m.p.: 208–209 °C (lit. m.p.: 209 °C¹³). IR (KBr, cm^{-1}): 3290 (v, -NH), 3139, 3098 (δ_s , -CH aromatic), 2983, 2974 (δ_{as} , -CH₃), 2902, 2897 (δ_s , -CH₃), 2217 (v, -CN), 1659 (amide band I), 1621 (amide band II), 1128 (v, -C-O). ¹H-NMR (200 MHz, DMSO-*d*₆, δ / ppm): 1.2 (3H, *t*, *J* = 7.0 Hz, -CH₂OCH₂CH₃), 2.2 (3H, *s*,

pyridone $-\text{CH}_3$), 3.5 (2H, *q*, $J = 7.0$ Hz, $-\text{CH}_2\text{OCH}_2\text{CH}_3$), 4.1 (2H, *s*, $-\text{CH}_2\text{OCH}_2\text{CH}_3$), 6.3 (1H, *s*, $-\text{CH}=\text{N}$), 12.5 (1H, *s*, NH). ^{13}C -NMR (50 MHz, $\text{DMSO}-d_6$, δ / ppm): 15.1 ($-\text{CH}_2\text{OCH}_2\text{CH}_3$), 19.4 (pyridone $-\text{CH}_3$), 66.3 ($-\text{CH}_2\text{OCH}_2\text{CH}_3$), 68.9 ($-\text{CH}_2\text{OCH}_2\text{CH}_3$), 115.3 ($-\text{CN}$), 96.6, 104.0, 152.9, 160.9, 161.2 (pyridone ring).

RESULTS AND DISCUSSION

Kinetic study

In order to perform the kinetic measurements under conditions that provide the maximum reaction rates, the influence of the initial enzyme concentration was tested. The effect of the initial enzyme concentration on the reaction rate and the yield of 3-cyano-4-(ethoxymethyl)-6-methyl-2-pyridone synthesis are shown in Fig. 2. The results indicate a linear increase in reaction rate with increasing enzyme concentration up to 1.2 % w/v, when the highest reaction rate of $1.49 \cdot 10^{-3} \text{ mol dm}^{-3} \text{ h}^{-1}$ was achieved. With further increase in enzyme concentration to 1.8 %, w/v, the reaction rate, as well as the yield of pyridone, remained constant. Thus, an enzyme concentration of 1.2 % w/v was chosen for the determination of the kinetic parameters.

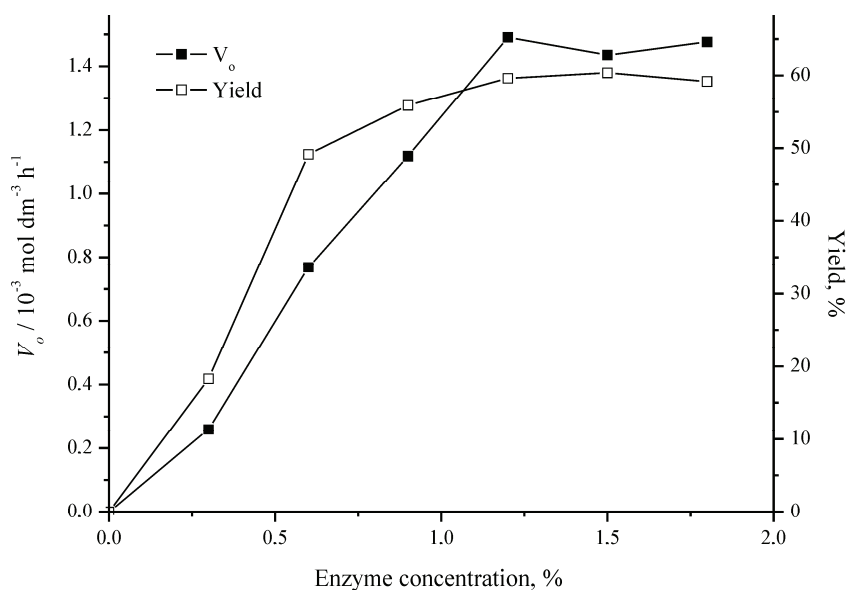


Fig. 2. Influence of the enzyme concentration on the initial reaction rate and the yield of pyridone. Concentrations of reactants were $2.6 \times 10^{-2} \text{ mol dm}^{-3}$ and 0.94 mol dm^{-3} for EPD and CAA, respectively. Lipase concentration was varied between 0.3 and 1.8 %, w/v.

The aim of this work was to elucidate the mechanism of the condensation of 2-cyanoacetamide and 1-ethoxy-2,4-pentanedione mediated by lipase from *C. rugosa*. For this purpose, initial reaction rate analysis was employed as the most useful method. The kinetic parameters of this bi-substrate reaction were deter-

mined by measuring the initial reaction rates for different sets of substrate concentrations. The effect of both substrates was investigated systematically over a wide range of concentrations: the concentration for 1-ethoxy-2,4-pentanedione was varied from 0.5×10^{-2} to 8×10^{-2} mol dm⁻³ and that for 2-cyanoacetamide from 0.2 to 4.8 mol dm⁻³. A large excess of 2-cyanoacetamide was applied since it was previously confirmed that an excess of this substrate significantly accelerates the lipase-catalyzed formation of pyridones.^{25–28}

Graphical representations of obtained initial rates against 2-cyanoacetamide (or 1-ethoxy-2,4-pentanedione) concentrations at several fixed values of 1-ethoxy-2,4-pentanedione (or 2-cyanoacetamide) concentrations are shown in Figs. 3 and 4.

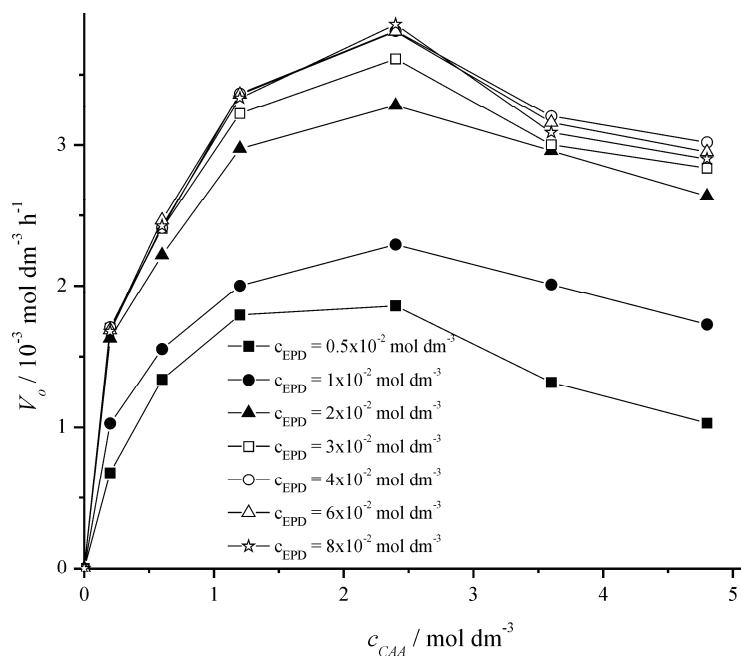


Fig. 3. The ping-pong model curves at a fixed concentration of 1-ethoxy-2,4-pentanedione.

It can be seen (Fig. 3) that with increasing concentration of 2-cyanoacetamide, the initial reaction rate increased up to an optimum value. The value of optimum 2-cyanoacetamide concentration slightly increased from 1.7 mol dm⁻³ for lower 1-ethoxy-2,4-pentanedione concentrations to 2.4 mol dm⁻³ for higher concentration. Nevertheless, at higher 2-cyanoacetamide concentrations a decrease of the initial velocity was observed, indicating that the excess 2-cyanoacetamide inhibited the catalytic activity of lipase. On the other hand, the effects of the 1-ethoxy-2,4-pentanedione concentration for various fixed concentrations of 2-cyanoacetamide (Fig. 4) resembled those typical Michaelis–Menten kinetics.

With increasing 1-ethoxy-2,4-pentanedione concentration, the reaction rates increased and slowly approached to a local maximum. The value of local maximum rate increased as the fixed concentration of 2-cyanoacetamide increased up to 2.4 mol dm^{-3} . Due to the inhibitory effect, with concentrations of 2-cyanoacetamide higher than 2.4 mol dm^{-3} , the local maximum rate were lower. Therefore, the maximum initial rate of $3.85 \times 10^{-3} \text{ mol dm}^{-3} \text{ h}^{-1}$ was achieved with $8 \times 10^{-2} \text{ mol dm}^{-3}$ of 1-ethoxy-2,4-pentanedione and 2.4 mol dm^{-3} of 2-cyanoacetamide.

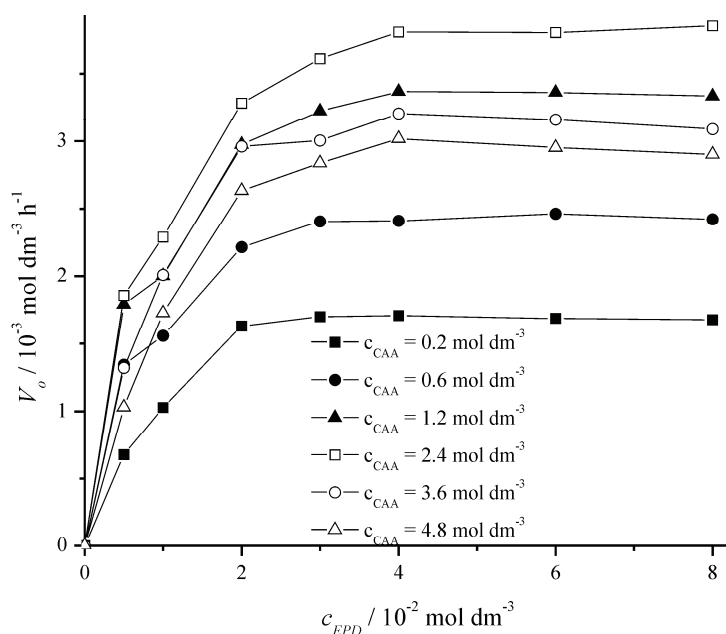


Fig. 4. The ping-pong model curves at a fixed concentration of 2-cyanoacetamide.

These results support a ping-pong mechanism with substrate inhibition, typical for lipase catalyzed reactions, and the same model was proposed in a previous study of the lipase-catalyzed synthesis of 4,6-dimethyl-3-cyano-2-pyridone.²⁹ A graphical illustration of the proposed mechanism is given in Fig. 5.

After statistical analysis, the ping-pong model with 2-cyanoacetamide inhibition was shown to be in good agreement with the experimental results, with a correlation coefficient of 0.94. According to this mechanism, the lipase was initially bound to 1-ethoxy-2,4-pentanedione forming a non-covalent complex, which was, with synchronal release of one water molecule, transformed to a 1-(ethoxymethyl)-3-oxo-but-1-enyl-enzyme complex. Subsequently, the modified enzyme reacted with the 2-cyanoacetamide and formed another binary complex which then released pyridone, water and the free enzyme. It is plausible that

inhibition by 2-cyanoacetamide occurs when a 2-cyanoacetamide molecule reacts with the enzyme directly to produce a dead-end complex (Fig. 6).

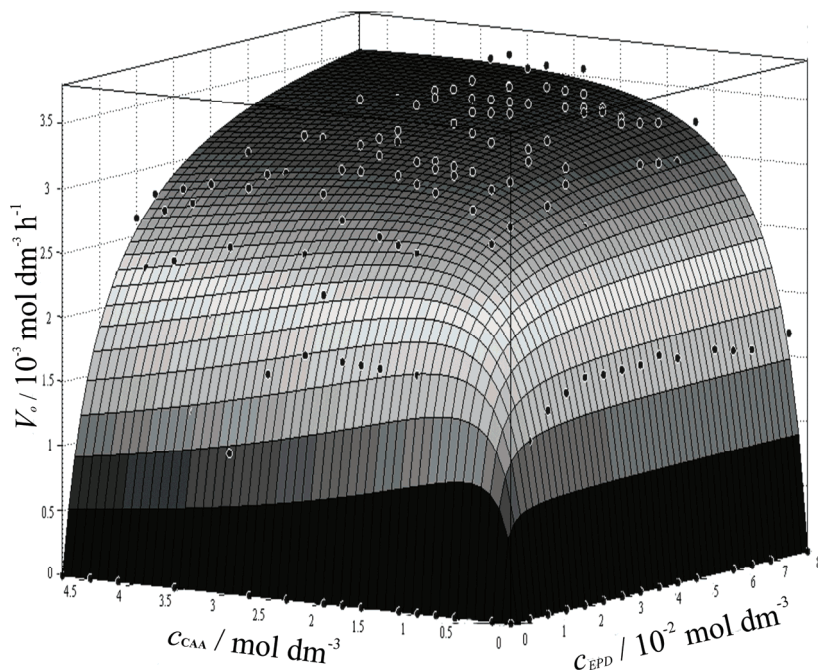


Fig. 5. Illustration of the proposed ping-pong bi-ter mechanism.

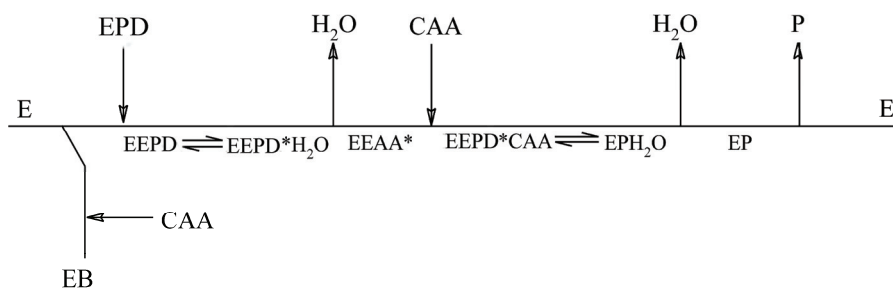


Fig. 6. Schematic representation of the ping-pong bi-ter mechanism: E: enzyme (lipase), CAA: 2-cyanoacetamide, EPD: 1-ethoxy-2,4-pentanedione, P: pyridone, EEPD and EP: complexes of lipase and EPD and P, respectively, EEPD*: 1-(ethoxymethyl)-3-oxo-but-1-enyl-enzyme complex and EB: dead-end inhibition complex of the enzyme with 2-cyanoacetamide.

The kinetic constants, given in Table I, were obtained by multiple regression fitting of the experimental data:

$$v = \frac{V_{\max} [A][B]}{K_m^B [A] + K_m^A [B] \left(1 + \frac{[B]}{K_{i,B}} \right) + [A][B]} \quad (1)$$

where v is the initial reaction rate, V_{\max} is the maximum reaction rate, $[A]$ and $K_{m,A}$ are the concentration and Michaelis constant of 1-ethoxy-2,4-pentanedione, $[B]$ and $K_{m,B}$ are the concentration and Michaelis constant of 2-cyanoacetamide, respectively, and $K_{i,B}$ is the inhibitory constant of 2-cyanoacetamide.

TABLE I. Estimated values of the kinetic parameters for the synthesis of 3-cyano-4-(ethoxymethyl)-6-methyl-2-pyridone

Parameter	Value
V_{\max}	$4.34 \times 10^{-3} \text{ mol dm}^{-3} \text{ h}^{-1}$
$K_{m,A}$	$0.315 \times 10^{-2} \text{ mol dm}^{-3}$
$K_{m,B}$	$0.347 \text{ mol dm}^{-3}$
$K_{i,B}$	$1.603 \text{ mol dm}^{-3}$
$K_{s,A}$	$0.106 \text{ dm}^3 \text{ g}^{-1} \text{ h}^{-1}$
$K_{s,B}$	$0.963 \times 10^{-3} \text{ dm}^3 \text{ g}^{-1} \text{ h}^{-1}$

Specificity constants, K_s , for A and B can be defined as $K_s = k_{\text{cat}}/K_m$, where k_{cat} is the rate constant for the catalyzed reaction. The high value of $K_{s,A}/K_{s,B}$ (109.6) indicates that the lipase from *C. rugosa* has a higher affinity towards the 1,3-diketone compared to 2-cyanoacetamide, which was also observed in a previous study.²⁹ The assumed reaction mechanism is schematically presented in Fig. 7.

By using specificity constant values, the preference of the enzyme for different 1,3-diketones (1-ethoxy-2,4-pentanedione and 2,4-pentanedione) can be compared. As the specificity constant of 2,4-pentanedione is about ninety fold higher than the specificity constant for 1-ethoxy-2,4-pentanedione, it is clear that lipase prefers 2,4-pentanedione as substrate. If the catalytic constants of these two reactions are compared, it is interesting to notice that the reaction was much faster (≈ 500 fold) with 2,4-pentanedione, although the higher polarity of the ethoxymethyl group facilitates the attack on the carbonyl group of 1-ethoxy-2,4-pentanedione. It seems that the mechanism of the enzymatic synthesis of substituted 2-pyridones is different to that operative in their chemical synthesis that leads to different selectivities, which could be an additional motive for wider application of lipase-catalyzed reactions. The explanation could be in the specific tunnel shape of the active center of the lipase from *C. rugosa*.³¹ The bulkier is the substrate, the more difficult is the approach to the catalytic triad and consequently the formation of the enzyme-substrate complex is slower.

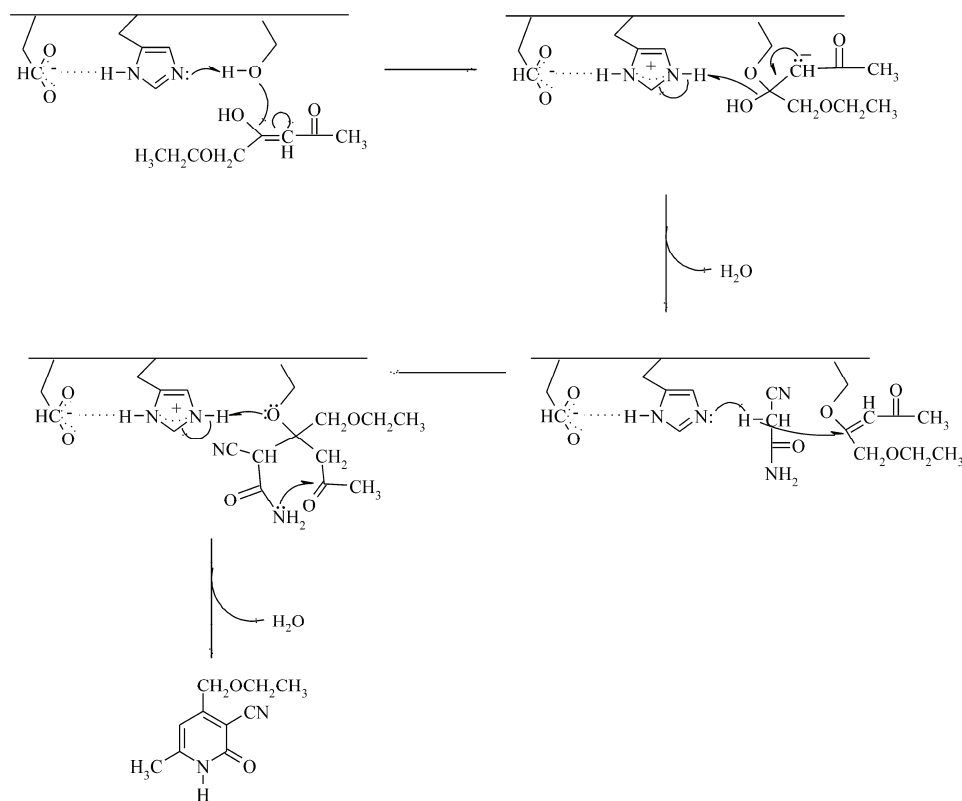


Fig. 7. Hypothetical mechanism of the enzyme catalyzed reaction of 1-ethoxy-2,4-pentanedione and 2-cyanoacetamide.

CONCLUSIONS

The enzymatic synthesis of 3-cyano-4-(ethoxymethyl)-6-methyl-2-pyridone, an important precursor for vitamin B₆, starting from 1-ethoxy-2,4-pentanedione and 2-cyanoacetamide was described. In addition, a kinetic study was performed. The results indicate a linear increase in reaction rate with increasing enzyme concentration up to 1.2 %, w/v. Moreover, the mechanism of 2-cyanoacetamide and 1-ethoxy-2,4-pentanedione condensation mediated by lipase from *Candida rugosa* was elucidated using the initial reaction rate analysis. The best fit of the experimental data was achieved using the ping-pong bi-ter mechanism with inhibition by 2-cyanoacetamide. Values of the kinetic parameters demonstrated higher affinity of lipase from *C. rugosa* for 1-ethoxy-2,4-pentanedione rather than for 2-cyanoacetamide. Moreover, the values of specificity constants of 2,4-pentanedione and 1-ethoxy-2,4-pentanedione clearly demonstrated a greater affinity towards 2,4-pentanedione and less bulky substrates.

Acknowledgements. The authors are grateful to the Ministry of Education, Science and Technological Development of the Republic of Serbia for financial support (Project Nos. 172013, III 46010 and 172049).

ИЗВОД

ЕНЗИМСКА СИНТЕЗА ПРЕКУРСОРА ВИТАМИНА Б₆

НЕВЕНА Ж. ПРЛАИНОВИЋ¹, ДЕЈАН И. БЕЗБРАДИЦА², ЗОРИЦА Д. КНЕЖЕВИЋ-ЈУГОВИЋ²,
ДУШАН В. ВЕЛИЧКОВИЋ³ и ДУШАН Ж. МИЛИН²

¹Иновациони центар Технолошко–металуршког факултета, Универзитет у Београду, Карнегијева 4, 11000 Београд, ²Технолошко–металуршки факултет, Универзитет у Београду, Карнегијева 4, 11000 Београд и ³Хемијски факултет, Универзитет у Београду, Студентски трг 16, 11000 Београд

3-Цијано-4-(етоксиметил)-6-метил-2-пиридон је веома важан прекурсор у синтези витамина Б₆. Добија се у реакцији између молекула 2-цијаноацетамида и 1-етокси-2,4-пентандиона катализованој липазом из *Candida rugosa* (триацилглицерол-ацил-хидролаза, ЕС 3.1.1.3). Резултати овог рада представљају сет нових експерименталних података брзине ензимске синтезе 3-цијано-4-(етоксиметил)-6-метил-2-пиридона. Математичким моделовањем ових података добијени су подаци о кинетици испитане реакције. Кинетичка мерења вршена су на температури од 50 °С при концентрацији ензима од 1,2 % m/v. Добијени резултати фитовани су са два различита математичка модела (пинг–понг модел са инхибицијом 2-цијаноацетамидом и секвенцијални модел са правилним редоследом везивања са инхибицијом 2-цијаноацетамидом). Вредности коефицијената линеарности показују да се почетне брзине реакције при различитим почетним концентрацијама супстрата најбоље могу описати пинг–понг би–тер моделом при чему постоји инхибиција 2-цијаноацетамидом. У раду је дат и графички приказ пинг–понг модела. Добијене константе специфичности указују на то да липаза из *C. rugosa* има већи афинитет према 1-етокси-2,4-пентандиону у поређењу са 2-цијаноацетамидом.

(Примљено 22. марта, ревидирано 10. маја 2013)

REFERENCES

1. K. Parmar, S. Prajapati, S. Joshi, K. Goswami, A. Patel, *Chem. Sin.* **2** (2011) 100
2. A. Abdel-Aziz, H. El-Subbagh, T. Kuniada, *Bioorg. Med. Chem.* **13** (2005) 4929
3. L. Qun, L. Mitscher, L. Shen, *Med. Chem. Rev.* **20** (2000) 231
4. R. L. T. Parreira, O. Abrahao Jr., S. E. Galembeck, *Tetrahedron* **57** (2001) 3243
5. W. Anderson, D. Dean, T. Endo, *J. Med. Chem.* **33** (1990) 1667
6. P. Thompson, V. Manganiello, E. Degerman, *Curr. Top. Med. Chem.* **7** (2007) 421
7. C. Altomare, S. Cellamare, L. Summo, P. Fossa, L. Mosti, *Bioorg. Med. Chem.* **8** (2000) 909
8. E. Presti, R. Boggia, A. Feltrin, G. Menozzi, P. Dorigo, L. Mosti, *Farmaco* **54** (1999) 465
9. G. Walker, B. Weaver, *J. Org. Chem.* **25** (1960) 484
10. S. Harris, K. Folkers, *J. Am. Chem. Soc.* **61** (1939) 3307
11. S. Harris, E. Stiller, K. Folkers, *J. Am. Chem. Soc.* **61** (1939) 1242
12. S. Harris, K. Folkers, *J. Am. Chem. Soc.* **61** (1939) 1245
13. S. Harris, N. Westfield, (Merck & Co.), US pat. 2,382,876 (1945)
14. M. Svedendahl, K. Hult, P. Berglund, *J. Am. Chem. Soc.* **127** (2005) 17988
15. J.-M. Xu, F. Zhang, B.-K. Liu, Q. Wu, X.-F. Lin, *Chem. Commun.* (2007) 2078
16. G. A. Strohmeier, T. Sovic, G. Steinkellner, F. S. Hartner, A. Andryushkova, T. Purkart-hofer, A. Glieder, K. Gruber, H. Griengl, *Tetrahedron* **65** (2009) 5663

17. M. Rahman, N. Chaibakhsh, M. Basri, R. Rahman, A. Salleh, S. Radzi, *J. Chem. Technol. Biotechnol.* **83** (2008) 1534
18. A. Petersson, L. Gustafsson, M. Nordblad, P. Borjesson, B. Mattiasson, P. Adlercreutz, *Green Chem.* **7** (2005) 837
19. Y. Liu, F. Wang, T. Tan, *J. Mol. Catal., B* **56** (2009) 126
20. R. de Souza, O. Antunes, W. Kroutil, C. Kappe, *J. Org. Chem.* **74** (2009) 6157
21. B. Davis, V. Boyer, *Nat. Prod. Rep.* **18** (2001) 618
22. K.-E. Jaeger, T. Eggert, *Curr. Opin. Biotechnol.* **13** (2002) 390
23. N. Turner, *Curr. Opin. Biotechnol.* **14** (2003) 401
24. J. Palomo, G. Fernández-Lorente, C. Ortiz, R. Segura, C. Mateo, M. Fuentes, J. Hermoso, R. Fernández-Lafuente, J. Guisán, *Med. Chem. Rev.* **2** (2005) 369
25. D. Mijin, D. Antonović, M. Mišić-Vuković, *Indian J. Chem., B* **33** (1994) 309
26. D. Mijin, M. Mišić-Vuković, *Indian J. Chem., B* **34** (1995) 348
27. D. Mijin, M. Mišić-Vuković, *Indian J. Chem., B* **37** (1998) 988
28. D. Mijin, B. Milić, M. Mišić-Vuković, *Indian J. Chem., B* **45** (2006) 61
29. N. Prlainović, D. Bezbradica, Z. Knežević-Jugović, R. Kozłowska, D. Mijin, *J. Braz. Chem. Soc.* **21** (2010) 2285
30. W. Bruce, H. Coover Jr., *J. Am. Chem. Soc.* **66** (1944) 2092
31. M. Cygler, J. Schrag, *Biochim. Biophys. Acta* **1441** (1999) 205.



J. Serb. Chem. Soc. 78 (10) 1503–1512 (2013)
JSCS–4513

High antioxidative potential and low toxic effects of selenosemicarbazone metal complexes

DRAGANA DEKANSKI¹, TAMARA TODOROVIĆ², DRAGANA MITIĆ², NENAD FILIPOVIĆ³, NATALIJA POLOVIĆ² and KATARINA ANĐELKOVIĆ^{2*}

¹Biomedical Research, R&D Institute, Galenika a.d., Pasterova 2, 11000 Belgrade, Serbia,

²Faculty of Chemistry, University of Belgrade, Studentski trg 12–16, 11000 Belgrade, Serbia

and ³Faculty of Agriculture, University of Belgrade –Nemanjina 6, 11080 Belgrade, Serbia

(Received 15 March, revised 27 March 2013)

Abstract: Novel metal-based compounds with therapeutic potential have become the subject of intense investigations in inorganic chemistry and biomedical science. Recently, strong dose-dependent cytotoxic activities of selenosemicarbazone metal complexes against several human cancer cell lines were demonstrated. The aim of the present study was to investigate *in vitro* antioxidative potential of Ni(II), Cd(II) and Zn(II) selenosemicarbazone complexes. All three investigated complexes exhibited high 2,2'-azinobis(3-ethylbenzothiazoline-6-sulphonic acid) radical cation (ABTS^{•+}) scavenging capacity, comparable with ascorbic acid. In an acute toxicity study, administration of the compounds was performed orally to mice at single doses. The mice were observed for clinical signs, body weight effects and mortality for 14 days, after which they were sacrificed for gross organ necropsy. The body weight did not vary after administration, and the autoptic analysis failed to show appreciable macroscopic alterations of internal organs. Generally, the compounds exhibited low toxic effects as required for further *in vivo* therapeutic studies.

Keywords: Ni(II), Cd(II) and Zn(II) complexes; selenosemicarbazones; antioxidative activity; *in vivo* toxicity.

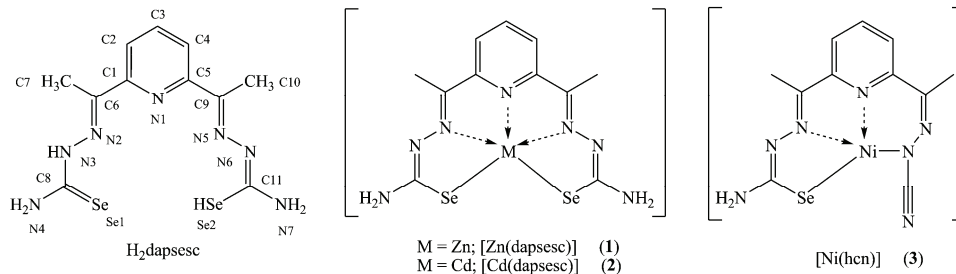
INTRODUCTION

Chalcogensemicarbazones are condensation derivatives of chalcogensemicarbazides and carbonyl compounds. Interest in (thio)semicarbazone ligands has been driven, in part, by potentially beneficial biological activity of ligands and their metal complexes, including, antifungal, antimicrobial, anticancer, anti-inflammatory and antiviral activities.^{1–4} However, total number of selenosemicarbazones and their metal complexes is much smaller in comparison to the corresponding O and S analogues, although results of few comparative studies

* Corresponding author. E-mail: kka@chem.bg.ac.rs
doi: 10.2298/JSC130315035D

indicated that isosteric replacement of other chalcogen atoms with selenium resulted in a much more active compounds.^{5–11} The biological action of chalcogensemicarbazones is attributed to their chelating properties.^{1–4}

Our research group has been engaged in the systematic investigation of selenosemicarbazones derived from *N*-heteroaromatic aldehydes and ketones, in order to determine the driving force behind the coordination behaviour of this type of ligands, as well as to explore their biological activity. Similar to their sulphur analogues, selenosemicarbazones exhibit various binding modes with d-metals. Selenosemicarbazones of aliphatic and aromatic carbonyl compounds can act as mono- or bidentate ligands, but when *N*-heteroaromatic carbonyl compound is used for synthesis of selenosemicarbazones, the coordination capacity can be extended by the presence of additional nitrogen atom suitable for chelation. Accordingly, 2,6-diacetylpyridine bis(selenosemicarbazone) ($H_2dapsesc$) is coordinated as pentadentate, *via* both selenium atoms, pyridine and both imine nitrogen atoms in Cd(II) and Zn(II) complexes (Scheme 1),¹² while during the formation of the Ni(II) complex, elimination of hydrogen selenide from one side chain of the $H_2dapsesc$ ligand occurred.¹² In the resulting Ni(II) complex, the modified ligand 2-{1-[6-(1-selenosemicarbazonoethyl)-2-pyridyl]ethylidene}-hydrazine carbonitrile (H_2hcn) is tetradentately coordinated (Scheme 1).



Scheme 1. Structures of the investigated compounds.

Over-production of activated oxygen species, generated by normal metabolic processes, is considered to be the main contributor of oxidative damage in biomolecules, thus inducing a broad spectrum of different diseases, in particular cardiovascular, neurodegenerative disease and cancer.¹³ It is known that oxidative stress plays a multistep role in carcinogenesis, through a process of both cell mutation and proliferation. Although most cancer cells exhibit elevated oxidative stress with increased metabolic activity and the production of reactive oxygen species (ROS), the mechanism of action of many cancer chemotherapeutic drugs involves ROS-mediated apoptosis. For example, the classic anticancer agents cisplatin and adriamycin appear to produce ROS at excessive levels, resulting in DNA damage and cell death.¹⁴ Most thiosemicarbazone complexes contain redox

metal ions that potentially can activate O₂ and generate OH-radicals. However, there are data that support but also data that exclude this activity as function of the nature of the ligand and the metal centre.⁴ The potential value of natural and synthetic antioxidants has already prompted scientists to search for cooperative effects of compounds which improve antioxidant activity and cytotoxicity.¹⁵ Previous investigations showed that selenosemicarbazone complexes exhibited strong dose-dependent cytotoxic activity against a panel of several human tumour cell lines, and this effect was comparable to that of cisplatin.^{16–19} This study was undertaken with the aim to investigate the *in vitro* antioxidative potential of Ni(II), Cd(II) and Zn(II) selenosemicarbazone complexes. The analysis of the toxicity level of chemical compounds is one of the most important steps required for further biological studies.²⁰ Bearing in mind the toxicity from high Se intake and that metal ions are generally toxic at high-dose levels, the second aim of the present study was to evaluate the acute oral toxicity of these novel metal-based compounds.

EXPERIMENTAL

Materials and methods

2,6-Diacetylpyridine (dap, 99 %), was obtained from Acros Organics, while Ni(CH₃COO)₂·4H₂O (*purum p.a.* ≥ 99.0 % KT), Zn(CH₃COO)₂·2H₂O (*purum p.a.* ≥ 99.0 % KT) and Cd(CH₃COO)₂·2H₂O (*purum p.a.* ≥ 99.0% KT) were obtained from Fluka. Dimethyl sulphoxide (DMSO dried, ≥ 99.5 %) was obtained from Merck (Darmstadt, Germany). 2,2'-Azino-bis(3-ethylbenzothiazoline-6-sulphonic acid) (ABTS, anal. grade) and vitamin C (ascorbic acid, *p.a.*) were purchased from Serva.

Elemental analyses (C, H, N) were performed by standard micro-methods using an ElementarVario ELIII C.H.N.S=O analyzer. The IR spectra were recorded on a Perkin–Elmer FT-IR 1725X spectrometer in the region 4000–400 and 400–200 cm⁻¹ as CsI tablets. Molar conductivities were measured at room temperature on a digital conductivity-meter Jenway-4009. The NMR spectra (in DMSO-*d*₆) were obtained using a Varian Gemini 2000 instrument (¹H at 200 MHz, ¹³C at 50.3 MHz).

Synthesis of the tested compounds

The ligand H₂dapsesc was synthesized as described previously¹² by the reaction of dap and selenosemicarbazide in the molar ratio 1:2. The complexes **1–3** (Scheme 1) were synthesized by adding an aqueous solution of Zn(CH₃COO)₂·2H₂O, Cd(CH₃COO)₂·2H₂O or Ni(CH₃COO)₂·4H₂O, respectively, into a suspension of H₂dapsesc in EtOH.¹² The Zn(II) and Cd(II) complexes were purified by vapour diffusion using DMSO as the inner solution and EtOH as the outer solvent. The purity of the synthesized compounds was tested by elemental analysis. The IR and NMR spectroscopy data, as well as the molar conductivity values were in good agreement with previously published data.¹²

Analytic and spectral data for the ligand and **1–3**

H₂dapsesc. Yield: 0.63 g (93 %); Anal. Calcd. for C₁₁H₁₅N₇Se (FW: 403.20): C, 32.77; H, 3.75; N, 24.32 %. Found: C, 32.96; H, 3.70; N, 23.79 %. IR (KBr, cm⁻¹): 3460 (s), 3375(s), 3333 (s), 3249 (s), 3147 (s), 1591 (vs), 1491 (vs), 1440 (vs), 1397 (vs), 1260 (vs), 1086 (vs), 786 (m). ¹H-NMR (200 MHz, DMSO-*d*₆, δ / ppm): 2.38 (3H, s, C7H₃), 2.58 (3H, s, C10H₃),

7.81 (1H, poorly resolved doublet, C4H), 8.01 (1H, poorly resolved triplet, C3H), 8.63 (1H, poorly resolved doublet, C2H), 8.65 and 8.75 (1H, *s*, N4H^aH^b), 8.97 (2H, *s*, N7H₂), 10.85 (1H, *s*, N3H), 14.16 (1H, *s*, Se2). ¹³C-NMR (50.3 MHz, DMSO-*d*₆, δ / ppm): 12.6 (C7+C10), 121.6 (C2+C4), 137.0 (C3), 149.9 (C6+C9), 153.7 (C1+C5), 175.5 (C8+C11).

Complex 1. Yield: 0.10 g (86 %); Anal. Calcd. for C₁₁H₁₃N₇Se₂Zn (FW: 466.58): C, 28.66; H, 3.52; N, 18.00 %. Found: C, 28.95; H, 3.51; N, 18.03 %. IR (KBr, cm⁻¹): 3411 (*m*), 3285 (*m*), 3157 (*m*), 1614 (*m*), 1482 (*s*), 1438 (*vs*), 1405 (*s*), 1285 (*m*), 1167 (*m*), 1024 (*m*), 714 (*w*). ¹H-NMR (200 MHz, DMSO-*d*₆, δ / ppm): 2.46 (6H, *s*, C7H₃+C10H₃), 6.82 (4H, *s*, N4H₂+N7H₂), 7.61 (2H, poorly resolved doublet, C2H+C4H), 7.92 (1H, poorly resolved triplet, C3H). ¹³C-NMR (50.3 MHz, DMSO-*d*₆, δ / ppm): 17.4 (C7+C10), 124.1 (C2+C4), 138.9 (C3), 153.6 (C6+C9), 155.8 (C1+C5), 173.0 (C8+C11). Conductivity ($A_M / \Omega^{-1}\text{cm}^2 \text{mol}^{-1}$ ($1 \times 10^{-3} \text{mol dm}^{-3}$ in DMF)): 0.73.

Complex 2. Yield 0.07 g (55 %); Anal. Calcd. for C₁₁H₁₃N₇Se₂Cd (FW: 513.60): C, 25.72; H, 2.55; N, 19.09 %. Found: C, 25.66; H, 2.54; N, 18.53 %. IR (KBr, cm⁻¹): 3476 (*m*), 3285 (*m*), 3162 (*w*), 1607 (*m*), 1495 (*s*), 1435 (*m*), 1407 (*s*), 1170 (*m*), 1019 (*w*), 702 (*w*). ¹H-NMR (200 MHz, DMSO-*d*₆, δ / ppm): 2.42 (6H, *s*, C7H₃+C10H₃), 6.93 (4H, *s*, N4H₂+N7H₂), 7.80 (2H, *d*, ³*J* = 7.9 Hz, C2H+C4H), 8.12 (1H, *t*, ³*J* = 7.9 Hz, C3H). ¹³C-NMR (50.3 MHz, DMSO-*d*₆, δ / ppm): 14.6 (C7+C10), 121.9 (C2+C4), 140.9 (C3), 145.4 (C6+C9), 150.5 (C1+C5), 174.6 (C8+C11). Conductivity ($A_M / \Omega^{-1}\text{cm}^2 \text{mol}^{-1}$ ($1 \times 10^{-3} \text{mol dm}^{-3}$ in DMF)): 1.17.

Complex 3. Yield 0.26 g (84 %); Anal. Calcd. for C₁₁H₁₁N₇SeNi (FW: 378.91): C, 34.87; H, 2.93; N, 25.88 %. Found: C, 34.64; H, 2.86; N, 25.47 %. IR (KBr, cm⁻¹): 3430 (*m*), 3315 (*m*), 3153 (*s*), 2176 (*vs*), 1648 (*s*), 1595 (*w*), 1535 (*s*), 1498 (*s*), 1444 (*m*), 1407 (*m*), 1370 (*m*), 1329 (*m*), 1289 (*m*), 1223 (*w*), 1172 (*m*), 1107 (*m*), 1076 (*m*), 1045 (*m*), 797 (*m*), 766 (*w*), 712 (*m*). ¹H-NMR (200 MHz, DMSO-*d*₆, δ / ppm): 2.34 (3H, *s*, C10H₃), 2.51 (3H, *s*, C7H₃), 7.87 (2H, *s*, N4H₂), 7.98 (1H, poorly resolved doublet, C2H), 8.18 (1H, poorly resolved doublet, C4H), 8.41 (1H, poorly resolved triplet, C3H). Conductivity ($A_M / \Omega^{-1}\text{cm}^2 \text{mol}^{-1}$ ($1 \times 10^{-3} \text{mol dm}^{-3}$ in DMF)): 1.35.

Free radical scavenging assay

The total antioxidant activity assay using ABTS cation radicals was performed according to the previously published procedure²¹ with some modifications. Briefly, ABTS was dissolved in water to a concentration of 7 mM and its cation radicals were produced in a reaction with 2.45 mM potassium persulphate. The resulting mixture was kept in the dark at room temperature for 12–16 h before use. Prior to the assay, the solution was diluted with miliQ water (about 1:79, v/v) to give an absorbance of 0.70±0.02 at 734 nm. After the addition of 2 mL of diluted ABTS cation radical solution to 0.2 mL of a fixed concentration of the compounds, the absorbance at 734 nm was recorded exactly 30 min after the initial mixing.

Results are presented as mean ± standard deviation. A minimum of three independent experiments were performed. The log sigmoid dose–response curves of free radical scavenging activity of tested compounds were generated using the Origin 7.0 software package (Microcal Software Inc., Northampton, MA, USA). The IC₅₀ values were determined by *post hoc* regression analysis of the linear segments of the sigmoid dose response curves. Calibration curves of the standards and samples were considered as linear if $R^2 > 0.98$.

Animals

This study was run in accordance to the statements of European Union regarding handling of experimental animals (86/609/EEC), and approved by the Ethical Committee for Labo-

ratory Animals, Galenika a.d., Belgrade (permit No 02/20.01.2012.). Adult, female (nulliparous and non-pregnant) NMRI/Han mice were provided by Biomedical Research Centre, R&D Institute, Galenika a.d. (Belgrade, Serbia). Before experiment, the mice were housed 5 per cage under constant environmental conditions (20–24 °C; 12 h light/dark cycle), and had access to standard pelleted food and water *ad libitum*.

Acute oral toxicity study

Acute oral toxicity test was run strictly in accordance with OECD *Guidelines for the Testing of Chemicals*, Section 4: Health Effects: Test No. 423: Acute Oral toxicity – Acute Toxic Class Method.²² The principle of the test is that, based on a stepwise procedure with the use of a minimum number of animals per step, sufficient information is obtained on the acute toxicity of a test substance. The substances were tested using a stepwise procedure. In each step, three female mice were used since they are generally slightly more sensitive. The absence or presence of compound-related mortality of the animals dosed at one step determined the next step, *i.e.*, no further testing is needed, dosing of three additional animals with the same dose, or dosing of three additional animals at the next higher or the next lower dose. The animals, which were 8–10 weeks old and weighed 22–30 g, were fasted for 4 h before the experiment and divided into experimental and control groups. Test samples were dissolved first in DMSO, and distilled water was added to obtain the final concentration of the tested compounds (the final concentration of DMSO was 20 %). The control group was treated with 20 % DMSO. A single dose of 300 and 2000 mg kg⁻¹ b.wt. of Ni (II), Cd(II) and Zn(II) complexes was administered intragastrically (*i.g.*) using a metal tube for gavage. Fixed volume of 0.5 mL was administered per mouse. Food was returned to the animals 3 h after dosing. Individual weights were determined at the start of the fasting time (day 0), immediately before the test substance was administered (day 0) and on the test days 1, 2, 4, 7, and 14. The animals were observed for clinical signs of toxicity while handled before and after fasting, during the first 30 min after dosing, at least two more times within 4–4.5 h after dosing, and daily thereafter. Observations for abnormal behavioural signs, somnolence, dizziness, restlessness, neurological signs, respiratory distress or mortality were conducted twice daily. At the end of the test (day 14), the mice were sacrificed by cervical dislocation, and gross pathological changes in the main organs (brain, liver, kidney, spleen, gastric and intestinal mucosa) were evaluated.

RESULTS AND DISCUSSION

The biological activities of semicarbazones and thiosemicarbazones were reported to increase upon coordination with the metal ions. The metal complex could be more active than the free ligand, and could exhibit biological activities that are not shown by the free ligand. In addition, some adverse effects may decrease upon complexation. Moreover, coordination may lead to significant reduction of drug-resistance. Therefore, studies on novel metal-based compounds with therapeutic potential have become an area of intense investigation in biomedicine and inorganic chemistry.^{23,24} In the present study, the antioxidative potential and acute toxicity level of three synthesised selenosemicarbazone metal complexes **1–3** (Scheme 1) were investigated.

There are various antioxidant activity assays, each having their specific target within the matrix and all of them with advantages and disadvantages. The

ABTS assay used in this study represents one of the most important and widely used assays.²⁵ This colorimetric test provides determination of the antioxidant capacity of natural and synthetic compounds since the ABTS radical decolorizes in the presence of antioxidants. The free radical scavenging capacity (FRSC in %) of the ligand H₂dapsesc, the complexes **1–3** and metal salts used in synthesis, as well as the ascorbic acid as positive control and DMSO as the vehicle control is expressed as 50 % inhibitory concentration (*IC*₅₀ in μM, Table I), defined as the concentration of the tested compound leading to a 50 % reduction of the free radical concentration. The *IC*₅₀ values for the tested compounds were calculated from log sigmoidal dose response inhibition curves by *post hoc* linear regression analysis. These results clearly indicated that the complexes **1–3** exhibited an excellent ABTS radical cation-scavenging effect, comparable to that of a reference antioxidant, Vitamin C. The antioxidative capacity of the ligand was lower by an order of magnitude compared to the activity of the complexes. It is to be noted that no significant radical scavenging activities were observed in the experiment carried out under the same experimental conditions with the metal salts used in the syntheses of the complexes, even up to the concentration of 1.0 mM. The *IC*₅₀ values (Table I) indicated that the ligand and the complexes showed antioxidant activity in the following order: **2** > **1** > **3** > H₂dapsesc. It can be assumed that coordination of the ligand in anionic form promotes the ligand-centered reduction of the CH₃C=N double bond in the complexes, which is reflected in the higher antioxidative potential of the complexes compared to the free ligand, as was registered for related Ga(III) complexes with thiosemicarbazones.²⁶

TABLE I. *IC*₅₀ values (in μM) calculated from ABTS radical cation scavenging assay of the tested compounds and the standard (vitamin C)

Compound	<i>IC</i> ₅₀ / μM
H ₂ dapsesc	557±54
[Zn(dapsesc)] (1)	29.51±1.50
[Cd(dapsesc)] (2)	21.62±0.83
[Ni(hcn)] (3)	35.59±5.30
Zn(CH ₃ COO) ₂ ·2H ₂ O	> 1000
Cd(CH ₃ COO) ₂ ·2H ₂ O	> 1000
Ni(CH ₃ COO) ₂ ·4H ₂ O	> 1000
Vitamin C	21.35±2.75

It is known that selenium represents one of the most important micro-nutrients in human diet regarding antioxidant activity. It does not act directly on free radicals but is an indispensable part of most antioxidant enzymes (metallo-enzymes, glutathione peroxidase) that would have no effect without it.²⁷ The mode of anticancer action of Se is not fully understood but several mechanisms including antioxidant protection by selenoenzymes have been proposed.²⁸ Furthermore, zinc is a bio-element that is important in the prevention of free radicals

formation. It plays a role as an inhibitor of NADPH oxidases, which catalyze the production of the superoxide radical anion from oxygen by using NADPH as an electron donor. Zinc is present in superoxide dismutase, an important antioxidant enzyme that converts the superoxide radical anion into hydrogen peroxide. Finally, zinc induces the production of metallothionein that is a scavenger of the hydroxyl radical, and also competes with copper for binding to the cell wall, thus decreasing the production of hydroxyl radicals.²⁹ Taken together, the present preliminary *in vitro* results and these known properties of selenium and zinc allow the proposal that these metal complexes are worthy of further investigation under *in vivo* conditions.

However, the toxicity and carcinogenicity of metal ions should not be neglected. The primary route for their toxicity is depletion of glutathione and bonding to sulfhydryl groups of proteins.³⁰ In addition, the unregulated intake of dietary or pharmacological selenium, mainly in the form of the inorganic Se compound, sodium selenite, could potentially expose the body tissues to toxic levels of Se with the subsequent negative consequences on DNA integrity. Due to a broad interest for the beneficial effects of Se on human health and cancer prevention and therapy, studies investigating the negative effects such as toxicity from high Se intake are also highly required.²⁸ Therefore, a toxicological study of the investigated selenosemicarbazone metal complexes was conducted as one of the most important steps required for further studies of biological activity. The acute toxicity evaluation was based on an established protocol, internationally recognized as a reference standard tool for chemical tests. The OECD 420 guideline – Fixed-Dose Procedure for Assessing Oral Acute Toxicity²² was followed. Acute oral toxicity refers to those adverse effects occurring following oral administration of a single dose of a substance. According to globally harmonized system of classification and labelling of chemicals (GHS),³¹ substances are assigned to one of the five toxicity categories based on LD_{50} (oral and dermal) or LC_{50} (inhalation). For the evaluation of acute oral toxicity, a single dose (300 and 2000 mg kg⁻¹) was orally administered to female mice. The doses used were based on the previous toxicological data on the structurally related substance, *N*-{4-[(*E*)-((aminothioxomethylhydrazono)methyl]phenyl}acetamide (thioacetazone), which was helpful in the selection of the most appropriate initial dose. Namely, the median lethal dose (LD_{50}) for thioacetazone was determined as 950 mg kg⁻¹ after oral administration in mouse.³¹ Thus a starting dose 300 mg kg⁻¹ was employed in the present study. The results are presented in Table II.

At the dose level of 300 mg kg⁻¹ body weight, no mortality was observed, but some signs and unusual symptoms during the first 4 h of the acute toxicity protocol were observed, such as exciting behavioural (agitation, touch response), inhibitory (sleepiness) and other characteristics (piloerection). It was observed that the compounds did not cause any gross behavioural alterations, such as

convulsion, dizziness or respiratory distress. No clinical signs of toxicity were observed in the group that received [Ni(hcn)] in the lower dose. After that, the toxicity level of the Ni(II), Cd(II) and Zn(II) selenosemicarbazone complexes were evaluated at the maximum dose of 2000 mg kg⁻¹ administered orally to the 4 h-fasted mice. At the higher dose, toxic symptoms, such mild agitation, touch response in one animal and sleepiness in the [Cd(dapsesc)] group, ataxia and somnolence with a fatal effect in [Ni(hcn)] group, were observed. During the study period of two weeks, no death occurred in the animals treated with the Cd(II) and Zn(II) selenosemicarbazone complexes, which indicates that the lethal dose of the compounds is above 2000 mg kg⁻¹ body weight in mice and that the compounds could be considered to be less harmful at this dose. No test substance-related effects on body weight occurred. The mean body weights of the test mice were similar to those of the control group throughout the study (data not shown). Sporadic body weight losses of up to 5 % were not considered test substance-related, because the decreases were only over a one- or two-day period and did not occur the day after dosing. No gross lesions were present in the mice at necropsy. In addition, macroscopic examination revealed that the organs taken presented aspects of colour, size and texture, showing no difference from the control group.

TABLE II. Parameters of acute toxicity observed in adult female mice, treated with different oral doses of Ni(II), Cd(II) and Zn(II) selenosemicarbazone complexes; -, no effect; +, mild effect; ++, moderate effect; +++, major effect

Clinical sign	Compound/Dose, mg kg ⁻¹						Control (20 % DMSO)
	[Ni(hcn)]		[Cd(dapsesc)]		[Zn(dapsesc)]		
	300	2000	300	2000	300	2000	
Agitation	-	-	-	+	+	-	-
Convulsion	-	-	-	-	-	-	-
Ataxia	-	+++	+	-	-	-	-
Touch response	-	-	+	+	-	-	-
Piloerection	-	-	-	-	+	-	-
Sleepiness	-	-	-	+	+	-	+
Somnolence	-	+++	-	-	-	++	-
Respiratory distress	-	-	-	-	-	-	-
Mortality	0/6	6/6	0/6	0/6	0/6	0/6	0/6

The absence of mortality at concentrations as high as 2000 mg kg⁻¹ b.wt. of the Cd(II) and Zn(II) complexes did not allow the calculation of the median lethal dose (*LD*₅₀) value. Hence, the Cd(II) and Zn(II) complexes investigated in this study belong to the so-called category 5 or unclassified according to GSH classification.³¹ Therefore, these compounds show low acute toxicological risk. The absence of gross behavioural alteration is also another indication of lack of toxicity of the compounds. Moreover, it is important to emphasize that a safe

therapeutic index or therapeutic ratio could be expected. A higher therapeutic index is preferable to a lower one, and means that much higher doses of these compounds are required to reach the lethal/toxic threshold than the dose which will lead to a therapeutic effect.

CONCLUSIONS

The investigated compounds showed high *in vitro* antioxidative potential. Accordingly, they are good candidates for the prevention or treatment of a broad range of pathological conditions mediated by uncontrolled oxidative processes. They also exhibited low toxic effects as required for further *in vivo* therapeutic studies. The obtained results invoke further preclinical studies that should show their efficacy in different oxidative stress related disorders. In addition, long-term toxicological studies with repeated doses are necessary for the final safety evaluation.

Acknowledgments. This research was supported by the Ministry of Education, Science and Technological Development of the Republic of Serbia (Innovation Project “Antioxidants based on selenium complex compounds – research and development” No. 451-03-2372-IP type 1/79).

ИЗВОД

ВИСОКИ АНТИОКСИДАТИВНИ ПОТЕНЦИЈАЛ И МАЛИ ТОКСИЧНИ ЕФЕКАТ СЕЛЕНОСЕМИКАРБАЗОНСКИХ КОМПЛЕКСА

ДРАГАНА ДЕКАНСКИ¹, ТАМАРА ТОДОРОВИЋ², ДРАГАНА МИТИЋ², НЕНАД ФИЛИПОВИЋ³, НАТАЛИЈА ПОЛОВИЋ² И КАТАРИНА АНЂЕЛКОВИЋ²

¹ Биомедицинска истраживања, Институт за истраживање и развој, Галеника а.д., Пастерова 2, 11000 Београд, ² Хемијски факултет, Универзитет у Београду, Студентски трг 12–16, 11000 Београд и ³ Пољопривредни факултет, Универзитет у Београду, Немањина 6, 11080 Београд

Нова једињења на бази метала са терапеутским дејством постала су предмет истраживања у неорганској хемији и биомедицинским наукама. Показана је јака дозно-зависна цитотоксична активност комплекса селеносемикарбазона на већем броју ћелијских линија хуманих ћелија канцера. Циљ рада је испитивање *in vitro* антиоксидативног дејства селеносемикарбазонских комплекса никла, цинка и кадмијума. Сва три испитивана комплекса показала су јаку антиоксидативну активност према ABTS радикалу, упоредиву са активношћу аскорбинске киселине. Током испитивања акутне токсичности, једињења су орално давана мишевима у појединачним дозама и праћени су клинички знаци, тежина тела и морталитет након 14 дана, а потом су животиње жртвоване ради аутопсије органа. Тежина тела није варирала након апликације. Генерално, једињења су показала мали токсични ефекат што и захтева будуће *in vivo* терапеутско испитивање.

(Примљено 15. марта, ревидирано 27. марта 2013)

REFERENCES

1. T. S. Lobana, R. Sharma, G. Bawa, S. Khanna, *Coord. Chem. Rev.* **253** (2009) 977
2. D. X. West, A. E. Liberta, S. B. Padhye, R. C. Chikate, P. B. Sonawane, A. S. Kumbhar, R. G. Yerande, *Coord. Chem. Rev.* **123** (1993) 49

3. D. X. West, S. B. Padhye, P. B. Sonawane, *Struct. Bond.* **76** (1991) 1
4. G. Pelosi, *Open Crystallogr. J.* **3** (2010) 16
5. C. R. Kowol, R. Eichinger, M. A. Jakupec, M. Galanski, V. B. Arion, B. K. Keppler, *J. Inorg. Biochem.* **101** (2007) 1946
6. C. Pizzo, P. Faral-Tello, G. Salinas, M. Flo, C. Robello, P. Wipfe, S. G. Mahler, *Med. Chem. Comm.* **3** (2012) 362
7. S. R. Turk, C. Shipman Jr., J. C. Drach, *J. Gen. Virol.* **67** (1986) 1625
8. C. Shipman Jr., S. H. Smith, J. C. Drach, D. L. Klayman, *Antiviral Res.* **6** (1986) 197
9. H. G. Mautner, W. D. Kumler, Y. Okano, R. Pratt, *Antibiot. Chemother.* **6** (1956) 51
10. M. D. Revenko, V. I. Prisacari, A. V. Dizdari, E. F. Stratulat, I. D. Corja, L. M. Proca, *Pharm. Chem. J.* **45** (2011) 351
11. K. C. Agrawal, B. A. Booth, R. L. Michaud, E. C. Moore, A. C. Sartorelli, *Biochem. Pharmacol.* **23** (1974) 2421
12. T. R. Todorović, A. Bacchi, G. Pelizzi, N. O. Juranić, D. M. Sladić, I. D. Brčeski, K. K. Anđelković, *Inorg. Chem. Commun.* **9** (2006) 862
13. E. E. Battin, J. L. Brumaghim, *Cell Biochem. Biophys.* **55** (2009) 1
14. J. E. Klaunig, L. M. Kamendulis, B. A. Hocevar, *Toxicol. Pathol.* **38** (2010) 96
15. S. Y. Chiang, J. Welch, F. J. Rauscher, T. A. Beerman, *Biochemistry* **33** (1994) 7033
16. N. Gligorijević, T. Todorović, S. Radulović, D. Sladić, N. Filipović, D. Godevac, D. Jeremić, K. Anđelković, *Eur. J. Med. Chem.* **44** (2009) 1623
17. S. Bjelogrić, T. Todorović, A. Bacchi, M. Zec, D. Sladić, T. Srdić-Rajić, D. Radanović, S. Radulović, G. Pelizzi, K. Anđelković, *J. Inorg. Biochem.* **10** (2010) 4673
18. T. Srdić-Rajić, M. Zec, T. Todorović, K. Anđelković, S. Radulović, *Eur. J. Med. Chem.* **46** (2011) 3734
19. M. Zec, T. Srdić-Rajić, A. Konić-Ristić, T. Todorović, K. Anđelković, I. Filipović-Ljesković, S. Radulović, *Anti-Cancer Agents Med. Chem.* **12** (2012) 1071
20. B. Ganter, S. Tugendreich, C. I. Pearson, E. Ayanoglu, S. Baumhueter, K. A. Bostian, L. Brady, L. J. Browne, J. T. Calvin, G. J. Day, N. Breckenridge, S. Dunlea, B. P. Eynon, L. M. Furness, J. Ferng, M. R. Fielden, S. Y. Fujimoto, L. Gong, C. Hu, R. Idury, M. S. Judo, K. L. Kolaja, M. D. Lee, C. McSorley, J. M. Minor, R. V. Nair, G. Natsoulis, P. Nguyen, S. M. Nicholson, H. Pham, A. H. Roter, D. Sun, S. Tan, S. Thode, A. M. Tolley, A. Vladimirova, J. Yang, Z. Zhou, K. Jarnagin, *J. Biotechnol.* **119** (2005) 219
21. R. Re, N. Pellegrini, A. Proteggente, A. Pannala, M. Yang, C. Rice-Evans, *Free Radical Biol. Med.* **26** (1999) 1231
22. OECD Guidelines for the Testing of Chemicals, Section 4/Test No. 420: Acute Oral Toxicity – Fixed Dose Procedure, 2001, DOI: 10.1787/9789264070943-en
23. H. Beraldo, D. Gambino, *Mini-Rev. Med. Chem.* **4** (2004) 31
24. S. M. Cohen, *Curr. Opin. Chem. Biol.* **11** (2007) 115
25. M. Carocho, I. C. Ferreira, *Food Chem. Toxicol.* **51** (2013) 15
26. C. R. Kowol, E. Reisner, I. Chiorescu, V. B. Arion, M. Galanski, D. V. Deubel, B. K. Keppler, *Inorg. Chem.* **47** (2008) 11032
27. A. Tabassum, R. G. Bristow, V. Venkateswaran, *Cancer Treat. Rev.* **36** (2010) 230
28. J. Brozmanová, D. Mániková, V. Vlčková, M. Chovanec, *Arch. Toxicol.* **84** (2010) 919
29. A. S. Prasad, B. Bao, F. W. Beck, O. Kucuk, F. H. Sarkar, *Free Radical Biol. Med.* **37** (2004) 1182
30. M. Valko, H. Morris, M. T. Cronin, *Curr. Med. Chem.* **12** (2005) 1161
31. United States National Library of Medicine, Toxicology data network, <http://toxnet.nlm.nih.gov/cgi-bin/sis/htmlgen?CHEM> (accessed January 2013).



J. Serb. Chem. Soc. 78 (10) 1513–1530 (2013)
JSCS–4514

Comparative study of reactions between μ -nitrido- or μ -oxo-bridged iron tetrasulfophthalocyanines and sulfur-containing reductants

ILIA A. DEREVEN'KOV¹, SVETLANA S. IVANOVA¹, EVGENY V. KUDRIK¹,
SERGEI V. MAKAROV^{1*}, ANNA S. MAKAROVA² and PAVEL A. STUZHIN¹

¹State University of Chemistry and Technology, Engels Str. 7, 153000 Ivanovo, Russia and

²G. A. Krestov Institute of Solution Chemistry of the RAS, Akademicheskaya Str. 1,
153045 Ivanovo, Russia

(Received 19 January, revised 11 February 2013)

Abstract: A comparative study of reactivity of μ -nitrido- and μ -oxo-dimers of iron tetrasulfophthalocyanine has been performed in aqueous solutions of various acidity. The substantially higher stability of the nitrido-bridged structure under both strongly acidic and strongly alkaline environments was demonstrated. The reactions of the complexes with sulfur-containing reductants (sodium dithionite, thiourea dioxide, sodium hydroxymethanesulfinate, L-cysteine) were studied. Differences in reduction processes were explained.

Keywords: μ -nitrido dimer, μ -oxo dimer, iron phthalocyanine, reduction.

INTRODUCTION

A selective low-temperature oxidation of hydrocarbons (especially of methane) is the challenging problem of great practical importance. The naturally occurring methane mono-oxygenase enzyme (MMO) converts methane to methanol in aqueous solutions under mild conditions.^{1,2} The active site of the enzyme includes two non-heme iron atoms linked together by an oxygen bridge, and this structural feature determines the unique reactivity of MMO. μ -Oxo-dimers of iron complexes with tetrapyrrole macrocycles (porphyrins and phthalocyanines) have been intensively used in model reactions of hydrocarbon oxidation for a long time.^{3,4} Their catalytic activity in the oxidation of unsaturated hydrocarbons and alkanes with active C–H bonds (tertiary, allyl and benzyl) was demonstrated.^{5–9} In 2009, it was discovered that the μ -nitrido-dimer of iron phthalocyanine catalyzes the low-temperature oxidation of methane by hydrogen peroxide.¹⁰ The authors showed that this complex reacts with hydrogen peroxide to

* Corresponding author. E-mail: makarov@isuct.ru
doi: 10.2298/JSC130119019D

form the strong oxidant $\text{Fe}^{\text{IV}}\text{NFe}^{\text{VO}}$ *via* heterolytic O–O bond cleavage in the peroxide and that the presence of the binuclear Fe–N–Fe motif is a prerequisite for an effective catalysis. Further possibilities of other substrate activations by μ -nitrido-dimers of iron phthalocyanines and porphyrins were evidenced later.^{11–14}

Recent DFT calculations performed on the Fe-porphyrazine model¹⁵ disclosed the fact that the unique catalytic activity of iron μ -nitrido-dimers may be connected with the ability of the nitrido-bridge (in contrast to the oxo-one) to bear an excessive charge in transient redox species in catalytic cycle and to stabilize their low-spin states.

Hence, as μ -nitrido(bis-iron phthalocyanines) are highly reactive in oxidations of organic substrates by hydrogen peroxide, it could be expected that oxygen activation is quite feasible *via* their mediation as well. The ability of Fe-porphyrazine μ -nitrido-dimer to bind reversibly dioxygen was proven earlier.¹⁶ Dioxygen activation in the catalytic cycle obligatorily requires the participation of reductants in a fully reversible reduction step. In the case of μ -oxo-dimers applied as models of the MMO active site, the action of relatively weak reductants leads to the cleavage of the Fe–O bonds, with the formation of monomers.^{17,18}

Recently, the first successful synthesis of the water-soluble sulfo-derivative of the μ -nitrido Fe-phthalocyanine dimer $\mu\text{-N}(\text{FeTSPc})_2$ was reported.¹⁹ The synthesis was performed in two alternative ways: *i*) *via* the sulfonation of μ -nitrido-bridged Fe-phthalocyanine and *ii*) *via* the thermolysis of the azide complex of Fe-tetrasulphophthalocyanine in acetic acid.¹⁹ This work presents a comparative analysis of the stability of $\mu\text{-N}(\text{FeTSPc})_2$ (I) and $\mu\text{-O}(\text{FeTSPc})_2$ (II) (Fig. 1) in aqueous solutions, as well as of reactivity in reduction processes with sulfur-containing compounds, *viz.*, sodium dithionite, thiourea dioxide (TDO), sodium hydroxymethanesulfinate (HMS)²⁰ and L-cysteine.

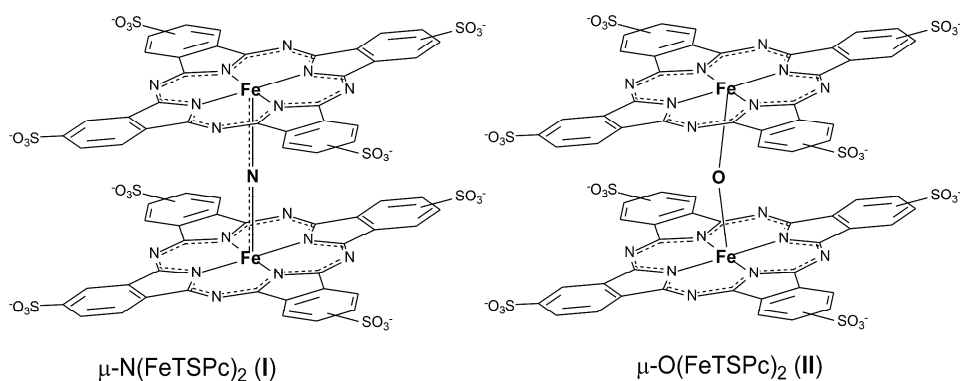


Fig. 1. The structures of the nitrido- and oxo-bridged complexes of iron tetrasulphophthalocyanine.

EXPERIMENTAL

Chemicals and methods

All reagents (Sigma–Aldrich) were used as received without further purification. Oxygen-free argon was used to deoxygenate the solutions. Britton–Robinson, phosphate and borate buffers were used to control the pH.

The IR-spectra were recorded on an Avatar 360 FT-IR spectrometer and the elemental composition of the complex was determined on a Flash EA CHNS-O Analyser. The UV–Vis spectra and kinetic traces were recorded on a thermostated Cary 50 spectrophotometer.

Experimental data were analyzed using the Origin 7.5 program. The rate constants were determined by fitting the absorbance vs. time curve to a single-exponential function implemented in the software. Calculations of equilibrium constants were performed by fitting the plots of absorbance vs. pH to sigmoidal (1) or double-sigmoidal (2) functions. The reported deviations are the calculated standard ones.

$$A = A_1 + \frac{A_1 - A_2}{1 + e^{(pH - pK_{a1})/d(pH)}} \quad (1)$$

$$A = A_1 + \frac{A_1 - A_2}{1 + e^{(pH - pK_{a1})/d(pH)}} + \frac{A_2 - A_3}{1 + e^{(pH - pK_{a2})/d(pH)}} \quad (2)$$

In these equations, A_1 , A_2 and A_3 are the absorbance values of the dominating species at each pH value.

Synthesis of μ -nitrido-bridged complex of iron tetrasulfophthalocyanine ammonium salt μ -N(FeTSPc)₂, I

μ -Nitrido-dimer of iron phthalocyanine μ -N(FePc)₂ (0.4 g), obtained according to a reported procedure,^{21,22} was dissolved in chlorosulfonic acid (15 ml). The mixture was heated for four hours at 150 °C and after cooling, the solution was left standing overnight. Then the mixture was poured on ice (300 g). The formed precipitate was collected by filtration, washed with cold water until the filtrate was sulfate-ion free and hydrolyzed in distilled water (100 mL) at 80 °C until fully dissolved. The solution was evaporated on a water bath, the residue was dissolved in 5 % ammonia solution (50 mL) and half of the solvent was evaporated. The solution of octa-ammonium salt **I** was purified by column chromatography (Molselect G10, eluent – water) collecting the middle fraction of blue zone. After solvent evaporation, the hydrate of the octa-ammonium salt **I** (0.34 g) was obtained. Yield: 48 %; Anal. Calcd. for (C₆₄H₃₂N₁₇S₈O₂₄Fe₂)·8NH₃·5H₂O: C, 38.10; H, 3.30; N, 17.36; S, 12.71 %. Found: C, 37.8; H, 3.2; N, 17.1; S, 12.6 %; IR (KBr, cm⁻¹): 913 (ν_{as} FeNFe), 1028 (ν_s S=O), 1151 (ν_{as} S=O); UV–Vis (DMSO) (λ_{max} / nm (ϵ / L mol⁻¹ cm⁻¹)): 336 (40800), 643 (43700).

Iron tetrasulfophthalocyanine was synthesized from 4-sulfophthalic anhydride as earlier proposed²³ and isolated as the μ -oxo-dimer μ -O(FeTSPc)₂, **II**. IR (KBr, cm⁻¹): 830 (ν_{as} FeOFe), 1029 (ν_s S=O), 1137, 1188 (ν_{as} S=O); UV–Vis (DMSO) (λ_{max} / nm (ϵ / L mol⁻¹ cm⁻¹)): 334 (112200), 636 (114800).

RESULTS AND DISCUSSION

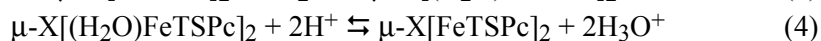
Stability in aqueous solutions

In the first step of the study, the stability of both complexes in aqueous aerobic solutions of various acidities was investigated. It was found that the

behavior of complexes **I** and **II** were substantially different in strongly acidic and strongly alkaline media.

Acidification of the μ -nitrido-dimer **I** solution resulted in a slight spectral change (Fig. 2a). During long storage in 0.1 M H₂SO₄, only a slow decrease at the initial absorption maxima was observed, which resulted from macrocycle destruction ($\tau_{1/2} = 15.5$ h at 25 °C), while no changes resulting from complex monomerization were observed. On the contrary, after the acidification of the μ -oxo-dimer **II** solution, the UV–Vis spectra were significantly altered, *i.e.*, the intensity of the initial Q-band at 632 nm decreased, the Q-band split with maxima at 642 and 679 nm, a small peak at 817 nm appeared and the Soret band shifted from 327 to 336 nm. After long exposure of complex **II** to 0.1 M H₂SO₄, a slow absorption decay was observed, indicating chromophore decomposition ($\tau_{1/2} = 12.5$ h at 25 °C). It should be noted that this spectral picture (Fig. 2b) was fully reversible, which confirms the acid–base character of the process.

In aqueous media, μ -dimers **I** and **II** (μ -X[FeTSPc]₂) axially bind water molecules and exist as di-aqua complexes (Reaction (3)):



There are several possible explanations of observed spectral changes in acidic media in the case of complex **II**. First, axial water molecules under acidic environment can be protonated and removed from the coordination sphere, which may lead to the formation of a five-coordinated μ -oxo-dimer (Reaction (4)). Due to an increase in excitonic interaction, the Q-band maximum in the spectra of six-coordinated μ -oxo-dimers is hypsochromically shifted as compared to the maximum of five-coordinated μ -oxo-complexes.²⁴ The same effect was also observed during the formation of six-coordinate dimers of Fe(III)-octaphenylporphyr-azine.²⁵

Secondly, in acidic media, acid–base interactions with the *meso*-nitrogen atoms of the macrocycle become possible. The splitting of the Q-band observed in UV–Vis spectrum of the product of μ -oxo-dimer **II** transformations at low pH values may result from the lowering of the symmetry of the *meso*-protonated phthalocyanine π -chromophore.

Thirdly, the protolytic dissociation of μ -dimers is possible in acidic media as previously observed, for example, in the case of Fe(III) μ -oxo-dimers of porphyrins, azaporphyrins and porphyrazines.^{26–28} The monomerization of iron μ -oxo-porphyrazines and μ -oxo-phthalocyanines was also shown to proceed in the presence of bases.¹⁷ Nevertheless, data on the monomerization of μ -nitrido-dimers is still unknown.

It should be noted that five-coordinated monomers of iron phthalocyanines are characterized by a single Q-band at 655–660 nm and an additional long-

wavelength band at ≈ 830 nm, but in the case of six-coordinated Fe-phthalocyanines, the Q-band is usually located at ≈ 680 nm in the UV-Vis spectrum.²⁹ The spectrum of an acidic solution of complex **II** includes peaks of all the above-mentioned species that may result from monomerization of complex **II**, giving a mixture of five- and six-coordinated iron tetrasulfophthalocyanines.

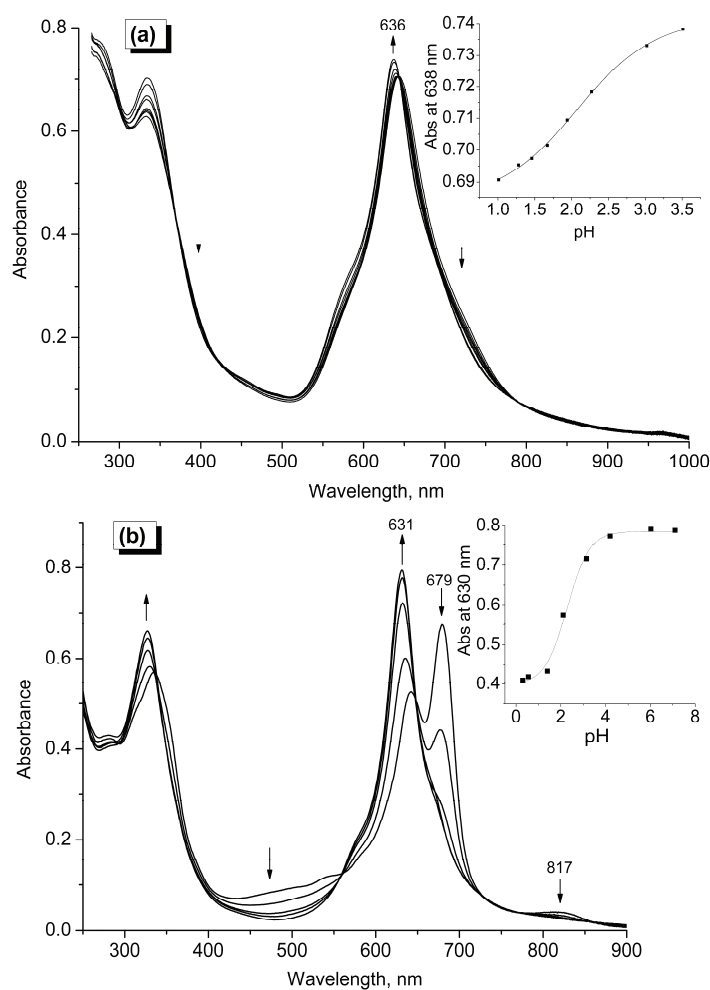


Fig. 2. UV-Vis spectral changes accompanied the pH-titration of both complex **I** ($c_{0,I} = 1.4 \times 10^{-5}$ M) (a) and **II** ($c_{0,II} = 6.1 \times 10^{-6}$ M) (b) during the titration from acidic media to neutral. Insets: pH-titration curves of both complex **I** and **II** at 25 °C, ionic strength = 0.2 M (ClO_4^-), aerobic conditions.

This suggestion is supported by the following experiments. The titration of complex **II** with thiocyanate in acidic media (pH 1.7) leads to a shift from a spec-

trum with the split Q-band to a spectrum with the single band at 679 nm (Fig. 3a). Simultaneously, the long-wave band at 817 nm, typical for five-coordinated iron(III) phthalocyanines, disappears. In the process, only one thiocyanate molecule became coordinated ($[\text{NCS}^-] \leq 0.1 \text{ M}$). Probably, the mixture of five- and six-coordinate Fe-tetrasulphophthalocyanine complexes after the addition of thiocyanate is transformed to a mixture of six-coordinated complexes. It is important to note that in weakly acidic media the addition of thiocyanate to complex **II** solution induces only slight spectral changes (Fig. 3b), which may be connected

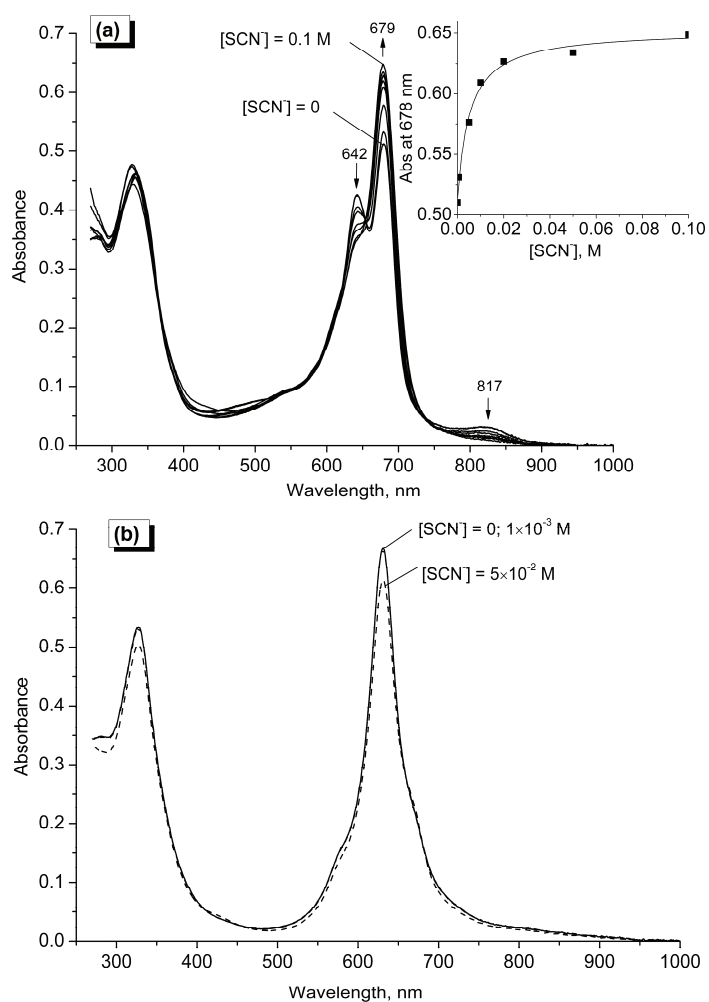
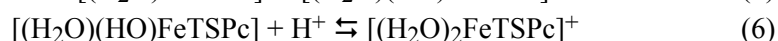
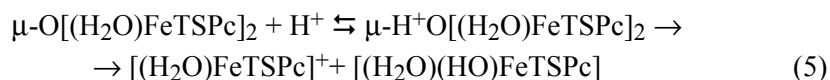


Fig. 3. UV-Vis spectral changes occurring during the titration of complex **II** ($c_{0,\text{II}} = 5.1 \times 10^{-6} \text{ M}$) by thiocyanate at pH 1.7 (a) and at pH 6.0 (b). Inset: titration curve of complex **II** by thiocyanate under aerobic conditions at pH 1.7, 25 °C, $I = 0.2 \text{ M}$ (ClO_4^-).

with difficulties in the substitution of an axial water in the oxo-dimer, as well as with the high stability of oxo-bridged structures to dissociation under the given conditions.

The observed value of $pK_{a(\text{obs})}$ determined during pH-titration of complex **II** (6.07×10^{-6} M) in acidic media and ionic strength 0.2 M was 2.29 ± 0.11 at 25 °C. After the addition of thiocyanate (0.1 M) to the mixture during the pH-titration in acidic media, a change of spectrum from one with a single Q-band at 679 nm to one with a single maximum at 631 nm was found. In the latter experiment, the $pK_{a(\text{obs})}$ value was increased up to 3.19 ± 0.02 . Thus, thiocyanate promotes oxo-dimer dissociation to monomeric species of Fe-tetrasulfophthalocyanine.

Thus, the above-mentioned differences in reactivity under environments of different acidities as well as spectral characteristics of the produced species indicate that complex **II** dissociates at low pH values giving a mixture of five- and six-coordinated Fe-tetrasulfophthalocyanine monomers (Reactions (5) and (6)):

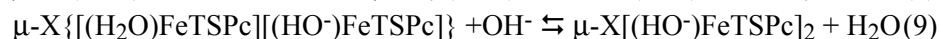
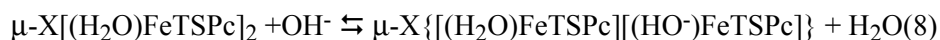


The value of $pK_{a(\text{obs})}$ can be recalculated using Eq. (7) to produce $pK_a = -3.10 \pm 0.11$, corresponding to Reaction (5):

$$pK_a = pK_{a(\text{obs})} + \log(2/3[\mathbf{II}]_0) \quad (7)$$

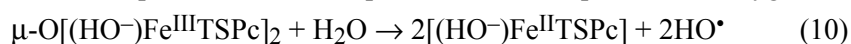
UV-Vis spectra recorded during the stage shown in Fig. 2a indicate relatively slight change in the structure of complex **I** after reaction with protons. The value of pK_a 2.09 ± 0.03 probably reflects both the protonation of the axial water molecule and its further dissociation (Reaction (4), protonation of the first water molecule).

Reactions of the oxo- and nitrido-dimers of iron tetrasulfophthalocyanine with hydroxide ions in alkaline media leads to the formation of aquahydroxo- and dihydroxocomplexes (Reactions (8) and (9)):



Complex **I** is relatively stable at pH 13 (the decrease in concentration was 3.7 % in 4 h at 25 °C), but a maximum at 667 nm, typical for $\text{Fe}^{\text{II}}\text{TSPc}$,³⁰ slowly appeared in the UV-Vis spectrum of complex **II** (observed rate constant is $k_{\text{obs.}} = (9.97 \pm 0.30) \times 10^{-5} \text{ s}^{-1}$ at pH 13 and 25 °C) simultaneously with the decay of $(\text{Fe}^{\text{III}}\text{TSPc})_2\text{O}$ peak (631 nm) (Fig. S-1 of the Supplementary material to this paper). The latter fact presumably resulted from reduction of complex **II** to $\text{Fe}^{\text{II}}\text{TSPc}$ (Reactions (10) and (11)). At the same time, the depletion of the oxo-bridged structure without electron transfer cannot be excluded, since the spectra of the six-coordinated $\text{Fe}^{\text{III}}\text{TSPc}$ and $\text{Fe}^{\text{II}}\text{TSPc}$ complexes are similar. This pro-

cess proceeds without chromophore decomposition under anaerobic conditions, but noticeable decomposition of the complex occurs in the presence of oxygen.



The pH-titration of complex **I** in alkaline media revealed the presence of two consecutive steps accompanied by weakly intensive but distinctly different spectral changes (Fig. S-2 of the Supplementary material to this paper). Probably, these steps correspond to the transformation of the nitrido-dimer to mono- and dihydroxo-species (Reactions (8) and (9), respectively, where X = N). The pK_a values of these equilibria were found to be 10.5 ± 0.1 and 12.9 ± 0.1 at 25 °C, respectively. These values were expectedly higher than those reported for Fe(III) complexes of octakis(benzenesulfonato)porphyrazine (7.5 and 11.16 at 25 °C³¹) and porphyrins (*e.g.*, for *meso*-tetrakis(4-*N*-methylpyridiniumyl)porphyrin, the pK_a values are of 5.0 and 11.9 at 25 °C³²), which results from the lesser propensity of the nitrido-dimer to bind axial ligands.

Reactions with reductants

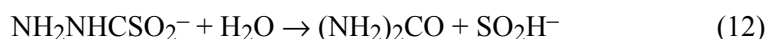
To date, the study of $\mu\text{-N}(\text{FePc})_2$ reduction in pyridine solution was the subject of only one paper.²² Particularly, it was shown that this complex can be involved in three reversible reduction steps, but at potentials lower than -1.29 V, the dimer structure is destroyed giving two reduced monomer moieties per one nitrido-dimer unit. Earlier reported data,²² summarized in Table I, demonstrates the substantial stabilization of high-valent iron ions in the nitrido-dimer as compared to corresponding monomer. The transfer of the first electron on the iron ion in the +3.5 formal oxidation state occurs in the potential region near to that of Fe^{2+} phthalocyanine monomer reduction. It is also known that the two-electron reduction of the Fe^{3+} phthalocyanine oxo-dimer proceeds fully irreversibly, leading to the decay of the dimer structure.³³

TABLE I. Potentials of reduction stages of $(\text{FePc})_2\text{N}$ and FePc ²²

Redox stage	$E_{1/2} / \text{V}$	
	$(\text{FePc})_2\text{N}$	FePc
0/-1	-0.83	-0.96
-1/-2	-1.02	-1.29
-2-3	-1.29	-

It should be noted that above-mentioned study of $\mu\text{-N}(\text{FePc})_2$ reduction was performed in the strongly coordinating solvent pyridine, which may facilitate the monomerization of dimers. Thus, some questions remain open, such as how fast does the decomposition of the nitrido-dimer to iron(II) phthalocyanine occur during its reduction in water and can complex **I** form more reduced states?

In the present study, the reduction of both complexes **I** and **II** with thiourea dioxide (TDO, $(\text{NH}_2)_2\text{CSO}_2$) was studied under anaerobic conditions. The reactions were accompanied by significant UV–Vis spectral changes and occurred at relatively low rates at pH 7.8. The latter is caused by the moderate rate of TDO decomposition in weakly alkaline solutions giving the strong reducing agent – sulfoxylate, SO_2H^- (SO_2^{2-}) (reaction (12)):³⁴



During the first reduction step of complex **I**, a sharp isosbestic point was observed at 498 nm that supports the presence in system of only two absorbing species; a slight shift of the Q-band from 636 to 631 nm also occurred. The second reduction step was accompanied by substantial changes in UV–Vis spectrum, *i.e.* a decrease in the intensity of the Q-band, the appearance of a new band at 500 nm and an absorption increase in the near-IR region (Fig. 4a). During the third step, both an increase of the absorption band at 655 nm and a decay of the band at 483 nm were observed (not shown). The same picture emerges during the use of either dithionite ($\text{S}_2\text{O}_4^{2-}$) or hydroxymethanesulfinate ($\text{HOCH}_2\text{SO}_2^-$) as the reductant under moderately alkaline conditions. The highest reduction rate was observed in the case of sulfoxylate (SO_2H^- has been obtained after TDO “aging” under strongly alkaline anaerobic conditions for four hours³⁵); a slower reaction proceeded when dithionite is used while the slowest reaction rates were observed using hydroxymethanesulfinate as the reductant. Moreover, the reaction rates at the final step had the highest values in neutral and weakly alkaline media and were substantially retarded at higher pH values, which was probably due to the transformation of the nitrido-dimer into the inert dihydroxocomplex.

The reduction of complex **II** included two consecutive stages (Fig. 4b): an increase in the UV–Vis maximum at 668 nm with a simultaneous absorption decrease at 631 nm and the subsequent appearance of a new band at 490 nm with a simultaneous decay of peak at 668 nm. These stages corresponded to the reduction of $(\text{Fe}^{\text{III}}\text{TSPc})_2\text{O}$ to $\text{Fe}^{\text{II}}\text{TSPc}$ and the reduction of $\text{Fe}^{\text{II}}\text{TSPc}$ to the Fe^{II} -anion-radical of tetrasulfophthalocyanine, respectively.³⁰ The use of sulfoxylate enabled the occurrence of the following electron transfers, which resulted in the formation of the formally Fe(0) state. According to DFT data, the most probable electromer of the latter species is the Fe^{II} -anion-biradical.^{30,36} Note, the latter process did not occur when dithionite or hydroxymethanesulfinate were added.

The distinct difference in UV–Vis changes during the reduction of complexes **I** and **II** is the absence in the first case of a species absorbing at ≈ 670 nm, which corresponds to $\text{Fe}^{\text{II}}\text{TSPc}$. To gain further insight into this fact, a titration of complex **I** with dithionite was performed. It is well known that dithionite serves as a two-electron reductant; thus, its application allows the exact number

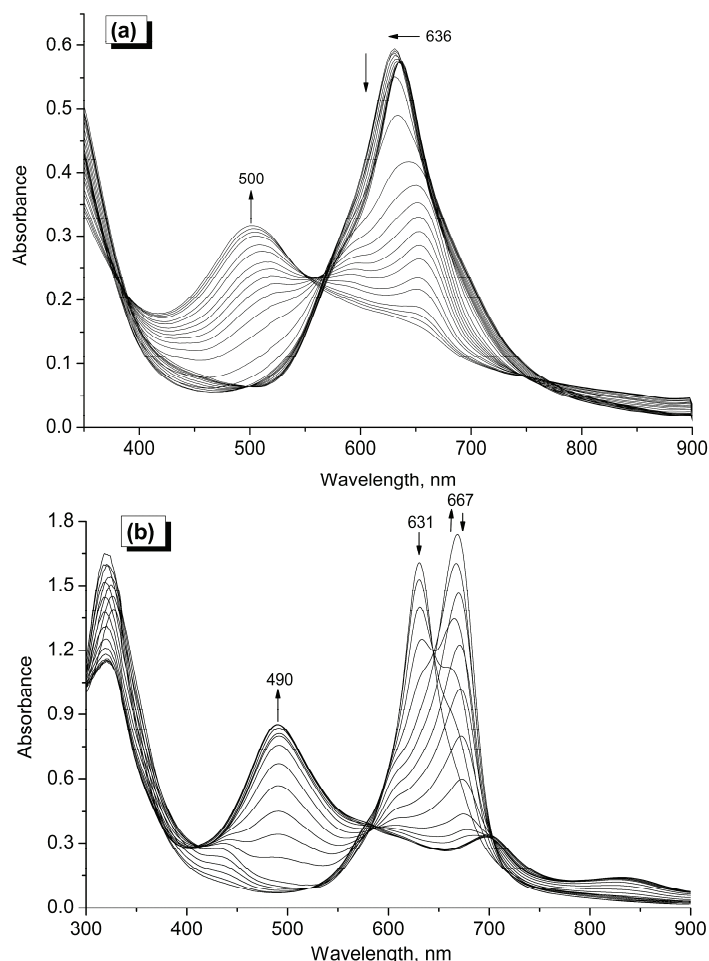


Fig. 4. Changes in the UV–Vis spectra during the reduction of complex **I** ($c_{0,I} = 1.1 \times 10^{-5}$ M, $\tau = 90$ min) (a) and complex **II** ($c_{0,II} = 1.3 \times 10^{-5}$ M, $\tau = 70$ min) (b) by TDO (5×10^{-4} M) at pH 7.8, 25 °C.

of electrons received by the complex during the reduction to be established. Moreover, dithionite possesses a significant reactivity in this process (reduction by dithionite at concentrations comparable with that of the nitrido-dimer occur in a few seconds or tens of minutes, depending on pH). The dithionite concentration can be exactly determined from the absorbance at 315 nm (extinction coefficient is $8043 \text{ M}^{-1} \text{ cm}^{-1}$).³⁷

The titration of complex **I** with dithionite (Fig. 5a) resulted in UV–Vis spectra different from those observed in the course of reaction between nitrido-dimer and excess of TDO. The transfer of the first electron from the added dithionite to the complex gave $\text{TSPcFe}^{\text{III}}\text{---N---Fe}^{\text{III}}\text{TSPc}$, which was accompanied by a slight

blue shift of the Q-band (similar to that observed during first reduction stage of complex **I** by TDO). However, the transfer of two or more electrons to the nitrido-dimer resulted in the appearance in the spectra of bands at 667 nm that were absent during reduction by excess TDO. It should be emphasized that the appearance of these bands in the UV-Vis spectrum corresponds to electron transfer(s) on the nitride-dimer and its further decomposition to monomer (*vide infra*). The UV-Vis spectrum of the final product formed after the three-electron reduction of $\text{TSPcFe}^{\text{III}/2}\text{---N---Fe}^{\text{III}/2}\text{TSPc}$ coincides with the spectrum of $\text{Fe}^{\text{II}}\text{TSPc}$. The spectra of two- and four-electron reduced $\text{TSPcFe}^{\text{III}/2}\text{---N---Fe}^{\text{III}/2}\text{TSPc}$ complexes include peaks of the corresponding monomers.

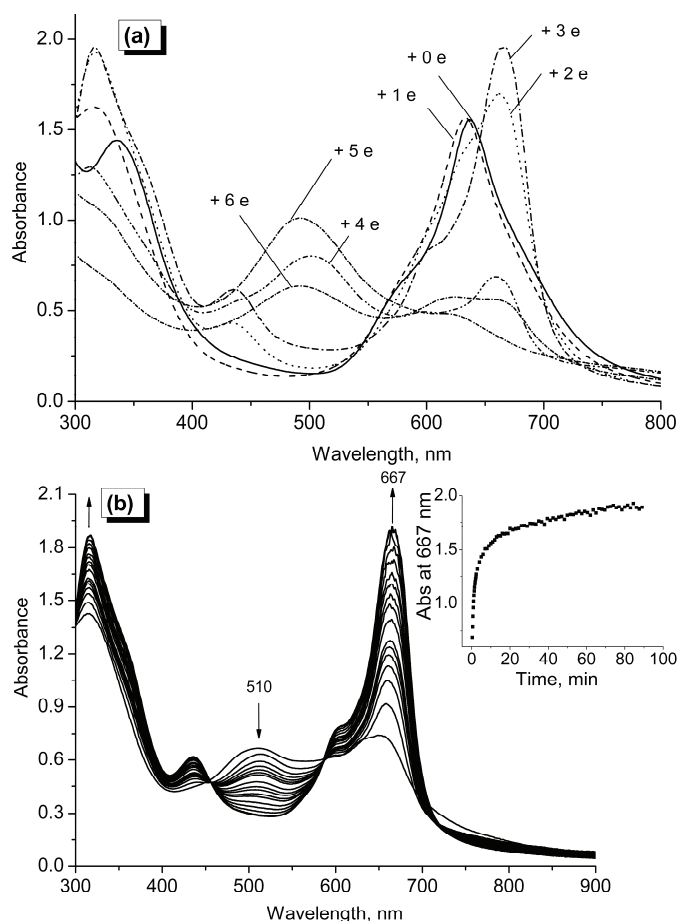


Fig. 5. UV-Vis spectra of dithionite reduced species of complex **I** recorded one hour after mixing the reagents (a) and the spectral changes during the decay of the three-electron reduced complex **I** ($c_{0,\text{I}} = 2.9 \times 10^{-5}$ M) (b) at pH 8.8, 25 °C. Inset: kinetic trace corresponding to the stage shown in Fig. 5b.

The addition of 1.5-fold excess of dithionite to complex **I** in weakly alkaline media resulted in a rapid spectral change (Fig. 5b, first spectrum) that likely resulted from the transfer of three electrons to the nitrido-dimer. Probably, the electrons are received in this case predominantly by the macrocycles since the UV–Vis spectrum of the product includes an absorption maximum at ≈ 500 nm, observed in the spectra of metallophthalocyanine anion-radicals.^{38–40} It is likely that $N(\text{Fe}^{\text{III}}\text{TSPc}^*)_2$ is formed during the three-electron transfer. The nitrido-dimer existing in this state is unstable and further decomposes to $\text{Fe}^{\text{II}}\text{TSPc}$. The rate constant of the decay stage was found to be $(1.18 \pm 0.05) \times 10^{-2} \text{ s}^{-1}$ (25 °C, pH 8.8). This value again indicates higher stability of the nitrido-dimer, since the oxo-dimer decomposition after achievement of the Fe^{II} -state proceeds much faster. The latter implies an important feature of the nitrido-dimer: in the presence of excess reducing agent, the fast reduction of unstable species and the achievement of lower oxidation states (being potentially more stable) become possible.

A comparative study of formally Fe^{I} -complexes produced after reduction of nitrido- and oxo-dimers was performed. Electromerism of tetrapyrroles existing in this oxidation state was the subject of some studies.^{41,42} DFT calculations performed on iron porphyrins models revealed evidence of macrocycle reduction in the course of electron transfer onto Fe^{II} , albeit electromerism remains possible depending on the nature of the axial and equatorial ligands. Phthalocyanines possess stronger electron-withdrawing properties than porphyrins used in above-mentioned calculations. Moreover, sulfo-groups result in a further increase of the electron-withdrawing properties of phthalocyanine. In addition, Fe^{I} -phthalocyanines have absorption maxima in the UV–Vis spectra at approximately 500 nm, *i.e.*, in the region of absorption maxima of phthalocyanines and porphyrins anion-radicals.^{38–40} Thus, the data mentioned above allows the conclusion that the formally Fe^{I} -oxidation state of tetrasulfophthalocyanines corresponded to the Fe^{II} -phthalocyanine-anion-radical structure.

The UV–Vis spectra of the Fe^{II} -anion-radicals of complexes **I** and **II** obtained after reduction by sodium dithionite are distinctly different. The spectrum of Fe^{II} -radical of nitrido-dimer significantly depended on the pH value of the solution, *i.e.*, in neutral media, the UV–Vis spectrum included one small intensity maximum at 480 nm, while in strongly alkaline media, intensive maxima at 330, 485 and 707 nm were observed (Fig. 6a). The same situation existed after use of TDO and HMS as reducing agents. The spectra of the Fe^{II} -anion-radicals obtained after reduction of the oxo-dimer by dithionite and TDO were pH-independent in neutral and alkaline media (Fig. 6b).

It was found that the Fe^{II} -radical of complex **I** participates in two acid–base equilibria in an alkaline environment. The $\text{p}K_{\text{a}}$ of the first transformation (8.3 ± 0.3) was found with a considerable degree of uncertainty because of an interference of a subsequent process. The $\text{p}K_{\text{a}}$ of the second equilibrium (10.01 ± 0.05) was found

by spectrophotometric titration at 707 nm where the influence of the first process is minimal. It is likely that during these stages, mono- (reaction (13)) and dihydroxo-species (reaction (14)) are formed. These transformations are supported by a significant reaction rate decrease of the subsequent reduction step in the case of both dithionite and HMS in strongly alkaline media, since hydroxo-species of metallo complexes are less reactive in redox processes as compared to their aqua forms:

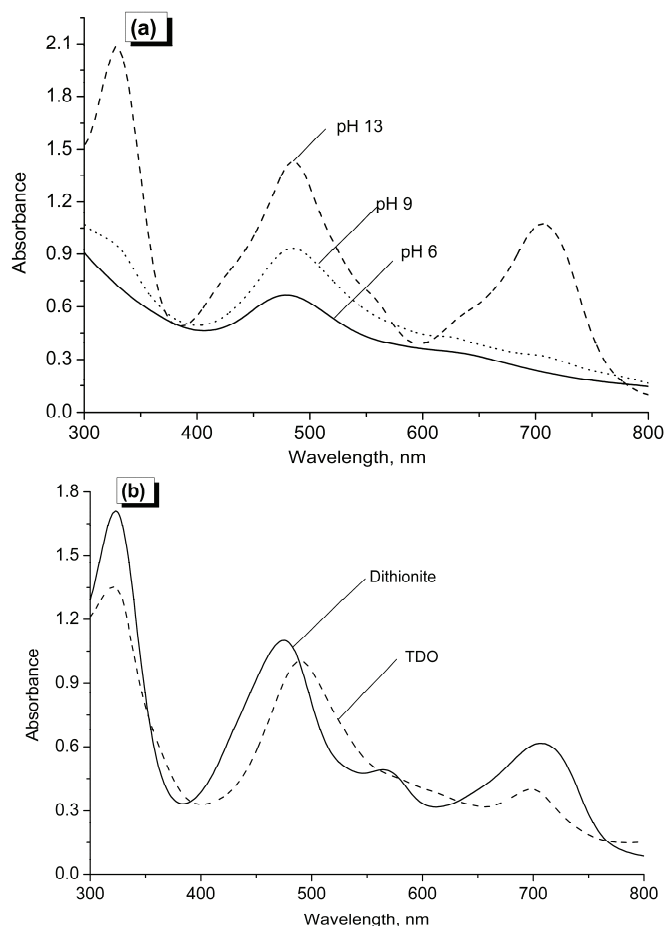
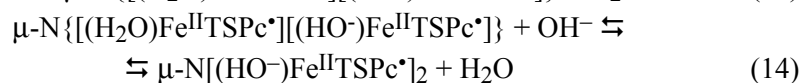
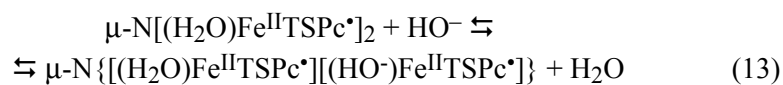
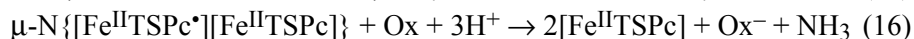


Fig. 6. UV-Vis spectra of Fe^{II} -phthalocyanine-radicals of complexes I (a) and II (b).
 $c_{0,\text{I}} = 2.7 \times 10^{-5} \text{ M}$; $c_{0,\text{II}} = 1.3 \times 10^{-5} \text{ M}$.

The noticeable difference in the UV–Vis spectra of the Fe^{II}-radicals of complexes **I** and **II** results from the inequality of their structures. In addition, the formed species possess different acid–base properties; the nitrido-dimer is capable of receiving one extra electron from both dithionite and HMS in contrast to the oxo-one. Perhaps, the strong reductant readily donates electrons to the nitrido-complex transiently existing in the unstable Fe^{II}-state and shifts it to the more stable Fe^{II}-anion-radical form.

Fe^{II}-anion-radicals are known to be potent reducing agents.^{30,43} The oxidation by air of Fe^{II}-anion-radicals prepared by the reaction between complex **II** and sulfur-containing reductants leads to Fe^{II}TSPc and further complex bleaching. Fe^{III}-state regeneration in this case is unfeasible. Bleaching in this case is likely to be connected with the formation of SO₅[−], being a strong oxidant produced by the reaction of sulfite with dioxygen (or reactive oxygen species)^{43,44} that is capable of destroying the macrocycle. In the presence of relatively mild oxidants (*e.g.*, nitrite), the Fe^{II}-anion-radical is oxidized to Fe^{II}TSPc without chromophore depletion. The oxidation of Fe^{II}-anion-radical of complex **I** by air also results in macrocycle destruction. Its oxidation by nitrite or iodine gives Fe^{II}-complexes spectrally similar to that of Fe^{II}TSPc and no complex bleaching in this case occurs. However, the latter oxidation process includes two-stages proceeding at different rates (*e.g.*, during the oxidation by nitrite at pH 7.8, 25 °C $k_1 = 0.21 \pm 0.01$ and $k_2 = 0.054 \pm 0.002 \text{ M}^{-1} \text{ s}^{-1}$), in contrast to the one-step oxidation of the Fe^{II}-anion-radical prepared from complex **I**. Probably, the first constant in this reaction corresponds to electron transfer from metallocomplex to the oxidant while the second is connected with the monomerization of dimer (reactions (15) and (16), respectively).



where Ox = oxidant.

The use of L-cysteine as a reductant of complex **I** and of complex **II** did not lead to the formation of any strongly reduced states. The UV–Vis spectra of the final reaction products are shown in Fig. 7. The same spectra could be obtained after careful aerial oxidation of a corresponding Fe^{II}-anion-radicals followed by L-cysteine addition. These complexes can be formed under both anaerobic and aerobic conditions, although in the latter case, the reaction proceeded much slower, that may have been caused either by aerial metallocomplex oxidation or by oxidative cysteine conversion to cystine. Apparently, the products of these processes were Fe^{II}-dithiolate complexes spectrally similar to other hexacoordinated complexes of Fe^{II}-phthalocyanines^{45,46} and porphyrazines.⁴⁷ An interaction of the complexes with nitrite resulted in their rapid reversion giving spec-

tra identical to those of the corresponding nitrite-oxidation product of the Fe^{II} -anion-radical.

Based on the herein presented experimental results and published data,^{22,33} two schemes for the reduction of complex **II** and of complex **I** are proposed (Scheme 1 and 2, respectively).

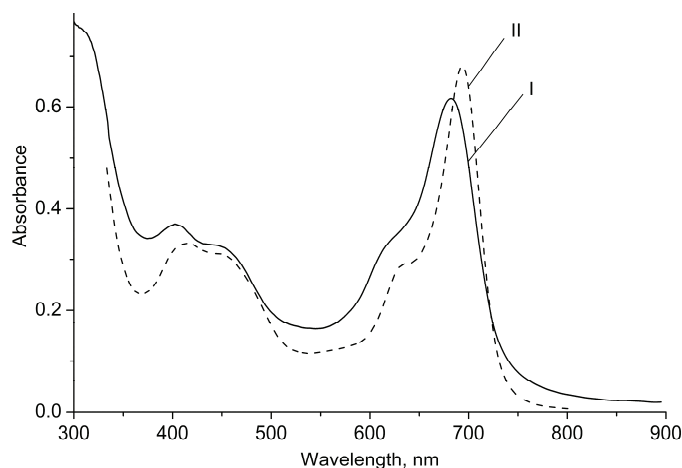
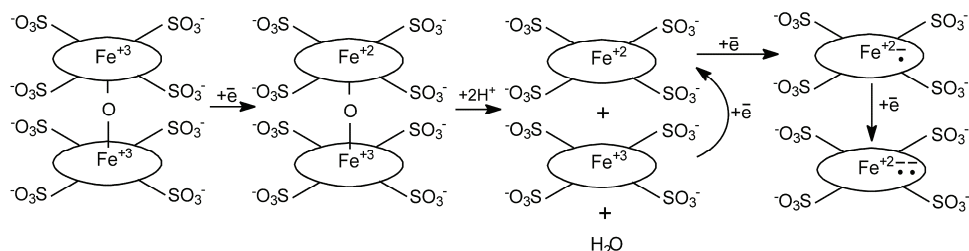
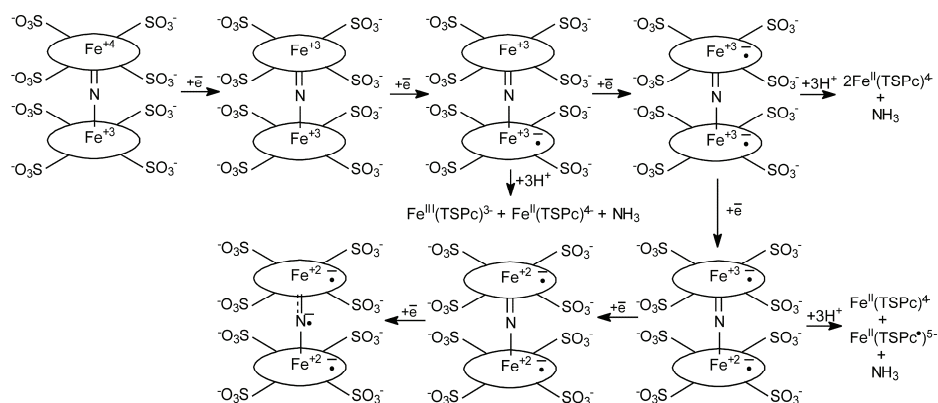


Fig. 7. UV-Vis spectra of L-cysteine (0.15 M) reduced complexes **I** ($c_{0,\text{I}} = 1.2 \times 10^{-5}$ M) and **II** ($c_{0,\text{II}} = 0.9 \times 10^{-5}$ M) at pH 10, 25 °C.



Scheme 1. Reduction of the μ -oxo-dimer of iron tetrasulfophthalocyanine.

To summarize, an investigation of reduction reactions of complexes **I** and **II** by sulfur-containing reductants demonstrated the low stability of Fe^{II} -dimers. It was established that stability of Fe^{II} -dimer with the nitrido-bridge was noticeably higher in comparison to oxo-one. Apparently, the nitrido-bridge provides the possibility for **I** to accept additional electrons without dimer structure decay in the presence of excess reductant. A comparison of the UV-Vis spectral data, acid-base properties and reactivity of the Fe^{II} -anion-radicals produced during the reduction of complexes unambiguously manifests their structural difference.

Scheme 2. Reduction of the μ -nitrido-dimer of iron tetrasulfophthalocyanine.

CONCLUSIONS

A comparative study of water-soluble μ -oxo- and μ -nitrido-dimers of iron tetrasulfophthalocyanine in aqueous media of various pH values has been presented. The higher stability of the nitrido-bridged structure in comparison to oxo-dimer in strongly acidic and strongly alkaline environments was demonstrated. The involvement of the nitrido-bridged complex in three reversible acid–base interactions was revealed. For the first time, the ability of a nitride-dimer to accept six electrons from strong reductants (*viz.*, dithionite, thiourea dioxide and hydroxymethanesulfinate) was evidenced. It was proved that both reduced dimers containing iron in +2 oxidation state possess low stability. The structural difference of Fe^{II}-anion-radicals was stressed. It was shown that the μ -nitrido-dimer moiety stabilizes iron cations in high oxidation states.

SUPPLEMENTARY MATERIAL

Figures S-1 and S-2 are available electronically at <http://www.shd.org.rs/JSCS/>, or from the corresponding author on request.

Acknowledgements. This work was supported by the Russian Foundation for Basic Research, Project No. 12-03-00563.

ИЗВОД

ИСПИТИВАЊЕ РЕАКЦИЈА ИЗМЕЂУ μ -НИТРИДО- И μ -ОКСО-ГВОЖЂЕ-
-ТЕТРАСУЛФОФТАЛОЦИЈАНИНА И РЕДУКЦИОНИХ СРЕДСТАВА
КОЈА САДРЖЕ СУМПОР

ILIA A. DEREVEN'KOV¹, SVETLANA S. IVANOVA¹, EVGENY V. KUDRIK¹, SERGEI V. MAKAROV¹, ANNA S. MAKAROVA² и PAVEL A. STUZHIN¹

¹ State University of Chemistry and Technology, Engels Str. 7, 153000 Ivanovo, Russia и ² G. A. Krestov Institute of Solution Chemistry of the RAS, Academicheskaya Str. 1, 153045 Ivanovo, Russia

У овом раду је упоређивана реактивност μ -нитридо- и μ -оксо-димера гвожђе-тетра-сулфофталоцијанина у воденој средини при различитим рН вредностима. Утврђено је да

је комплекс са нитридо-мосним лигандом знатно стабилнији у киселој и у базној средини. Испитиване су реакције одговарајућих комплекса са редукционим средствима која садрже сумпор (натријум-дитионит, тиоуреа-диоксид, натријум-хидроксиметансулфинат и L-цистеин) и објашњене разлике у одговарајућим редокс процесима.

(Примљено 19. јануара, ревидирано 11. фебруара 2013)

REFERENCES

1. A. C. Rosenzweig, C. A. Frederick, S. J. Lippard, P. Norlund, *Nature* **366** (1993) 537
2. H. Basch, K. Mogi, D. G. Musaev, K. Morokuma, *J. Am. Chem. Soc.* **121** (1999) 7249
3. S. V. Barkanova, V. M. Derkacheva, I. A. Zheltukhin, O. L. Kaliya, E. A. Luk'yanets, *Zh. Org. Khim.* **21** (1985) 2018 (in Russian)
4. P. E. Ellis Jr., J. E. Lyons, *Coord. Chem. Rev.* **105** (1990) 181
5. L. Weber, G. Haufe, D. Rehorek, H. Hennig, *J. Chem. Soc., Chem. Commun.* (1991) 502
6. H.-Y. Hu, Q. Jiang, Q. Liu, J.-X. Song, W.-Y. Ling, C.-C. Guo, *J. Porphyrins Phthalocyanines* **10** (2006) 948
7. X.-T. Zhou, Q.-H. Tang, H.-B. Ji, *Tetrahedron Lett.* **50** (2009) 6601
8. H. M. Neu, V. V. Zhdankin, V. N. Nemykin, *Tetrahedron Lett.* **51** (2010) 6545
9. H. M. Neu, M. S. Yusubov, V. V. Zhdankin, V. N. Nemykin, *Adv. Synth. Catal.* **351** (2009) 3168
10. A. B. Sorokin, E. V. Kudrik, D. Bouchu, *Chem. Commun.* **22** (2008) 2562
11. E. V. Kudrik, P. Afanasiev, D. Bouchu, J.-M. M. Millet, A. B. Sorokin, *J. Porphyrins Phthalocyanines* **12** (2008) 1078
12. P. Afanasiev, D. Bouchu, E. V. Kudrik, J.-M. M. Millet, A. B. Sorokin, *Dalton Trans.* **44** (2009) 9828
13. E. V. Kudrik, A. B. Sorokin, *Macroheterocycles* **4** (2011) 154
14. E. V. Kudrik, P. Afanasiev, L. X. Alvarez, P. Dubourdeaux, M. Clémancey, J.-M. Latour, G. Blondin, D. Bouchu, F. Albrieux, S. E. Nefedov, A. B. Sorokin, *Nature Chem.* **4** (2012) 1024
15. R. Silaghi-Dumitrescu, S. V. Makarov, M.-M. Uta, I. A. Dereven'kov, P. A. Stuzhin, *New J. Chem.* **35** (2011) 1140
16. P. A. Stuzhin, L. Latos-Grazynski, A. Jezierski, *Transition Met. Chem. (London)* **14** (1989) 341
17. F. Monacelli, *Inorg. Chim. Acta* **254** (1997) 285
18. A. Mot, K. Zoltan, D. A. Svistunenko, G. Damian, R. Silaghi-Dumitrescu, S. V. Makarov, *Dalton Trans.* **39** (2010) 1464
19. P. A. Stuzhin, S. S. Ivanova, I. Dereven'kov, S. V. Makarov, R. Silaghi-Dumitrescu, H. Homborg, *Macroheterocycles* **5** (2012) 175
20. S. V. Makarov, R. Silaghi-Dumitrescu, *J. Sulfur Chem.* **34** (2013) 444
21. B. J. Kennedy, K. S. Murray, H. Homborg, W. Kalz, *Inorg. Chim. Acta* **134** (1987) 19
22. L. A. Bottomlley, J.-N. Gorce, V. L. Goedken, C. Ercolani, *Inorg. Chem.* **24** (1985) 3733
23. J. N. Weber, D. H. Busch, *Inorg. Chem.* **4** (1965) 469
24. S. Sieversten, K. S. Murray, B. Moubaraki, K. J. Berry, Y. Korbatieh, J. D. Cashion, L. J. Brown, H. Homborg, *Z. Anorg. Allg. Chem.* **620** (1994) 1203 (in German)
25. P. A. Stuzhin, I. S. Migalova, B. D. Berezin, *Russ. J. Inorg. Chem.* **43** (1998) 1536
26. P. A. Stuzhin, M. Hamdush, B. D. Berezin, *Russ. J. Phys. Chem.* **70** (1996) 747
27. O. A. Golubchikov, B. D. Berezin, I. M. Kazakova, M. B. Berezin, *Zh. Obshch. Khim.* **52** (1982) 83 (in Russian)

28. P. A. Stuzhin, A. Ul-Haq, S. E. Nefedov, R. S. Kumeev, O. I. Koifman, *Eur. J. Inorg. Chem.* **16** (2011) 2567
29. B. J. Kennedy, K. S. Murray, P. R. Zwack, H. Homborg, W. Kalz, *Inorg. Chem.* **25** (1986) 2539
30. E. V. Kudrik, S. V. Makarov, A. Zahl, R. van Eldik, *Inorg. Chem.* **44** (2005) 6470
31. A. Theodoridis, J. Maigut, R. Puchta, E. V. Kudrik, R. van Eldik, *Inorg. Chem.* **47** (2008) 2994
32. S. C. M. Gandini, E. A. Vidoto, O. R. Nascimento, M. Tabak, *J. Inorg. Biochem.* **94** (2003) 127
33. L. A. Bottomley, C. Ercolani, J.-N. Gorce, G. Pennesi, G. Rossi, *Inorg. Chem.* **25** (1986) 2338
34. S. V. Makarov, *Russ. Chem. Rev.* **70** (2001) 885
35. S. V. Makarov, E. V. Kudrik, R. van Eldik, E. V. Naidenko, *J. Chem. Soc., Dalton Trans.* (2002) 4074
36. Z. Kis, R. Silaghi-Dumitrescu, *Int. J. Quantum Chem.* **110** (2010) 1848
37. C. E. McKenna, W. G. Gutheil, W. Song, *Biochim. Biophys. Acta* **1075** (1991) 1091
38. J. Mack, M. J. Stillman, *Inorg. Chem.* **36** (1997) 413
39. J. Mack, M. J. Stillman, *J. Porphyrins Phthalocyanines* **5** (2001) 67
40. A. Erdoğan, I. A. Akinbulu, T. Nyokong, *Polyhedron* **29** (2010) 2352
41. C. S. Porro, D. Kumar, S. P. de Visser, *Phys. Chem. Chem. Phys.* **11** (2009) 10219
42. R. Silaghi-Dumitrescu, S. V. Makarov, *J. Biol. Inorg. Chem.* **15** (2010) 977
43. E. S. Ageeva, E. A. Vlasova, S. V. Makarov, A. S. Makarova, *Izv. Vyssh. Uchebn. Zaved., Khim. Khim. Tekhnol.* **53** (2010) 74 (in Russian)
44. A. S. Pogorelova, S. V. Makarov, E. S. Ageeva, R. Silaghi-Dumitrescu, *Russ. J. Phys. Chem., A* **83** (2009) 2050
45. E. A. Ough, M. J. Stillman, *Inorg. Chem.* **33** (1994) 573
46. V. N. Nemykin, I. N. Tret'yakova, S. V. Volkov, V. D. Li, N. G. Mekhryakova, O. L. Kaliya, E. A. Luk'yanets, *Russ. Chem. Rev.* **69** (2000) 325
47. P. A. Stuzhin, *Macroheterocycles* **2** (2009) 114 (in Russian).

SUPPLEMENTARY MATERIAL TO
Comparative study of reactions between μ -nitrido- or μ -oxo-bridged iron tetrasulfophthalocyanines and sulfur-containing reductants

ILIA A. DEREVEN'KOV¹, SVETLANA S. IVANOVA¹, EVGENY V. KUDRIK¹,
 SERGEI V. MAKAROV^{1*}, ANNA S. MAKAROVA² and PAVEL A. STUZHIN¹

¹State University of Chemistry and Technology, Engel's Str. 7, 153000 Ivanovo, Russia and

²G. A. Krestov Institute of Solution Chemistry of the RAS, Academicheskaya Str. 1, 153045 Ivanovo, Russia

J. Serb. Chem. Soc. 78 (10) (2013) 1513–1530

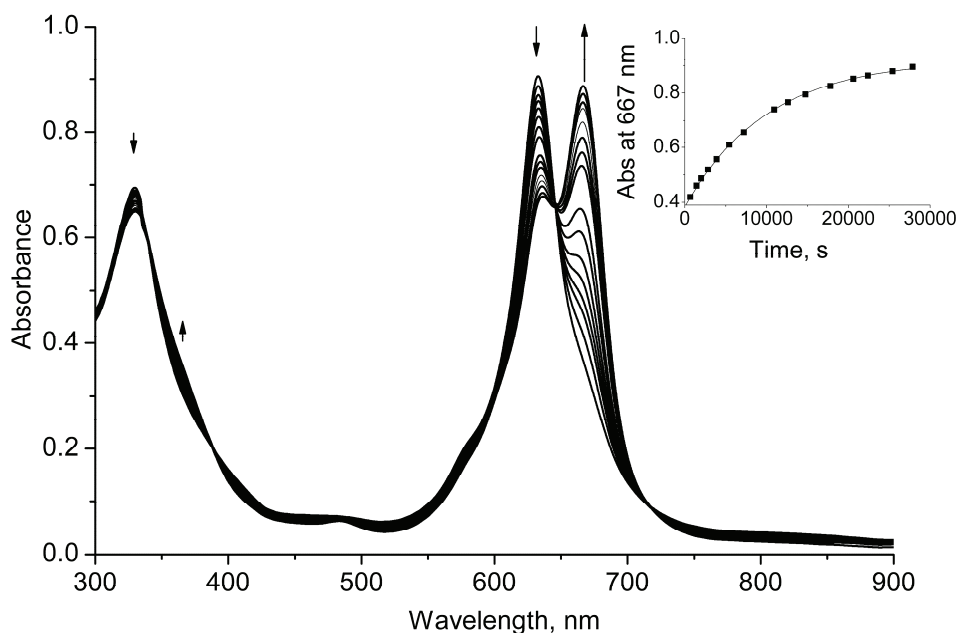


Fig. S-1. UV–Vis spectral changes recorded during the reaction of complex **II** ($c_{0,II} = 7 \times 10^{-6}$ M) with alkali. Inset: kinetic curve of above-mentioned process at pH 13, at 25 °C under anaerobic conditions.

* Corresponding author. E-mail: makarov@isuct.ru

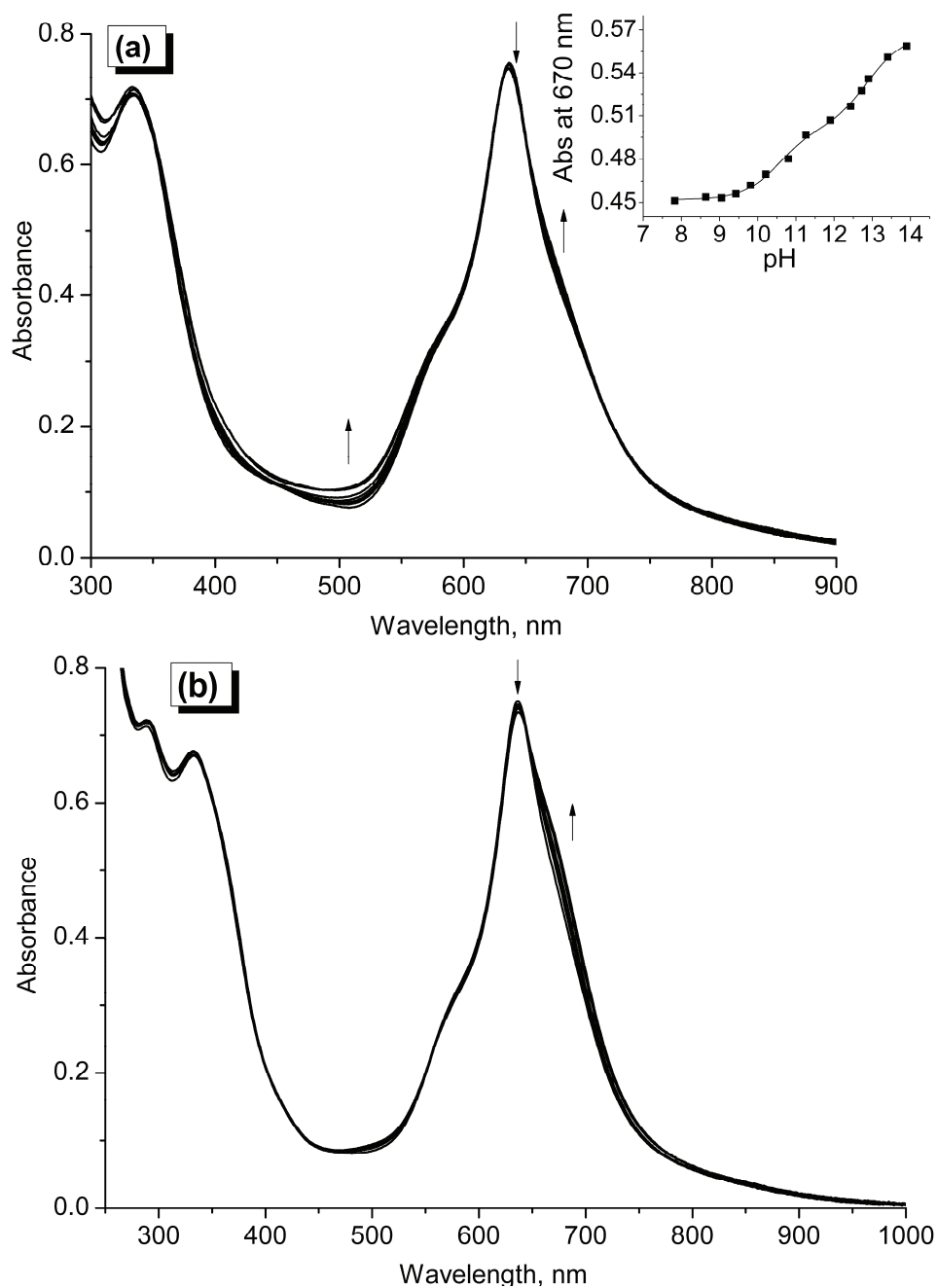
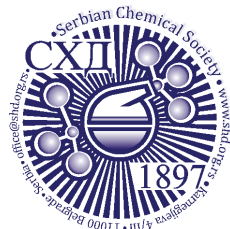


Fig. S-2. Spectral changes accompanied the titration of complex I (1.4×10^{-5} M) in alkaline media: pH 7.5–11.0 (a) and 11.0–14.0 (b). Inset: pH-titration curve of complex I at 25 °C under aerobic conditions.



J. Serb. Chem. Soc. 78 (10) 1531–1537 (2013)
JSCS–4515

SHORT COMMUNICATION

**Synthesis, characterization and crystal structure of butyl
N-(3-chloropropyl)-(2*S*)-alaninate hydrochloride**

DEJANA P. DIMITRIJEVIĆ¹, SLAĐANA B. NOVAKOVIĆ^{2*}, GORDANA R. RADIĆ³,
VERICA V. JEVTIĆ^{1#}, LAURA MENÉNDEZ-TABOADA⁴, SANTIAGO
GARCÍA-GRANDA⁴ and SREĆKO R. TRIFUNOVIĆ^{1#}

¹Department of Chemistry, Faculty of Science, University of Kragujevac, Radoja Domanovića
12, 34000 Kragujevac, Serbia, ²Vinča Institute of Nuclear Sciences, Laboratory of Theoretical
Physics and Condensed Matter Physics, University of Belgrade, P. O. Box 522, 11001
Belgrade, Serbia, ³Faculty of Medical Sciences, University of Kragujevac, Svetozara
Markovića 69, 34000 Kragujevac, Serbia and ⁴Physical and Analytical Chemistry
Department, University Oviedo, Faculty of Chemistry, C/ Julian Claveria, 8,
33006 Oviedo, Asturias, Spain

(Received 14 February, revised 9 May 2013)

Abstract: The synthesis of butyl *N*-(3-chloropropyl)-(2*S*)-alaninate hydrochloride is reported here. The compound was characterized by elemental analysis, infrared, and ¹H- and ¹³C-NMR spectroscopy. The structure of butyl *N*-(3-chloropropyl)-(2*S*)-alaninate hydrochloride was confirmed by single-crystal X-ray analysis.

Keywords: asymmetric ligand; infrared; ¹H- and ¹³C-NMR spectroscopy; X-ray analysis.

INTRODUCTION

Six-membered cyclic urethanes and their derivatives are an important class of compounds that can serve as small building blocks for the synthesis of pharmaceutical compounds¹ or 1,3-amino alcohols.² The preparation, spectral characterization and crystal structure of (2*S*)-2-(2-oxo-1,3-oxazinan-3-yl)propanoic acid, as a six-membered cyclic urethane, was previously described.³ After opening the cyclic form of this compound, the obtained derivatives could be used as suitable precursors for the synthesis of numerous asymmetric ligands. In this paper, the preparation and characterization of the (2*S*)-2-(2-oxo-1,3-oxazinan-3-yl)propanoic acid derivative, *i.e.*, *N*-(3-chloropropyl)-(2*S*)-alaninate, are

* Corresponding author. E-mail: snovak@vin.bg.ac.rs

Serbian Chemical Society member.

doi: 10.2298/JSC130214054D

reported. Furthermore, the single crystal X-ray structure determination of butyl *N*-(3-chloropropyl)-(2*S*)-alaninate hydrochloride is reported.

EXPERIMENTAL

Reagents and instruments

The commercially available chemicals were used without further purification except that 1-butanol was dried according to a standard laboratory method. (2*S*)-2-(2-Oxo-1,3-oxazinan-3-yl)propanoic acid was prepared as previously described.³

Infrared spectra were recorded on a Perkin-Elmer Spectrum One FT-IR spectrometer using the KBr pellet technique (4000–400 cm⁻¹). The ¹H- and ¹³C-NMR spectra were recorded on a Varian Gemini-2000 (200 MHz) spectrometer in D₂O using tetramethylsilane as the internal standard. Elemental microanalyses for C, H and N were performed by standard methods using a Vario EL III C, H, N elemental analyzer.

Preparation of butyl *N*-(3-chloropropyl)-(2*S*)-alaninate hydrochloride

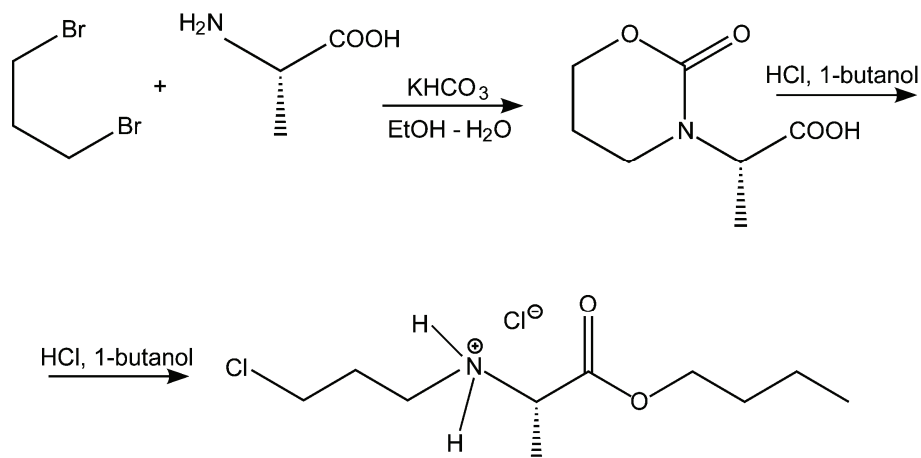
To 50 mL of dry 1-butanol saturated with gaseous HCl, 1.50 g (8.7 mmol) of (2*S*)-2-(2-oxo-1,3-oxazinan-3-yl)propanoic acid was added and the mixture was refluxed for 12 h. The mixture was allowed to reach room temperature, filtered off and the filtrate was left in refrigerator for two days. The obtained white powder was filtered off and washed with diethyl ether.

X-ray data collection

Appropriate crystals for X-ray crystal structure determination were collected after recrystallization of butyl *N*-(3-chloropropyl)-(2*S*)-alaninate hydrochloride from water. Data were collected at room temperature on an Oxford Diffraction Xcalibur Gemini S diffractometer equipped with CuK_α radiation ($\lambda = 1.54184 \text{ \AA}$).

RESULTS AND DISCUSSION

The synthesis route of butyl *N*-(3-chloropropyl)-(2*S*)-alaninate hydrochloride is given in Scheme 1.



Scheme 1. Synthesis of butyl *N*-(3-chloropropyl)-(2*S*)-alaninate hydrochloride.

Analytic and spectroscopic measurements

Butyl N-(3-chloropropyl)-(2S)-alaninate hydrochloride. Yield: 1.515 g (67.45 %); Anal. Calcd. for $C_{10}H_{21}Cl_2NO_2$ (FW: 258.178): C, 46.52; H, 8.20; N, 5.34 %. Found: C, 45.92; H, 8.95; N, 5.43 %. IR (KBr, cm^{-1}): 3435, 2938, 1743, 1447, 1315, 1207, 1112, 1087, 960, 839, 735. 1H -NMR (200 MHz, D_2O , δ / ppm): 0.91 (3H, *t*, $^3J = 7.01$ Hz, C^5H_3), 1.37 (2H, *m*, C^4H_2), 1.57 (3H, *d*, $^3J = 6.96$ Hz, C^7H_2), 1.68 (2H, *m*, C^3H_2), 2.22 (2H, *m*, C^9H_2), 2.89 (2H, *t*, $^3J = 7.12$ Hz, C^8H_2), 3.29 (2H, *t*, $^3J = 6.96$ Hz, $C^{10}H_2$), 3.71 (2H, *t*, $^3J = 6.51$ Hz, C^2H_2), 3.29 (1H, *q*, $^3J = 6.96$ Hz, C^6H). ^{13}C -NMR (50 MHz, D_2O , δ / ppm): 16 (C^5H_3), 17 (C^7H_3), 21 (C^4H_2), 31 (C^3H_2), 33 (C^9H_2), 44 ($C^{10}H_2$), 47 (C^8H_2), 59 (C^6H), 70 (C^2H_2), 173 ($C^{10}OBU$).

The microanalysis results confirmed the composition of the titled compound. The proposed structure based on its infrared and NMR (1H and ^{13}C) spectra is given in Fig. 1. This structure was confirmed by crystal structure analysis.

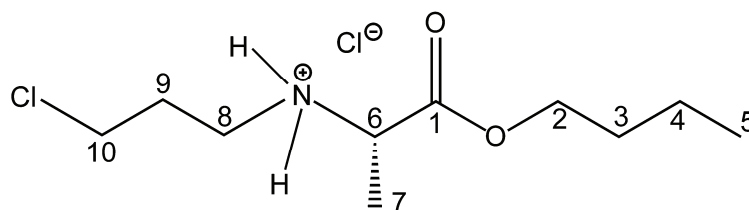


Fig. 1. Numbering of butyl *N*-(3-chloropropyl)-(2*S*)-alaninate hydrochloride used for the NMR data.

Thus, in the IR spectrum of the compound, the absorption band for secondary ammonium group $\nu(R_2NH_2^+)$ was observed at 3435 cm^{-1} . The absorption band at 1743 cm^{-1} is characteristic for an ester group,⁴ while the bands at 1207 and 2938 cm^{-1} arise from C–O and methyl groups, respectively.

The expected resonances were found in 1H -NMR spectrum. The chemical shift for methyl protons was found at 0.91 ppm. In the ^{13}C -NMR spectrum of the title compound, the ester carbon resonance was found as expected at around 173 ppm.⁵

Crystal structure of butyl N-(3-chloropropyl)-(2S)-alaninate hydrochloride

Data for X-ray crystal structure determination were processed with CrysAlis software⁶ and corrected for absorption by an analytical numeric method.⁷ The crystal structure was solved by direct methods, using Sir2002⁸ and refined using SHELXL.⁹

H atoms bonded to C atoms were placed at the geometrically calculated positions with C–H distances fixed to 0.97 and 0.96 Å and isotropic displacement parameters equal to $1.2U_{eq}$ and $1.5U_{eq}$ of the parent methylene and methyl C

atoms, respectively. H atoms bonded to the N atom were located in the difference Fourier map and refined isotropically. The correct absolute structure of the compound was confirmed by the Flack parameter¹⁰ of 0.01(3). A summary of crystallographic data is given in Table I. The software used for the preparation of the material for publication were WinGX,¹¹ PLATON,¹² PARST¹³ and ORTEP.¹⁴

TABLE I. Crystal data and structure refinement for butyl *N*-(3-chloropropyl)-(2*S*)-alaninate hydrochloride

Empirical formula	C ₁₀ H ₂₁ Cl ₂ NO ₂
Formula weight	258.18
Temperature / K	293(2)
Wavelength / Å	1.54184
Crystal system	Orthorhombic
Space group	<i>P</i> 2 ₁ 2 ₁ 2
Unit cell dimensions	
<i>a</i> / Å	7.2650(4)
<i>b</i> / Å	14.8864(7)
<i>c</i> / Å	13.308(1)
<i>V</i> / Å ³	1439.3(2)
<i>Z</i>	4
μ / mm ⁻¹	3.939
<i>F</i> (000)	552
<i>D</i> _{calc} / g cm ⁻³	1.191
Crystal size / mm ³	0.19 × 0.06 × 0.04
θ range for data collection / °	3.32–67.5
Reflections collected	8742
Independent reflections	2903
Flack parameter ¹⁰	0.01 (3)
Goodness-of-fit on <i>F</i> ²	1.075
<i>R</i> _{int}	0.0361
<i>R</i> ₁ , <i>wR</i> ₂ [<i>I</i> > 2 σ (<i>I</i>)]	0.0492, 0.1436

The title compound crystallizes in the orthorhombic space group *P*2₁2₁2. The asymmetric unit contains one ester molecule protonated on the N atom, which is neutralized by the chloride anion (Fig. 2). The bond lengths and angles (Table II) are comparable to those of R₂edda-type esters (R refers to the isopropyl⁴ or cyclopentyl⁵ group), which comprise similar CH₂–CH₂–NH₂+–CH(CH₃)–COO fragments and also crystallize as hydrochloride salts. In the present compound, the torsion angles within the long, heteroatomic chain vary from 173.2(3) to 178.8(3)°, which describes a fully extended conformation. The backbone of the molecule is therefore approximately planar with the R.M.S. deviation for all non-H atoms, except the alaninate methyl C, of 0.09 Å. This is unlike the above mentioned R₂edda derivatives,^{4,5} in which the ester group significantly deviates from the rest of the aliphatic chain. Namely, in two previously reported examples, the dihedral angle between the best plane of the

–COO fragment and the plane passing through the rest of non-H atoms of the chain exceeds 50°. In the present compound, the corresponding dihedral angle has the value of 5.2(7)°. This difference in orientation of ester group can be related with the fact that the extended *n*-butyl ester moiety points away from the rest of the molecule and, in contrast to the bulky isopropyl ester and cyclopentyl ester fragments, can avoid possible steric hindrance. It could also be suggested that the *n*-butyl ester moiety better complies with all the *trans*-conformation of the aliphatic chain, resulting in an extended molecule with more efficient crystal packing.

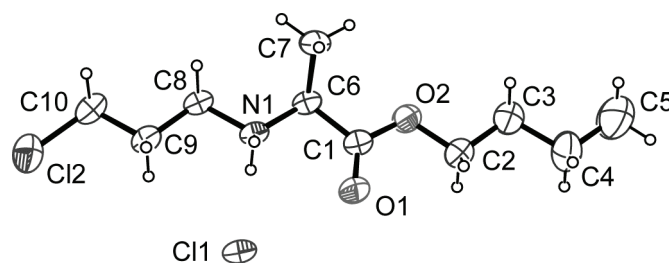


Fig. 2. Molecular structure of butyl *N*-(3-chloropropyl)-(2*S*)-alaninate hydrochloride. Displacement ellipsoids are drawn at the 40 % probability level.

TABLE II. Selected bond lengths (Å) and angles (°)

Bonds		Angles	
C12–C10	1.773(5)	C9–C10–C12	112.5(3)
O1–C1	1.194(4)	O1–C1–O2	124.7(3)
O2–C1	1.313(5)	C1–O2–C2	116.2(3)
O2–C2	1.462(5)	O2–C2–C3	109.1(4)
N1–C6	1.483(5)	N1–C6–C1	107.2(3)
N1–C8	1.497(4)	N1–C6–C7	112.2(3)
C6–C7	1.523(5)	N1–C8–C9	110.9(3)

The crystal packing is dominated by two N1–H···Cl1 hydrogen bonds formed between the protonated amino group and the Cl anion (Table III). These rather strong interactions with nearly linear interaction angles connect the screw-related molecules into a zigzag chain parallel to the *a* axis (Fig. 3). The *n*-butyl ester and chloropropyl moieties of the adjusted molecules point to the same side of the chain, giving rise to a secondary, weak C10–H10a···O1 interaction. The

TABLE III. Geometry of the hydrogen bonds (Å, °); symmetry codes: *i*) *x*, *y*, *z*; *ii*) *x*–1/2, –*y*+1/2, –*z*+1; *iii*) *x*+1/2, –*y*+1/2, –*z*+1

D–H···A	D–H	D···A	H···A	D–H···A
N1–H1a···Cl1 ^{<i>i</i>}	0.94(4)	3.150(3)	2.21(4)	177(3)
N1–H1b···Cl1 ^{<i>ii</i>}	0.92(4)	3.114(3)	2.20(4)	172(3)
C10–H10a···O1 ^{<i>iii</i>}	0.97	3.200(5)	2.50	129

chains of the molecules can be considered as principal packing motifs of this crystal structure. The further molecular arrangement is mostly based on van der Waals interactions. In contrast to the chloride anion, which represents the most important hydrogen bonding acceptor site, the Cl atom of the chloropropyl moiety plays no role in intermolecular interactions. The closest donor, the butyl ester C2–H2b fragment, is placed at a distance of 3.08 Å.

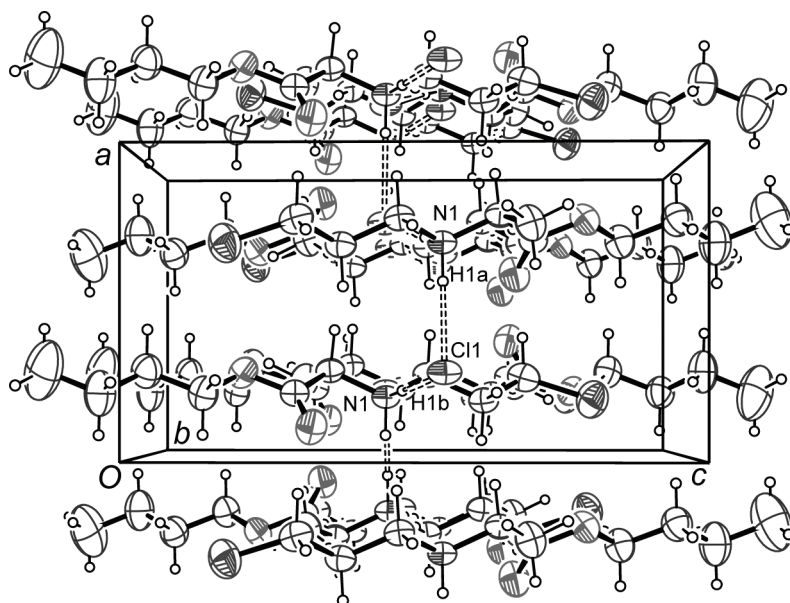


Fig. 3. Segment of crystal packing as viewed down the *b* axis. The strongest N–H...Cl hydrogen bonds are represented as dashed lines.

CONCLUSIONS

In reaction of (2*S*)-2-(2-oxo-1,3-oxazinan-3-yl)propanoic acid and dry 1-butanol saturated with gaseous HCl, butyl *N*-(3-chloropropyl)-(2*S*)-alaninate hydrochloride was prepared. The compound was characterized by NMR spectroscopy, IR spectroscopy and elemental analysis. The compound crystallizes in the orthorhombic space group $P2_12_12$. In the crystal packing, the molecules of *N*-(3-chloropropyl)-(2*S*)-alaninate hydrochloride are linked into chains by two strong N–H...Cl hydrogen bonds. The molecules further interact by means of weak van der Waals interactions.

SUPPLEMENTARY DATA

Crystallographic data for the structural analysis have been deposited with the Cambridge Crystallographic Data Centre CCDC No. 891442. The data are available free of charge *via* www.ccdc.cam.ac.uk/data_request/cif (or from the CCDC,

12 Union Road, Cambridge CB2 1EZ, UK; +44 1223 336033; e-mail: deposit@ccdc.cam.ac.uk).

Acknowledgements. The authors are grateful for the financial support to the Ministry of Education, Science and Technological Development of the Republic of Serbia (Projects No. 172016 and 172035).

ИЗВОД

СИНТЕЗА, КАРАКТЕРИЗАЦИЈА И КРИСТАЛНА СТРУКТУРА БУТИЛ-*N*-(3-ХЛОПРОПИЛ)-(2*S*)-АЛАНИНАТ-ХИДРОХЛОРИДА

ДЕЈАНА П. ДИМИТРИЈЕВИЋ¹, СЛАЂАНА Б. НОВАКОВИЋ², ГОРДАНА Р. РАДИЋ³, ВЕРИЦА В. ЈЕВТИЋ¹, LAURA MENÉNDEZ-TABOADA⁴, SANTIAGO GARCÍA-GRANDA⁴ и СРЕЉКО Р. ТРИФУНОВИЋ¹

¹Институт за хемију, Природно–математички факултет, Универзитет у Крагујевцу, Радоја Домановића 12, 34000 Крагујевац, ²Институт за нуклеарне науке „Винча“, Лабораторија за физику кондензоване материје, Универзитет у Београду, п. пр. 522, 11001 Београд, ³Факултет медицинских наука, Универзитет у Крагујевцу, Светозара Марковића 69, 34000 Крагујевац и ⁴Physical and Analytical Chemistry Department, University Oviedo, Faculty of Chemistry, C/ Julian Claveria, 8, 33006 Oviedo, Asturias, Spain

У раду је описана синтеза бутил-*N*-(3-хлорпропил)-(2*S*)-аланинат-хидрохлорида. Једињење је окарактерисано елементалном анализом, инфрацрвеном, ¹H- и ¹³C-NMR спектроскопијом. Структура *N*-(3-хлорпропил)-(2*S*)-аланинат-хидрохлорида је потврђена рендгенском структурном анализом.

(Примљено 14. фебруара, ревидирано 9. маја 2013)

REFERENCES

1. G. Wang, J.-R. Ella-Menye, V. Sharma, *Bioorg. Med. Chem. Lett.* **16** (2006) 2177
2. A. Bogini, G. Cardillo, M. Orena, G. Poorzi, S. Sandrini, *Chem. Lett.* (1988) 67
3. S. Trifunović, D. Dimitrijević, G. Vasić, N. Radulović, M. Vukićević, F. W. Heinemann, R. Vukićević, *Synthesis-Stuttgart* **6** (2010) 943
4. B. B. Krajinović, G. N. Kaluđerović, D. Steinborn, H. Schmidt, C. Wagner, Ž. Žižak, Z. D. Juranić, S. R. Trifunović, T. J. Sabo, *J. Inorg. Biochem.* **102** (2008) 892
5. B. B. Zmejkovski, G. N. Kaluđerović, S. Gómez-Ruiz, Ž. Žižak, D. Steinborn, H. Schmidt, R. Paschke, Z. D. Juranić, T. J. Sabo, *Eur. J. Med. Chem.* **44** (2009) 3452
6. Oxford Diffraction, CrysAlis CCD and CrysAlis RED, version 1.171.32.24, Oxford Diffraction Ltd., Abingdon, Oxfordshire, 2008
7. R. C. Clark, J. S. Reid, *Acta Crystallogr., A* **51** (1995) 887
8. M. C. Burla, M. Camalli, B. Carrozzini, G. L. Cascarano, C. Giacovazzo, G. Polidori, R. Spagna, *J. Appl. Crystallogr.* **36** (2003) 1103
9. G. M. Sheldrick, *Acta Crystallogr., A* **64** (2008) 112
10. H. D. Flack, *Acta Crystallogr., A* **39** (1983) 876
11. L. J. Farrugia, WinGX, *J. Appl. Crystallogr.* **32** (1999) 837
12. A. L. J. Spek, *J. Appl. Crystallogr.* **36** (2003) 7
13. M. Nardelli, *Comput. Chem.* **7** (1983) 95
14. L. J. Farrugia, *J. Appl. Crystallogr.* **30** (1997) 565



J. Serb. Chem. Soc. 78 (10) 1539–1546 (2013)
JSCS–4516

A test of Clar aromatic sextet theory

IVAN GUTMAN*#, SLAVKO RADENKOVIĆ#, MARIJA ANTIĆ
and JELENA ĐURĐEVIĆ

Faculty of Science, University of Kragujevac, P. O. Box 60, 34000 Kragujevac, Serbia

(Received 20 May, revised 28 May 2013)

Abstract. The Clar aromatic sextet theory predicts that the intensity of cyclic conjugation in chevron-type benzenoid hydrocarbons monotonically decreases along the central chain. This regularity has been tested by means of several independent theoretical methods (by the energy effects of the respective six-membered rings, as well as by their HOMA, NICS, and SCI values, calculated at the B3LYP/6-311G(d,p) level of DFT theory). Our results show that the predictions of Clar theory are correct only for the first few members of the chevron homologous series, and are violated at the higher members. This indicates that Clar theory is not universally applicable, even in the case of fully conjugated benzenoid molecules.

Keywords: Clar theory, aromatic sextet, cyclic conjugation, benzenoid hydrocarbons, chevron homologous series.

INTRODUCTION

Benzenoid hydrocarbons form a class of conjugated π -electron systems the theory of which has been elaborated in due detail.^{1–7} Cyclic conjugation in benzenoid hydrocarbons was especially much studied, see the papers^{8–14} and the references cited therein. The “aromatic sextet theory” of Erich Clar^{1,3} provides the simplest and most direct way by which an insight into the dominant modes of cyclic conjugation of a benzenoid molecule can be gained. In the Clar theory, so-called “Clar formulas” are constructed by placing “aromatic sextets” into some rings of a benzenoid molecule, obeying certain formal rules^{3,15} (*cf.* Fig. 1). Rings in which “aromatic sextets” are located are predicted to have a high intensity of cyclic conjugation. The original version of the Clar method is qualitative and has no direct foundation in quantum theory. Eventually, much effort was devoted to providing a quantitative and theoretically founded re-formulation of the Clar model (see the recent works^{18–26} and the references cited therein). In earlier

* Corresponding author. E-mail: gutman@kg.ac.rs

Serbian Chemical Society member.

doi: 10.2298/JSC130520057G

studies,^{13,14,27,28} examples of benzenoid hydrocarbons were found in which the predictions of Clar theory were violated. However, the benzenoid systems in these examples contained fixed single and double carbon–carbon bonds, and thus, it could be argued that the Clar theory was not strictly applicable to them. Herein, a class of fully conjugated benzenoid molecules (*i.e.*, molecules without fixed single and double carbon–carbons bonds) has been detected in which the modes of cyclic conjugation are not in full agreement with the Clar model. These are the members of the chevron homologous series,^{16,17} see Fig. 1.

CLAR FORMULAS OF CHEVRONS

For $n \geq 2$, the formula of the chevron molecule Ch_n (see Fig. 1) is $C_{8n+6}H_{2n+8}$ and the number of its hexagons is $3n$. It will now be shown that this benzenoid system has a total of $(1/6)n(n-1)(2n-1)$ Clar formulas.

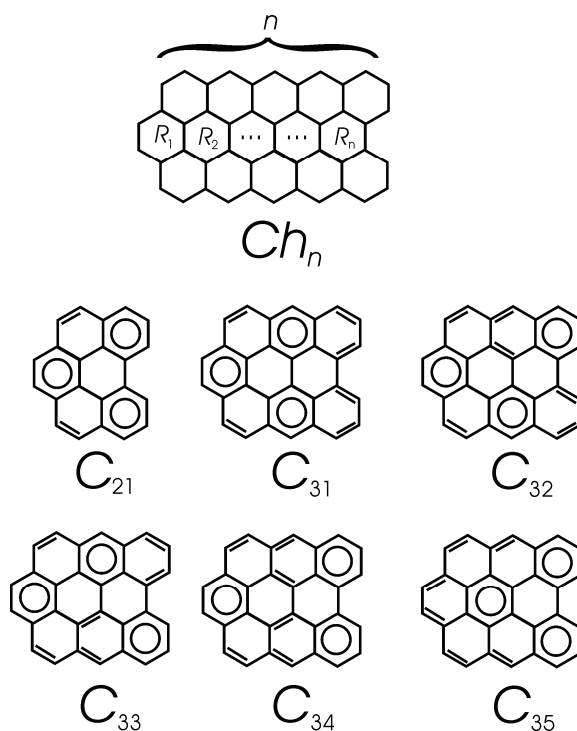


Fig. 1. The general formula of the chevron-type^{16,17} benzenoid hydrocarbon (Ch_n) and the labeling of its central rings. The first member (Ch_2) of this homologous series has a unique Clar formula (C_{21}), but the second member (Ch_3) has already five Clar formulas (C_{31} – C_{35}).

Suppose that the central hexagons of Ch_n are labeled as indicated in Fig. 1. Then, if an aromatic sextet is placed in hexagon R_1 , an additional aromatic sextet can be placed in the upper chain of Ch_n in $n-1$ different ways. The same is the

case with an aromatic sextet in the lower chain of Ch_n . Consequently, there are $(n-1) \times (n-1) = (n-1)^2$ Clar formulas when an aromatic sextet is placed in ring R_1 , see diagram D_1 in Fig. 2. If an aromatic sextet is placed in the central ring R_2 , then the aromatic sextets in the upper and lower chains can each be arranged in $n-2$ different ways, resulting in a total of $(n-2)^2$ Clar formulas, see diagram D_2 in Fig. 2.

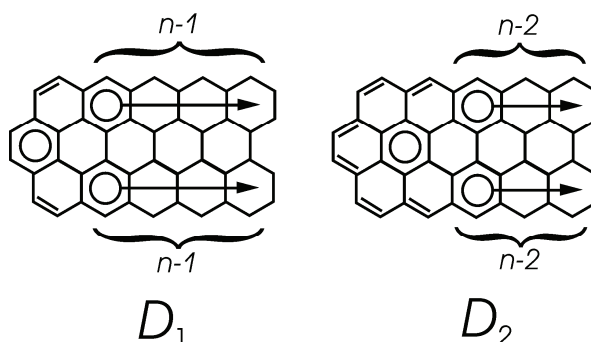


Fig. 2. Diagram D_1 is the usual abbreviated representation^{1,2} of the $(n-1)^2$ Clar formulas of the chevron Ch_n with an aromatic sextet in position R_1 . Diagram D_2 represents the $(n-1)^2$ Clar formulas with an aromatic sextet in position R_2 .

Continuing this argument, it can be seen that there are $(n-i)^2$ Clar formula in which an aromatic sextet is positioned in the central ring R_i , $i = 1, 2, \dots, n$. Thus the total number of Clar formulas is $\sum_{i=1}^n (n-i)^2$, which by direct calculation yields the expression $(1/6)n(n-1)(2n-1)$.

Notice that for $i = 1, 2, \dots, n$, the term $(n-i)^2$ monotonically decreases. Thus, the number of Clar formulas in which the ring R_i has an aromatic sextet (rapidly) decreases along the central chain of the chevron Ch_n .

The Clar theory yields a pictorial and qualitative description of the conjugation models of the π -electrons in benzenoid molecules. From an analysis of Clar formulas, it is not possible (or, at least, it is very risky) to obtain any quantitative result concerning cyclic conjugation. However, it is doubtless that the rings of a benzenoid system in which an aromatic sextet is placed in the majority (or all) Clar formulas must be viewed as possessing a high degree of cyclic conjugation. On the other hand, the rings in which an aromatic sextet is placed only in a few (or no) Clar formulas must be predicted as those in which the intensity of cyclic conjugation is low. In other words, the fundamental assumption of Clar theory is that the greater is the number of Clar formulas in which a ring R has an aromatic sextet, the stronger is the cyclic conjugation in this ring.

In the case of the central rings of the chevron-type benzenoids, the Clar theory implies a simple regularity: going along the central chain of Ch_n , starting

at the ring R_1 and ending at the ring R_n , the intensity of cyclic conjugation should monotonically decrease.

The aim of the present work is to check if this regularity is a true π -electron property or an artifact of the Clar theory.

A PRELIMINARY TEST

A quantitative, graph-theory based measure of cyclic conjugation in π -electron systems, especially in benzenoid hydrocarbons, is achieved by the energy-effect of the respective cycles. Details of this method have been earlier described several times, *e.g.*, in the review.⁸ Thus, $ef = ef(Z)$ is the energy-effect caused by cyclic conjugation of π -electrons along the cycle Z in the underlying conjugated molecule. As usual, in what follows, ef will be expressed in the units of the carbon-carbon resonance integral β , where $\beta \approx -137 \text{ kJ mol}^{-1}$. Note that since β is negative-valued, large (positive) ef -values mean a large stabilizing energy-effect caused by conjugation in the cycle Z , providing an energetic measure of the intensity of cyclic conjugation in Z .

The energy-effects of the central rings of the first few members of the chevron series are presented in Table I. The calculated ef -values indicate that the monotonicity rule is obeyed only for Ch_2 and Ch_3 , but is already violated at Ch_4 and for all higher chevron homologues. Thus, according to the ef -values, if n is large enough, the cyclic conjugation along the central chain of Ch_n , starting at the ring R_1 and ending at the ring R_n , first decreases, then increases reaching a maximum around the center of the chain, and then decreases again. This is in stark contrast with the predictions of Clar theory.

In view of the fact that the energy-effects are computed based on a relatively crude graph-theory-based model,⁸ the results based on ef -values (shown in Table I) cannot be considered as sufficient proof of the inadequacy of the Clar theory. Therefore, in order to strengthen the arguments, several other criteria, based on much more sophisticated quantum-chemical approaches, were employed.

TABLE I. Energy effects (in β -units, $\beta \approx -137 \text{ kJ mol}^{-1}$) of the central rings R_1, R_2, \dots, R_n of the chevrons Ch_n for $n = 2, 3, 4, 5, 6, 7$ and 8 . The labeling of the rings is indicated in Fig. 1

n	R_1	R_2	R_3	R_4	R_5	R_6	R_7	R_8
2	0.0794	0.0256						
3	0.0792	0.0361	0.0270					
4	0.0757	0.0369	0.0375	0.0280				
5	0.0740	0.0361	0.0376	0.0392	0.0280			
6	0.0737	0.0356	0.0366	0.0393	0.0392	0.0278		
7	0.0738	0.0355	0.0363	0.0381	0.0393	0.0388	0.0277	
8	0.0739	0.0355	0.0363	0.0376	0.0381	0.0390	0.0386	0.0277

There are several methods for assessing the intensity of cyclic conjugation in individual rings (often referred to as “local aromaticity”) based on high-level *ab*

initio molecular orbital (MO) and density-functional theoretic (DFT) approaches. Of these, the harmonic oscillator model (HOMA),^{29–31} nucleus-independent chemical shifts (NICS),^{19,32–34} and multicenter (six-center) bond indices (SCI) were used in this work.^{35–38}

NUMERICAL WORK

The DFT calculations on the chevrons Ch_n were performed for $n = 2, 3, 4, 5, 6, 7$ and 8 , using the Gaussian 09W package, version 0.1, at the B3LYP/6-311G(d,p) level of theory.³⁹ Geometry optimization confirmed that the molecules were perfectly planar. By frequency calculations, it was confirmed that the geometry determined corresponds to a true energy minimum. Bond lengths were taken from the optimized geometry.

The HOMA index^{29–31} was calculated by means of the formula:

$$\text{HOMA} = 1 - \frac{1}{N} \sum_{i=1}^N \alpha (d_{\text{opt}} - d_i)^2$$

where N is the number of bonds of the ring considered, $\alpha = 25.77 \times 10^{-3}$ is a normalization constant fixed to give HOMA = 0 for a model anti-aromatic system and HOMA = 1 for a fully delocalized π -electron system; $d_{\text{opt}} = 138.8$ pm, and d_i is an actual bond length.

NICS values^{32–34} were calculated at the B3LYP/6-311G(d,p) level through the gauge-including atomic orbital method (GIAO).⁴⁰ The NICS-values reported below were calculated 1 Å above the ring center.

The SCI indices^{35–38} were calculated from the B3LYP/6-31G(d) density matrices obtained, starting from the B3LYP/6-311G(d,p) optimized geometries. Calculations of SCI were performed using in-house software.

The numerical values of these three indicators of cyclic conjugation in individual rings of the central rings R_1, R_2, \dots, R_n of Ch_n for $n = 2, 3, 4, 5, 6, 7$ and 8 , are given in Tables II–IV.

TABLE II. HOMA values of the rings R_1, R_2, \dots, R_n . Other details are the same as in Table I

n	R_1	R_2	R_3	R_4	R_5	R_6	R_7	R_8
2	0.7867	0.3769						
3	0.8197	0.6659	0.3372					
4	0.8012	0.7163	0.6375	0.3314				
5	0.7850	0.7081	0.6893	0.6381	0.3322			
6	0.7792	0.6937	0.6819	0.6917	0.6394	0.3314		
7	0.7797	0.6863	0.6674	0.6846	0.6932	0.6343	0.3277	
8	0.7815	0.6850	0.6597	0.6703	0.6873	0.6883	0.6272	0.3242

DISCUSSION AND CONCLUDING REMARKS

First, by inspection of the data in Tables II–IV, it can be seen that the results of the preliminary test (based on energy-effects) were only partially confirmed. Namely, the DFT-based indices indicate that the predictions of the Clar theory are correct up to $n = 5$ (or, in the case of NICS, up to $n = 6$), but, again, are violated for the higher members of the chevron series.

Nevertheless, the main conclusion of the preliminary test remains. According to the HOMA, NICS, and/or SCI indices, if n is large enough, the cyclic

conjugation along the central chain of Ch_n first decreases, then increases reaching a maximum around the center of the chain, and then decreases again. This breakdown of the Clar theory occurs at $n = 6$ or $n = 7$.

TABLE III. NICS(1) values of the rings R_1, R_2, \dots, R_n . Other details are the same as in Table I. Note that the more negative NICS(1) is, the more intense is the respective cyclic conjugation

n	R_1	R_2	R_3	R_4	R_5	R_6	R_7	R_8
2	-13.39	-2.62						
3	-14.13	-7.96	+0.54					
4	-13.30	-10.70	-4.78	+2.07				
5	-12.30	-10.88	-8.54	-3.58	+2.96			
6	-11.70	-9.83	-9.44	-8.33	-3.13	+3.74		
7	-11.55	-8.67	-8.47	-9.98	-8.67	-2.52	+4.64	
8	-11.64	-7.85	-6.93	-9.25	-10.96	-8.53	-1.46	+5.73

TABLE IV. SCI values of the rings R_1, R_2, \dots, R_n , multiplied by 10^3 . Other details are the same as in Table I. Note that the greater SCI is, the more intense is the respective cyclic conjugation

n	R_1	R_2	R_3	R_4	R_5	R_6	R_7	R_8
2	17.02	6.02						
3	17.51	8.86	5.12					
4	16.48	9.95	7.83	5.27				
5	15.72	9.70	8.96	8.05	5.39			
6	15.46	9.28	8.81	9.23	8.23	5.40		
7	15.47	9.07	8.46	9.11	9.42	8.20	5.35	
8	15.55	9.03	8.27	8.77	9.31	9.38	8.09	5.30

In the earlier chemical literature, countless examples have been offered, demonstrating the correctness of the Clar aromatic sextet theory. The most convincing of these examples (see, for instance, in the books^{1,3,6}) are based on the comparison of the predictions of Clar theory and experimental findings. It happens, however, that all these example-based confirmations of the validity of Clar theory pertain to relatively small benzenoid molecules. In the present work also, it was found that the Clar theory performs well for the smaller members of the chevron series. Violations of Clar theory seem to occur at larger benzenoids. In the present case, these are the chevron-type species $C_{54}H_{20}$, $C_{62}H_{22}$.

The main conclusion is thus the following. There is a size-limit above which the π -electrons of benzenoid molecules behave in a way that violates the predictions of the Clar aromatic sextet theory. Consequently, this theory may be used only for smaller and moderate-sized benzenoids, and then only with a due degree of caution.

Acknowledgement. The authors thank the Serbian Ministry of Education, Science and Technological Development of the Republic of Serbia for support (Grant No. 174033).

ИЗВОД

ПРОВЕРА КЛАРОВЕ ТЕОРИЈЕ АРОМАТИЧНОГ СЕКСТЕТА

ИВАН ГУТМАН, СЛАВКО РАДЕНКОВИЋ, МАРИЈА АНТИЋ и ЈЕЛЕНА БУРЂЕВИЋ

Природно–математички факултет Универзитета у Крагујевцу

Кларова теорија ароматичног секстета предвиђа да интензитет цикличне конјугације у бензеноидним угљоводоникима шеvronског типа монотонно опада дуж централног ланца. Ова правилност је проверена помоћу неколико независних теоријских метода (са енергетским ефектима одговарајућих шесточланих прстенова, као и помоћу њихових НОМА, NICS и SCI вредности, рачунатих на B3LYP/6-311G(d,p) нивоу теорије функционала густине). Резултати показују да предвиђања Кларове теорије важе само код првих чланова хомологног низа шеvronа, док се код виших чланова јављају одступања. То указује на то да Кларова теорија није универзално применљива, чак ни код потпуно конјугованих бензеноидних молекула.

(Примљено 20. маја, ревидирано 28. маја 2013)

REFERENCES

1. E. Clar, *The Aromatic Sextet*, Wiley, London, 1972
2. J. R. Dias, *Handbook of Polycyclic Hydrocarbons. Part A. Benzenoid Hydrocarbons*, Elsevier, Amsterdam, 1987
3. I. Gutman, S. J. Cyvin, *Introduction to the Theory of Benzenoid Hydrocarbons*, Springer, Berlin, 1989
4. I. Gutman, S. J. Cyvin, Eds., *Advances in the Theory of Benzenoid Hydrocarbons*, Springer, Berlin, 1990
5. I. Gutman, Ed., *Advances in the Theory of Benzenoid Hydrocarbons II*, Springer, Berlin, 1992
6. M. Zander, *Polycyclische Aromaten*, Teubner, Stuttgart, 1995
7. J. R. Dias, *J. Chem. Inf. Model.* **47** (2007) 707
8. I. Gutman, *Monatsh. Chem.* **136** (2005) 1055
9. A. T. Balaban, J. Đurđević, I. Gutman, S. Jeremić, S. Radenković, *J. Phys. Chem., A* **114** (2010) 5870
10. B. Furtula, I. Gutman, S. Jeremić, S. Radenković, *J. Serb. Chem. Soc.* **75** (2010) 83
11. S. Jeremić, S. Radenković, I. Gutman, *J. Serb. Chem. Soc.* **75** (2010) 943
12. M. Marković, J. Đurđević, I. Gutman, *J. Serb. Chem. Soc.* **77** (2012) 751
13. I. Gutman, J. Đurđević, Z. Matović, M. Marković, *J. Serb. Chem. Soc.* **77** (2012) 1401
14. I. Gutman, J. Đurđević, S. Radenković, Z. Matović, *Monatsh. Chem.* **143** (2012) 1649
15. A. T. Balaban, *Polyc. Arom. Comp.* **24** (2004) 83
16. S. J. Cyvin, *J. Mol. Struct. (Theochem)* **133** (1985) 211
17. S. J. Cyvin, I. Gutman, *Kekulé Structures in Benzenoid Hydrocarbons*, Springer, Berlin, 1988, pp. 110–120
18. J. Aihara, *J. Phys. Chem., A* **107** (2003) 11553
19. G. Portella, J. Poater, M. Solá, *J. Phys. Org. Chem.* **18** (2005) 785
20. M. Randić, A. T. Balaban, *J. Chem. Inf. Model.* **46** (2006) 57
21. S. Gojak, I. Gutman, S. Radenković, A. Vodopivec, *J. Serb. Chem. Soc.* **72** (2007) 673
22. M. Randić, A. T. Balaban, *J. Phys. Chem., A* **112** (2008) 4148
23. K. Salem, S. Klavžar, A. Vesel, P. Žigert, *Discr. Appl. Math.* **157** (2009) 2565
24. M. Randić, D. Plavšić, *Acta Chim. Sloven.* **58** (2011) 448

25. C. P. Chou, H. A. Witek, *MATCH Commun. Math. Comput. Chem.* **68** (2012) 3
26. C. P. Chou, H. A. Witek, *MATCH Commun. Math. Comput. Chem.* **68** (2012) 31
27. I. Gutman, N. Turković, J. Jovičić, *Monatsh. Chem.* **135** (2004) 1389
28. I. Gutman, N. Turković, B. Furtula, *Indian J. Chem.* **45A** (2006) 1601
29. M. Krygowski, M. Cyranski, *Tetrahedron* **52** (1996) 1713
30. T. M. Krygowski, M. Cyranski, *Chem. Rev.* **101** (2001) 1385
31. M. Cyranski, *Chem. Rev.* **105** (2005) 3773
32. P. Raguè Schleier, C. Maerker, A. Drausfeld, H. Jiao, N. J. R. van Eikema Hommes, *J. Am. Chem. Soc.* **118** (1996) 6371
33. P. Raguè Schleier, H. Jiao, *Pure Appl. Chem.* **68** (1996) 209
34. Z. Chen, C. S. Wannere, C. Corminboeuf, R. Puchta, P. Raguè Schleyer, *Chem. Rev.* **105** (2005) 3842
35. M. Giambiagi, M. S. Giambiagi, C. D. Dos Santos, A. P. Figueiredo, *Phys. Chem. Chem. Phys.* **2** (2000) 3381
36. P. Bultinck, R. Ponec, S. Van Damme, *J. Phys. Org. Chem.* **18** (2005) 706
37. R. Bochicchio, R. Ponec, A. Torre, L. Lain, *Theor. Chem. Acc.* **105** (2001) 292
38. J. Đurđević, I. Gutman, R. Ponec, *J. Serb. Chem. Soc.* **74** (2009) 549
39. Gaussian 09, Revision A.01, Gaussian, Inc., Wallingford, CT, 2009
40. K. Wolinski, J. F. Hilton, P. Pulay, *J. Am. Chem. Soc.* **112** (1990) 8251.



J. Serb. Chem. Soc. 78 (10) 1547–1559 (2013)
JSCS–4517

Calculation of the stability constants for complex formation of dioxovanadium(V) with methyliminodiacetic acid in various H₂O + CH₃OH solutions using the Kamlet–Abboud–Taft equation

KAVOSH MAJLESI*, SAGHAR REZAIENEJAD, NAZILA DOUSTMAND SARABI,
MEHRDOKHT FAHMI and FERESHTEH TAHAMTAN

Department of Chemistry, Science and Research Branch, Islamic Azad University, Tehran, Iran

(Received 17 March, revised 21 June 2013)

Abstract: The stability constants for the complex formation of VO₂⁺ with methyliminodiacetic acid (MIDA) were determined in this study for various volume fractions of methanol (0–45 %, v/v) at $T = 298$ K, $I = 0.1$ mol dm⁻³ (sodium perchlorate). Potentiometric and UV spectrophotometric methods were utilized for the collection of experimental data. Different species were investigated but the best model contained VO₂HL and VO₂L⁻ for the employed data treatment. One-, two- and three-parameter Kamlet–Abboud–Taft (KAT) equations were applied for the determination and calculation of the solvatochromic regression coefficients for the KAT models.

Keywords: vanadium(V); linear solvation energy relationships; solvent effects; methanol; methyliminodiacetic acid.

INTRODUCTION

Yamada and coworkers reported a value of the stability constant for the formation of only one species, VO₂L⁻ (L = MIDA) in the complexation of dioxovanadium(V) with MIDA at $I = 1.0$ mol dm⁻³ sodium perchlorate.¹ The present study was performed in H₂O + CH₃OH medium with the aim of comparing the results with those of a previously published paper obtained at different ionic strengths.² Vanadium(V) oxometalates have found application as analytical reagents for the determination of various pharmacologically active substances and biochemical parameters. The antitumoral effects of vanadium can be evaluated by the determination of different parameters, such as cell proliferation, morphology and disruption of cellular architecture. The biological effects of vanadium(V) vary greatly in different biological systems.³ Vanadium plays a catalytic role in metalloenzyme systems, such as nitrogenase and haloperoxi-

* Corresponding author. E-mail: kavoshmajlesi@srbiau.ac.ir; kavoshmajlesi@gmail.com
doi: 10.2298/JSC130317072M

dases.⁴ Aminopolycarboxylic acids complexes with metals are usually very stable and have been used in different fields, such as selective NMR line broadening, magnetic resonance imaging (MRI), chelation therapy and several other industrial applications.⁵ In the present study, the aim was to clarify the role of various specific and nonspecific interactions in solution by application of the KAT equation, similarly to previous reports concerning the complexation of dioxovanadium(V) and molybdenum(VI) with ethylene glycol bis(2-aminoethyl ether)-*N,N,N',N'*-tetraacetic acid (EGTA) and ethylenediamine-*N,N'*-diacetic acid (EDDA).⁶⁻⁸

EXPERIMENTAL

MIDA, 99 % (Fig. 1) was obtained from Aldrich. Sodium perchlorate, 99%; sodium hydroxide titrisol solution (1 mol dm⁻³); anhydrous sodium monovanadate, minimum 99%; sodium carbonate anhydrous, 99.5%; perchloric acid, 60%; potassium hydrogen carbonate \geq 99.5%; hydrochloric acid, 37% and methanol, 99.8% were purchased from Merck as analytical reagent grade materials. The chemicals were used as were received.

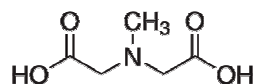


Fig. 1. The chemical structure of MIDA.

Anhydrous sodium monovanadate was dissolved in perchloric acid solution for the preparation of the vanadium(V) stock solution and prevention of decavanadate formation.⁹ Isopolyvanadates should not be present, therefore the solution was left overnight before use in order to obtain only the VO₂⁺.^{9,10} Titrisol solutions were used for the preparation of the NaOH solutions. Several titrations with standard HCl were performed to obtain their concentration. KHCO₃ and sodium carbonate solutions were used for the standardization of dilute perchloric and hydrochloric acids solutions, respectively. The specific conductance of the double-distilled water used for the preparation of the stock solutions was (1.3±0.1) μS cm⁻¹.

The medium for all measurements at $T = 298$ K had an ionic strength of 0.10 mol dm⁻³ of sodium perchlorate. The pH values were measured with a Metrohm pH-meter, 827. A Metrohm combination electrode, model 6.0228.010 was used for the hydrogen ion concentration measurements. A standard solution of hydrogen ion concentration was employed which consists of a 0.01 mol dm⁻³ perchloric acid solution, and 0.09 mol dm⁻³ sodium perchlorate for the ionic strength adjustment to 0.10 mol dm⁻³. The liquid junction potential was calculated using Eq. (1).⁶

$$\text{pH}(\text{real}) = \text{pH}(\text{measured}) + a + b[\text{H}^+](\text{measured}) \quad (1)$$

Adjustment of the ionic medium was realized by hydrogen ion concentration measurement of two different solutions of HClO₄ with sufficient NaClO₄ and in this way, the values of a and b were obtained.⁶ Literature survey shows the glass electrode calibration for various methanol mixtures.^{6,11} For an aqueous methanol solution, the value of pH is denoted by B (which was measured using the pH meter) and the following equation shows its relation to the hydrogen ion concentration:⁶

$$-\log [\text{H}^+] = B + \log \mu_{\text{H}} \quad (2)$$

Different aqueous methanol solutions containing a known concentrations of sodium perchlorate and perchloric acid were used to maintain a constant ionic strength of 0.10 mol dm^{-3} and for the calculation of the B values.⁶ The values of the correction term $\log \mu_{\text{H}} = \log(\mu_{\text{H}}^0 \gamma_{+})$ were obtained based on the difference between the logarithm of known hydrogen ion concentrations and the corresponding values of B .⁶ The value of μ_{H}^0 is only dependent on the solvent composition.⁶ The mean activity coefficient of perchloric acid in the solvent mixtures is denoted by γ_{+} .⁶ Three titrations have been performed for each volume fraction of methanol and approximately 200 points were used in the calculations at each volume fraction of methanol.^{2,12}

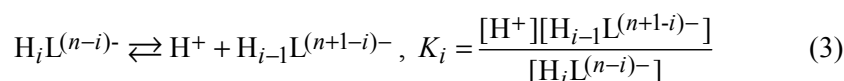
A flow type cell has been used for the spectrophotometric measurements, which were performed using a Varian Cary 300 UV-Vis spectrophotometer. The absorbance values were collected in the wavelength range 245–280 nm in a thermoregulated matched 10-mm quartz cells. The acquisition of the couple of data A versus λ (nm) was performed by means of the built in computer program of the UV-Vis spectrophotometer. Simultaneous measurement of pH and absorbance was enabled by using a Masterflux pump that circulated the solution between the potentiometric and spectrophotometric cells.

Different metal and ligand concentrations and ligand–metal mole ratios were tested and finally $c_{\text{L}} = 2.0 \times 10^{-2}$ and $c_{\text{VO}_2} = 5.0 \times 10^{-4} \text{ mol dm}^{-3}$ gave good fits and speciation patterns with minimum error functions. Thus, 50 ml acidic solutions of dioxovanadium(V) ($5.0 \times 10^{-4} \text{ mol dm}^{-3}$) were titrated with basic solutions of MIDA ($2.0 \times 10^{-2} \text{ mol dm}^{-3}$) at different volume fractions of methanol. The absorbance and pH of the solutions were measured simultaneously after each addition. VO_2^{+} is dominant when a large excess of ligand was present in the acidic solution ($\text{pH} < 3.0$).^{6,10} All experiments were repeated three times, and the average values of experimental dissociation and stability constants along with their deviations from the average are given.

RESULTS AND DISCUSSION

Dissociation constants

The two dissociation constants for MIDA are given by the following equilibria:



L^{2-} represents the fully deprotonated ligand. The values of the dissociation constants were obtained using the potentiometric technique and Microsoft Excel 2003 software.^{2,12} The experimental, calculated and literature data are gathered in Tables I–IV.^{2,5} The experimental data for 0 % methanol in the first lines of Tables I–IV were from the literature² but all the calculated values were obtained in this work based on the KAT equation, which will be discussed later.

Data treatment

Various stoichiometric models were investigated in order to find the best one. Finally, two species were identified that allowed the attainment of suitable fitting and distribution diagrams, similar to a previous work pertaining to complex formation of VO_2^{+} with MIDA at different ionic strengths.² The values of

stability constants can be calculated from the summation of dissociation and formation constants. The two equations for complex formation of dioxovanadium(V) with MIDA are represented below:

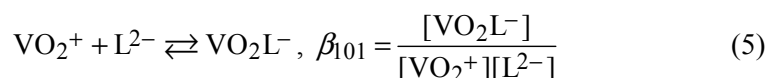
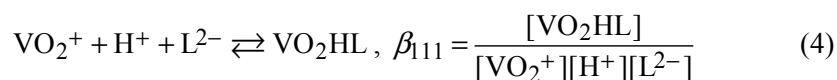


TABLE I. Average experimental and calculated values of $\log K_1$ at $I = 0.1 \text{ mol dm}^{-3}$ of NaClO_4 and different aqueous solutions of CH_3OH for MIDA, based on one and three solvatochromic parameters: α , hydrogen bond donor acidity; β , hydrogen bond acceptor basicity; π^* , dipolarity/polarizability. $T = 298 \text{ K}$

Methanol content % (v/v)	Experimental	Calculated			
		α	β	π^*	α, β, π^*
0	2.54±0.04	2.54±0.02	2.53±0.03	2.53±0.02	2.54±0.01
5	2.58±0.02	2.58±0.02	2.57±0.03	2.60±0.02	2.58±0.01
10	2.64±0.03	2.61±0.02	2.61±0.03	2.61±0.02	2.62±0.01
15	2.65±0.01	2.65±0.02	2.65±0.03	2.64±0.02	2.65±0.01
20	2.67±0.02	2.69±0.02	2.70±0.03	2.69±0.02	2.69±0.01
25	2.72±0.02	2.73±0.02	2.74±0.03	2.72±0.02	2.72±0.01
30	2.76±0.01	2.77±0.02	2.78±0.03	2.77±0.02	2.76±0.01
35	2.79±0.02	2.81±0.02	2.82±0.03	2.81±0.02	2.80±0.01
40	2.85±0.01	2.85±0.02	2.86±0.03	2.86±0.02	2.84±0.01
45	2.95±0.01	2.92±0.02	2.90±0.03	2.92±0.02	2.95±0.01
0	2.12±0.09 ^a	–	–	–	–
0	2.28±0.02 ^b	–	–	–	–
0	2.32±0.03 ^c	–	–	–	–
0	2.40±0.10 ^d	–	–	–	–

^a $I = 0.1 \text{ mol dm}^{-3}$ KCl, $T = 298 \text{ K}$; ^b $I = 0.5 \text{ mol dm}^{-3}$ NaClO_4 , $T = 298 \text{ K}$; ^c $I = 0.5 \text{ mol dm}^{-3}$ KNO_3 , $T = 298 \text{ K}$; ^d $I = 1.0 \text{ mol dm}^{-3}$ NaClO_4 , $T = 298 \text{ K}$ (a, b, c and d data were taken from the literature⁵)

The absorbance data in the UV range 255 to 280 nm were collected for minimizing the error function base on the Gauss–Newton nonlinear least squares method in the Microsoft Excel 2003 software based on the function $A = f(\text{pH})$. Error function calculation could be realized according to the following equation:²

$$U = \sum (A_{\text{exp}} - A_{\text{cal}})^2 \quad (6)$$

A_{exp} values were obtained from the UV spectrophotometric measurements at different pH values, wavelengths and volume fractions of methanol. A_{cal} values were determined for the model consisting of VO_2HL and VO_2L^- species. A_{exp} and A_{cal} values at $T = 298 \text{ K}$, $I = 0.10 \text{ mol dm}^{-3}$, 5 % volume fraction of methanol and 270 nm are shown in Fig. 2. After optimization of error function, the values of $U = 0.00243$ and standard error of y , $SE(y) = 0.00834$ were obtained for

Fig. 2, which shows a good fit. The other volume fractions of methanol showed similar fits.

TABLE II. Average experimental and calculated values of $\log K_1$ at $I = 0.1 \text{ mol dm}^{-3}$ of NaClO_4 and different aqueous solutions of CH_3OH for MIDA, based on two solvatochromic parameters: α , hydrogen bond donor acidity; β , hydrogen bond acceptor basicity; π^* , dipolarity/polarizability. $T = 298 \text{ K}$

Methanol content, % (v/v)	Experimental	Calculated		
		α, β	α, π^*	β, π^*
0	2.54±0.04	2.54±0.01	2.54±0.02	2.53±0.02
5	2.58±0.02	2.58±0.01	2.57±0.02	2.60±0.02
10	2.64±0.03	2.62±0.01	2.61±0.02	2.61±0.02
15	2.65±0.01	2.65±0.01	2.65±0.02	2.64±0.02
20	2.67±0.02	2.69±0.01	2.69±0.02	2.69±0.02
25	2.72±0.02	2.72±0.01	2.73±0.02	2.72±0.02
30	2.76±0.01	2.76±0.01	2.77±0.02	2.77±0.02
35	2.79±0.02	2.80±0.01	2.81±0.02	2.80±0.02
40	2.85±0.01	2.83±0.01	2.85±0.02	2.85±0.02
45	2.95±0.01	2.95±0.01	2.92±0.02	2.93±0.02

TABLE III. Average experimental and calculated values of $\log K_2$ at $I = 0.1 \text{ mol dm}^{-3}$ of NaClO_4 and different aqueous solutions of CH_3OH for MIDA, based on one and three solvatochromic parameters: α , hydrogen bond donor acidity; β , hydrogen bond acceptor basicity; π^* , dipolarity/polarizability. $T = 298 \text{ K}$

Methanol content % (v/v)	Experimental	Calculated			
		α	β	π^*	α, β, π^*
0	9.67±0.10	9.63±0.02	9.62±0.03	9.62±0.02	9.63±0.03
5	9.68±0.06	9.68±0.02	9.68±0.03	9.71±0.02	9.69±0.03
10	9.70±0.06	9.73±0.02	9.73±0.03	9.73±0.02	9.73±0.03
15	9.76±0.01	9.78±0.02	9.78±0.03	9.77±0.02	9.78±0.03
20	9.83±0.08	9.83±0.02	9.84±0.03	9.83±0.02	9.83±0.03
25	9.87±0.07	9.88±0.02	9.89±0.03	9.87±0.02	9.88±0.03
30	9.95±0.12	9.93±0.02	9.94±0.03	9.94±0.02	9.94±0.03
35	9.97±0.10	9.98±0.02	9.99±0.03	9.98±0.02	9.98±0.03
40	10.06±0.07	10.03±0.02	10.05±0.03	10.04±0.02	10.04±0.03
45	10.13±0.09	10.13±0.02	10.10±0.03	10.13±0.02	10.13±0.03
0	9.65±0.07 ^a	—	—	—	—
0	9.59±0.02 ^b	—	—	—	—
0	9.43±0.03 ^c	—	—	—	—
0	9.46±0.03 ^d	—	—	—	—
0	9.48±0.06 ^e	—	—	—	—

^a $I = 0.1 \text{ mol dm}^{-3} \text{ KCl}$, $T = 293 \text{ K}$; ^b $I = 0.1 \text{ mol dm}^{-3} \text{ KCl/KNO}_3$, $T = 298 \text{ K}$; ^c $I = 0.5 \text{ mol dm}^{-3} \text{ NaClO}_4$, $T = 298 \text{ K}$; ^d $I = 0.5 \text{ mol dm}^{-3} \text{ KNO}_3$, $T = 298 \text{ K}$; ^e $I = 1.0 \text{ mol dm}^{-3} \text{ NaClO}_4$, $T = 298 \text{ K}$ (a, b, c, d and e data were taken from the literature⁵)

The distribution diagrams are gathered in Fig. 3 for different volume fractions of methanol. The combination of the formation constants, mass-balance and

the Lambert–Beer law enabled the determination of the A_{cal} values for the model including VO_2HL and VO_2L^- ($\text{L} = \text{MIDA}$):²

$$A = \varepsilon_0[\text{VO}_2^+] + \varepsilon_{\text{VO}_2\text{HL}}[\text{VO}_2\text{HL}] + \varepsilon_{\text{VO}_2\text{L}^-}[\text{VO}_2\text{L}^-] \quad (7)$$

$$c_{\text{VO}_2^+} = [\text{VO}_2^+] + [\text{VO}_2\text{HL}] + [\text{VO}_2\text{L}^-] \quad (8)$$

$$c_{\text{L}} = [\text{VO}_2\text{HL}] + [\text{VO}_2\text{L}^-] + [\text{H}_2\text{L}] + [\text{HL}^-] \quad (9)$$

$$\text{VO}_2^+ + \text{H}_2\text{L} \rightleftharpoons \text{VO}_2\text{HL} + \text{H}^+, \quad K_{\text{VO}_2\text{HL}} = \frac{[\text{VO}_2\text{HL}][\text{H}^+]}{[\text{VO}_2^+][\text{H}_2\text{L}]} \quad (10)$$

$$\text{VO}_2\text{HL} \rightleftharpoons \text{VO}_2\text{L}^- + \text{H}^+, \quad K_{\text{VO}_2\text{L}^-} = \frac{[\text{VO}_2\text{L}^-][\text{H}^+]}{[\text{VO}_2\text{HL}]} \quad (11)$$

TABLE IV. Average experimental and calculated values of $\log K_2$ at $I = 0.1 \text{ mol dm}^{-3}$ of NaClO_4 and different aqueous solutions of CH_3OH for MIDA, based on two solvatochromic parameters: α , hydrogen bond donor acidity; β , hydrogen bond acceptor basicity; π^* , dipolarity/polarizability. $T = 298 \text{ K}$

Methanol content, % (v/v)	Experimental	Calculated		
		α, β	α, π^*	β, π^*
0	9.67±0.10	9.63±0.02	9.63±0.02	9.62±0.02
5	9.68±0.06	9.68±0.02	9.69±0.02	9.70±0.02
10	9.70±0.06	9.73±0.02	9.73±0.02	9.73±0.02
15	9.76±0.01	9.78±0.02	9.78±0.02	9.77±0.02
20	9.83±0.08	9.83±0.02	9.83±0.02	9.83±0.02
25	9.87±0.07	9.88±0.02	9.88±0.02	9.88±0.02
30	9.95±0.12	9.93±0.02	9.94±0.02	9.94±0.02
35	9.97±0.10	9.98±0.02	9.98±0.02	9.98±0.02
40	10.06±0.07	10.03±0.02	10.04±0.02	10.04±0.02
45	10.13±0.09	10.13±0.02	10.13±0.02	10.12±0.02

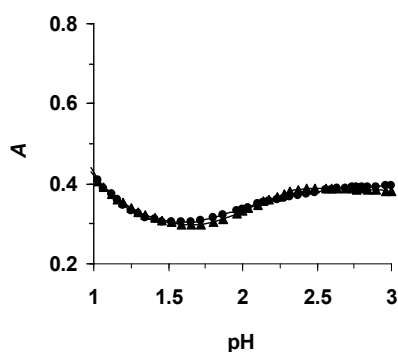


Fig. 2. A_{exp} and A_{cal} values at $T = 298 \text{ K}$, $I = 0.10 \text{ mol dm}^{-3}$, 5 % (v/v) and 270 nm. ●, A_{cal} ; ▲, A_{exp} for the model including VO_2HL , and VO_2L^- . $SE(y) = 0.00834$.

Comparison with literature data

Yamada and coworkers published the value of $\log \beta_{101} = 10.16 \pm 0.12$ at $I = 1.0 \text{ mol dm}^{-3}$ (NaClO_4) for the formation of only one species VO_2L^- .¹ On the

other hand, stability constants for the formation of two species, VO_2HL and VO_2L^- , at different ionic strengths of sodium perchlorate in the range of $0.1 < I < 1.0 \text{ mol dm}^{-3}$ was previously reported.² A difference exists between the stability constants data (Tables V and VII) at 0 % methanol reported in this work and those presented in the previously published paper ($1.00 < \text{pH} < 2.50$, $c_{\text{L}} = 5.18 \times 10^{-2}$ and $c_{\text{VO}_2^+} = 1.00 \times 10^{-3} \text{ mol dm}^{-3}$), especially for the values of $\log \beta_{101}$ (Tables V and VII).² It seems that the main reason is due to the selection of different concentrations and pH range for the calculations, which was up to pH 3.00 in the current work. Values of $\log \beta_{111}$ and $\log \beta_{101}$ from the literature together with the results of the present work are gathered in Tables V and VII.

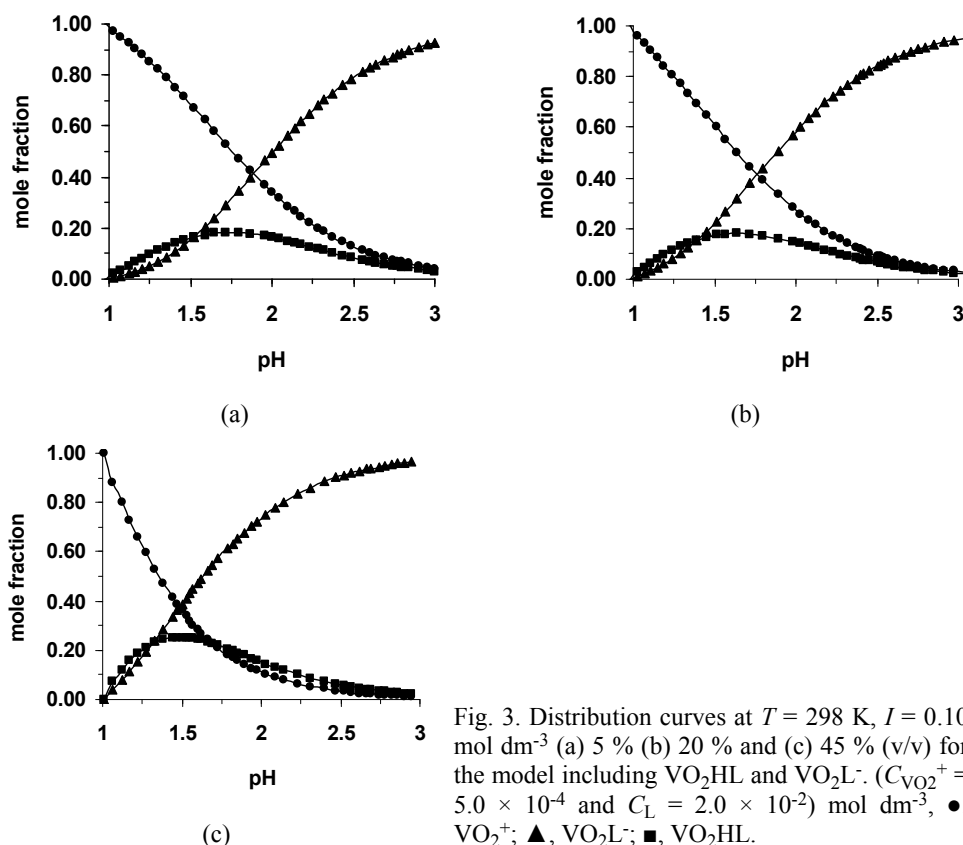


Fig. 3. Distribution curves at $T = 298 \text{ K}$, $I = 0.10 \text{ mol dm}^{-3}$ (a) 5 % (b) 20 % and (c) 45 % (v/v) for the model including VO_2HL and VO_2L^- . ($C_{\text{VO}_2^+} = 5.0 \times 10^{-4}$ and $C_{\text{L}} = 2.0 \times 10^{-2}$) mol dm^{-3} , \bullet , VO_2^+ ; \blacktriangle , VO_2L^- ; \blacksquare , VO_2HL .

Solvent effect investigation in the complex formation reaction using the KAT equation

The Kamlet–Abboud–Taft equation is a subset of linear solvation energy relationships (LSER), which has been used for the interpretation of different interactions in solution:^{13–37}

$$\log K = A_0 + p(\pi^* + d\delta) + a\alpha + b\beta \quad (12)$$

where A_0 is the value for $\log K$ in the setup when α , β , and π^* are all zero. α is the solvent hydrogen-bond donor (HBD) acidity. A solvent can give a proton to a solute and form a hydrogen bond. The α values are between zero for non-HBD solvents up to 1.0 for methanol.¹³ β is the solvent hydrogen-bond acceptor (HBA) basicity. A solvent can accept a proton from a solute during hydrogen bond formation. The β values vary from zero for non-HBA solvents up to 1 for hexamethylphosphoric acid triamide (HMPT).¹³ π^* is an index of the solvent dipolarity/polarizability. In other words, it is the capability of a solvent regarding charge, dipole and dielectric contributions. The π^* value is 0.00 and 1.00 for cyclohexane and dimethyl sulfoxide respectively.¹³ δ is discontinuous polarizability correlation term. The value of δ is 0.0 for non-chloro-substituted aliphatic solvents, 0.5 for poly-chloro-substituted aliphatics, and 1.0 for aromatic solvents.¹³ In the current work, δ is equal to zero.

TABLE V. Average experimental and calculated values of $\log \beta_{111}$ at $I = 0.1 \text{ mol dm}^{-3}$ of NaClO_4 and different aqueous solutions of CH_3OH for MIDA, based on one and three solvatochromic parameters: α , hydrogen bond donor acidity; β , hydrogen bond acceptor basicity; π^* , dipolarity/polarizability. $T = 298 \text{ K}$

Methanol content % (v/v)	Experimental	Calculated			
		α	β	π^*	α, β, π^*
0	12.50±0.04	12.43±0.07	12.41±0.06	12.40±0.07	12.41±0.07
5	12.60±0.10	12.60±0.07	12.58±0.06	12.68±0.07	12.61±0.07
10	12.75±0.06	12.77±0.07	12.76±0.06	12.75±0.07	12.76±0.07
15	12.87±0.04	12.94±0.07	12.94±0.06	12.90±0.07	12.93±0.07
20	13.01±0.20	13.10±0.07	13.12±0.06	13.11±0.07	13.11±0.07
25	13.25±0.02	13.27±0.07	13.29±0.06	13.25±0.07	13.28±0.07
30	13.51±0.10	13.44±0.07	13.47±0.06	13.46±0.07	13.46±0.07
35	13.69±0.10	13.61±0.07	13.65±0.06	13.60±0.07	13.63±0.07
40	13.82±0.15	13.77±0.07	13.82±0.06	13.81±0.07	13.81±0.07
45	14.04±0.10	14.11±0.07	14.00±0.06	14.09±0.07	14.04±0.07
0	12.79±0.15 ²	–	–	–	–

TABLE VI. Average experimental and calculated values of $\log \beta_{111}$ at $I = 0.1 \text{ mol dm}^{-3}$ of NaClO_4 and different aqueous solutions of CH_3OH for MIDA, based on two solvatochromic parameters: α , hydrogen bond donor acidity; β , hydrogen bond acceptor basicity; π^* , dipolarity/polarizability. $T = 298 \text{ K}$

Methanol content, % (v/v)	Experimental	Calculated		
		α, β	α, π^*	β, π^*
0	12.50±0.04	12.41±0.06	12.42±0.07	12.40±0.06
5	12.60±0.10	12.59±0.06	12.63±0.07	12.62±0.06
10	12.75±0.06	12.76±0.06	12.76±0.07	12.76±0.06
15	12.87±0.04	12.94±0.06	12.92±0.07	12.92±0.06
20	13.01±0.20	13.11±0.06	13.10±0.07	13.11±0.06

TABLE VI. Continued

Methanol content, % (v/v)	Experimental	Calculated		
		α, β	α, π^*	β, π^*
25	13.25±0.02	13.29±0.06	13.26±0.07	13.28±0.06
30	13.51±0.10	13.46±0.06	13.45±0.07	13.47±0.06
35	13.69±0.10	13.63±0.06	13.60±0.07	13.63±0.06
40	13.82±0.15	13.81±0.06	13.79±0.07	13.82±0.06
45	14.04±0.10	14.04±0.06	14.10±0.07	14.03±0.06

TABLE VII. Average experimental and calculated values of $\log \beta_{101}$ at $I = 0.1 \text{ mol dm}^{-3}$ of NaClO_4 and different aqueous solutions of CH_3OH for MIDA, based on one and three solvatochromic parameters: α , hydrogen bond donor acidity; β , hydrogen bond acceptor basicity; π^* , dipolarity/polarizability. $T = 298 \text{ K}$

Methanol content % (v/v)	Experimental	Calculated			
		α	β	π^*	α, β, π^*
0	10.96±0.10	10.90±0.09	10.86±0.07	10.86±0.09	10.86±0.08
5	11.08±0.20	11.09±0.09	11.07±0.07	11.18±0.09	11.10±0.08
10	11.27±0.10	11.28±0.09	11.27±0.07	11.26±0.09	11.27±0.08
15	11.45±0.05	11.47±0.09	11.47±0.07	11.42±0.09	11.46±0.08
20	11.57±0.20	11.66±0.09	11.68±0.07	11.66±0.09	11.67±0.08
25	11.77±0.20	11.85±0.09	11.88±0.07	11.83±0.09	11.87±0.08
30	12.06±0.30	12.04±0.09	12.08±0.07	12.07±0.09	12.08±0.08
35	12.33±0.20	12.24±0.09	12.28±0.07	12.23±0.09	12.28±0.08
40	12.58±0.10	12.43±0.09	12.49±0.07	12.47±0.09	12.49±0.08
45	12.70±0.10	12.81±0.09	12.69±0.07	12.79±0.09	12.70±0.08
0	11.74±0.25 ²	—	—	—	—
0	10.16±0.12 ^a	—	—	—	—

^a $I = 1.0 \text{ mol dm}^{-3} \text{ NaClO}_4$, $T = 298 \text{ K}$ (data were taken from the literature¹)

Different trends exist for the variation of solvatochromic parameters with the change in the concentration of various alcohols. Values of α , β and π^* for various aqueous solutions of methanol are listed in Table IX.⁶ The α and π^* values decrease but the β values increase with increasing methanol (Table IX). Several interactions exist in solution that are mainly classified as specific and non-specific interactions. All of these interactions can be defined as solvent polarity or solvation power. The famous specific interactions include different kinds of hydrogen bonding. All the other interactions except hydrogen bonding have been classified as non-specific interactions. The main intention of this work was to determine the contributions of different interactions by calculation of the regression coefficients a , b and p . Different one and two parameters KAT equations for the dissociation and stability constants are gathered in Table X.

TABLE VIII. Average experimental and calculated values of $\log \beta_{101}$ at $I = 0.1 \text{ mol dm}^{-3}$ of NaClO_4 and different aqueous solutions of CH_3OH for MIDA, based on two solvatochromic parameters: α , hydrogen bond donor acidity; β , hydrogen bond acceptor basicity; π^* , dipolarity/polarizability. $T = 298 \text{ K}$

Methanol content, % (v/v)	Experimental	Calculated		
		α, β	α, π^*	β, π^*
0	10.96±0.10	10.87±0.08	10.88±0.09	10.86±0.08
5	11.08±0.20	11.07±0.08	11.14±0.09	11.09±0.08
10	11.27±0.10	11.27±0.08	11.27±0.09	11.27±0.08
15	11.45±0.05	11.47±0.08	11.45±0.09	11.46±0.08
20	11.57±0.20	11.67±0.08	11.66±0.09	11.67±0.08
25	11.77±0.20	11.88±0.08	11.84±0.09	11.87±0.08
30	12.06±0.30	12.08±0.08	12.06±0.09	12.08±0.08
35	12.33±0.20	12.28±0.08	12.23±0.09	12.27±0.08
40	12.58±0.10	12.48±0.08	12.45±0.09	12.48±0.08
45	12.70±0.10	12.70±0.08	12.80±0.09	12.71±0.08

TABLE IX. Solvatochromic parameters for different aqueous solutions of methanol from the literature⁶

Methanol content, % (v/v)	α	β	π^*
0	1.17	0.47	1.09
5	1.16	0.48	1.05
10	1.15	0.49	1.04
15	1.14	0.50	1.02
20	1.13	0.51	0.99
25	1.12	0.52	0.97
30	1.11	0.53	0.94
35	1.10	0.54	0.92
40	1.09	0.55	0.89
45	1.07	0.56	0.85

TABLE X. Different KAT equations with one and two solvatochromic parameters together with their standard errors and square values of the correlation coefficients (r^2) for the dissociation and stability constants at $T = 298 \text{ K}$, $I = 0.1 \text{ mol dm}^{-3}$ of NaClO_4 and different aqueous solutions of methanol: α , hydrogen bond donor acidity; β , hydrogen bond acceptor basicity; π^* , dipolarity/polarizability; $n = 10$

KAT Equation	r^2
$\log K_1 = (7.08 \pm 0.20) - (3.88 \pm 0.18)\alpha$	0.98
$\log K_1 = (0.62 \pm 0.15) + (4.07 \pm 0.29)\beta$	0.96
$\log K_1 = (4.30 \pm 0.08) - (1.63 \pm 0.09)\pi^*$	0.98
$\log K_1 = (13.86 \pm 2.79) - (7.94 \pm 1.67)\alpha - (4.31 \pm 1.77)\beta$	0.99
$\log K_1 = (7.22 \pm 1.99) - (4.08 \pm 2.77)\alpha + (0.08 \pm 1.16)\pi^*$	0.98
$\log K_1 = (5.68 \pm 2.07) - (1.53 \pm 2.30)\beta - (2.23 \pm 0.91)\pi^*$	0.98
$\log K_2 = (15.52 \pm 0.27) - (5.03 \pm 0.24)\alpha$	0.98
$\log K_2 = (7.13 \pm 0.15) + (5.31 \pm 0.29)\beta$	0.98
$\log K_2 = (11.92 \pm 0.10) - (2.11 \pm 0.10)\pi^*$	0.98
$\log K_2 = (14.54 \pm 5.13) - (4.44 \pm 3.07)\alpha + (0.62 \pm 3.25)\beta$	0.98

TABLE X. Continued

KAT Equation	r^2
$\log K_2 = (13.78 \pm 2.61) - (2.60 \pm 3.65)\alpha - (1.02 \pm 1.53)\pi^*$	0.98
$\log K_2 = (10.84 \pm 2.51) + (1.20 \pm 2.78)\beta - (1.64 \pm 1.10)\pi^*$	0.98
$\log \beta_{111} = (32.02 \pm 0.80) - (16.74 \pm 0.71)\alpha$	0.99
$\log \beta_{111} = (4.07 \pm 0.36) + (17.73 \pm 0.69)\beta$	0.99
$\log \beta_{111} = (20.06 \pm 0.30) - (7.02 \pm 0.31)\pi^*$	0.98
$\log \beta_{111} = (13.75 \pm 13.37) - (5.81 \pm 8.02)\alpha + (11.61 \pm 8.48)\beta$	0.99
$\log \beta_{111} = (27.45 \pm 7.69) - (10.34 \pm 10.75)\alpha - (2.69 \pm 4.51)\pi^*$	0.99
$\log \beta_{111} = (9.31 \pm 6.52) + (11.93 \pm 7.24)\beta - (2.31 \pm 2.87)\pi^*$	0.99
$\log \beta_{101} = (33.27 \pm 1.05) - (19.12 \pm 0.93)\alpha$	0.98
$\log \beta_{101} = (1.32 \pm 0.42) + (20.30 \pm 0.82)\beta$	0.99
$\log \beta_{101} = (19.61 \pm 0.38) - (8.03 \pm 0.39)\pi^*$	0.98
$\log \beta_{101} = (3.78 \pm 16.33) - (1.47 \pm 9.79)\alpha + (18.74 \pm 10.36)\beta$	0.99
$\log \beta_{101} = (26.35 \pm 10.02) - (9.42 \pm 14.00)\alpha - (4.08 \pm 5.88)\pi^*$	0.98
$\log \beta_{101} = (4.82 \pm 7.94) + (16.43 \pm 8.81)\beta - (1.54 \pm 3.49)\pi^*$	0.99

CONCLUSIONS

In general, it could be stated that increasing the methanol concentration (lower solvation and decrease in the polarity of the mixture) in the concentration range studied in this research cause an increase in the values of the dissociation and stability constants for the complexation of dioxovanadium(V) with aminopolycarboxylic acids. The standard errors for three parameters KAT equations were too high due to the strong intercorrelation of the methanol parameters. The standard errors for the two-parameter KAT equation in Table X are relatively high in comparison to those of the one parameter KAT equation. Therefore only one and two parameters KAT equations are presented in Table X. Although relatively good results were obtained with the one-parameter KAT equation, it could be concluded that KAT equation may not be applicable in the current research because the solvatochromic substances may be preferentially solvated to a greater or lesser degree than the substances involved in the studied chemical reaction. For the methanol + water system in the current work, it is very difficult to determine exactly the role of the KAT parameters because the variations in the stability and dissociation constants with the methanol concentration are linear and strong correlation exist for the KAT parameters.

ИЗВОД

ИЗРАЧУНАВАЊЕ КОНСТАНТИ СТАБИЛНОСТИ ЗА ФОРМИРАЊЕ КОМПЛЕКСА
ДИОКСОВАНАДИЈУМА(V) СА МЕТИЛИМИНОДИСИРЋЕТНОМ КИСЕЛИНОМ У
РАЗЛИЧИТИМ $\text{H}_2\text{O} + \text{CH}_3\text{OH}$ РАСТВОРИМА КОРИШЋЕЊЕМ
КАМЛЕТ–АВБОУД–ТАФТ-ОВЕ ЈЕДНАЧИНЕ

KAVOSH MAJLESI, SAGHAR REZAIENEJAD, NAZILA DOUSTMAND SARABI, MEHRDOKHT FAHMI
и FERESHTEH TAHAMTAN

Department of Chemistry, Science and Research Branch, Islamic Azad University, Tehran, Iran

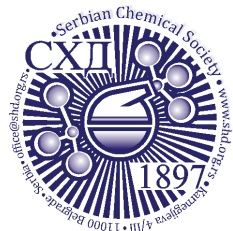
Константе стабилности за формирање комплекса VO_2^+ са метилиминодисирћетном киселином (MIDA) су одређене у овом раду за различите запреминске уделе метанола (0–45 %, v/v) на $T = 298 \text{ K}$, $I = 0,1 \text{ mol dm}^{-3}$ натријум-перхлората. Потенциометријска и УЉ спектрофотометријска метода су примењене за прикупљање података. Различите врсте су испитиване, а најбољи модел садржи VO_2HL и VO_2L^- ($L = \text{MIDA}$) за наш третман података. Једно-, дво- и тропараметарске Камлет–Аббод–Тафт-ове (КАТ) једначине су примењене за одређивање и израчунавање КАТ модела солватохромних регресионих коефицијената.

(Примљено 17. марта, ревидирано 21. јуна 2013)

REFERENCES

1. S. Yamada, J. Nagase, S. Funahashi, M. Tanaka, *J. Inorg. Nucl. Chem.* **38** (1976) 617
2. K. Majlesi, S. Rezaiejad, *J. Chem. Eng. Data* **55** (2010) 882
3. A. Tracey, G. Willsky, E. Takeuchi, *Vanadium: Chemistry, Biochemistry, Pharmacology and Technical Applications*, CRC Press, Boca Raton FL, USA, 2007
4. D. Rehder, *Bioinorganic Vanadium Chemistry*, Wiley, New York, USA, 2008.
5. G. Anderegg, F. A-Neu, R. Delgado, J. Felcman, K. Popov, *Pure Appl. Chem.* **77** (2005) 1445
6. K. Majlesi, S. Rezaiejad, *J. Chem. Eng. Data* **55** (2010) 4491
7. K. Majlesi, N. Momeni, *J. Chem. Eng. Data* **54** (2009) 2479
8. K. Majlesi, *Chin. J. Chem.* **28** (2010) 1973
9. K. Majlesi, S. Rezaiejad, *J. Solution Chem.* **41** (2012) 937
10. P. Lagrange, M. Schneider, J. Lagrange, *J. Chim. Phys.* **95** (1998) 2280
11. R. G. Bates, *Determination of pH*, Wiley, New York, USA, 1964
12. J. E. Billo, *Excel for Chemists*, 2nd ed., Wiley, New York, USA, 2001
13. C. Reichardt, *Solvents and Solvent Effects in Organic Chemistry*, Wiley-VCH, Weinheim, Germany, 2004
14. S. F. Hmuda, N. R. Banjac, N. P. Trišović, B. Đ. Božić, N. V. Valentić, G. S. Ušćumlić, *J. Serb. Chem. Soc.* **78** (2013) 627
15. S. Ž. Drmanić, J. B. Nikolić, B. Ž. Jovanović, *J. Serb. Chem. Soc.* **77** (2012) 569
16. S. Ž. Drmanić, J. B. Nikolić, A. D. Marinković, B. Ž. Jovanović, *J. Serb. Chem. Soc.* **77** (2012) 1311
17. A. S. Alimmari, A. D. Marinković, D. Ž. Mijin, N. V. Valentić, N. Todorović, G. S. Ušćumlić, *J. Serb. Chem. Soc.* **75** (2010) 1019
18. N. D. Divjak, N. R. Banjac, N. V. Valentić, G. S. Ušćumlić, *J. Serb. Chem. Soc.* **74** (2009) 1195
19. G. S. Ušćumlić, J. B. Nikolić, *J. Serb. Chem. Soc.* **74** (2009) 1335
20. S. Ž. Drmanić, A. D. Marinković, B. Ž. Jovanović, *J. Serb. Chem. Soc.* **74** (2009) 1359
21. J. B. Nikolić, G. S. Ušćumlić, *J. Serb. Chem. Soc.* **72** (2007) 1217

22. J. B. Nikolić, G. S. Ušćumlić, V. Krstić, *J. Serb. Chem. Soc.* **69** (2004) 601
23. G. S. Ušćumlić, A. A. Kshad, D. Ž. Mijin, *J. Serb. Chem. Soc.* **68** (2003) 699
24. H. Uslu, *J. Chem. Eng. Data* **57** (2012) 3685
25. W. E. Acree Jr., G. A. Baker, A. L. Revelli, J. C. Moise, F. Mutelet, *J. Chem. Eng. Data* **57** (2012) 3510
26. M. Prezhdo, V. Zubkova, V. Prezhdo, *J. Chem. Eng. Data* **57** (2012) 1945
27. J. Planeta, P. Karásek, M. Roth, *J. Chem. Eng. Data* **57** (2012) 1064
28. H. Uslu, *J. Chem. Eng. Data* **57** (2012) 902
29. F. Mutelet, J. C. Moise, A. Skrzypczak, *J. Chem. Eng. Data* **57** (2012) 918
30. S. Seifert, F. Simon, G. Baumann, M. Hietschold, A. Seifert, S. Spange, *Langmuir* **27** (2011) 14279
31. Y.-S. Shih, S.-M. Chou, Y.-H. Peng, M. Shih, *J. Chem. Eng. Data* **56** (2011) 4950
32. K. Khimeche, P. Alessi, A. Dahmani, I. Kikic, A. Cortesi, *J. Chem. Eng. Data* **56** (2011) 4651
33. F. Mutelet, V. Ortega-Villa, J. C. Moise, J. N. Jaubert, W. E. Acree Jr., *J. Chem. Eng. Data* **56** (2011) 3598
34. J. P. Hallett, T. Welton, *Chem. Rev.* **111** (2011) 3508
35. K. Paduszynski, U. Domanska, *J. Phys. Chem., B* **115** (2011) 8207
36. R. W. Taft, J. L. M. Abboud, M. J. Kamlet, *J. Org. Chem.* **49** (1984) 2001
37. M. J. Kamlet, J. L. M. Abboud, M. H. Abraham, R. W. Taft, *J. Org. Chem.* **48** (1983) 2877.



J. Serb. Chem. Soc. 78 (10) 1561–1567 (2013)
JSCS–4518

Autoprotolysis in water/methanol/NaCl ternary systems

ALI FARAJTABAR^{1*}, FERESHTEH NADERI² and FARROKH GHARIB³

¹Young Researchers Club, Jouybar Branch, Islamic Azad University, Jouybar, Iran,

²Department of Chemistry, Shahr-e-Qods branch, Islamic Azad University, Tehran, Iran and

³Chemistry Department, Faculty of Sciences, Shahid Beheshti University, Tehran, Evin, Iran

(Received 4 January, revised 10 March 2013)

Abstract: A potentiometric method was used to determine the autoprotolysis constant for aqueous solutions containing 0, 20 and 40 mass % of methanol over a wide range of NaCl concentrations at 25 °C. The ionic strength ranged between 0.25 and 2.00 mol L⁻¹ at intervals of 0.25 units. The osmotic and activity coefficients of the mixed solvents were calculated as a function of ionic strength. The dependence on ionic strength was analyzed using the original specific ion interaction theory. The specific ion interaction parameters associated with the thermodynamic autoprotolysis constant were extracted. Results indicate that interaction between ions increases with increasing methanol content in the mixture.

Keywords: autoprotolysis; water–methanol; sodium chloride; specific ion interaction theory.

INTRODUCTION

Mixed solvent electrolyte systems, especially water/organic/salt mixtures, frequently occur in wide variety of chemical industries, such as supercritical technologies, environmental applications, production of energy sources and separation, electrochemical and hydrometallurgical processes.¹ A comprehensive knowledge of the physicochemical properties of mixed solvents is mandatory for the development of modeling a successful process in the chemical industry. The autoprotolysis constant is one of the most important properties of each medium that is essential for pH definition, chemical speciation and acid–base equilibrium calculation.² An autoprotolysis constant describes quantitatively the extent of self ionization of solvent molecules SH, when a solvated proton, SH₂⁺, and lyate ion, S⁻, are produced in a chemical reaction:



* Corresponding author. E-mail: a_farajtabar@yahoo.com
doi: 10.2298/JSC130104039F

Although autoprotolysis of various aqueous electrolytes and solvent mixtures has been extensively investigated in the literature,²⁻⁵ to best of our knowledge, no effort has been made on the determination of the autoprotolysis constant of mixed solvent electrolyte systems. Therefore, in this work, the autoprotolysis constants of methanol–water mixtures (0, 20 and 40 mass % of methanol) were determined over a wide range of NaCl electrolyte concentrations. The autoprotolysis constant was modeled utilizing the specific ion interaction theory (SIT).

EXPERIMENTAL

All chemicals were purchased from Merck. Methanol was of highest available purity and used without further purification. Sodium chloride was dried under vacuum at room temperature for at least 72 h before use. NaOH and HCl solutions were prepared from a titrisol solution and their concentration was determined by several titrations. Water was double distilled with a conductivity equal to $1.3 \pm 0.1 \mu\Omega^{-1} \text{ cm}^{-1}$. A Jenway research potentiometer, model 3520, with a combined glass pH electrode was used for electromotive force (e.m.f) measurement in the potentiometric titrations. The electrode was modified by replacing its aqueous KCl solution with NaCl solution (0.10 mol L^{-1}) saturated with AgCl in aqueous methanol mixture.³ This method is useful to improve the response speed of the glass electrode and to keep the liquid junction potential constant at a small value.

The autoprotolysis constant of a mixed solvent was determined by the potentiometric titration method at 25°C at different ionic strengths from 0.5 to 2.0 mol L^{-1} , supplied by sodium chloride as an inert electrolyte. 25 mL of acidic solution (0.01 mol L^{-1} HCl) in a double-walled thermostated reaction vessel was titrated with NaOH (0.10 mol L^{-1}) at each ionic strength. Potentiometric data were taken after every addition of titrant, after which the stabilization of e.m.f data was checked manually. The criterion for a stable e.m.f was $\pm 0.1 \text{ mV}$ deviation, which was achieved in a period of 1 min.

RESULTS AND DISCUSSION

Computation of the autoprotolysis constant

According to Eq. (1), the thermodynamic autoprotolysis constant, K° , can be defined by Eq. (2):

$$K^\circ = \frac{a_{\text{SH}_2^+} a_{\text{S}^-}}{a_{\text{SH}}^2} = \frac{\gamma_{\text{SH}_2^+} [\text{SH}_2^+] \gamma_{\text{S}^-} [\text{S}^-]}{a_{\text{SH}}^2} = K \frac{\gamma_{\text{SH}_2^+} \gamma_{\text{S}^-}}{a_{\text{SH}}^2} \quad (2)$$

where γ_i and a_i are the activity coefficient and the activity of the species, respectively. K is a conditional autoprotolysis constant and $[\text{SH}_2^+][\text{S}^-]$ the product at each constant ionic strength.

During a potentiometric titration, the potential of a potentiometric cell equipped with a glass electrode in the acidic region can be formulated as:⁶

$$E = E^\circ + k \log a_{\text{SH}_2^+} = E^\circ + k \log \gamma_{\text{SH}_2^+} + k \log [\text{SH}_2^+] \quad (3)$$

E° is value of the standard electromotive force; k is the Nernst slope equal to $2.303RT/F$ in which R , T and F have their usual meaning. At constant ionic

strength, the activity coefficient of species should be constant; therefore, Eq. (3) can be rewritten as Eq. (4), with E_a being $E^\circ + k \log \gamma$:

$$E = E_a + k \log[\text{SH}_2^+] \quad (4)$$

The hydrogen ion concentration can be easily calculated by:

$$[\text{H}^+] = \frac{M_{\text{H}}V_0 - M_{\text{OH}}V_1}{V_0 + V_1} \quad (5)$$

where M_{H} and M_{OH} are the molarities of the acid and base, and V_0 and V_1 are the initial volume of acid and the added volume of sodium hydroxide solution, respectively.

By introducing Eq. (2) into Eq. (4), the e.m.f value in the alkaline region can be represented as:

$$E = E_a + k \log K - k \log[\text{S}^-] \quad (6)$$

The experimental e.m.f data were fitted simultaneously to Eqs. (4) and (6) using nonlinear least squares analysis to find the optimum values for the negative logarithm of K ($\text{p}K$). For each experiment at constant ionic strength, the slopes obtained from the least squares analysis were close to the theoretical Nernst value (59.167 mV at 25 °C) with correlation coefficients of nearly $r^2 = 0.99$. The $\text{p}K$ values in both the molar and molal concentration scales are reported in Tables I–III. The average standard deviations of the calculated $\text{p}K$ values were less than 0.01 units. Conversion from the molar to the molal scale was realized using literature data for the density of NaCl solution in water–methanol mixtures.⁷

TABLE I. Values of $\text{p}K$, activity coefficient of NaCl, osmotic coefficient and solvent activity in methanol–water mixture containing 0 % methanol in different ionic strengths at 25 °C

$I / \text{mol L}^{-1}$	$I / \text{mol kg}^{-1}$	$\text{p}K / \text{mol}^2 \text{L}^{-2}$	$\text{p}K / \text{mol}^2 \text{kg}^{-2}$	γ_{NaCl}	ϕ	a_{SH}
0.10	0.10	13.781	13.777	0.778	0.934	0.996
0.25	0.25	13.754	13.748	0.720	0.924	0.991
0.50	0.51	13.717	13.700	0.681	0.919	0.982
0.75	0.76	13.711	13.699	0.664	0.923	0.973
1.00	1.02	13.719	13.702	0.656	0.931	0.963
1.25	1.28	13.734	13.713	0.653	0.941	0.954
1.50	1.55	13.761	13.733	0.654	0.952	0.943
1.75	1.82	13.794	13.760	0.657	0.964	0.933
2.00	2.09	13.834	13.796	0.663	0.977	0.923

Computation of the activity and the osmotic coefficient of mixed solvent

The activity and osmotic coefficient of a mixed solvent were calculated according to Eqs. (7) and (8) from activity coefficients of NaCl and then tabulated in Tables I–III:

$$\ln a_{\text{SH}} = \frac{-M_s \nu m_j}{1000} \phi \quad (7)$$

$$\phi = 1 + \frac{1}{m_j} \int_0^{m_j} m_j d \ln \gamma_j \quad (8)$$

The symbol ν is the stoichiometric index, m_j stands for the molality of the salt. M_s and ϕ are the molecular weight and osmotic coefficient of the solvent, respectively. The activity coefficients of NaCl in water–methanol mixtures were taken from the literature.⁸

TABLE II. Values of pK, activity coefficient of NaCl, osmotic coefficient and solvent activity in methanol–water mixture containing 20 % methanol in different ionic strengths at 25 °C

$I / \text{mol L}^{-1}$	$I / \text{mol kg}^{-1}$	$\text{pK} / \text{mol}^2 \text{L}^{-2}$	$\text{pK} / \text{mol}^2 \text{kg}^{-2}$	γ_{NaCl}	ϕ	a_{SH}
0.10	0.10	13.720	13.689	0.720	0.910	0.996
0.25	0.26	13.684	13.651	0.643	0.892	0.991
0.50	0.52	13.598	13.564	0.592	0.883	0.982
0.75	0.79	13.591	13.546	0.571	0.890	0.973
1.00	1.06	13.631	13.580	0.563	0.905	0.963
1.25	1.33	13.697	13.643	0.563	0.923	0.953
1.50	1.60	13.769	13.713	0.567	0.944	0.942
1.75	1.88	13.826	13.764	0.576	0.966	0.931
2.00	2.16	13.846	13.779	0.588	0.988	0.919

TABLE III. Values of pK, activity coefficient of NaCl, osmotic coefficient and solvent activity in methanol–water mixture containing 40 % methanol in different ionic strengths at 25 °C

$I / \text{mol L}^{-1}$	$I / \text{mol kg}^{-1}$	$\text{pK} / \text{mol}^2 \text{L}^{-2}$	$\text{pK} / \text{mol}^2 \text{kg}^{-2}$	γ_{NaCl}	ϕ	a_{SH}
0.10	0.11	13.830	13.766	0.675	0.896	0.996
0.25	0.27	13.654	13.588	0.596	0.877	0.990
0.50	0.54	13.674	13.607	0.545	0.869	0.980
0.75	0.82	13.738	13.660	0.523	0.877	0.969
1.00	1.10	13.838	13.755	0.514	0.892	0.958
1.25	1.38	13.906	13.820	0.512	0.910	0.947
1.50	1.66	14.003	13.915	0.515	0.930	0.935
1.75	1.95	14.141	14.047	0.522	0.953	0.922
2.00	2.25	14.221	14.119	0.532	0.976	0.909

Ionic strength effect

To account for the ionic strength effect, the results were analyzed using the specific ion interaction theory (SIT) in which activity coefficient of ion i with charge z_i can be expressed by Eq. (9) in a solution of ionic strength I (in the molal scale) at 25 °C:^{5,9–14}

$$\log \gamma_i = -z_i^2 \frac{A\sqrt{I}}{1 + Ba_i\sqrt{I}} + \sum_j \epsilon_{ij} m_j \quad (9)$$

where a_i is the effective diameter of the hydrated ion i . A and B are Debye–Hückel constants, the values of which can be calculated by:

$$A = 1.8247 \times 10^6 \frac{\rho^{0.5}}{(DT)^{1.5}} \quad (10)$$

$$B = 50.2901 \frac{\rho^{0.5}}{(DT)^{0.5}} \quad (11)$$

where ρ , D and T are the density, dielectric constant and temperature of the solvent, respectively. Dielectric constants were taken from the literature,¹⁵ and are listed in Table IV. The ion interaction coefficient ε_{ij} interprets the specific short-range interactions of ion i with ion j in its molal concentration m_j .

TABLE IV. Values of pK° and $\Delta\varepsilon$ for every methanol–water mixture at 25 °C

Methanol content, mass %	D	pK°	$\Delta\varepsilon / \text{kg mol}^{-1}$	r^2
0	78.38	13.992±0.006	0.090±0.005	0.981
20	70.00	13.899±0.023	0.158±0.018	0.915
40	60.94	13.945±0.021	0.317±0.022	0.966

Introducing the SIT model into the logarithmic form of Eq. (2), the effect of the NaCl concentration on the autoprotolysis constant can be modeled as:

$$pK + 2 \log a_{\text{SH}} = pK^\circ - \frac{2A\sqrt{I}}{1+B\sqrt{I}} + \Delta\varepsilon I \quad (12)$$

where

$$\Delta\varepsilon = \varepsilon_{\text{SH}_2^+, \text{Cl}^-} + \varepsilon_{\text{S}^-, \text{Na}^+} \quad (13)$$

The pK° and $\Delta\varepsilon$ values were optimized by least squares analysis for all methanol–water mixture. The results are tabulated together with the correlation coefficient of the fitting procedure (r^2) in Table IV.

The value of ion interaction coefficient was positive and increased with increasing methanol content in the mixture. It is worthwhile to consider the effect of changing the dielectric constant on interaction parameter. As shown in Fig. 1, there is a linear dependence of the ion interaction coefficient on the reciprocal of dielectric constant.

The same behavior was found for β^1 , an interaction parameter in the Pitzer Model, in the thermodynamic treatment of the activity coefficients of 1:1 electrolytes in mixed solvents.^{15–22} Similar to β^1 , the principal contribution to ε_{ij} in SIT model originated from the short-range interactions between ions of opposite charge. Based on the exponential form of the Debye–Hückel theory, Gupta showed that the radial distribution function for unlike charged ions, namely g_{+-} (which contributes to β^1 and ε_{ij}) is a function of the dielectric constant that

increases greatly with decreasing dielectric constant.¹⁸ This explanation is consistent with the presented results. The positive values of $\Delta\varepsilon$ indicate that there is an attractive force between unlike ions. Moreover, the linear dependency of $\Delta\varepsilon$ on the inverse of dielectric constant shows that this attractive force mainly originated from electrostatic interactions. This is reasonable because the electrostatic interaction between unlike charged ions increases with decreasing polarity of the media.

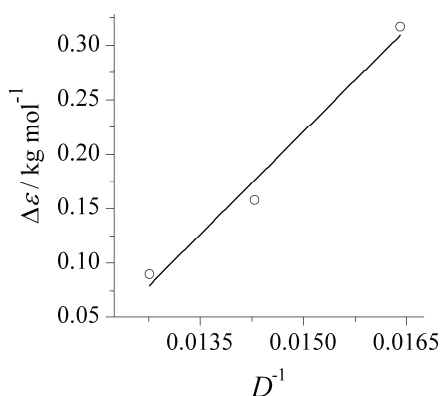


Fig. 1. Plot of $\Delta\varepsilon$ values as a function of the reciprocal of dielectric constant in water–methanol mixtures at 25 °C.

CONCLUSIONS

The autoprotolysis of some methanol–water mixture were successfully determined by an accurate potentiometric method over a wide range of ionic strength supplied by sodium chloride at 25 °C. The SIT theory was applied to describe the ionic strength dependency of the pK values. The thermodynamic autoprotolysis constant at infinite dilution was calculated together with the overall specific ion interaction coefficients.

Acknowledgement. The authors gratefully acknowledge the financial support from the Research Council of the Islamic Azad University, Jouybar Branch, Iran.

ИЗВОД

АУТОПРОТОЛИЗА У СИСТЕМУ ВОДА/МЕТАНОЛ/NaCl

ALI FARAJTABAR¹, FERESHTEH NADERI² и FARROKH GHARIB³

¹Young Researchers Club, Jouybar Branch, Islamic Azad University, Jouybar, Iran, ²Department of Chemistry, Shahr e Qods Branch, Islamic Azad University, Shahr e Qods, Tehran, Iran и ³Chemistry Department, Faculty of Sciences, Shahid Beheshti University, Tehran, Evin, Iran

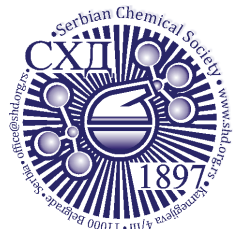
Потенциометријска метода је коришћена за одређивање константе аутопротолизе за водене растворе који садрже 0, 20 и 40 мас. % метанола у широком опсегу концентрација NaCl на 25 °C. Вредности јонске јачине биле су између 0,25 и 2,00 mol L⁻¹, са интервалима од 0,25 јединица. Осмотски коефицијенти и коефицијенти активности помешаних растварања израчунати су у зависности од јонске јачине. Зависност од јонске јачине анализирана је коришћењем теорије специфичних јонских интеракција. Пара-

метри специфичне јонске интеракције добијени су заједно са термодинамичком константом аутопротолизе. Резултати указују да интеракција између јона расте са порастом садржаја метанола у смеси.

(Примљено 4. јануара, ревидирано 10 марта 2013)

REFERENCES

1. A. Anderko, P. Wang, M. Rafal, *Fluid. Phase Equilib.* **194–197** (2002) 123
2. T. Mussini, A. K. Covington, P. Longhi, S. Rondinini, *Pure. Appl. Chem.* **57** (1985) 865
3. E. Kiliç, N. Aslan, *Microchim. Acta* **151** (2005) 89
4. R. M. Dzudovic, L. N. Jaksic, *J. Serb. Chem. Soc.* **75** (2010) 1575
5. P. Sipos, *J. Mol. Liq.* **143** (2008) 13
6. F. Naderi, A. Farajtabar, F. Gharib, *J. Solution Chem.* **41** (2012) 1033
7. T. Guetachew, S. Ye, I. Mokbel, J. Jose, P. Xans, *J. Solution Chem.* **25** (1996) 895
8. A. Basili, P. R. Mussini, T. Mussini, S. Rondinini, *J. Chem. Thermodyn.* **28** (1996) 923
9. C. Bretti, C. De Stefano, C. Foti, S. Sammartano, G. Vianelli, *J. Chem. Thermodyn.* **44** (2012) 154
10. J. N. Brønsted, *J. Am. Chem. Soc.* **44** (1922) 877
11. F. Gharib, A. Farajtabar, *J. Mol. Liq.* **135** (2007) 27
12. F. Gharib, M. Jabbari, A. Farajtabar, *J. Mol. Liq.* **144** (2009) 5
13. E. A. Guggenheim, J. C. Turgeon, *Trans. Faraday Soc.* **51** (1955) 747
14. M. Faraji, A. Farajtabar, F. Gharib, *J. Serb. Chem. Soc.* **78** (2012) 681
15. F. Hernandez-Luis, M. V. Vazquez, M. A. Estesó, *J. Mol. Liq.* **108** (2003) 283
16. K. S. Pitzer, *Activity Coefficients in Electrolyte Solutions*, CRC Press, Boca Raton, FL, 1991
17. K. S. Pitzer, *Thermodynamics*, McGraw-Hill, New York, USA, 1995
18. R. A. Gupta, *J. Phys. Chem.* **83** (1979) 2986
19. D. S. P. Koh, K. H. Khoo, C.-Y. Chen, *J. Solution Chem.* **14** (1985) 635
20. F. Hernandez-Luis, H. R. Galleguillos, T. A. Graber, M. E. Taboada, *Ind. Eng. Chem. Res.* **47** (2008) 2056
21. F. Deyhimi, B. Ghalami-Chooabar, *J. Mol. Liq.* **122** (2005) 116
22. F. Deyhimi, B. Ghalami-Chooabar, *Fluid Phase Equilib.* **246** (2006) 185.



J. Serb. Chem. Soc. 78 (10) 1569–1581 (2013)
JSCS–4519

JSCS-info@shd.org.rs • www.shd.org.rs/JSCS
UDC 546.47'711+66.022.3+547.571:
544.654.2

Original scientific paper

The influence of substituted aromatic aldehydes on the electrodeposition of Zn–Mn alloy

MIHAEL BUČKO^{1#}, UROŠ LAČNJEVAC^{2#} and JELENA BAJAT^{1**}

¹Faculty of Technology and Metallurgy, University of Belgrade, Karnegijeva 4, 11000 Belgrade, Serbia and ²Institute for Multidisciplinary Research, University of Belgrade, P. O. Box 33, 11030 Belgrade, Serbia

(Received 18 January, revised 20 February 2013)

Abstract: Additives are necessary in the electrodeposition of Zn–Mn alloys at high current densities, in order to reduce the hydrogen evolution reaction and prevent dendrite formation. The influences of two aromatic aldehydes, 4-hydroxy-benzaldehyde and 3,4-dimethoxy-benzaldehyde, as additives in the Zn–Mn plating electrolyte, were examined in this study. The characterization of the coatings by scanning electron microscopy and X-ray energy dispersive spectroscopy, as well as an examination of the effect of the additives by electrochemical methods, indicated a complex involvement of additive molecules in hydrogen evolution, as well as in Zn²⁺ and Mn²⁺ reduction. Consequently, a levelling action could be achieved and the chemical composition of the Zn–Mn alloy tailored by the addition of the proper type and concentration of additive in the plating electrolyte.

Keywords: Zn–Mn alloy; plating additive; hydrogen inhibitor; leveller; surface morphology.

INTRODUCTION

Among the various zinc alloys, Zn–Mn alloy coatings have received wide attention in the automotive industry, due to their attractive features.¹ It has been reported that alloy coatings with a high Mn content (10–30 at. % Mn) show the highest corrosion resistance known among zinc alloys.^{2,3}

The large scale production of Zn–Mn coatings with varying Mn contents seems achievable by electrochemical deposition.⁴ However, the incorporation of higher percent of Mn in an alloy is a difficult issue, since the standard electrode potentials of the Zn²⁺/Zn and Mn²⁺/Mn couples are significantly different, *i.e.*, $-0.76 V_{SHE}$ for Zn vs. $-1.18 V_{SHE}$ for Mn.⁵ One way of overcoming this issue is

* Corresponding author. E-mail: jela@tmf.bg.ac.rs

Serbian Chemical Society member.

doi: 10.2298/JSC130118025B



to shift the deposition potential of Zn closer to that of Mn by using a complexing agent, as realized, for instance, with sodium citrate or EDTA² in an acidic sulphate bath, or pyrophosphate ion in an alkaline bath.⁶ The deposition process in these cases has important drawbacks, particularly with regards to process control and current efficiency.⁷

On the contrary, a simple bath without strong complexing agent shows several benefits, such as high current efficiency and good bath stability.⁵ A simple electrolyte consisting of boric acid, potassium, and zinc and manganese chlorides was proposed for Zn–Mn electrodeposition in the past decade,⁸ and this electrolyte was chosen for examination in the present study. However, in order to obtain a Mn-rich deposit from a simple chloride bath, significant cathodic polarization or high deposition current density (c.d.) is necessary. Under such conditions, the Zn reduction is under diffusion control, leading to the formation and growth of dendrites,^{9,10} and additionally, the accompanying intensive hydrogen evolution decreases the current efficiency and may lead to porous coatings.¹¹

Dendritic deposit formation and hydrogen co-deposition during Zn–Mn electrodeposition at high c.d.s, could be prevented by the use of plating additives. As a matter of fact, in the industrial production of pure Zn coatings, plating additives are mainly necessary,^{12,13} and the list of compounds investigated for this purpose is extremely long.^{12,14} Concerning pure Mn plating, sulphur and selenium compounds are normally used as additives, in order to increase the current efficiency, but at the cost of contamination of the Mn deposit with sulphur and selenium inclusions.¹⁵ The effect of various additives (*e.g.*, gelatine, agar-agar,¹⁶ ascorbic acid, alcohols, aromatic aldehydes and ketones,¹⁷ thiourea and thiocarbamide¹⁸) are well understood in Zn–Mn electrodeposition from a sulphate electrolyte. Contrarily, the list of additives studied in chloride electrolytes is appreciably shorter, including Fra 700 (a commercial additive for pure Zn),⁸ poly(ethylene glycol)⁵ and ammonium thiocyanate.¹⁹

The scope of the present study was to investigate the influence of plating additives on the Zn–Mn alloy electrodeposits obtained from a chloride electrolyte, at a high c.d., where the onset of dendrite formation was observed, *i.e.*, at 90 mA cm⁻². The additives were expected to inhibit both dendritic growth and the hydrogen evolution reaction. According to the literature, substituted aromatic aldehydes are good candidates for both purposes.²⁰

The effects of two substituted aromatic aldehydes, namely 4-hydroxy-benzaldehyde (HBA) and 3,4-dimethoxy-benzaldehyde (DMBA), shown in Fig. 1, were studied in this work. Electrochemical techniques were used to investigate the role of the additives in the electrodeposition process, and scanning electron microscopy (SEM) coupled with X-ray energy dispersive spectroscopy (EDS) was used to characterize the deposits obtained under different plating conditions.

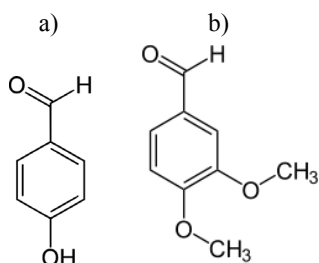


Fig. 1. a) The structure of 4-hydroxy-benzaldehyde and b) the structure of 3,4-dimethoxy-benzaldehyde.

EXPERIMENTAL

Electrolyte preparation

The electrodeposition of Zn–Mn alloys and the electrochemical experiments were performed using a chloride electrolyte containing 1.25 mol dm^{-3} KCl, 0.4 mol dm^{-3} H_3BO_3 , 0.3 mol dm^{-3} ZnCl_2 and 1 mol dm^{-3} MnCl_2 , pH 4.50. HBA and DMBA were added in concentrations of 0.25 or 0.5 g dm^{-3} . The electrolytes were prepared with analytical grade reagents and double distilled water.

Substrate preparation

The substrates for all experiments were steel (AISI 4340) panels with an active surface area of 3.68 cm^2 . Prior to each experiment, the steel surface was abraded successively with emery papers of the following grades: 600, 1000 and 1200, and then degreased in a saturated solution of NaOH in ethanol, pickled with 2 mol dm^{-3} HCl for 30 s and finally rinsed with distilled water.

Electrochemical studies and coating electrodeposition

A three-electrode cell arrangement was used for both the electrochemical (voltammetric and chronopotentiometric) studies and alloy electrodeposition, at the temperature of $25 \text{ }^\circ\text{C}$ without stirring. The reference electrode was a saturated calomel electrode (SCE) mounted in a Luggin capillary. All potentials in this paper are referred to this electrode. The counter electrode was a Zn plate (high purity Zn).

The Zn–Mn alloy coatings were electrodeposited galvanostatically at a c.d. of 90 mA cm^{-2} , using a PAR M173 galvanostat as the power supply. The deposition time was chosen to obtain layers of $10 \text{ }\mu\text{m}$ thickness, verified by a coating thickness measuring instrument Dualscope MPOR.

The voltammetric experiments (with IR correction) were performed at 5 mV s^{-1} between -800 and -1700 mV vs. SCE scanning to negative potentials, by using a ZRA Reference 600 potentiostat, Gamry Instruments.

Zn–Mn coating characterization

Surface morphology of the coatings was examined by scanning electron microscopy (SEM), using a Tescan, VEGA TS 5130 MM instrument. Chemical analysis of the deposits was performed by an attached energy dispersive X-ray spectrometer (EDS), INCAPenta-FETex3, Oxford Instruments.

The measurement of the surface roughness of the samples was performed using a TR200 surface roughness tester, over a length of 2.5 mm . The measured parameter was the average roughness, R_a , as denoted in Eq. (1), where “y” is the distance between the profile line and the average line:

$$R_a = \frac{1}{n} \sum_{i=1}^n |y_i| \quad (1)$$

RESULTS AND DISCUSSION

Effect of additives on the morphology of the Zn–Mn deposits

Zn–Mn coatings were preliminary electrodeposited from the chloride electrolyte free of organic additives, and it was observed that the samples obtained at c.d.s of up to 80 mA cm⁻² were smooth and homogeneous, *i.e.*, commercially acceptable deposits. However, the SEM photograph of a Zn–Mn coating plated at 90 mA cm⁻² (Fig. 2a) shows a deposit with cauliflower morphology and a very rough surface, on which precursors of dendrites are visible.⁹ Therefore, the effect of plating additives was further studied at 90 mA cm⁻², in order to clarify whether the additives could extend the operation window for the applied current density.

The morphologies of Zn–Mn deposits plated from the baths containing different concentrations of HBA or DMBA additive, are presented in Fig. 2b–e. It can be seen that the additive concentration had a higher impact on the coating morphology than the additive type. Namely, no dendrites are visible in Fig. 2b and c, but grain globules, ranging from 2–4 μm, are found for the Zn–Mn deposits plated from the baths containing 0.25 g dm⁻³ HBA or DMBA. Thus, both HBA and DMBA are powerful additives for depressing the formation of dendrites on Zn–Mn deposits formed at high c.d.s, *i.e.*, they act as levelling agents. The substituted aromatic aldehydes were reported as dendrite inhibitors due to their specific adsorption on the metallic surface and slow diffusion to the cathode.^{20,21} Namely, the rate of metal deposition is inhibited on the cathode locations where the additive molecules are adsorbed. Since the additive bulk concentration is very low, the adsorption of organic molecule is highly influenced by mass transport, *i.e.*, the molecules are preferentially adsorbed on those parts of the surface that are more accessible, *i.e.* on the precursors of dendrites. As a result, protrusions receive more additive molecules by diffusion and consequently become smaller as the deposit grows.²¹

When the concentration of HBA and DMBA additives was increased to 0.5 g dm⁻³, two strong effects could be observed, as shown in Fig. 2d and e. The Zn–Mn globules no longer exist, meaning that the growth of the crystallites perpendicular to the surface was inhibited, and they spread across the surface as smooth layers to produce deposits which are rather flat on the microscopic scale. It should be noticed that the deposits obtained appeared bright, as observed by the naked eyes. Thus, the levelling action of the additives examined in this study, strongly depended on their concentration. This is in agreement with data for some other additives. Thus, it was shown, for example, that coumarone in Ni plating produced levelled or bright deposits only as a function of its concentration.²² A similar result was found for thiourea and saccharin in Ni–P and Cu deposition.²³ In fact, aldehydes

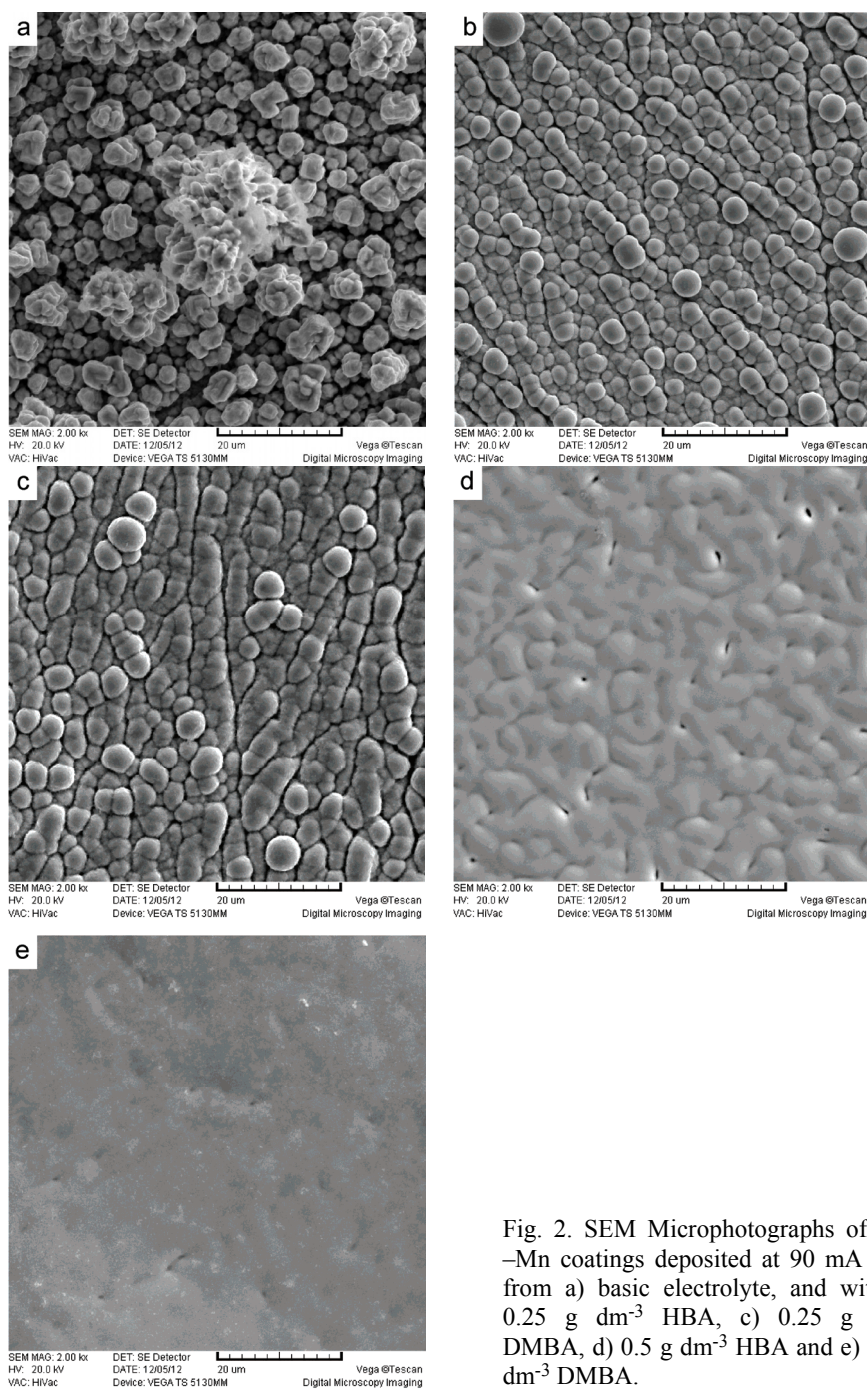


Fig. 2. SEM Microphotographs of Zn–Mn coatings deposited at 90 mA cm^{-2} from a) basic electrolyte, and with b) 0.25 g dm^{-3} HBA, c) 0.25 g dm^{-3} DMBA, d) 0.5 g dm^{-3} HBA and e) 0.5 g dm^{-3} DMBA.

are widely used as brightening agents in Zn electrodeposition, improving grain fineness.^{13,14,24} Additives that smooth the surface at the 1–500 μm lateral length are known as levellers and the ones responsible for surface brightening at 1–1000 nm lateral distance are known as brighteners.²⁵ Apart from visual examination, no additional experiment was conducted in order to evaluate further the brightening effect of the two additives in the present article.

However, as a second effect of the change in additive concentration from 0.25 to 0.5 g dm^{-3} was that an insufficient coalescence of the deposits could be noticed, with pitting-like morphology, particularly for the coating obtained with HBA (Fig. 2d), probably indicating that the additives and/or products of their decomposition act as organic contaminants in the electrolyte. As a matter of fact, many organic compounds, above some critical concentration in a plating bath, bond to specific parts of the substrate and consequently may be trapped in the deposit or cause a noticeable hydrogen gas bubbling, increasing thereby the chances for the formation of gas pits in that area. The pitting of the deposit due to organic impurities is a serious problem in Ni²² and Cr²⁶ electrodeposition, and probably is present in this work, for higher additive concentration (0.5 g dm^{-3}).

In order to additionally examine the levelling effect of substituted aromatic aldehydes, the macroscopic roughness was measured for the Zn–Mn coatings deposited at different concentrations of the two additives, and the values of average roughness are presented in Table I. Similarly to the SEM observations, it is clear from Table I that the roughness of the samples depended strongly on the concentration of the additives, regardless of their structure, in terms of a decrease in the average roughness on addition of more additive to the plating solution. The lower R_a values for the samples deposited in the presence of additives, compared to the sample from blank electrolyte, clearly denote the smoothening effect. This is particularly visible for 0.5 g dm^{-3} of additives, where the R_a values of $\approx 0.5 \mu\text{m}$ indicate very flat deposits.

TABLE I. The values of average roughness, R_a , for Zn–Mn coatings deposited from different plating electrolytes

Additive type	Additive concentration / g dm^{-3}	$R_a / \mu\text{m}$
No additive	0	1.65
HBA	0.25	1.03
	0.5	0.47
DMBA	0.25	0.98
	0.5	0.62

EDS Analysis

The chemical composition analysis revealed that in addition to Zn and Mn, various amounts of oxygen were present in the Zn–Mn coatings obtained at 90 mA cm^{-2} . The atomic contents of Mn and O in the samples deposited from

electrolytes with different additive concentrations are shown in Fig. 3. The oxygen content was between 5 and 7 at. % for the samples obtained in the presence of additives, which could be related to alloy oxidation during air-exposure.¹ On the contrary, the coating obtained in the blank electrolyte contained 18 at. % oxygen, indicating either rapid corrosion of the dendritic sample or, more probably, the inclusion of metallic hydroxides, due to the increased pH in the near-cathodic layer, as a result of fast hydrogen evolution.²⁷ The issue of hydroxide inclusions was reported for Mn alloy coatings obtained at high c.d.s, where the oxygen content reached even 60 at. %, ^{11,27} and also for pure Zn coatings, where 18 mass % of oxygen was reported.²⁸

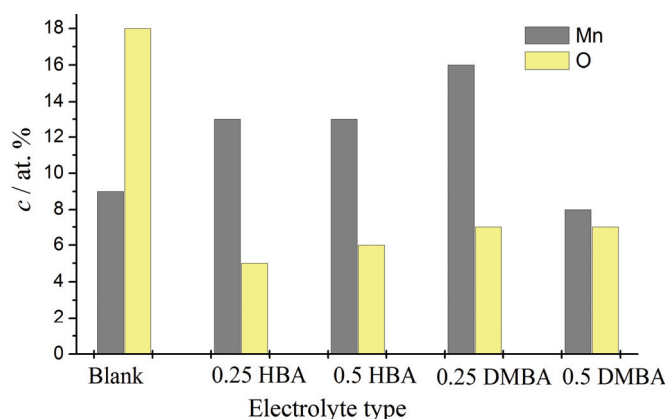


Fig. 3. The dependence of the Mn and O content in the Zn–Mn coatings obtained at 90 mA cm⁻² on the type and concentration of the plating additive.

Hence, the low oxygen percent in the coatings obtained with additives, probably means that the deposits were hydroxide-free, *i.e.*, the hydrogen evolution process during alloy deposition is not fast enough to create alkaline media in the near-cathodic layer.²⁹ It could be concluded that the EDS analysis gives circumstantial, but strong evidence that the additives are hydrogen inhibitors in Zn–Mn electrodeposition.

When it is assumed that the total applied deposition c.d. is related to Zn and Mn reduction and hydrogen formation, then the zinc and manganese atomic percentage determined by EDS, allows an evaluation of the partial current densities for each reaction.³⁰ While the surface morphology was quite similar for both additives, the elemental composition of the Zn–Mn deposits depended greatly on the additive type. The Mn content was 9 % in the coating obtained at 90 mA cm⁻² without additives in the electrolyte (Fig. 3) and it increased to 13 % when HBA was added, independent of the additive concentration. This indicates that the adsorbed HBA molecules do not affect the reduction of both metals equally, *i.e.*, either Zn reduction is more inhibited or Mn reduction is favoured in the presence

of HBA. On the other hand, in the case of DMBA, the role of its concentration is quite ambiguous, because at the lower DMBA concentration, the Mn content in the deposit reached 16 %, whereas it was only 8 % when 0.5 g dm^{-3} DMBA was present in the electrolyte.

Linear sweep voltammetry

In order to further examine the influence of additives on the coating morphology and chemical composition, electrochemical techniques were applied. For characterization of the substituted benzaldehydes as hydrogen evolution inhibitors, linear voltammetry was performed at 5 mV s^{-1} . The polarization curves, shown in Fig. 4, were recorded in plating solutions free of Zn and Mn ions; thus the increase in the cathodic current could be attributed to only one process, *i.e.*, hydrogen evolution. The polarization curves in Fig. 4 reveal that hydrogen evolution started at the same potential, around -1200 mV , in all electrolytes. However, at more negative potentials, the suppression of hydrogen evolution by the additives was seen as a decrease in the j - E slope.³¹ According to the literature, substituted aromatic aldehydes are strong hydrogen evolution inhibitors, due to the interaction of the negative charge centre in the organic molecule ($-\text{CHO}$) with the positive charge carriers at the cathode/electrolyte interface, *i.e.*, with the adsorbed hydrogen ions from acidic plating baths.³² It is also clear from Fig. 4 that HBA provides stronger inhibition as compared to DMBA.

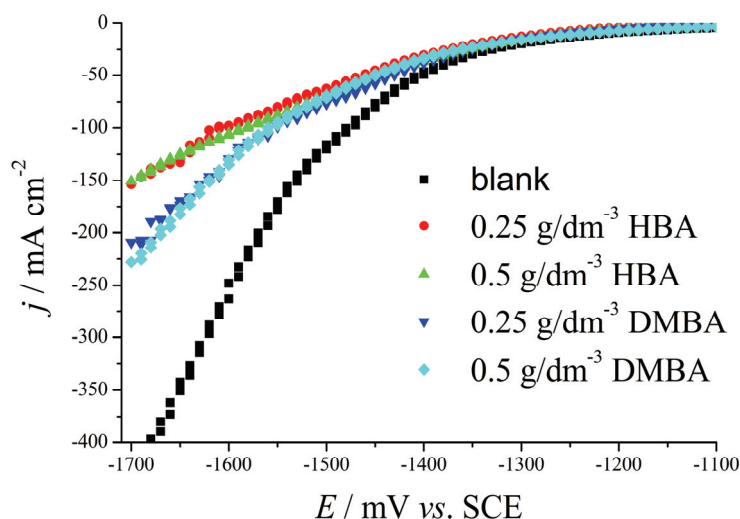


Fig. 4. Linear voltammograms of a steel electrode in $1.25 \text{ mol dm}^{-3} \text{ KCl} + 0.4 \text{ mol dm}^{-3} \text{ H}_3\text{BO}_3$, with different concentrations of HBA and DMBA additives.

It should be additionally stressed that the increase in the additives concentration from 0.25 to 0.5 g dm^{-3} did not bring any improvement in the suppression

of hydrogen evolution. In fact, it is quite common with many additives that the slopes of the cathode potential vs. additive concentration curves decrease with increasing additive concentration, and that a polarization plateau is reached at a certain amount of additive.³³

To conclude, it is clear that both additives are beneficial for Zn–Mn electrodeposition because they inhibit the hydrogen evolution reaction, thus increasing the current efficiency and preventing coating porosity. Moreover, as the most important fact, they enable the formation of hydroxide-free Zn–Mn deposits even at 90 mA cm^{-2} .

Chronopotentiometric study

From the previous analysis, it could be concluded that two general effects were noticed concerning the influence of the additives: an increase in the smoothness of the samples with increasing additive concentration and the Mn content change in the alloys. A number of theories concerning the influence of additives on metal deposition start from the principle of electrosorption of additives at the metal/electrolyte interface;²⁹ hence this approach may also be used to relate the structure and concentration of the additives analysed in this work with their effect on Zn–Mn deposits. A strong influence of additives on the cathodic overpotential is often used as a selection criterion for efficient plating agents. It is thought that the main cause of the changes in the cathode potential is the coverage of the electrode interface by additive molecules, which increases the effective c.d. and, consequently, the overvoltage.³³

The effect of HBA and DMBA additives on the cathodic potential related to the Zn–Mn electrodeposition at a c.d. of 90 mA cm^{-2} is shown in Fig. 5. It can be seen that the curves recorded in the presence of the additives are 55–70 mV more negative as compared to the curve of the blank electrolyte. The SEM photographs showed that such an overpotential difference is sufficient for the production of smooth, non-dendritic deposits with a fine-grained structure.

When the influence of additive concentration is analyzed, it is seen that the overpotential only slightly increases when the additives concentration increases from 0.25 to 0.5 g dm^{-3} , *i.e.*, the change is approximately 5–20 mV. Nevertheless, it seems possible that such a small increase in the cathodic overpotential is related to the change in surface morphology from spherical agglomerates to a completely flat surface, as SEM analysis showed. This is consistent with the literature, because it was reported, for example, that the brightening of a nickel deposit was accompanied by a cathode polarization of only 20 mV.³⁴ Based on the overpotential change seen in Fig. 5, it could be assumed that a more uniform distribution of the adsorbed additive molecules could occur on the surface when a higher additive concentration is applied, leading to significant reduction in the Zn–Mn aggregate size, which resulted in a smoother appearance.²⁵

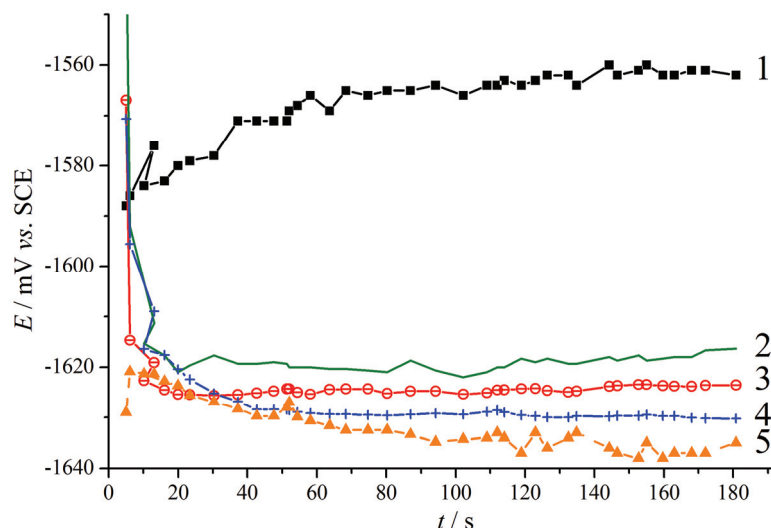


Fig. 5. Potential – time transients for Zn–Mn alloy electrodeposition at 90 mA cm^{-2} from: 1) basic electrolyte, with 2) 0.25 and 3) 0.5 g dm^{-3} HBA; with 4) 0.25 and 5) 0.5 g dm^{-3} DMBA.

Concerning the additive structure, an analysis of the voltammograms shown in Fig. 4, which refer to hydrogen evolution, and of the $E-t$ curves in Fig. 5, where the main reactions are Zn and Mn reduction, indicates that the DMBA additive is a weaker inhibitor for hydrogen evolution, as compared to HBA additive, but it has a stronger inhibiting influence on the reduction of metal ions. Furthermore, the EDS analysis showed that the Mn at. % in the Zn–Mn deposits was principally higher for the depositions in the presence of additives and, additionally, that DMBA had a more pronounced effect on the Mn content in alloy deposit. Based on all these results, it could be inferred that the molecular structure of the investigated additives plays an important role in their interaction with Zn^{2+} , Mn^{2+} or H^+ reduction.

The adsorption of aromatic aldehydes, such as vanillin and its derivatives, is well documented and examined,^{32,35} and it was shown that the adsorption on a steel surface would occur through carbonyl, methoxy and hydroxyl functional groups arranged on the benzene ring.³⁵ In addition, it was assumed that the organic molecules preferably interact with the positive cathodic sites, and the strength of the negative charge centre in the molecule (carbonyl group) is influenced by side groups of the benzene ring ($-\text{OH}$, $-\text{OCH}_3$).³² It should be emphasized that besides adsorbed hydrogen ions, the metallic species participating in Zn–Mn deposition may also be positive charge carriers adsorbed on the cathode (for instance, Zn_{ad}^+ , ZnH_{ad}^+ , etc.).³⁶ As Fig. 1 shows, the HBA molecule has a hydroxyl, while the DMBA molecule has two methoxy groups as functional side

groups. It can be summarized that due to different side groups, the molecules have different affinities to various adsorbed species, which results in the slight overpotential deviations observed in Fig. 5, but leads to significant changes in Mn at. % in the coatings.

CONCLUSIONS

The effects of the addition of two aromatic aldehydes to the plating electrolyte on the properties of Zn–Mn alloy electrodeposits were studied. The SEM micrographs showed that the Zn–Mn coatings obtained at 90 mA cm^{-2} in the presence of additives were smooth and homogeneous. A levelling action was observed with 0.25 g dm^{-3} additive and that it increased when the additive concentration was increased to 0.5 g dm^{-3} , regardless of the additive type.

The EDS results showed that the sample deposited from the electrolyte free of additive possesses high amount of oxygen, indicating rapid corrosion or metallic hydroxide inclusions in the sample. The very low oxygen percent in the samples deposited with additives, as well as a voltammetric examination, gave evidence for strong inhibiting actions of the additives on hydrogen evolution. Furthermore, the observed changes in Zn and Mn atomic content in the coatings revealed that the additive molecules interact with all reactions in the process, *i.e.*, the Zn^{2+} , Mn^{2+} and hydrogen ion reduction. It is assumed that the molecule structure of the additives (*i.e.*, the presence of methoxy or hydroxyl groups) affects their adsorption ability and, consequently, modifies the kinetic parameters of all reactions participating in the electrodeposition of Zn–Mn alloys.

It could be concluded that the employed aromatic aldehydes are beneficial additives for Zn–Mn alloy electrodeposition, because they extend the operative window of the current density, thereby increasing the Mn content and enabling the formation of smooth deposits.

Acknowledgement. This research was financed by the Ministry of Education, Science and Technological Development of the Republic of Serbia, Contract No. III 45019.

ИЗВОД

УЛОГА СУПСТИТУИСАНИХ АРОМАТИЧНИХ АЛДЕХИДА У ЕЛЕКТРОХЕМИЈСКОМ ТАЛОЖЕЊУ Zn–Mn ЛЕГУРА

МИХАЕЛ БУЧКО¹, УРОШ ЛАЧЊЕВАЦ² И ЈЕЛЕНА БАЈАТ¹

¹Технолошко–металуршки факултет, Универзитет у Београду, Карнегијева 4, 11000 Београд и

²Институт за мултидисциплинарна истраживања, Универзитет у Београду, п. пр. 33, 11030 Београд

У циљу успоравања реакције издвајања водоника и спречавања настајања дендрита приликом електрохемијског таложња Zn–Mn легура високим густинама струје, неопходна је примена специфичних додатака. У овом раду је испитиван утицај два ароматична алдехида, 4-хидрокси-бензалдехида и 3,4-диметокси-бензалдехида, као специфичних додатака у таложњу Zn–Mn легура. Карактеризација превлака скенирајућом електронском микроскопијом и енергетском дисперзионом спектроскопијом X-зрака, као и испитивање утицаја специфичних додатака на процес таложња електрохемијским

методама, указују на сложене интеракције молекула ароматичних алдехида у процесима издвајања водоника и редукције јона цинка и мангана. У раду је показано да се само применом одређене концентрације и врсте специфичног додатка може мењати хемијски састав Zn–Mn легуре и могу се добијати превлаке мање храпавости.

(Примљено 18. јануара, ревидирано 20. фебруара 2013)

REFERENCES

1. Z. I. Ortiz, P. Diaz-Arista, Y. Meas, R. Ortega-Borges, G. Trejo, *Corr. Sci.* **51** (2009) 2703
2. C. Muller, M. Saret, T. Andreu, *J. Electrochem. Soc.* **149** (2002) C600
3. L. Diaz-Ballote, R. Ramanauskas, P. Bartolo-Perez, *Corros. Rev.* **18** (2000) 41
4. B. Bozzini, V. Accardi, P. L. Cavallotti, F. Pavan, *Met. Finish.* **97** (1999) 33
5. D. Sylla, J. Creus, C. Savall, O. Roggy, M. Gadouleau, Ph. Refait, *Thin Solid Films* **424** (2003) 171
6. M. Bučko, J. Rogan, S. I. Stevanović, A. Perić-Grujić, J. B. Bajat, *Corr. Sci.* **53** (2011) 2861
7. M. Bučko, S. Stevanović, M. Tomić, M. Pavlović, J. B. Bajat, *Hem. Ind.* **65** (2011) 295 (in Serbian)
8. C. Savall, C. Rebere, D. Sylla, M. Gadouleau, Ph. Refait, J. Creus, *Mater. Sci. Eng., A* **430** (2006) 165
9. N. Nikolić, K. Popov, Lj. Pavlović, M. Pavlović, *J. Electroanal. Chem.* **588** (2006) 88
10. G. Orhan, G. G. Gezgin, *J. Serb. Chem. Soc.* **77** (2012) 651
11. J. Gong, G. Zangari, *Mat. Sci. Eng., A* **344** (2003) 268
12. C. A. Loto, *Asian J. Appl. Sci.* **5** (2012) 314
13. N. D. Nikolić, G. Novaković, Z. Rakočević, D. R. Đurović, K. I. Popov, *Surf. Coat. Technol.* **298** (2002) 188
14. N. D. Nikolić, Z. Rakočević, K. I. Popov, *J. Solid State Electrochem.* **8** (2004) 526
15. P. Wei, O. E. Hileman, M. R. Bateni, X. Deng, A. Petric, *Surf. Coat. Technol.* **201** (2007) 7739
16. G. Govindarajan, V. Ramakrishnan, S. Ramamurthi, V. Subramanian, N. Parthasaradhy, *Bull. Electrochem.* **5** (1990) 485
17. N. Boshkov, *Surf. Coat. Technol.* **172** (2003) 217
18. B. Bozzini, E. Griskonis, A. Fanigliulo, A. Sulcius, *Surf. Coat. Technol.* **154** (2002) 294
19. P. Diaz-Arista, Z. I. Ortiz, H. Ruiz, R. Ortega, Y. Meas, G. Trejo, *Surf. Coat. Technol.* **203** (2009) 1167
20. N. D. Nikolić, K. I. Popov, Z. Rakočević, D. R. Đurović, M. Pavlović, M. Stojanović, *J. Serb. Chem. Soc.* **65** (2000) 819
21. M. S. Aroyo, *Plat. Surf. Finish.* **121** (1995) 53
22. N. V. Mandich, H. Geduld, *Met. Finish.* **100** (2002) 38
23. M. Quinet, F. Lallemand, L. Ricq, J. Y. Hihn, P. Delobelle, C. Arnould, Z. Mekhalif, *Electrochim. Acta* **54** (2009) 1529
24. J. C. Hsieh, C. C. Hu, T. C. Lee, *J. Electrochem. Soc.* **155** (2008) D675
25. A. Chrzanowska, R. Mroczka, *Electrochim. Acta* **78** (2012) 316
26. N. V. Mandich, *Met. Finish.* **97** (1999) 30
27. J. Gong, G. Wei, J. A. Barnard, G. Zangari, *Metall. Mater. Trans., A* **36** (2005) 2705
28. R. Ramanauskas, R. Juskenas, A. Kalinichenko, L. F. Garfias-Mesias, *J. Solid. State Electrochem.* **8** (2004) 416
29. S. Nineva, Ts. Dobrovolska, I. Krastev, *J. Appl. Electrochem.* **41** (2011) 1397

30. F. Lallemand, L. Ricq, M. Wery, P. Bercot, J. Pagetti, *Appl. Surf. Sci.* **228** (2004) 326
31. B. Jović, U. Lačnjevac, V. Jović, Lj. Gajić-Krstajić, N. Krstajić, *J. Serb. Chem. Soc.* **77** (2012) 211
32. H. Dietz, G. Hoogestraat, S. Laibach, D. von Borstel, K. Wiesener, *J. Power Sources* **53** (1995) 359
33. L. Oniciu, L. Muresan, *J. Appl. Electrochem.* **21** (1991) 565
34. S. Nakahara, R. Weil, *J. Electrochem. Soc.* **120** (1973) 1462
35. X. Li, S. Deng, H. Fu, *Prog. Org. Coat.* **67** (2010) 420
36. K. Raeissi, A. Saatchi, M. A. Golozar, A. Tufani, J. A. Szpunar, *Electrochim. Acta* **53** (2008) 4674.



J. Serb. Chem. Soc. 78 (10) 1583–1594 (2013)
JSCS–4520

Comparison of the electrochemical behavior of cast and sintered CuAg 4 at. % alloy during thermomechanical treatment

MIRJANA M. RAJČIĆ-VUJASINOVIĆ*#, VESNA J. GREKULOVIĆ#,
ZORAN M. STEVIĆ, SVETLANA D. NESTOROVIĆ#, IVANA I. MARKOVIĆ#
and SLAVKO B. SIMOV

University of Belgrade, Technical faculty in Bor, V. J. 12, 19210 Bor, Serbia

(Received 24 December 2012, revised 13 March 2013)

Abstract: The paper presents a comparison of the electrochemical behavior of samples of CuAg 4 at. % alloy obtained by the powder metallurgy method and the same alloy obtained by melting and casting during oxidation in an alkaline medium. The investigated alloys exhibited the anneal hardening effect. Hence, they were examined in each stage of thermomechanical treatment resulting in this effect. Cyclic voltammetry investigations showed that both the sintered and cast samples after cold rolling to a final reduction of 60 % behaved as completely homogenous phases. In this stage of thermomechanical treatment, peaks corresponding to reactions on silver did not appear and the currents on the cyclic voltammograms were the lowest. After annealing below the recrystallization temperature, both samples exhibited anneal hardening; in this stage, the sintered alloy retained its corrosion stability, whereas the current densities for the cast alloy increased and peaks characteristic for silver appeared again. Further annealing above the recrystallization temperature led increasing current density on voltammograms for samples obtained by both methods and all characteristic current peaks for silver reappeared.

Keywords: copper; silver; anodic oxidation; anneal hardening; recrystallization.

INTRODUCTION

Copper–silver alloys can be obtained by the so-called ingot metallurgy (IM) method, *i.e.*, by melting and casting, as well as by the powder metallurgy (PM) method.^{1–3} The Ag–Cu binary alloy is a characteristic example of a eutectic system, with full solubility in the liquid state and mutually restricted solubility in the solid state.⁴ The maximum solubility of silver in copper at the eutectic temperature is 4.9 at. % and it decreases with decreasing temperature. Cu–Ag alloys have wide range of electrical applications because of good combinations of high

* Corresponding author. E-mail: mrajcic@tf.bor.ac.rs

Serbian Chemical Society member.

doi: 10.2298/JSC121224049R

mechanical properties and high electrical conductivity. Tensile strengths up to 1 GPa and electrical conductivities of about 60–70 % of the International Annealed Copper Standard (IACS) make them particularly suitable for applications such as pulsed high-field solenoids and conductor materials for Bitter type magnets.^{5,6} Additional improvements in properties such as electrical conductivity, corrosion resistance, strength and maintenance of strength at high temperatures can be achieved by application of proper thermomechanical treatments. Anneal hardening is a genuine hardening mechanism that occurs in some copper-based alloys, including Cu–Ag alloys, where alloying elements segregate on dislocation after cold deformation and annealing below the recrystallization temperature. Anneal hardening of Cu–Ag alloys was observed in the annealing temperature range from 140 to 400 °C, the hardness increasing with the degree of pre-deformation.^{2,3} The phenomenon was observed in alloys synthesized by both the IM and the PM method.

Oxidation and passivity of pure copper and silver have been widely investigated in the electrochemical literature.^{7–13} Cu–Ag alloys have been less examined, but some recent papers deal with electrochemical characteristics of this binary alloy.^{14–21} Taking into account that the method of synthesis of an alloy may influence its corrosion stability, the goal of the current work was to compare the electrochemical behavior of CuAg 4 at. % alloy obtained by the PM method with the same alloy obtained by the IM method. The samples obtained by the two different methods were compared in the corresponding stages of thermo-mechanical treatment that results in anneal hardening.

EXPERIMENTAL

Electrochemical characterization was performed using a standard three-electrode system consisting of a saturated calomel electrode (SCE) as the reference electrode, platinum as the counter electrode and CuAg 4 at. % alloy, as the working electrode material. The active surface area of the working electrodes was 0.25 cm² and that of the counter electrode was 2 cm². The investigations were performed in a 0.1 M NaOH solution (pH 12.7) by cyclic voltammetry and open-circuit potential measurement under the following conditions: temperature, 25 °C and scan rates of 10, 20, 50, 75 and 100 mV s⁻¹.

The CuAg 4 at. % alloy for the working electrodes was obtained by both the PM and IM methods. The sample marked as IM1 (pre-saturated solid solution) was prepared in the following usual metallurgical way: metallic silver and electrolytic copper wire with a purity of 99.99 % were weighed in the required ratio, melted in a laboratory electric furnace and cast in a sand clay mould; the obtained ingots were subjected to homogenization annealing at 800 °C for 34 h, pre-final cold rolling, solution annealing and quenching in ice water.

Electrolytic copper powder and silver powder with purities of 99.7 and 99.9 %, respectively (the silver powder content in the mixture was 4 at. %) were used to prepare the samples marked as PM. Powder mixture compacts measuring 6–7 mm in height, 30 mm in length and 12 mm in width were prepared by the method of one sided pressing at a pressure of 300 MPa on a hydraulic press (sample PM1 for electrochemical investigations). The compacts were sintered at 790 °C in a horizontal tube furnace under an atmosphere of high purity dry

hydrogen for 1 h to obtain the sample marked as PM1. Detailed synthesis and thermomechanical treatment to obtain starting samples are described in previous works.^{2,3,18,19} The samples for testing are chosen in corresponding different stages of thermomechanical treatment that resulted in anneal hardening for both the IM and PM samples. This treatment included final cold rolling and annealing at different temperatures below the recrystallization temperature. Finally, the samples were subjected to annealing above the recrystallization temperature. The sample assignments and descriptions of preparation are given in Table I.

TABLE I. Sample abbreviations and descriptions of preparation

Abbreviation	Description of preparation
IM1	Pre-saturated α solid solution obtained by melting, casting, annealing at 700 °C for 1 h and quenching in ice water (the treatment is fully described in ref. 16)
IM2	Cold rolled sample IM1 after a final reduction of 60 %
IM3	Sample IM2 annealed at 260 °C for 90 min (exhibited anneal hardening)
IM4	Sample IM3 annealed at 600 °C for 60 min
PM1	Powder mixture pressed at a pressure of 300 MPa and sintered at 790 °C for 1 h with a two-phases structure
PM2	Cold rolled PM1 after a final reduction of 60 %
PM3	Sample PM2 annealed at 260 °C for 150 min (exhibited anneal hardening)
PM4	Sample PM3 annealed at 600 °C for 60 min

Five measurements of hardness and electrical conductivity were performed on each chosen sample. The hardness measurements were realized using a Vickers hardness tester VEB Leipzig with a load of 5 kg and a dwell time of 15 s. Electrical conductivity was measured using a “Sigmatest” conductometer.

For electrochemical measurements, all the investigated samples were prepared in the form of electrodes. Electrical contact between the copper wire and the electrode material was achieved using conducting silver glue IM-P3014 (Iritel, Belgrade) and then mounted in cold polymerized SIMGAL mass (Galenika, Belgrade). For each set of experiments, working electrodes were ground with the finest grinding paper, polished with alumina (0.05 μm), washed with distilled water and alcohol, dried, and finally drowned into electrolyte. Before each experiment, the working electrode was polished with alumina.

The system for electrochemical measurements consisted of hardware (PC, AD–DA converter NI-6251 produced by National Instruments and an analog interface) and software for excitation and measurement (LabView 8.2 platform, National Instruments, Austin, TX, and application software) both fully developed by the Technical Faculty in Bor, Serbia.^{22,23} The investigations were performed in 0.1 M NaOH by cyclic voltammetry and open circuit potential measurements.

RESULTS AND DISCUSSION

Hardness, electrical conductivity and steady-state open circuit potentials of all the investigated samples are presented in Table II. The table illustrates the changes in the mechanical and electrical characteristics of the CuAg 4 at. % alloy during thermomechanical treatment resulting in so-called anneal hardening.

It can be seen that sample PM1 had lower hardness and electrical conductivity values in comparison with those of the IM1 sample. The porosity of the

sintered material decreased its properties in comparison with the more compact cast material.

TABLE II. Some properties of the CuAg 4 at. % alloys in different stages of thermo-mechanical treatment

Abbreviation	Hardness, HV	Electrical conductivity, MS m ⁻¹	Steady-state open circuit potential, V vs. SCE
IM1	80	42.6	-0.200
IM2	170	40.4	-0.209
IM3	194	42.1	-0.152
IM4	97	50	-0.157
PM1	48	38	-0.198
PM2	156	46.3	-0.208
PM3	182	46.9	-0.205
PM4	93	50.4	-0.210

The hardness of both samples increased during cold rolling, due to deformation strengthening. Although the PM2 sample still had lower hardness in comparison with the suitable hardness of the IM2 sample, a more intensive hardness increase was achieved with the PM2 sample, because porosity elimination and deformation strengthening occurred simultaneously. The electrical conductivity of the PM sample was increased after cold rolling but the electrical conductivity of the IM sample decreased with deformation. This was the result of two opposing effects.² A porosity decrease during cold rolling increases the electrical conductivity (effect 1). However, lattice distortion (effect 2) during the cold rolling decreases the electrical conductivity. In the PM sample, the first effect was stronger than the second one and as a result, the electrical conductivity increased. On the other hand, with the IM sample, the second effect was stronger than the first one, which resulted in a decrease in the electrical conductivity.

The anneal hardening effect appeared in both cold deformed samples during annealing at 260 °C as the result of silver segregation to dislocations, analogous to the formation of Cottrell atmospheres in interstitial solid solutions, which resulted in increases in the hardness and electrical conductivity of samples IM3 and PM3.

After annealing the cold deformed samples at 600 °C, the hardness of both samples dropped significantly, because of the formation and growth of new undeformed grains, *i.e.*, recrystallization starts to occur. The hardness values for the IM4 and, especially, for the PM4 sample were higher compared to those of the initial state, implying that the recrystallization had not occurred in full. Annealing at 600 °C led to an increase in the electrical conductivity, because of recovery and the beginning of recrystallization (samples IM4 and PM4).

The electrochemical investigations included measurements of the open-circuit potential (OCP) and cyclic voltammetry. The open-circuit potentials for all

the samples are given in Table II. It is obvious that there is no big difference in the OCP values between the samples obtained by the two different metallurgical techniques. On the other hand, annealing led to some positive change in the OCP of casted samples, because silver as the nobler component appeared as an independent phase, while all PM samples had very similar OCP values (around -0.200 mV vs. SCE). The voltammograms were recorded from -1.6 up to 1.0 V vs. SCE, *i.e.*, from hydrogen evolution up to the beginning of gaseous oxygen evolution. To recognize which current wave corresponds to copper and which one to silver, the voltammograms obtained for the alloy (samples IM4 and PM1) were compared with those obtained on the pure metals, copper and silver (Fig. 1). The results of the first scan obtained at a scan rate of 20 mV s^{-1} are presented.

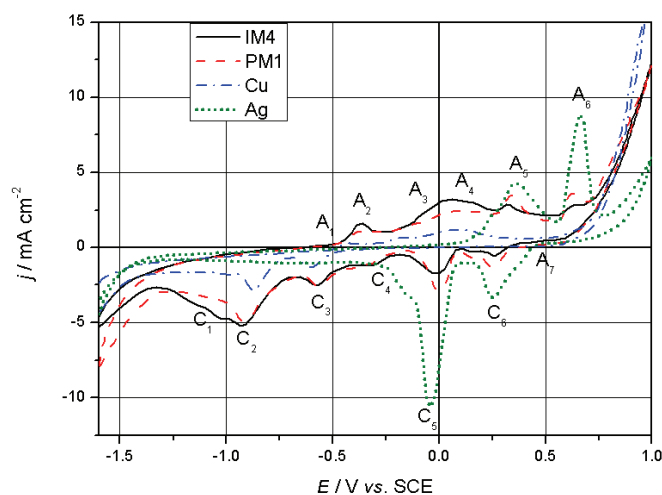


Fig. 1. Cyclic voltammograms of pure metals Cu and Ag, and samples IM4 and PM1 in 0.1 M NaOH at a scan rate of 20 mV s^{-1} .

The voltammograms in Fig. 1 proved that the mechanism of the anodic oxidation of the alloy in NaOH medium consisted of at least six steps. The first step in the oxidation process of the investigated alloy was the formation of a monolayer of adsorbed OH^- species.^{18,19} This reaction is attributed to the current peak marked as A_1 . The next step during the anodic polarization was the formation of a lower copper oxide, Cu_2O , connected with the peak A_2 . Peak A_2 appeared only on the voltammograms for samples of the alloy, both IM4 and PM1, and for pure copper. The same was valid for the peak A_3 ; hence, this peak is connected with formation of a higher oxide of copper, CuO . Current peaks A_4 , A_5 and A_6 , registered on the voltammogram for pure silver, are very well defined on the voltammogram for the sample of alloy obtained by the PM method, but they appear only as waves on voltammogram for the sample IM4. Peaks or waves A_4 and A_5 are

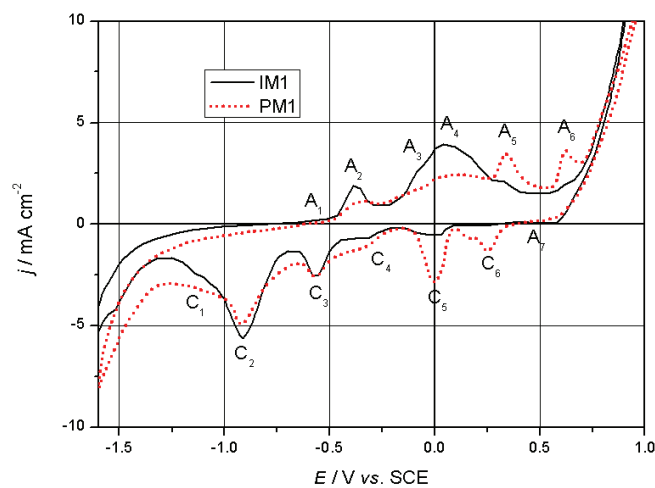
connected with formation of the lower oxide of silver, Ag₂O (type I and type II), and the peak A₆ is related with formation of higher silver oxide, AgO.^{11–13,18–21} In the cathodic direction, the anodic reaction products are sequentially reduced in the corresponding reverse order, C₆, C₅, C₄, C₃, C₂, and C₁. The anodic current wave A₇, on the cathodic part of voltammograms, is associated with additional oxidation of elemental silver to Ag₂O.^{20,21,24,25}

Within the aim of comparing the behavior of CuAg 4 at. % obtained by the IM method with the same alloy obtained by the PM method, first the sample IM1 was compared with the sample PM1 (Fig. 2), because these two samples are considered as the primary step for further thermomechanical treatment. The sample IM1 is a pre-saturated α solid solution, the synthesis procedure of which is described in detail elsewhere.¹⁸ An optical microphotograph of the IM1 sample (Fig. 2b) shows that the structure was generally homogeneous with equiaxial grains of average size 50–100 μm . The sample PM1 was obtained by pressing an appropriate powder mixture at a pressure of 300 MPa and sintering at 790 °C for 1 h (Table I). The optical microphotograph of the sintered PM1 sample (Fig. 2c) shows a relatively homogeneous structure with equiaxial grains and spherical pores. According to the phase diagram, the PM1 structure mainly consists of a Cu-rich α solid solution with a small amount of an Ag-rich β solid solution. The structure of the sintered sample was more fine-grained compared to the coarse-grained cast structure. The obtained voltammograms, presented in Fig. 2a, confirmed that in sample PM1, silver-rich grains still existed because the independent current peaks corresponding to silver are very well defined. It is obvious that the time of sintering was not long enough to complete the process of alloying.

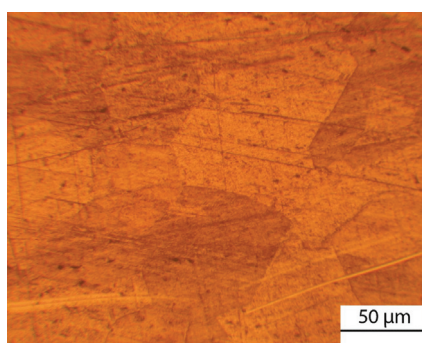
On voltammogram for the cast alloy (sample IM1), the anodic currents are lightly higher than those obtained for the sintered sample and the current peaks A₃ and A₄ are hardly distinguishable because they overlap. Other current peaks on this voltammogram corresponding to the oxidation of silver are noticeable only as small shoulders because all these peaks are superposed on the current wave of copper oxidation. This indicates that the highest amount of silver present in the alloy was in form of a solid solution in copper. However, low but noticeable waves at potentials corresponding to the formation of silver oxide on the voltammogram obtained for the sample IM1 indicate that a small amount of silver was also present as an independent component.

The thermomechanical treatment that leads to anneal hardening consisted of cold rolling and further annealing below the recrystallization temperature. For this reason, in the next step of thermomechanical treatment, the IM1 and PM1 samples were subjected to final reduction of 20, 40 and 60 % by cold rolling. The samples obtained after the reduction of 60 % were chosen as samples IM2 and PM2 for electrochemical investigations because they resulted in highest final hardening. Voltammetric curves of samples IM2 and PM2 are presented in Fig. 3a,

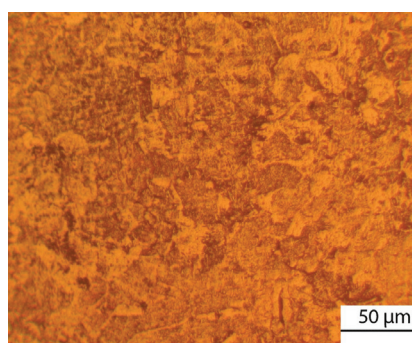
from which it could be seen that the voltammograms of the CuAg 4 at. % alloys obtained by the PM and IM method, both cold rolled to a final reduction of 60 %, almost do not exhibit any peak that would correspond to the formation of silver oxide, which indicated that the highest amount of silver present in the alloy was in the form of a solid solution in copper. At this stage of thermomechanical treatment, both samples behaved as a homogenous phase and the peak currents were the lowest. Optical microphotographs of the IM2 and PM2 samples presented in Fig. 3a and b, respectively, show that the equiaxial grains had been deformed and elongated in the rolling direction. Moreover, in PM2 sample, porosity had decreased significantly due to sealing of the pores. In previous studies, it was shown that the slip lines in the cast samples formed during the plastic defor-



(a)



(b)

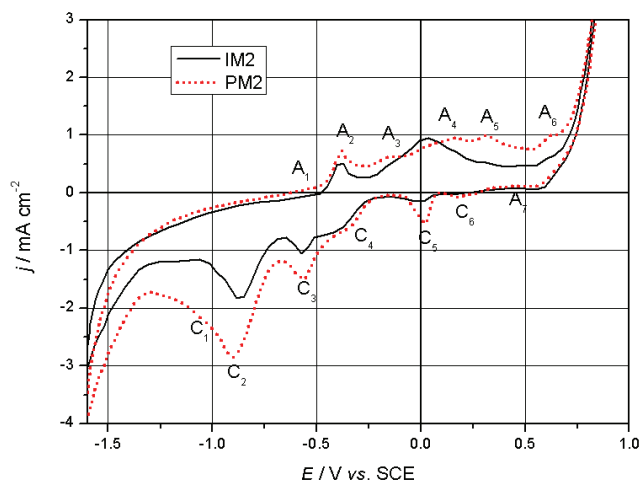


(c)

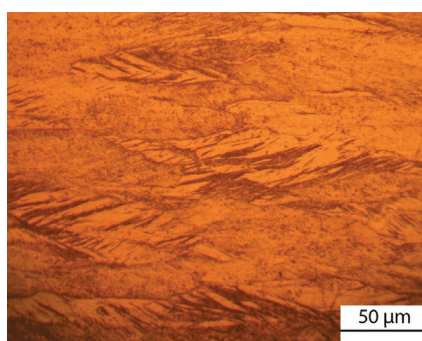
Fig. 2. Comparison of the CuAg 4 at. % alloys obtained by the IM method when in form of an undeformed α solid solution and by the PM method after pressing and sintering; a) cyclic voltammograms under the conditions: $\nu = 20 \text{ mV s}^{-1}$, 0.1 M NaOH, $t = 25 \pm 0.5 \text{ }^\circ\text{C}$; optical microphotographs of the b) IM1 and c) PM1 sample.

mation were more extensive than in the sintered samples,^{2,3,18,19} as is evident in Fig. 3b and c. This could be an explanation for differences in behavior between these samples during further treatment.

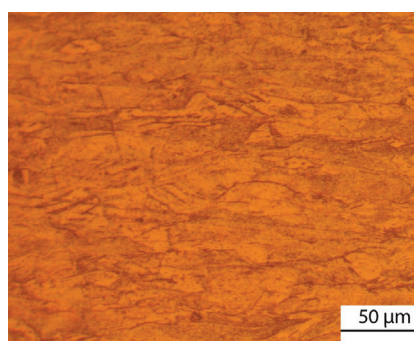
Cyclic voltammograms of the CuAg 4 at. % alloy obtained by IM and PM method in a stage when they exhibit anneal hardening effect (samples IM3 and PM3) are presented in Fig. 4a, from which, it could be seen that after annealing below the recrystallization temperature, the sintered alloy retained its corrosion stability, whereas the peak currents for the cast alloy increased. The current peaks corresponding to the oxidation of silver were hardly distinguishable for the sample obtained by the PM method, while on the voltammogram obtained for the sample synthesized by melting and casting (IM3), these peaks reappeared. After



(a)



(b)



(c)

Fig. 3. Comparison of the CuAg 4 at. % alloys obtained by the IM and PM methods, both cold rolled to final reduction of 60 %; a) cyclic voltammograms under the conditions: $\nu = 20 \text{ mV s}^{-1}$, 0.1 M NaOH, $t = 25 \pm 0.5 \text{ }^\circ\text{C}$; optical microphotographs of the b) IM2 and c) PM2 sample.

annealing at 260 °C, the oxidation of silver in the cast CuAg 4 at. % alloy sample was more pronounced because of segregation of solute atoms (silver) on the dislocations and the higher non-homogeneity of the structure. The microstructures of the cold rolled IM and PM alloys after annealing at 260 °C, which led to a hardening of their structures due to anneal hardening effect, are shown in Fig. 4b and c, respectively. Several explanations have been proposed for the origin of this phenomenon, among which two propositions are thought to be rational. The first proposition is the formation and collapse of short-range order and the second one is the segregation of solute atoms to stacking faults. The grains are still elongated along the rolling direction and the slip lines and slip bands are still very clear, especially for the IM3 sample.

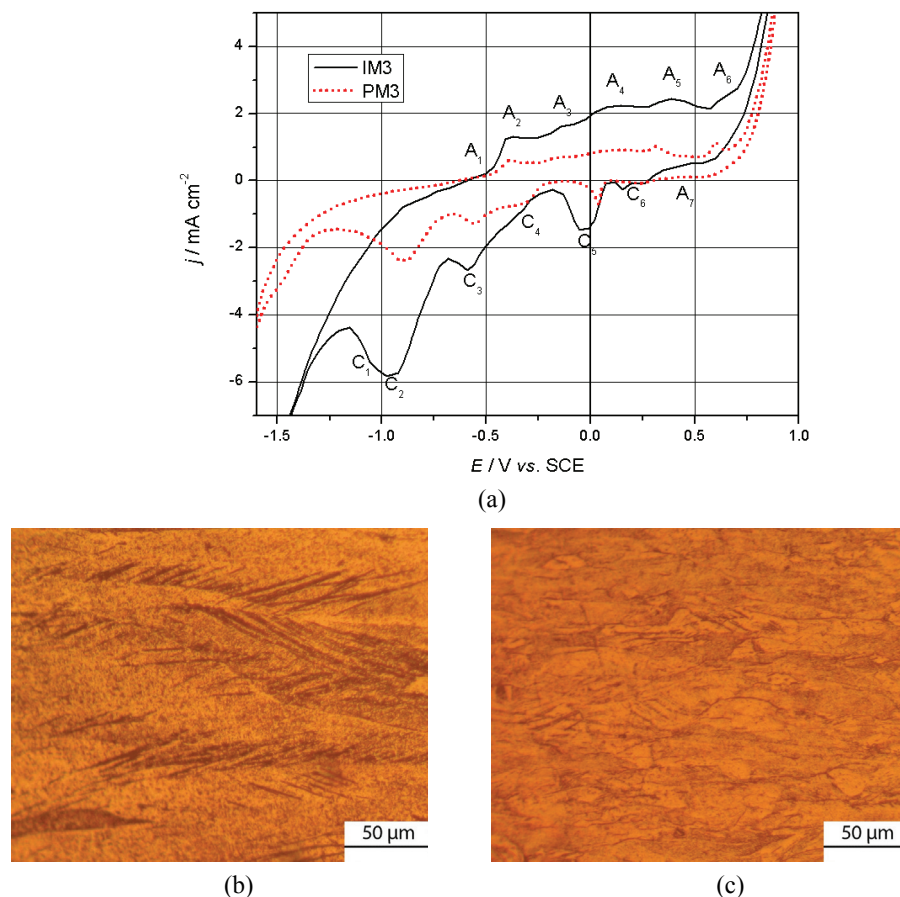


Fig. 4. Comparison of the CuAg 4 at. % alloys obtained by the IM and PM methods, both exhibiting the anneal hardening effect; a) cyclic voltammograms under the conditions: $\nu = 20 \text{ mV s}^{-1}$, 0.1 M NaOH, $t = 25 \pm 0.5 \text{ }^\circ\text{C}$; optical microphotographs of the b) IM3 and c) PM3 sample.

The voltammograms of both the IM and PM samples annealed above the recrystallization temperature (IM4 and PM4) are presented in Fig. 5a. The voltammograms of both samples contain distinctly separate current waves of silver oxide formation, which means that silver, that was in the form of a solid solution, remained in that form after cold rolling, whereas in the annealing process, it was extracted as a second pure metal phase. After recrystallization annealing at 600 °C for 30 min, the peak currents increased to the value they had before cold deformation and the current densities were lower for the sample PM4, obtained by the powder metallurgy method, than for the sample IM4. The microstructure of the samples IM4 and PM4 are shown in Fig. 5b and c, respectively. No newly deformed, recrystallized grains were observed in the structures. In PM4 sample,

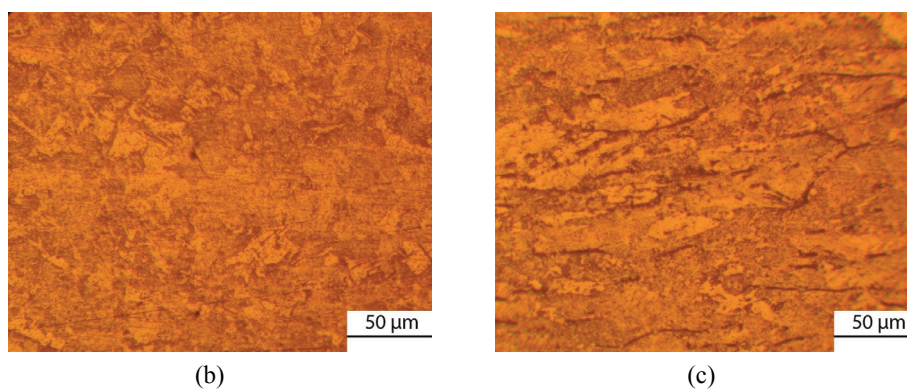
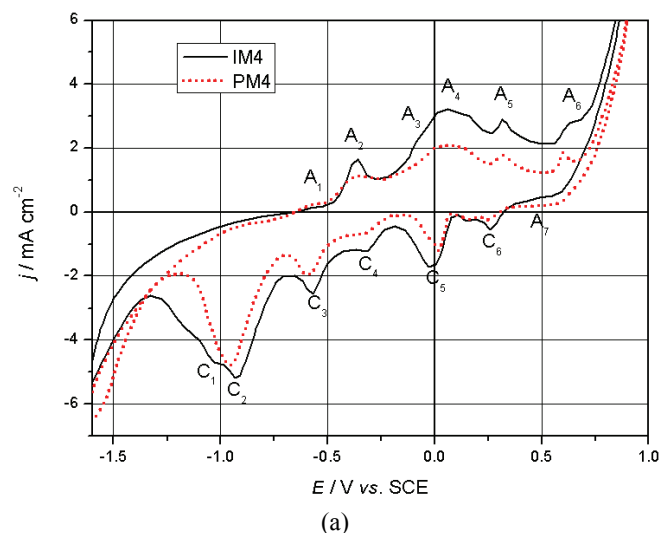


Fig. 5. Comparison of the CuAg 4 at. % alloys obtained by the IM and PM methods after recrystallization annealing; a) cyclic voltammograms under the conditions: $\nu = 20 \text{ mV s}^{-1}$, 0.1 M NaOH, $t = 25 \pm 0.5 \text{ }^\circ\text{C}$; optical microphotographs of the b) IM4 and c) PM4 sample.

some places with elongated grains were still visible, implying that the recrystallization was not complete, which is in agreement with the results of the hardness measurements.

CONCLUSIONS

The electrochemical behavior of samples of CuAg 4 at. % alloy obtained by the powder metallurgy method during oxidation in an alkaline medium was compared with behavior of the same alloy obtained by melting and casting (so-called ingot metallurgy). It was shown in cyclic voltammetric investigations that the oxidation of both copper and silver in the CuAg 4 at. % alloy samples obtained by the ingot metallurgy method was more pronounced than in the samples obtained by the powder metallurgy technique in all stages of thermomechanical treatment leading to anneal hardening. This was the consequence of the more fine-grained structure of the sintered samples in comparison to the cast structure. The oxidation was the slowest in the case when only the α phase (solid solution of silver in copper) was present in the structure. This structure was obtained after cold rolling to a final reduction of 60 %.

Annealing below the recrystallization temperature led to anneal hardening of both the IM and PM samples. In this stage, sintered alloy retained its corrosion stability, whereas the current densities for the cast alloy increased and peaks characteristic for silver reappeared. The oxidation of the silver in the cast CuAg 4 at. % alloy samples after annealing at 260 °C was more pronounced because of segregation of the solute atoms (silver) onto the dislocations and inhomogeneities of the structure.

Acknowledgement. This work was supported by the Ministry of Education, Science and Technological Development of the Republic of Serbia, Project No. 172060: "New approaches in the design of materials for energy conversion and energy storage systems."

ИЗВОД

ПОРЕЂЕЊЕ ЕЛЕКТРОХЕМИЈСКОГ ПОНАШАЊА ЛИВЕНЕ И СИНТЕРОВАНЕ ЛЕГУРЕ CuAg 4 ат. % У ТОКУ ТЕРМОМЕХАНИЧКЕ ОБРАДЕ

МИРЈАНА М. РАЈЧИЋ-ВУЈАСИНОВИЋ, ВЕСНА Ј. ГРЕКУЛОВИЋ, ЗОРАН М. СТЕВИЋ,
СВЕТЛАНА Д. НЕСТОРОВИЋ, ИВАНА И. МАРКОВИЋ и СЛАВКО Б. СИМОВ

Универзитет у Београду, Технички факултет у Бору, В. Ј. 12, 19210 Бор

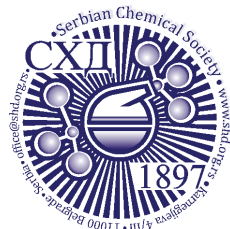
У раду је приказано поређење електрохемијског понашања у алкалној средини легура CuAg 4 ат. % добијених по две различите металуршке методе – методом металургије праха и такозваном ингот методом. Ова легура је посебно интересентна због тога што испољава ефекат ојачавања жарењем после одговарајуће термомеханичке обраде. Због тога је поређење изведено у свим фазама које та термомеханичка обрада подразумева. Методом цикличне волтаметрије утврђено је да је легура електрохемијски најстабилнија у фази након хладног ваљања са степеном деформације од 60 % без обзира на методу којом је легура синтетизована. Тада се легура понаша као хомогена фаза, на волтаграмима се не појављују пикови карактеристични за сребро и густине струје су

најниже. Накнадно жарење испод температуре рекристализације, које доводи до ојачавања, донекле нарушава хомогеност ливене легуре, док синтерована легура задржава хомогеност и стабилност достигнуту након ваљања. Рекристализационо жарење, међутим, доводи до повећања густине струје на волтамограмима и до поновне појаве свих струјних пикова карактеристичних за оксидацију и редукцију оба присутна метала у легури.

(Примљено 24. децембра 2012, ревидирано 13. марта 2013)

REFERENCES

1. K. Dies, *Kupfer und Kupferlegierungen in der Technik*, Berlin/Heidelberg/New York, 1967 (in German)
2. S. Nestorović, I. Rangelov, D. Marković, *Powder Metall.* **54** (2011) 36
3. S. Nestorović, D. Marković, I. Marković, *J. Alloys Compd.* **489** (2010) 582
4. P. Gertik, *Noble Metals*, GIP "Slobodan Jovic", Belgrade, 1997 (in Serbian)
5. J. Freudenberger, *High Strength Copper-Based Conductor Materials*, in *Copper Alloys: Preparations, Properties and Applications*, M. Naboka, J. Giordano, Eds., Nova Science Publishers, New York, USA, 2011, Ch. 9, p. 159
6. A. Benghalem, D. G. Morris, *Acta Mater.* **45** (1997) 397
7. J. Kunze, V. Maurice, L. H. Klein, H. H. Strehblow, P. Marcus, *J. Electroanal. Chem.* **554–555** (2003) 113
8. H. H. Strehblow, V. Maurice, P. Marcus, *Electrochim. Acta* **46** (2001) 3755
9. J. Kunze, V. Maurice, L. H. Klein, H. H. Strehblow, P. Marcus, *Corros. Sci.* **46** (2004) 245
10. N. D. Nikolić, Lj. J. Pavlović, M. G. Pavlović, K. I. Popov, *J. Serb. Chem. Soc.* **72** (2007) 1369
11. B. M. Jović, V. D. Jović, *J. Serb. Chem. Soc.* **69** (2004) 153
12. T. Uk Hur, W. Sub Chung, *J. Electrochem. Soc.* **152** (2005) A179
13. J. Ambrose, R. G. Barradas, *Electrochim. Acta* **19** (1974) 781
14. O. A. Hazzazi, A. M. Zaky, M. A. Amin, S. S. Abd El Rehim, *Int. J. Electrochem. Sci.* **3** (2008) 489
15. F. H. Assaf, A. M. Zaky, S. S. Abd El-Rehim, *Appl. Surf. Sci.* **18** (2002) 18
16. A. M. Zaky, *Electrochim. Acta* **51** (2006) 2057
17. S. M. Skogvold, Ø. Mikkelsen, G. Billon, C. Garnier, L. Lesven, *Anal. Bioanal. Chem.* **384** (2006) 1567
18. M. Rajčić-Vujasinović, S. Nestorović, V. Grekulović, I. Marković, Z. Stević, *Corrosion* **66** (2010) 105004-1
19. M. Rajčić-Vujasinović, S. Nestorović, V. Grekulović, I. Marković, Z. Stević, *Metall. Mater. Trans., B* **41** (2010) 955
20. V. Grekulović, M. Rajčić-Vujasinović, *Corrosion* **68** (2012) 025003-1
21. V. Grekulović, M. Rajčić-Vujasinović, B. Pešić, Z. Stević, *Int. J. Electrochem. Sci.* **7** (2012) 5231
22. Z. Stević, M. Rajčić-Vujasinović, *Hem. Ind.* **61** (2007) 1
23. Z. Stević, Z. Andjelković, D. Antić, *Sensors* **8** (2008) 1819
24. P. Stonehart, *Electrochim. Acta* **13** (1968) 1789
25. H. Ha, J. Payer, *Electrochim. Acta* **56** (2010) 2781.



J. Serb. Chem. Soc. 78 (10) 1595–1607 (2013)
JSCS–4521

Electrocatalytic oxidation and determination of homocysteine at nanotubes-modified carbon paste electrode using dopamine as a mediator

SAFOORA MOHAMMADZADEH¹ and MASOUD FOULADGAR^{2*}

¹ Department of Chemistry, Payame Noor University, P. O. Box 19395-3697 Tehran, Iran and

² Department of Biochemistry, Falavarjan Branch, Islamic Azad University, Falavarjan, Iran

(Received 29 October 2012, revised 11 January 2013)

Abstract: A carbon paste electrode modified with multiwall carbon nanotubes (MWCNTPE) was prepared to study the electrocatalytic activity of dopamine (DP) in the presence of homocysteine (HCy) and it was used for the determination of HCy. The diffusion coefficient of HCy ($D = 6.79 \times 10^{-6} \text{ cm}^2 \text{ s}^{-1}$), and the kinetic parameters of its oxidation, such as electron transfer coefficient ($\alpha = 0.46$), and rate constant ($k_h = 7.44 \times 10^2 \text{ dm}^3 \text{ mol}^{-1} \text{ s}^{-1}$) were also determined using electrochemical approaches. Under the optimum pH of 5.0, the peak current of oxidation of HCy at MWCNTPE in the presence of DP occurred at a potential of about 530 mV and the results showed that the oxidation peak current of HCy at the modified carbon nanotubes electrode was higher than on the unmodified electrode. The peak current of differential pulse voltammograms of HCy solutions increased linearly in the range 3.0–600 μM HCy with a detection limit of 2.08 μM HCy. This method was also examined for determination of HCy in physiological serum and urine samples.

Keywords: homocysteine; dopamine; electrocatalytic effect; carbon nanotubes, carbon paste electrode; voltammetry.

INTRODUCTION

Homocysteine (HCy), as an important sulfur-containing amino acid, plays a considerable role in many biochemical processes.¹ HCy was discovered by Butz and Du Vigneaud in 1932 by heating methionine in sulfuric acid.² The produced compound was found to have chemical properties similar to those of cysteine.

The concentration of HCy can be an independent risk factor for disease in human society.^{3,4} Mild hyperhomocysteinemia has no signs but it provides the conditions for developed premature coronary disease in the third or fourth decade of life.⁴ Thus, early determination of the HCy plasma concentration is necessary and essential. Based on clinical studies, the normal total plasma HCy concen-

*Corresponding author. E-mail: Fouladgar@iaufala.ac.ir
doi: 10.2298/JSC121019022M

tration range has been confirmed as 5–15 μM in the fasting state and elevated level of HCy has been classified in three range, moderate (16–30 μM) medium (30–100 μM) and severe (>100 μM).^{5,6} The total plasma HCy includes, 75 % homocysteine bound to various proteins *via* disulfide bonds and the remaining 25 % free HCy includes oxidized homocysteine dimers (homocystine) or as homocysteine–cysteine hetero dimers. Only 1–2 % of HCy is in the reduced state and is distributed among different tissues, cells, and intracellular compartments. In addition, small metabolic changes of HCy affect many physiological concentrations.^{7,8}

According to many researches, elevated plasma HCy concentrations are known to be a factor implicated in the appearance and progression of various diseases, such as coronary artery and cerebro vascular disease.^{4,9,10}

To date, due to the importance of the determination of HCy, different techniques have been employed its measurement. The direct methods included the enzyme immunoassay (EIA),^{11,12} the fluorescence polarization immunoassay (FPIA),^{13–15} and the enzyme-linked immunosorbent assay (ELISA).^{16,17} Gas chromatography (GC),^{18–21} liquid chromatography (LC),^{22,23} high-performance liquid chromatography (HPLC),^{24–31} capillary electrophoresis (CPE)^{28,32,33} and electrochemical methods^{1,5,34–41} fall in the category of indirect methods. The advantages of electrochemical methods, such as sensitivity, selectivity, facile, high performance, low cost, high accuracy and precision, aroused the attention of many researchers.^{1,5,35,41–51} Other methods such as immunoassay kits and chromatographic methods require sample preparation that consumes a long time, are expensive and necessitate the use environmentally hazardous solvents.^{1,5,35}

In the present work, we applied a carbon nanotubes-modified graphite paste electrode for determination of HCy using dopamine (DP) as an electrocatalytic mediator. The nanotubes interconnect the graphite powder particles together to form a continuous conductive network. The small diameters of the nanotubes enabled the nanotubes to be homogeneously distributed in the thin electrode material and to introduce a larger surface area to react with the electrolyte. The improved electrical conductivity of the electrode was related to the high electrical conductivity of the tubes, and the function of the electrical bridge between the graphite particles. In the presence of carbon nanotubes, the anodic signal increased, which could be due to the increase in the active surface of electrode and increase the conductivity of the electrode.^{52–61} Effective parameters on anodic signal were studied and a method was proposed for determination of HCy in biological serum and urine samples.

EXPERIMENTAL

Reagents and apparatus

All employed chemical were of analytical grade and purchased from Merck, Aldrich and Fluka. Homocysteine ($\geq 95\%$) and DP (99 %) were purchased from Aldrich.

Spectrally pure graphite powder (particle size $<50\ \mu\text{m}$) from Merck and multiwall carbon nanotubes ($> 90\%$, MWCNTs, $d \times l$, $100\text{--}70\ \text{nm} \times 5\text{--}9\ \mu\text{m}$) from Fluka were used as the substrate for the preparation of the carbon paste electrode as a working electrode (WE). High viscosity paraffin ($\rho = 0.88\ \text{kg L}^{-1}$) from Merck was used as the pasting liquid for the preparation of the paste electrodes.

Universal buffer solutions (0.04 M acetic acid, boric acid, phosphoric acid and 0.2 M sodium hydroxide) contain the 0.1 M potassium chloride with different pH values were prepared to examine and provide the optimum pH value.

All aqueous solutions were prepared from deionized water by passing through a Milli-Q water purification system (resistance $>18\ \text{MW cm}^{-1}$).

The homocysteine and DP solutions, $1.0 \times 10^{-2}\ \text{M}$, were prepared daily by dissolving 0.0068 g homocysteine, respectively, 0.0095 g dopamine in the buffer solution and then diluting to 5 ml in two volumetric flasks. The solution was kept in a refrigerator at $4\ ^\circ\text{C}$ in the dark. More dilute solutions were prepared by serial dilution of these solutions with water.

All electrochemical experiments including cyclic voltammetry (CV) and differential pulse voltammetry (DPV) were performed using a computerized potentiostat/galvanostat (Autolab PGSTAT101, Eco Chem. Utrecht, The Netherlands). A Pentium IV computer controlled all settings and data processing of the system. All the electrochemical studies were performed at $25 \pm 1\ ^\circ\text{C}$. The system was connected to a three-electrode cell assembly consisting of a 50 mL glass cell containing an Ag/AgCl electrode as the reference electrode (RE), a platinum wire counter electrode and a MWCNTPE working electrode. All of the measured potentials are reported vs. the Ag/AgCl reference electrode. The pH of the solutions was controlled with a Metrohm pH meter (model 827). The electrode prepared with carbon nanotubes was characterized by scanning electron microscopy (SEM) (Seron Tech. AIS 2100).

Preparation of the modified electrode (MWCNTPE)

A mixture of 0.10 g carbon nanotubes (CNT) and 0.9 g graphite powder was hand mixed using a pestle and mortar. To achieve a uniform mixture, diethyl ether was added to the mixture, the mixture was mixed again, and the diethyl ether allowed adequately to evaporate. Paraffin oil, about of 0.4 g, was added to the mixture and mixed well for 20 min until a uniformly wetted paste was obtained. The prepared paste was inserted into a glass tube (internal radius 2.2 mm) with a copper wire in it for electrical connection. A fresh surface was obtained after pushing out an excess of the paste and polishing it on a weighing paper.

For comparison, a uniform carbon paste electrode (CPE) was obtained in the same way without addition of CNT to the mixture.

Electrochemical procedure

The MWCNTPE as working electrode was located in an electrochemical cell containing 10 ml of buffer solution (universal pH 5 and 0.10 M KCl) including $400\ \mu\text{M}$ DP to record the voltammetric measurements. The voltammograms were recorded with a scan rate $20\ \text{mV s}^{-1}$ to give the blank signal from initial to final potentials of 0.1 mV to 0.7 mV vs. the Ag/AgCl reference electrode. Subsequently, different amounts of HCy solution were added to the cell and the same procedure was repeated to give the analytical signal. Differential pulse voltammetry (DPV) curves were recorded with a pulse height and pulse width of 50 mV and 0.005 s, respectively, using the same procedure to obtain blank and analytical signals. The difference between the blank and the analytical signal was obtained as a net peak current that was proportional to the concentration of HCy. Calibration curves were constructed by plotting the net peak current vs. concentration of HCy.

Preparation of real sample

Urine sample was stored in a refrigerator (at 4 °C) immediately after collection. Ten milliliters of the sample was centrifuged for 15 min at 1500 rpm and the supernatant solution was filtered through a 0.45 µm filter. Then, the solution was diluted ten times with buffer solution (pH 5.0 and 0.10 M KCl) and was transferred into the electrochemical cell, where it was analyzed without any further pretreatment. The standard addition method was used for the determination of Hcy in real samples.

Physiological serum solutions (0.9 % NaCl) were analyzed directly after 1:1 diluted with buffer solution (pH 5 and 0.10 M KCl) without any further preparation.

RESULTS AND DISCUSSION

SEM characterization of electrodes

The SEM image of the CPE and MWCNTPE has been shown in the Fig. 1. As can be seen, multiwall carbon nanotubes were dispersed to the carbon paste matrix and were caused increasing the surface area of the active sites of the electrode.

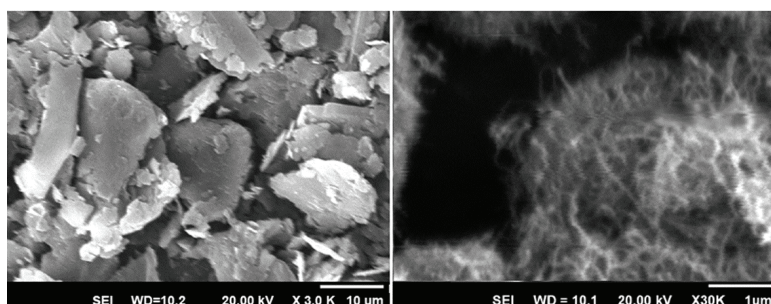


Fig. 1. SEM Image of A) CPE and B) MWCNTPE.

Electrochemical behavior of dopamine (DP) on MWCNTPE

The electrochemical behavior of DP on MWCNTPE in buffer solution (pH 5.0 and 0.10 M KCl) was characterized by cyclic voltammetry. The cyclic voltammogram (Fig. 2) of DP showed well-defined and reproducible anodic and cathodic peaks with a peak separation potential of $\Delta E_p = E_{pa} - E_{pc} = 620$ mV. This value was greater than the value of $59/n$ mV for reversible behavior and was indicative of quasi-reversible behavior. The influence of potential scan rate (20 to 500 mV s^{-1}) on the anodic peak current of DP was studied by cyclic voltammetry. The peak currents of DP grew with increasing scan rate and the anodic peak current increased linearly with square root of the scan rate ($I = 0.986v^{1/2} - 0.534$, $R^2 = 0.995$). Such a dependence shows that the oxidation reaction of DP on the MWCNTPE is diffusion-controlled (Fig. 2).⁶²

pH Effect

As the oxidation of DP is accomplished with the exchange of two electrons and two protons, the dependence of the redox reaction of DP on pH could be con-

cluded. The voltammetric response of DP showed that with increasing pH of the solution, the peak potential shifted to less positive potentials. In addition, the effect of pH solution on the electrocatalytic oxidation of Hcy in the presence of DP at the surface of MWCNTPE was investigated using cyclic voltammetry. The optimum pH was investigated by varying the pH from 3.0 to 6.0. As can be seen in Fig. 3, maximum peak current was obtained at pH 5.0. Hence, this pH was selected as optimum pH for further experiments.

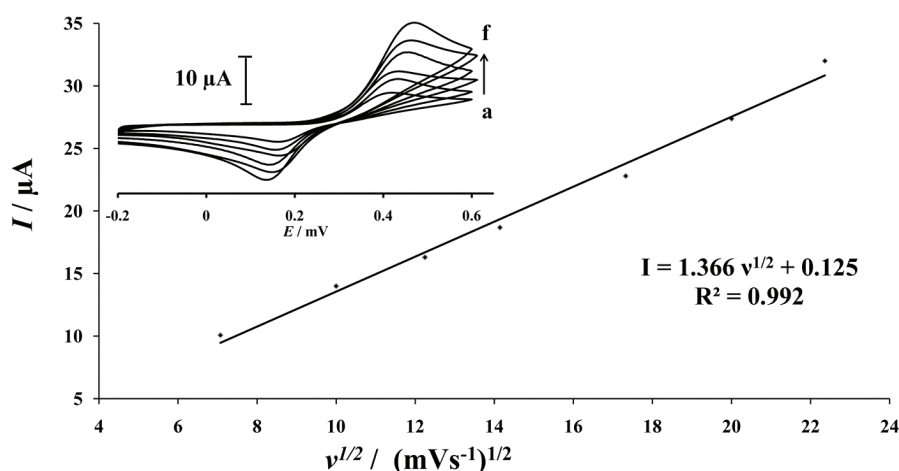


Fig.2. Plot of I vs. $v^{1/2}$ for 400 μM DP at the MWCNTPE. Inset: cyclic voltammograms at various scan rates of a) 50, b) 100, c) 150, d) 200, e) 300 and f) 400 mV s^{-1} in the universal buffer (pH 5).

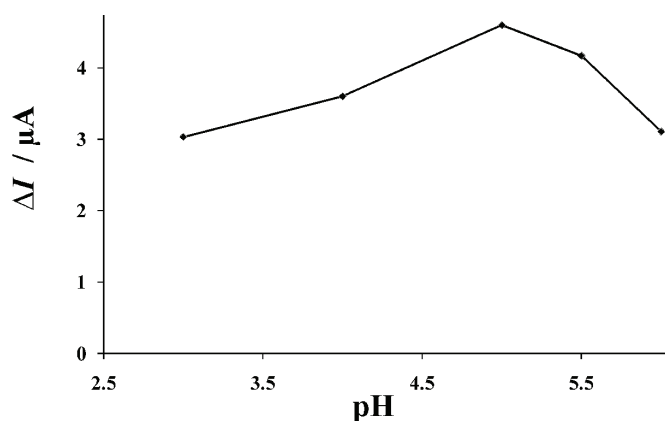


Fig. 3. Effect of pH on the electrocatalytic current.

Optimization of the dopamine (DP) concentration

The effect of DP concentration on the peak currents was studied by varying its concentration in the range of 100–600 μM at pH 5.0. The electrocatalytic

response was optimized and the maximum value of the oxidation peak current was achieved by increasing the DP concentration up to 400 μM . This value was selected as the optimum concentration for further experiments.

Electrocatalytic oxidation of HCy on MWCNTPE

HCy, as an oxidizable compound, can be detected by electrochemical methods based on its anodic oxidation.⁸ The voltammetric response of HCy at MWCNTPE was investigated in presence and absence of DP in pH 5.0 buffer solution using cyclic voltammetry at a scan rate of 20 mV s^{-1} . The recorded cyclic voltammograms of HCy in the absence of DP did not show a significant redox peak for HCy (Fig. 4, curve d). Moreover, a pair of well-defined redox peaks was observed as the voltammetric behavior of DP (400 μM) in the absence of HCy (Fig. 4, curve c). Upon the addition of 500 μM HCy, the anodic peak current increased sharply and no cathodic current was observed in the reverse scan (Fig. 4, curve a). Therefore, HCy can be detected in the presence of DP potential about 0.53 V vs. Ag/AgCl at the surface of a MWCNTPE. As can be seen, the oxidation of HCy on a CPE in presence of DP (Fig. 4, curve b) has a lower peak current compare to that on the MWCNTPE. In the other words, the presence of multiwall carbon nanotubes increased the conductivity and effective surface area of the electrode for the oxidation of HCy.^{53,54} Based on the the obtained information, the electrocatalytic mechanism shown in Scheme 1 is suggested for the oxidation of HCy. In the first step, DP is oxidized on the surface of the MWCNTPE. Then, the oxidized form of DP is reduced by HCy, whereby HCy is converted to its oxidized form.⁸

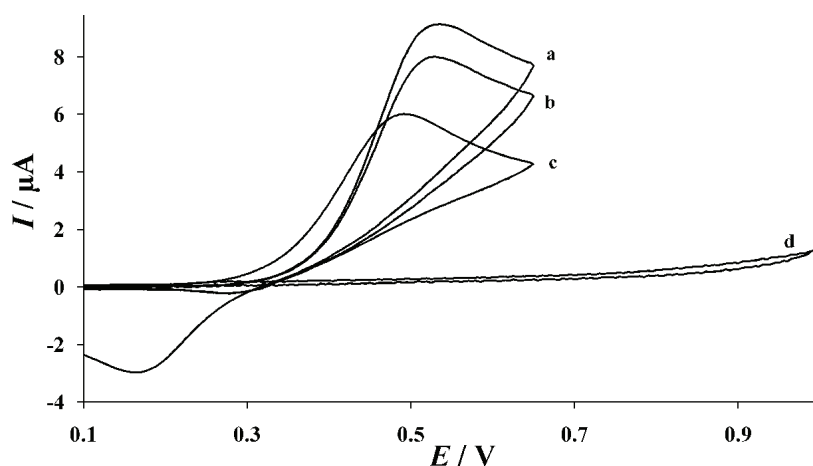
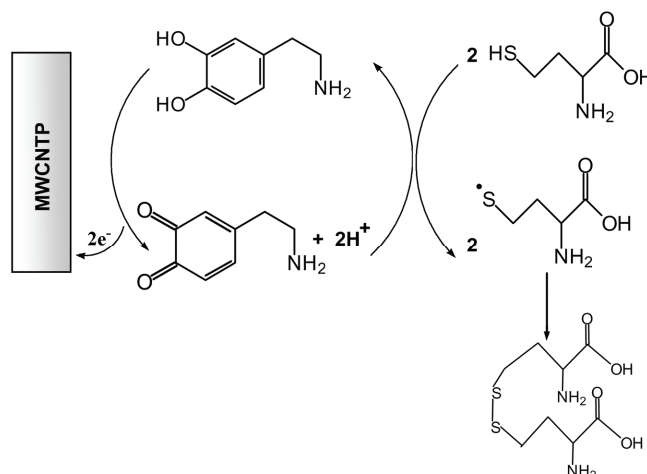


Fig.4. Cyclic voltammograms recorded at a scan rate of 20 mV s^{-1} in universal buffer solution pH 5.0. a) 400 μM DP at the MWCNTPE in the presence of 500 μM HCy, b) as a) but at the CPE, c) 400 μM DP at the MWCNTPE, d) 500 μM HCy at the MWCNTPE in the absence of DP.



Scheme 1. Electrocatalytic mechanism for the oxidation of Hcy at the surface of the modified electrode.

Cyclic voltammograms of 500 μM Hcy in presence of 400 μM DP at pH 5.0 were recorded in the potential range -0.1 to 0.6 V at various sweep rates. With increasing scan rate from 5 to 40 mV s^{-1} , the peak currents of Hcy increased (Fig. 5, inset). The results showed, there was a linear relationship between the peak current and the square root of the scan rate ($v^{1/2}$) with the regression equation:

$$I (\mu\text{A}) = 1.621v^{1/2} (\text{mV s}^{-1})^{1/2} + 0.820$$

$$(R^2 = 0.997)$$

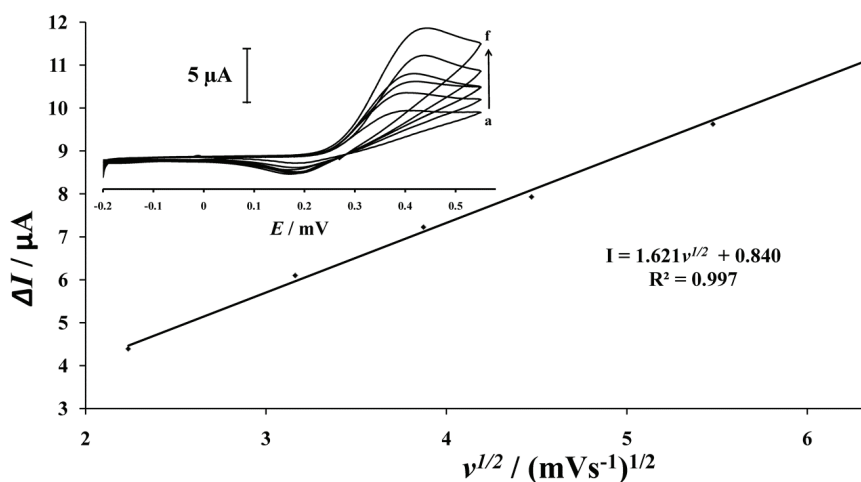


Fig. 5. Plot of I vs. $v^{1/2}$ for 500 μM Hcy in the presence of 400 μM DP at the MWCNTPE. Inset: cyclic voltammograms recorded at various scan rates: a) 5, b) 10, c) 15, d) 20, e) 30 and f) 40 mV s^{-1} in the universal buffer (pH 5.0).

This equation confirms that the process is diffusion controlled (Fig. 5). In addition, by increasing in the scan rate and following the shift of the oxidation peak potential towards more positive potential, the kinetic limitation of the electrochemical reaction was verified.⁶³

In order to obtain information on the rate determining step, Tafel plot was obtained from raising part of the current–voltage curve at scan rate of 20 mV s⁻¹ (Fig. 6). The slope of the Tafel plot was equal to $2.3RT/n(1-\alpha)F$, which was 0.108 V decade⁻¹. Using this data and assuming $n = 1$, then $\alpha = 0.46$.

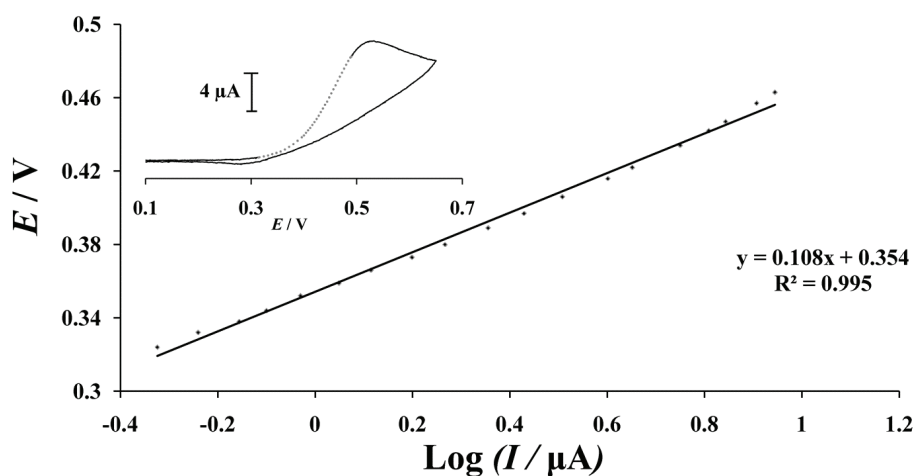


Fig. 6. Tafel plot for 500 μM HCy in the presence of 400 μM DP (pH 5.0) at the MWCNTPE.

Chronoamperometric study

The electrochemical response of HCy at the MWCNTPE was investigated using various concentrations of HCy by chronoamperometry. The chronoamperograms were obtained in buffered solution by employing and adjusting a double-step potential from 0.3 (first step) to 0.7 V (second step) vs. Ag/AgCl (Fig. 7). The linearity of the electrocatalytic current vs. $t^{-1/2}$ indicates that the current must have been under diffusion control. The inset in Fig. 7 shows the linear relationships between I vs. $t^{-1/2}$ for different concentrations of HCy. The Cottrell Equation is given by:

$$I = \frac{nFAc\sqrt{D}}{\sqrt{\pi t}} \quad (1)$$

where I is the current (A), n the number of electrons involved in the process, F is the Faraday constant, A is the area of the electrode (cm²), c is the initial concentration of HCy (mol cm⁻³), D is the diffusion coefficient (cm² s⁻¹) and t is time (s).

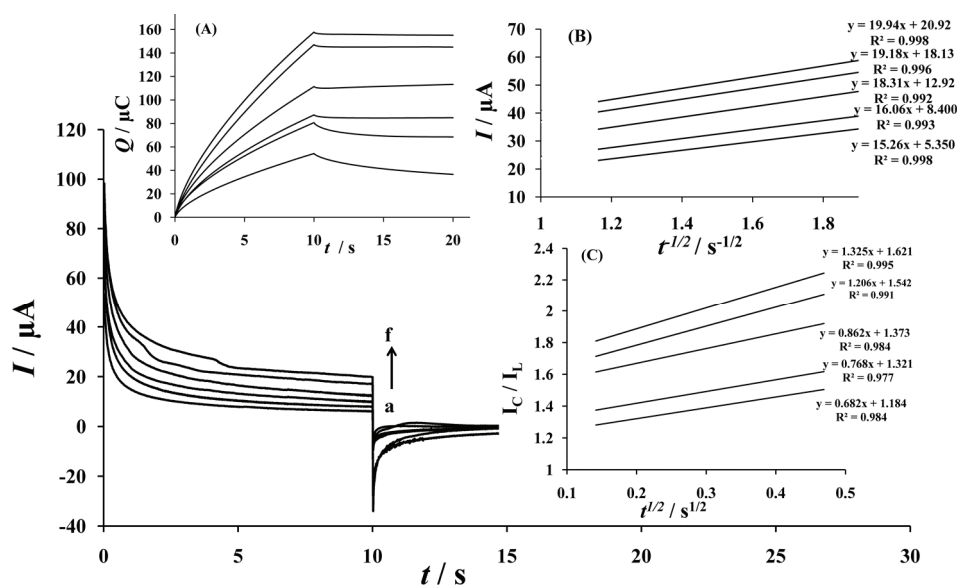


Fig.7. Chronoamperograms obtained at MWCNTPE in the absence (a), and in the presence of b) 100, c) 300, d) 700, e) 900 and f) 1000 μM HCY in buffer solution (pH 5.0). Inset (A): charge–time curves; inset (B): the Cottrell plot for data from the chronoamperograms; inset (C): dependence of I_C/I_L on $t^{1/2}$ derived from the chronoamperographic data.

From the Cottrell Equation and the obtained slope values for different concentrations of HCY, the diffusion coefficient could be calculated and was found to be $6.79 \times 10^{-6} \text{ cm}^2 \text{ s}^{-1}$.⁶²

In addition, the chronoamperometry method was applied to obtain the rate constant of the catalytic oxidation (k_h) of HCY. For this purpose, the Galus Method was used:

$$I_C/I_L = \pi^{1/2} \gamma^{1/2} = \pi^{1/2} (k_h c t)^{1/2} \quad (2)$$

where I_C is catalytic current of HCY in the presence of DP at the MWCNTPE, I_L is the limiting current in the absence of HCY, and t is the time elapsed (s). Based on the slope of the I_C/I_L vs. $t^{1/2}$ plots, k could be obtained for different concentrations of HCY. The average value of k_h was calculated to be $7.44 \times 10^2 \text{ dm}^3 \text{ mol}^{-1} \text{ s}^{-1}$.

Analytical features of the method

Differential pulse voltammetry method (DPV) was used for preparation of the calibration plot. The DP voltammograms were recorded for the determination of HCY in the buffer solution (pH 5.0 and 0.10 M KCl). The electrocatalytic current of MWCNTPE increased with increasing HCY concentration in the pre-

sence of 400 μM DP. The results showed that there is a linear dynamic range of 3.0–600 μM for HCy.

$$I (\mu\text{A}) = 0.008c_{\text{HCy}} + 0.873, R^2 = 0.997$$

The limit of detection was 2.08 μM and the relative standard deviations (*RSD*) for six replicated analyses of 200 and 400 μM HCy at 20 mV s^{-1} were 1.15 and 2.3 %, respectively.

Interference study

To evaluate the ability of proposed method for determination of HCy in real samples, such as urine, the interference effects due to some potential interfering species that are commonly found in urine, were studied under the optimum conditions with 400 μM HCy at pH 5.0. The tolerance limit was taken as the maximum concentration of foreign substances that caused no more than ± 5 % relative error in the determination of HCy. Some cations may form complexes with HCy or DP and disrupt or effect on electrocatalytic mechanism, but no interference was observed for the following cations: Pb^{2+} , Ni^{2+} , Ba^{2+} and Ca^{2+} (1000 fold) or Fe^{2+} (100 fold). The results are presented in Table I.

TABLE I. Interference study

Tolerance limit (M/M_{HCy})	Species
1000	Pb^{2+} , NO_3^{2-} , Ni^{2+} , SO_4^{2-} , Ba^{2+} , Cl^- , Ca^{2+} , glucose, methionine, phenylalanine, ethanol, fructose, lactose, sucrose, urea
100	Fe^{2+}
50	Citric acid
10	Uric acid
1	Ascorbic acid, L-cysteine

Determination of HCy in real samples

The utility of the proposed sensor for the electrocatalytic determination of HCy was investigated in physiological serum solution and urine samples. The centrifuged urine sample and physiological serum were diluted ten and two times, respectively, with buffer and then various amounts of HCy were added to the physiological serum and urine samples. The recovery of HCy was obtained using the standard addition method. The results are given in Table II, from which it could be seen the proposed method had good recoveries of the spiked HCy.

TABLE II. Determination of HCy in real samples

No.	Biological sample	HCy added μM	Expected μM	Found $\pm SD$ ($n = 3$) μM	Recovery %
1	Serum	–	–	< Detection limit	
2		50.0	50.0	50.6 ± 1.1	101.2
3		100.0	150.0	148.9 ± 1.2	99.3

TABLE II. Continued

No.	Biological sample	HCy added μM	Expected μM	Found \pm SD ($n = 3$) μM	Recovery %
4	Urine	–	–	< Detection limit	–
5		50.0	50.0	48.7 \pm 0.6	97.4
6		50.0	100.0	102.2 \pm 0.7	102.2
7		100.0	200.0	198.6 \pm 0.8	99.3

CONCLUSIONS

In this paper, DP was proposed as a homogeneous mediator for determination of HCy by electrochemical oxidation at a multiwall carbon nanotubes graphite paste electrode (MWCNTPE). The electrochemical behavior of HCy was studied using cyclic voltammetry, differential pulse voltammetry and chronoamperometry in a buffer solution (pH 5.0 and 0.10 M KCl). The peak current of HCy oxidation was at 0.53 V on the MWCNTPE in the presence of DP, while in the absence of DP oxidation of HCy did not occur at the surface of the carbon nanotube graphite paste electrode. The kinetic parameters of the electrocatalytic process and the diffusion coefficients of HCy in an aqueous solution were determined. The proposed method has a good linear dynamic range and was applied for the determination of HCy in biological serum and urine samples.

Acknowledgments. The authors gratefully acknowledge the National Foundation for Iranian Elites, the research councils of Islamic Azad University, Falavarjan branch, and Payame Noor University, Iran, for their support of this work.

ИЗВОД

ЕЛЕКТКАТАЛИТИЧКА ОКСИДАЦИЈА И ОДРЕЂИВАЊЕ ХОМОЦИСТЕИНА НА ЕЛЕКТРОДИ ОД УГЉЕНИЧНЕ ПАСТЕ МОДИФИКОВАНОЈ ДОПАМИНОМ КАО МЕДИЈАТОРОМ

SAFOORA MOHAMMADZADEH¹ и MASOUD FOULADGAR²

¹Department of Chemistry, Payame Noor University, P. O. Box 19395-3697 Tehran, Iran и

²Department of Biochemistry, Falavarjan Branch, Islamic Azad University, Falavarjan, Iran

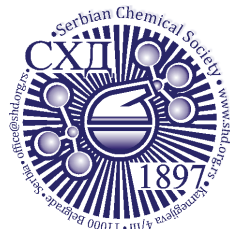
Електрода од угљеничне пасте која је модификована вишеслојним угљеничним наноцевима припремљена је за испитивање електрокаталитичке активности допамина у присуству хомоцистеина и коришћена за одређивање хомоцистеина у раствору. На основу електрохемијских мерења одређен је коефицијент дифузије хомоцистеина ($D = 6,79 \times 10^{-6} \text{ cm}^2 \text{ s}^{-1}$) и кинетички параметри за његову оксидацију, као што су коефицијент прелаза ($\alpha = 0.46$) и константа брзине ($k_h = 7,44 \times 10^2 \text{ dm}^3 \text{ mol}^{-1} \text{ s}^{-1}$). При оптималној вредности рН 5,0 максимум струје оксидације хомоцистеина на електроди од угљеничне пасте модификованој допамином постиже се на потенцијалу од око 530 mV. Запажено је да је тај максимум виши него на немодификованој електроди. Струјни максимум за оксидацију хомоцистеина одређен диференцијалном пулсном волтаметријом повећавао се линеарно у опсегу концентрације 3,0–600,0 μM са границом детекције 2,08 μM хомоцистеина. Ова метода је такође тестирана за одређивање хомоцистеина у физиолошком серуму и у узорцима урина.

(Примљено 29. октобра 2012, ревидирано 11. јануара 2013)

REFERENCES

1. S. Timur, D. Odaci, A. Dincer, F. Zihnioglu, A. Telefoncu, L. Gorton, *Sensors Actuators, B* **125** (2007) 234
2. L. W. Butz, V. Du Vigneaud, *J. Biol. Chem.* **99** (1932) 135
3. A. A. Z. Sanjay Kaul, P. K. Shah, *J. Am. Coll. Cardiol.* **48** (2006) 914
4. G. N. Welch, J. Loscalzo, *N. Engl. J. Med.* **338** (1998) 1042
5. L. Agüí, C. Peña-Farfal, P. Yáñez-Sedeño, J. M. Pingarrón, *Talanta* **74** (2007) 412
6. G. Zhang, D. Liu, S. Shuang, M. M. F. Choi, *Sensors Actuators, B* **114** (2006) 936
7. T. G. Williams, *JANA* **7** (2004) 11
8. F. Gholami-Orimi, F. Taleshi, P. Biparva, H. Karimi-Maleh, H. Beitollahi, H. R. Ebrahimi, M. Shamshiri, H. Bagheri, M. Fouladgar, A. Taherkhani, *J. Anal. Methods Chem.* 2012 (2012), Article ID 902184, doi: 10.1155/2012/902184
9. H. S. Collaboration, *JAMA* **288** (2002) 2015
10. J. Perla-Kajan, T. Twardowski, H. Jakubowski, *Amino Acids* **32** (2007) 561
11. A. D. Paramonov, S. V. Moiseev, V. V. Fomin, M. V. Kopeleva, L. I. Stankevich, A. I. Martynov, N. A. Mukhin, *Terapevt. Arkh.* **76** (2004) 67
12. A. Khosrowbeygi, H. Ahmadvand, *Bangladesh Med. Res. Counc. Bull.* **37** (2011) 106
13. J. Wan, Y. Deng, J. Guo, G. Xiao, D. Kuang, Y. Zhu, Y. Duan, G. Wang, *Exp. Mol. Pathol.* **91** (2011) 411
14. C. Huang, L. Zhang, Z. Wang, H. Pan, J. Zhu, *Acta Cardiol.* **66** (2011) 773
15. Y. J. Lai, W. L. Tseng, *Talanta* **91** (2012) 103
16. C. Sanli, D. Oguz, R. Olgunturk, F. S. Tunaoglu, S. Kula, H. Pasaoglu, O. Gulbahar, A. Cevik, *Pediatr. Cardiol.* **33** (2012) 1323
17. M. Y. Alsagaff, M. Thaha, M. Aminuddin, R. M. Yogiarto, M. Yogiartoro, Y. Tomino, *J. Int. Med. Res.* **40** (2012) 340
18. F. Wang, L. Han, Y. Yang, X. Gu, J. Ye, W. Qiu, H. Zhang, Y. Zhang, X. Gao, Y. Wang, *J. Inherit. Metab. Dis.* **33** Suppl. 3 (2010) 435
19. Z. Svagera, D. Hanzlikova, P. Simek, P. Husek, *Anal. Bioanal. Chem.* **402** (2012) 2953
20. J. Kaluzna-Czaplinska, M. Michalska, J. Rynkowski, *Nutr. Res.* **31** (2011) 318
21. J. Kaluzna-Czaplinska, M. Michalska, J. Rynkowski, *Acta Biochim. Pol.* **58** (2011) 31
22. S. Zhang, F. Huang, J. Zhao, L. Wen, F. Zhou, P. Yang, *Talanta* **58** (2002) 451
23. Y. Rao, M. McCooeye, Z. Mester, *Anal. Chim. Acta* **721** (2012) 129
24. S. Tokgz, C. Bulgu, E. C. Akir, M. K. Erbul, T. Kutluay, *Turk. J. Med. Sci.* **33** (2003) 71
25. A. Khan, M. I. Khan, Z. Iqbal, Y. Shah, L. Ahmad, S. Nazir, D. G. Watson, J. A. Khan, F. Nasir, Ismail, *Talanta* **84** (2011) 789
26. O. Chailapakul, W. Siangproh, B. V. Sarada, C. Terashima, T. N. Rao, D. A. Tryk, A. Fujishima, *Analyst* **127** (2002) 1164
27. C. M. Pfeiffer, D. L. Huff, E. W. Gunter, *Clin. Chem.* **45** (1999) 290
28. K. Kuśmierk, G. Chwatko, R. Głowacki, P. Kubalczyk, E. Bald, *J. Chromatogr., B* **879** (2011) 1290
29. M. Zhang, C. M. Pfeiffer, *Clin. Chim. Acta* **340** (2004) 195
30. A. A. Ghanem, S. M. Mady, H. E. El Awady, L. F. Arafa, *Curr. Eye Res.* **37** (2012) 712
31. M. Lopez-Alarcon, A. Chavez-Negrete, I. Montalvo-Velarde, J. Maldonado-Hernandez, V. S. Vital-Reyes, *Cir Cir* **79** (2011) 432
32. S. A. Pasas, N. A. Lacher, M. I. Davies, S. M. Lunte, *Electrophoresis* **23** (2002) 759
33. A. Zinellu, S. Sotgia, B. Scanu, E. Pisanu, M. Sanna, S. Sati, L. Deiana, S. Sengupta, C. Carru, *Talanta* **82** (2010) 1281
34. Z. Chen, Y. Zu, *J. Electroanal. Chem.* **624** (2008) 9

35. N. S. Lawrence, J. Davis, R. G. Compton, *Talanta* **53** (2001) 1089
36. M. K. Halbert, R. P. Baldwin, *Anal. Chim. Acta* **57** (1985) 591
37. M. Heyrovský, S. Vavříčka, *Bioelectrochem. Bioenerg.* **48** (1999) 43
38. P. Kalimuthu, S. A. John, *Bioelectrochemistry* **79** (2010) 168
39. K. Gong, Y. Dong, S. Xiong, Y. Chen, L. Mao, *Biosen. Bioelectron.* **20** (2004) 253
40. E. Sharifi, A. Salimi, E. Shams, *Bioelectrochemistry* **86** (2012) 9
41. H. Han, H. Tachikawa, *Front. Biosci.* **10** (2005) 931
42. V. K. Gupta, R. Jain, K. Radhapyari, N. Jadon, S. Agarwal, *Anal. Biochem.* **408** (2011) 179
43. R. Jain, V. K. Gupta, N. Jadon, K. Radhapyari, *Anal. Biochem.* **407** (2010) 79
44. R. N. Goyal, V. K. Gupta, S. Chatterjee, *Biosensors Bioelectron.* **24** (2009) 3562
45. R. N. Goyal, V. K. Gupta, A. Sangal, N. Bachheti, *Electroanalysis* **17** (2005) 2217
46. R. Jain, V. K. Gupta, N. Jadon, K. Radhapyari, *J. Electroanal. Chem.* **648** (2010) 20
47. Y. Li, Y. Umasankar, S. M. Chen, *Anal. Biochem.* **388** (2009) 288
48. Y. Umasankar, T. Y. Huang, S. M. Chen, *Anal. Biochem.* **408** (2011) 297
49. A. P. Periasamy, Y. J. Chang, S. M. Chen, *Bioelectrochemistry* **80** (2011) 114
50. A. K. Upadhyay, T. W. Ting, S. M. Chen, *Talanta* **79** (2009) 38
51. A. P. Periasamy, Y. H. Ho, S. M. Chen, *Biosensors Bioelectron.* **29** (2011) 151
52. M. Fouladgar, M. R. Hadjmohammadi², M. A. Khalilzadeh, P. Biparva, N. Teymoori, H. Beitollah, *Int. J. Electrochem. Sci.* **6** (2011) 1355
53. M. Fouladgar, H. Karimi-Maleh, R. Hosseinzadeh, *Ionics* **19** (2013) 665
54. M. Fouladgar, H. Karimi-Maleh, *Ionics* **19** (2013) 1163
55. M. Keyvanfard, A. A. Ensafi, H. Karimi-Maleh, *J. Solid State Electrochem.* **16** (2012) 2949
56. A. Mokhtari, H. Karimi-Maleh, A. A. Ensafi, H. Beitollahi, *Sensors Actuators, B* **169** (2012) 96
57. H. Karimi-Maleh, M. A. Khalilzadeh, Z. Ranjbarha, H. Beitollahi, A. A. Ensafi, D. Zareyee, *Anal. Methods* **4** (2012) 2088
58. H. Beitollahi, H. Khabazzadeh, H. Karimi-Maleh, A. Akbari, *Chin. Chem. Lett.* **23** (2012) 719
59. M. Roodbari Shahmiri, A. Bahari, H. Karimi-Maleh, R. Hosseinzadeh, N. Mirnia, *Sensors Actuators, B* **177** (2013) 70
60. M. Keyvanfard, R. Shakeri, H. Karimi-Maleh, K. Alizad, *Mat. Sci. Eng., C* **33** (2013) 811
61. H. Beitollahi, A. Mohadesi, S. Khalilzadeh Mahani, H. Karimi-Maleh, *Turk. J. Chem.* **36** (2012) 526
62. A. G. Bard, L. R. Faulkner, *Electrochemical Methods, Fundamentals and Principles*, Wiley, New York, USA, 2001
63. M. Fouladgar, *Int. J. Electrochem. Sci.* **6** (2011) 705
64. Z. Galus, *Fundamentals of Electrochemical Analysis*, Ellis Horwood, New York, USA, 1976.



J. Serb. Chem. Soc. 78 (10) 1609–1616 (2013)
JSCS–4522

Preparation and *in vitro* drug delivery response of doxorubicin-loaded poly(acrylic acid)-coated magnetite nanoparticles

REYHAN OMIDIRAD*, FARZANEH HOSSEINPOUR RAJABI
and BAHMAN VASHEGHANI FARAHANI

*Department of Chemistry, Faculty of Science, Imam Khomeini International University,
Qazvin, Iran*

(Received 25 December 2012, revised 12 March 2013)

Abstract: In this study, spherical superparamagnetic iron oxide nanoparticles (SPION) with mean diameter of 6 nm were prepared by a reduction–precipitation method. The surface of SPION were coated with poly(acrylic acid) 5000 (PAA-5000) and followed by loading with the anticancer drug doxorubicin (DOX). The drug loading efficiency was (14.64±0.29). *In vitro* drug release studies were realized for 8 h at two different pH values 4.2 and 7.4. The drug release rate at pH 4.2 (100 % DOX released in 2 h) was much faster than that at pH 7.4 (≈78 % DOX released in 8 h). These results indicate that these DOX-carrier nanoparticles have a high drug loading capacity and favourable release property for magnetic drug targeting. The drug release kinetics followed the Korsmeyer–Peppas model at pH 4.2, while at pH 7.4 the zero order model was fitted the best. The drug release mechanism followed super-case II transport in acidic and basic medium. The samples were characterized by XRD, SEM, TEM, FTIR, and UV–Vis.

Keywords: magnetite drug targeting; functionalization; poly(acrylic acid); anti-cancer drug; controlled delivery; release kinetic studies.

INTRODUCTION

Recently, Fe₃O₄ magnetic nanoparticles (MNs) have been widely used in biology and medicine in fields such as immunoassay, drug delivery and magnetic resonance imaging (MRI) due to their favourable characteristics, such as chemical stability, low toxicity and ultra-fine size, *etc.*^{1,2} Bare magnetite nanoparticles on account of their large surface area/volume ratio tend to agglomerate. To prevent agglomeration, a variety of polymeric coatings have been applied to nanoparticles.^{3,4} Of these polymers, poly(acrylic acid) (PAA) has been identified as being highly effective.

* Corresponding author. E-mail: reyhana.omidirad@gmail.com
doi: 10.2298/JSC121225041O

The PAA shell reduces the interactions of the electrostatic particles and as a result significantly augments the stability of the diffusion colloid. Poly(acrylic acid) is an aqueous soluble polymer with a high density of reactive functional groups, well known for its biocompatibility and widely used in drug delivery systems, especially as a mucoadhesive drug carrier.⁵ Surface-modified Fe₃O₄ nanoparticles have been explored as drug carriers. Doxorubicin (DOX) is an efficient anti-neoplastic agent commonly used in the treatment of a variety of cancers, such as leukaemia, ovarian cancer and, especially, late-stage breast cancer.⁶ The clinical use of DOX is limited by the resistance developed by cancer cells and the strong side effects of DOX, namely dose-dependent cardiotoxicity.⁷ Drug targeting (drug delivery to the tumour site) can prevent side effects and increase the cytotoxicity of doxorubicin. One of the possible approaches for drug targeting is delivery using magnetic nanoparticles, which can be retained in a tumour by application of an external magnetic field.^{8,9}

In this research, one kind of novel nano-scale carrier for doxorubicin was prepared using Fe₃O₄ nanoparticles as the core, PAA as a polymeric shell and doxorubicin as a drug to form drug-loaded magnetic nanoparticles.

EXPERIMENTAL

Materials

All chemicals were of analytical grade and used without further purification, iron(III) chloride hexahydrate (FeCl₃·6H₂O, Merck), poly(acrylic acid) 5000 (PAA-5000, Polysciences), anhydrous sodium sulphite (Na₂SO₃, Merck), ferrous ammonium sulphate ((NH₄)₂Fe(SO₄)₂·6H₂O, Carlo Erba), doxorubicin hydrochloride (DOX, Pharmacia Italia SpA, Milan, Italy), tris hydroxymethyl aminomethane (Tris, Merck).

Chemical synthesis of Fe₃O₄ nanoparticles

Fe₃O₄ nanoparticles were prepared using the reduction–precipitation method.¹⁰ Briefly, aqueous solutions of 0.3M FeCl₃·6H₂O (45 ml) and 2 M HCl (0.5 ml) were placed into a 200-ml glass beaker and subsequently aqueous solution of 0.3 M Na₂SO₃ (15 ml) was put into the beaker under stirring; Meanwhile, in another clean 1000-ml glass beaker, 50.8 ml of concentrated ammonia was diluted to a total volume of 800 ml with deionised water. In the smaller beaker, the colour of solution could be seen to turn into red from light yellow immediately upon mixing Fe³⁺ and SO₃²⁻, implying the formation of complex ions. Then, when the colour had returned from red to yellow, the solution was quickly poured into the dilute ammonia solution under intensive stirring. After continuation of the stirring for 30 min, the beaker with the suspension was placed on a permanent magnet. A black powder could be observed rapidly precipitating on the bottom of the beaker. The supernatant was discarded and fresh water added to the beaker. This technique was performed 5 times until a great part of the ions in the suspension had been removed. The powders were extracted by filtration and dried at room temperature.

Preparation of PAA-functionalized magnetite nanoparticles

The as produced nanoparticles were washed 3 times in absolute ethanol, centrifuged, and vacuum-dried overnight. Then, the dried nanoparticles were dispersed in deionised water using ultrasound. A solution of PAA in deionised water were added into the suspension under

stirring, and stirred for 24 h. The Fe₃O₄:PAA mass ratio was 1:2. The product was washed with deionised water and freeze-dried under vacuum at -20 °C for 24 h.

Preparation of DOX-SPION

A solution of DOX-Fe²⁺ complex of 1.5:1 drug:iron molar ratio was obtained by adding an aqueous solution of (NH₄)₂Fe(SO₄)₂·6H₂O to DOX in tris buffer pH 7.6. Then the DOX-Fe²⁺ complex was incubated in the dark with the PAA-coated SPION (PS), the mass ratio of DOX:PS was 0.31 mass %. After incubation for 30 min, the drug-loaded PS were separated by centrifugation at 19000 rpm for 15 min (4 °C). Finally, the resulting solid product was washed with ice-cold fresh aqueous buffer pH 7.6 and used immediately afterwards.

Drug loading determination

The DOX loading, %, was defined as the weight fraction of the drug in doxorubicin-loaded PS (DLPS). To measure the loaded drug, particles equivalent to 5 mg were accurately weighed and re-suspended for 20 min in acetate buffer (pH 4.0), conditions that lead to complete dissociation of the DOX-Fe²⁺ complex and therefore to the release of 100 % of DOX. Then, the sample was centrifuged and the DOX concentration measured by means of UV-Vis using the DOX absorbance at 480 nm.

The drug-loading capacity, %, was determined using the following equation:

$$\text{Drug loading} = 100 \frac{W_1 - W_2}{W_1} \quad (1)$$

where W_1 is the initial weight of DOX that was incorporated into the PS and W_2 is the weight of free drug (unincorporated DOX). Each determination was performed in triplicate.

Kinetics of drug release

In order to understand the kinetics and mechanism of drug release from DLPS, the drug-loaded nanoparticles were suspended in 50 ml of acetate buffer (pH 4.2) or phosphate buffer (pH 7.4) at 37 °C for 8 h under constant stirring (200 rpm) by a mechanical stirrer. At given time intervals, 2 mL of the release medium was removed for analysis and replaced with 2 mL of same buffer solution. The concentration of drug released was determined from the absorbance at 480 nm (measured using a UV-Vis spectrophotometer) and previously established calibration curves.

The results of the *in vitro* drug release study were fitted with zero order model (cumulative drug release vs. time), first order model (ln (cumulative drug remaining) vs. time), Higuchi model (cumulative drug release vs. $t^{1/2}$), Hixson-Crowell model (cube root of drug remaining in the matrix vs. time) and the Korsmeyer-Peppas model (log (cumulative drug released) vs. log t). The kinetic model that best fitted the dissolution data was evaluated by comparing the regression coefficient (r^2) values of the various models. The “ n ” (release exponent) value of the Korsmeyer-Peppas model used to characterize the different mechanisms of drug release from polymeric systems. For nanoparticles of spherical shape, values of $n \leq 0.43$ mean Fickian diffusion, between 0.43 to 0.85 mean anomalous (non-Fickian) diffusion, $n = 0.85$ for case II transport and $n > 0.85$ for super-case II transport.¹¹ To determine the drug release mechanism, first 60 % of the drug release data was fitted to the Korsmeyer-Peppas model.

Characterization of nanoparticles

Powder X-ray diffraction (XRD) patterns were acquired from dried nanoparticle samples employing a Rigaku D/max rA X-ray diffractometer using CuK α radiation. A Philips-CM120

transmission electron microscope (TEM) at an accelerating voltage of 120 KV and a Hitachi S-4160 field emission scanning electron microscope (FE-SEM) at an accelerating voltage of 15 kV were used to observe the morphologies of the Fe_3O_4 MNs and PS. Fourier transform infrared (FTIR) spectra were taken on a Bruker FTIR spectrometer (Tensor 27) and the UV–Vis absorption spectra were recorded using a Camspec-M350 double beam spectrophotometer.

RESULTS AND DISCUSSION

XRD Analysis

The XRD patterns of the bare Fe_3O_4 and PS are shown in Fig. 1. These patterns detect the nanocrystalline structure of the nanoparticles and the mean particle size. The seven diffraction peaks visible in both patterns are consistent with the diffraction peaks of (220), (311), (400), (422), (511), (440) and (533), ascertained by comparison with Joint Committee on Powder Diffraction Standards (JCPDS card, File No. 79-0418). These coincidences suggests that the crystalline structure of Fe_3O_4 did not change on modification of the particles with PAA chains and shows that the PAA coating occurred only at the surface of Fe_3O_4 MNs and resulted in no detectable chemical/physical change in bulk of the nanoparticles.

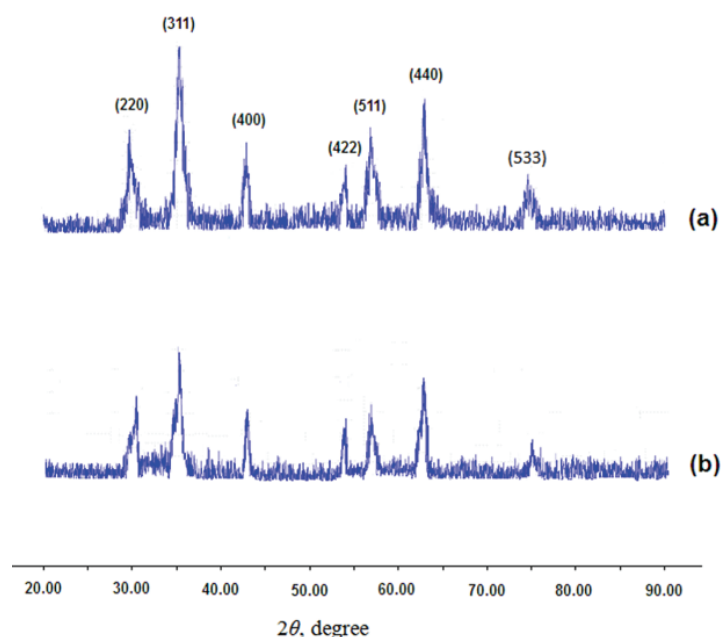


Fig. 1. XRD Patterns of a) uncoated Fe_3O_4 MNs and b) PAA-coated Fe_3O_4 MNs.

Particle sizes can be quantitatively evaluated from XRD data using the Debye–Scherrer equation.

$$D = K\lambda/(\beta \cos \theta) \quad (2)$$

where, K (=0.89) is the Scherrer constant, λ is the X-ray wavelength, β is the peak width at half-maximum height and θ is the Bragg diffraction angle.

The crystallite sizes of the Fe₃O₄ and PS were found to be about 6 and 11 nm, respectively.

FE-SEM and TEM analysis

The morphologies of magnetic nanoparticles were investigated by FE-SEM and TEM, as shown in Fig. 2a–d. These images showed that the prepared nanoparticles had regular spherical shape and a core–shell structure. Due to large specific surface area and high surface energy, some bare magnetite nanoparticles were aggregated (Fig. 2a). However, after being coated with PAA, the nanoparticles were well dispersed (Fig. 2b). Therefore, PAA coating reduced the aggregation and enhanced the particle dispersion. It is an important factor in drug delivery applications that nanoparticles are individually dispersed and are not agglomerated because aggregation would reduce the effective magnetization of nanoparticles and cause difficulties during drug delivery to the desired site.¹²

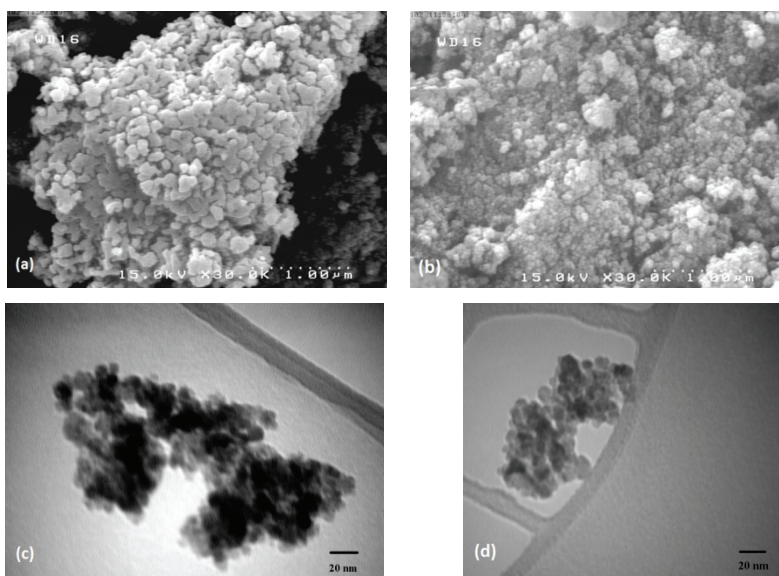


Fig. 2. FE-SEM Images of a) uncoated Fe₃O₄ MNs, b) PAA coated Fe₃O₄ MNs and TEM images of c) uncoated Fe₃O₄ MNs and d) doxorubicin-loaded PAA-coated Fe₃O₄ MNs.

FTIR Analysis

The FTIR spectra of bare Fe₃O₄ MNs (a) and PS (b) are shown in Fig. 3. The IR peak at approximately 603 cm⁻¹ was assigned to Fe–O,¹³ and the peak at

3434 cm^{-1} was attributed to the stretching vibrations of $-\text{OH}$, which resulted from OH^- absorbed by Fe_3O_4 nanoparticles. Moreover, Fig. 3b shows additional peak of the $\text{C}=\text{O}$ stretching band at 1710 cm^{-1} , the COO^- stretching bands at 1423 and 1554 cm^{-1} , and $-\text{CH}_2-$ bending band at 1492 cm^{-1} . These results suggested that the Fe_3O_4 MNPs had been successfully coated by PAA-5000.

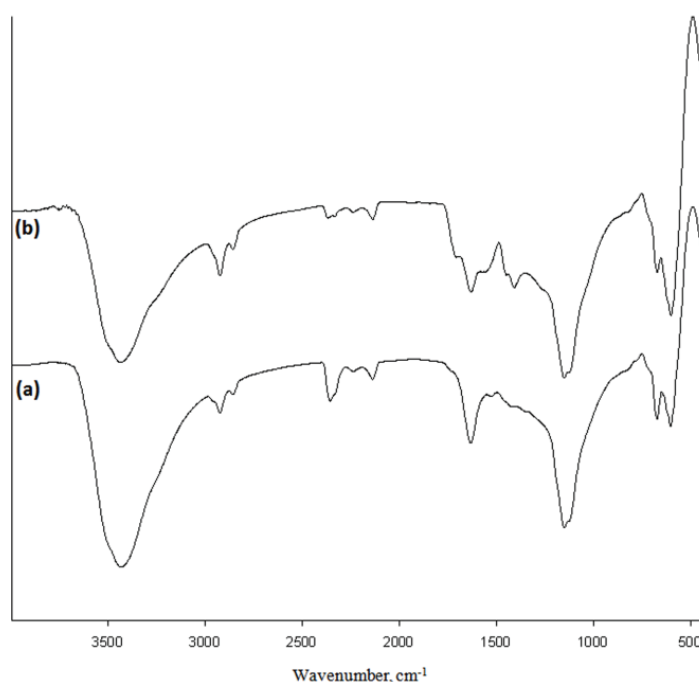


Fig. 3. FTIR Spectra of a) bare Fe_3O_4 MNPs and b) PAA-coated Fe_3O_4 MNPs.

Drug loading and in vitro release analysis

The drug loading efficiency of DLPS was (14.64 ± 0.29) . The low values of the standard deviation indicate uniformity of the drug content in the nanocarriers. The drug-loaded nanoparticles were incubated in acetate buffer and phosphate buffer at different pH values to examine the drug release. The chosen pH levels replicated those found in the acidity environment of cancer cells (pH 4.2), as well as blood (pH 7.4). As shown in Fig. 4, the drug release at pH 4.2 was much faster than that at pH 7.4. This is likely due to protonation of the phenol group of DOX in the acidic environment, which leads to the faster dissociation of the DOX-iron complex.¹⁴

Kinetic modelling of release data

The regression coefficient (r^2) values for DLPS are tabulated in Table I. The model that gave higher r^2 values was considered as best fit model. Based on the

r^2 values, it was also observed that the release of drug from DLPS at pH 4.2 followed the Korsmeyer–Peppas kinetic model while at pH 7.4, the zero-order kinetic model was best fitted. The ‘ n ’ values of the Korsmeyer–Peppas equation for DLPS suggested that the drug release behaviour was super case II transport at the two pH values. These experiments were performed twice.

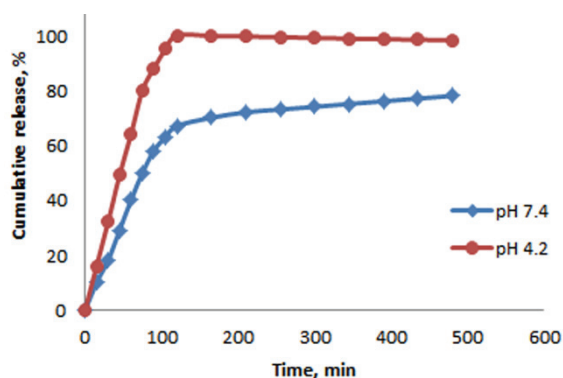


Fig. 4. *In vitro* drug release of DLPS into pH 4.2 and 7.4 solutions

TABLE I. *In vitro* release kinetics studies of DLPS

pH	Regression coefficient, r^2 , values					Release exponent “ n ” values
	Zero order	First order	Higuchi	Hixson Crowell	Korsmeyer–Peppas	
4.2	0.9998	0.9802	0.9946	0.9919	0.9999	1.0058
	0.9987	0.9871	0.9938	0.9883	0.9999	1.0193
7.4	0.9986	0.9950	0.9910	0.9973	0.9981	1.0085
	0.9991	0.9906	0.9927	0.9964	0.9973	1.0047

CONCLUSIONS

Spherical magnetite particles, prepared using a reduction–precipitation method, were successfully modified with PAA and confirmed by FTIR spectroscopy. Based on X-ray diffraction, introduction of the PAA coating did not affect the crystalline structure of Fe₃O₄, whereas, based on FE-SEM, it enhanced the uniform dispersion of the nanoparticles. Drug loading was confirmed by UV-Vis and *in vitro* release behaviour was investigated. Approximately 78 % of DOX was released into phosphate buffer, pH 7.4, within 8 h but up to 100 % of drug was released at pH 4.2 within approximately 2 h. At pH 4.2, Korsmeyer–Peppas kinetics of drug release were observed while at pH 7.4, drug release kinetics followed the zero order model. The values of the release exponent “ n ” suggested a super-case II transport release mechanism in both phosphate and acetate buffer.

ИЗВОД

ПРИПРЕМА И *IN VITRO* ИСПИТИВАЊЕ БРЗИНЕ ОТПУШТАЊА ДОКСОРУБИЦИНА
ИНКАПСУЛИРАНОГ У НАНОЧЕСТИЦАМА МАГНЕТИТА ПРЕКРИВЕНИМ
ПОЛИАКРИЛНОМ КИСЕЛИНОМ

REYHAN OMIDIRAD, FARZANEH HOSSEINPOUR RAJABI и ВАХМАН VASHEGHANI FARAHANI

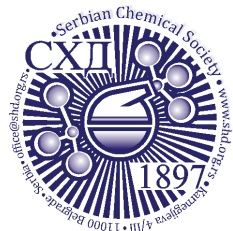
Department of Chemistry, Faculty of Science, Imam Khomeini International University, Qazvin, Iran

Предмет овог рада је добијање сферичних, супермагнетних наночестица оксида гвожђа, средњег пречника 6 nm, методом редукционе преципитације. Површина наночестица је обложена поли-акрилном киселином 5000, након чега је у честице инкапсулиран лек доксорубицин. Степен инкапсулације лека износио је $14,64 \pm 0,29$. Ослобађање лека из наночестица праћено је *in vitro* током 8 h у два система са различитим рН вредностима (4,2 и 7,4). Отпуштање лека при рН вредности од 4,2 (100 % лека је ослобођено током 2 h) значајно је брже од отпуштања на рН 7,4 (~78 % током 8 h). Ови резултати указују на то да добијене наночестице имају потенцијал као носачи доксорубицина у системима за контролисано отпуштање под дејством магнетног поља. Кинетика ослобађања лека из наночестица описана је Korsmeuер–Peppas моделом у раствору рН 4,2, док је процес у раствору рН 7,4 могуће описати кинетиком нултог реда. Сви узорци су окарактерисани коришћењем различитих аналитичких метода: XRD, SEM, TEM, FTIR и UV–Vis.

(Примљено 25. децембра 2012, ревидирано 12. марта 2013)

REFERENCES

1. J. Dobson, *Drug. Dev. Res.* **67** (2006) 55
2. S. I. Park, J. H. Kim, J. H. Lim, C. O. Kim, *Curr. Appl. Phys.* **8** (2008) 706
3. Y. Zhang, N. Kohler, M. Zhang, *Biomaterials* **7** (2002) 1553
4. E. Osterberg, K. Bergstrom, K. Holmberg, *Colloids Surfaces, A* **77** (1993) 159
5. K. Burugapalli, V. Koul, A. K. Dinda, *J. Biomed. Mater. Res., A* **68** (2004) 210
6. E. M. Hoke, C. A. Maylock, E. Shacter, *Free Radical Biol. Med.* **39** (2005) 403
7. A. Bast, H. Kaiserová, G. J. M. Den Hartog, G. R. M. M. Haenen, W. J. F. Van Der Vijgh, *Cell Biol. Toxicol.* **23** (2007) 39
8. V. P. Torchilin, *Adv. Drug Deliv. Rev.* **58** (2006) 1532
9. A. S. Lübbe, C. Alexiou, C. Bergemann, *Surg. Res.* **95** (2001) 200
10. S. Qu, H. Yang, D. Ren, S. Kan, G. Zou, D. Li, M. Li, *J. Colloid Interface Sci.* **215** (1999) 190
11. J. Siepmann, F. Siepmann, *Int. J. Pharm.* **364** (2008) 328
12. J. Zhang, S. Rana, R. S. Srivastava, R. D. K. Misra, *Acta Biomater.* **4** (2008) 40
13. J. Ge, Y. Hu, M. Biasini, C. Dong, J. Guo, W. P. Beyermann, Y. Yin, *Chem. Eur. J.* **13** (2007) 7153
14. E. Munnier, S. Cohen-Jonathan, C. Linassier, L. Douziech-Eyrolles, H. Marchais, M. Soucé, K. Hervé, P. Dubois, I. Chourpa, *Int. J. Pharm.* **363** (2008) 170.



J. Serb. Chem. Soc. 78 (10) 1617–1632 (2013)
JSCS–4523

Influence of different carbon monolith preparation parameters on pesticide adsorption

MARIJA VUKČEVIĆ^{1*#}, ANA KALIJDIS², BILJANA BABIĆ³, ZORAN LAUŠEVIĆ²
and MILA LAUŠEVIĆ^{1#}

¹Faculty of Technology and Metallurgy, University of Belgrade, P. O. Box 494, 11001 Belgrade, Serbia, ²Laboratory of Physics, Vinča Institute of Nuclear Sciences, University of Belgrade, P. O. Box 522, 11001 Belgrade, Serbia and ³Laboratory of Material Science, Vinča Institute of Nuclear Sciences, University of Belgrade, P. O. Box 522, 11001 Belgrade, Serbia

(Received 27 December 2012, revised 14 January 2013)

Abstract: The capacity of carbon monolith for pesticide removal from water, and the mechanism of pesticide interaction with the carbon surface were examined. Different carbon monolith samples were obtained by varying the carbonization and activation parameters. In order to examine the role of surface oxygen groups on pesticide adsorption, the carbon monolith surface was functionalized by chemical treatment in HNO₃, H₂O₂ and KOH. The surface properties of the obtained samples were investigated by determination of the Brunauer, Emmett and Teller (BET) surface area, pore size distribution and temperature-programmed desorption. Adsorption of pesticides from aqueous solution onto the activated carbon monolith samples was studied using five pesticides belonging to different chemical groups (acetamiprid, dimethoate, nicosulfuron, carbofuran and atrazine). The presented results show that higher temperature of carbonization and amount of activating agent enable microporous carbon monolith with higher numbers of surface functional groups to be obtained. The adsorption properties of the activated carbon monolith were more readily affected by the number of surface functional groups than by the specific surface area. Results obtained after carbon monolith functionalization showed that π - π interactions were the driving main force for adsorption of pesticides with an aromatic structure, while acidic groups played an important role in adsorption of pesticides with no aromatic ring in their chemical structure.

Keywords: carbon monolith; activation; surface properties; adsorption; pesticides.

* Corresponding author. E-mail: marijab@tmf.bg.ac.rs

Serbian Chemical Society member.

doi: 10.2298/JSC131227006V

INTRODUCTION

The possibility of producing carbon materials with high specific surface areas, microporous structure, high adsorption capacity and high degree of surface reactivity brings a variety of applications for these materials. Carbon monolith (CM) is a relatively new carbon material. Depending on the application, CM can be produced with the desired shape and morphology, and controlled composition, structure and porosity. CMs are potentially useful in a wide variety of applications, such as residential water filtration, volatile organic compound emission control,^{1–4} indoor air purification, chemical separation,⁵ catalysis, biocatalysts,⁶ adsorption, *etc.* In a previous work, cylindrical CM impregnated with silver was successfully used for the disinfection of drinking water.⁷ Due to the fact that finer silver particles had higher resistance to attrition from the surface of the carbon material in comparison to larger ones,⁸ the CM surface was efficiently modified and an Ag deposit was obtained in the form of fine crystals with small crystallite sizes.⁹ The last few years have been marked with a growing interest in carbon monolith as an alternative for conventional carbon materials. In the present study, an attempt was made to use activated CM as an adsorbent for the removal of pesticides from aqueous solutions.

Pesticides are the group of hazardous compounds that, due to their extensive application in agriculture, may contaminate surface and groundwater with potential risks for wildlife and human health.¹⁰ Environmental contamination occurs when pesticides drift away from the application sites and infiltrate the groundwater by leaching through the soil.^{11,12} Several methods are available for removal of pesticides, such as photocatalytic degradation, combined photo-Fenton and biological oxidation, advanced oxidation processes, aerobic degradation, nanofiltration, ozonation and adsorption.¹³ Adsorption on activated carbon is the most widespread technology used to deal with the purification of water contaminated by pesticides.^{14–17} The adsorption capacity as one of the most important properties is directly determined by the surface structure of the activated carbon material.

As the surface characteristics of a carbon material depend on the nature of the carbon precursor and the processing conditions during production,¹⁸ the main objective of this work was to determine the appropriate carbonization and activation parameters in order to obtain a material with good adsorption properties toward pesticides. Chemical activation, either through carbonization followed by activation, or through a direct activation, as one of the most important steps during the preparation, has attracted extensive attention.^{19–21} Basta *et al.*²² found that a 2-step KOH activation was much more advantageous than a single-step activation for obtaining carbon materials with a high Brunauer, Emmett and Teller (BET) surface area. The factor that influence the final porous texture of activated carbon materials obtained by chemical activation are the activation agent, the activating agent/carbon material ratio, the heating rate and the acti-

vation temperature.¹⁹ In the present work, different carbon monolith samples were obtained by changing the carbonization temperature and the amount of potassium hydroxide used as the activation agent. The adsorption properties of the resulting CM samples were determined by adsorption of five pesticides: acetamiprid, dimethoate, nicosufurone, carbofuran and atrazine. The influence of the carbonization temperature and the activation parameters on the specific surface area, surface functional groups and adsorption properties of the activated CM samples were studied. Additionally, in order to examine the role of surface oxygen groups in pesticide adsorption, the carbon monolith surface was functionalized by different chemical treatments.

EXPERIMENTAL

Material

CMs precursor in the shape of cylinder (length 3.0 cm, diameter 1.8 cm) with 8600 parallel capillary channels (each with a diameter of 80 μm) inside the cylinder were purchased from Fractal Carbon (London, UK). The design and structure of the employed CM is shown in Fig. 1. This is a composite material, consisting of a glassy carbon bed and activated carbon on the inner capillary walls.

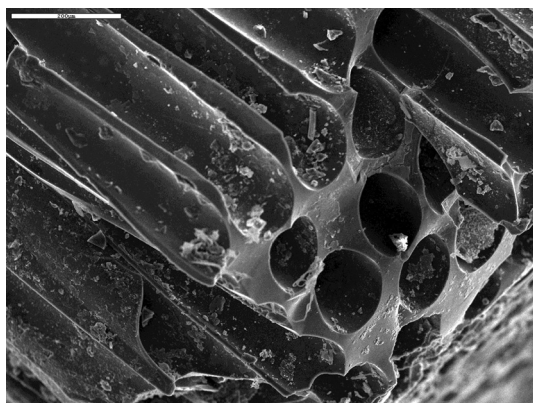


Fig. 1. SEM Photograph of the carbon monolith and cross-section (magnification: 100 \times).

Activation of the carbon monolith

The carbon precursor was first carbonized at two different temperatures, 700 and 1000 $^{\circ}\text{C}$, under a constant nitrogen flow rate, at a heating rate of 5 $^{\circ}\text{C min}^{-1}$, and the samples CM7 and CM1, respectively, were obtained. Only sample CM1 was further tested and compared with samples activated with KOH, as sample CM7 was not fully carbonized due to its lower carbonization end-temperature. The carbonized samples, CM7 and CM1, were mixed with KOH pellets in different weight ratio of KOH:carbonized material (1:1 and 2:1). The samples were placed in a furnace and heated at a rate of 5 $^{\circ}\text{C min}^{-1}$ to 900 $^{\circ}\text{C}$. The activation process was realized under a constant nitrogen flow rate. The resulting products were thoroughly washed with tap water and finally distilled water to remove the residual KOH until the pH value of the washed solution ranged from 6 to 7. Four samples obtained in this way were used for further examination. The scheme of activated carbon monolith production is shown in Fig. 2. The samples were denoted as CM719, CM729, CM119 and CM129. The first number in the

sample code represents a temperature of carbonization: 7 for 700 °C and 1 for 1000 °C; the second number in the sample code represents the amount of activating agent used: 1 for the KOH:carbon material ratio 1:1, and 2 for the ratio 2:1; the last number specifies the activating temperature: 9 for the 900 °C.

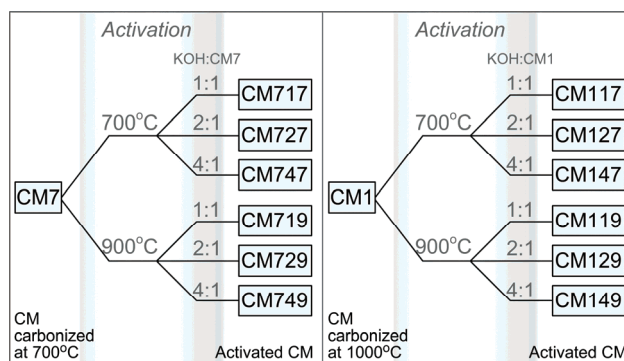


Fig. 2. Scheme for the production of activated carbon monolith.

Chemical surface treatment

The chemical treatments involved submerging the sample CM719 in HNO₃, KOH and H₂O₂ solution. The chemically treated samples were designated CM/A, CM/B and CM/P, respectively. Samples CM/A and CM/B were obtained by heating CM719 in 4 M HNO₃ and 4 M KOH, respectively, for 2 h, while CM/P was obtained by submerging CM719 in 4 M H₂O₂ at room temperature until complete decomposition of the H₂O₂ (when there was no further gas evolution). After chemical treatment, modified samples were thoroughly washed with distilled water to neutral pH and dried at 110 °C for 24 h. All samples were stored in a dessicator until use.

pH_{slurry} of the chemically treated samples

The pH values of aqueous slurries of the CMs samples were measured. The slurries were prepared with boiled distilled water in the ratio of 10 ml g⁻¹; these suspensions were stirred and the pH values were measured several times until a constant value was reached.

Specific surface area and porosity

Specific surface area of all CM samples was determined by nitrogen adsorption at liquid nitrogen temperature using an automatic surface area analyzer, model 4200 (Leeds & Northrup Instruments, USA). The N₂ adsorption and desorption isotherms of samples CM119, CM129, CM719 and CM729 were measured at -196 °C, using the gravimetric McBain method. The specific surface area, S_{BET} , pore size distribution, mesopore including external surface area, S_{meso} , and micropore volume, V_{mic} , for the samples were calculated from the isotherms. The pore size distribution was estimated by application of the Barret, Joyner and Halenda (BJH) method²³ to the desorption branch of the isotherms. Mesopore surface and micropore volume were estimated using the high resolution α_s plot method.²⁴ Micropore surface, S_{mic} , was calculated by subtracting S_{meso} from S_{BET} .

Surface oxygen groups

Temperature-programmed desorption (TPD) in combination with mass spectrometry was used to investigate the nature and the thermal stability of the CM surface oxygen groups. The

TPD profiles were obtained using a custom-built set-up, consisting of a quartz tube placed inside an electrical furnace. A CM sample was outgassed in the quartz tube and subjected to TPD at a constant heating rate of $10\text{ }^{\circ}\text{C min}^{-1}$ to $900\text{ }^{\circ}\text{C}$ under high vacuum. The amounts of CO (Q_{CO}) and CO_2 (Q_{CO_2}) released from the carbon monolith sample (0.1 g) were monitored using an Extorr 300 quadrupole mass spectrometer (Extorr Inc., USA).

Pesticide adsorption

Adsorption of pesticides (acetamiprid, dimethoate, nicosulfuron, carbofuran and atrazine) by the CM samples (0.5 g) was performed from 50 ml of an aqueous solution of pesticide in batch system with constant shaking. The initial concentration of each pesticide was 500 ppb. The concentration of pesticides was determined at the end of 2 h adsorption period using an HPLC–MS/MS method.²⁵

HPLC–MS/MS Analysis

Surveyor HPLC system (Thermo Fisher Scientific, USA) was used for the separation of the analytes on the reverse-phase Zorbax Eclipse XDB-C18 column, 75 mm long, 4.6 mm i.d. and $3.5\text{ }\mu\text{m}$ particle size (Agilent Technologies, USA). The mobile phase consisted of methanol (A), water (B) and acetic acid (C). The composition was linearly changed as follows: 0 min 59 % A, 40 % B, 1 % C; 10 min 99 % A, 1 % C; 15 min 59 % A, 40 % B, 1 % C. The flow rate of the mobile phase was 0.5 ml min^{-1} . A $10\text{ }\mu\text{l}$ aliquot of the aqueous solution was injected into HPLC system. Quadrupole ion trap mass spectrometer, LCQ Advantage (Thermo Fisher Scientific, USA), was used for detection and quantification of pesticides. The electrospray ionization technique was used and all pesticides were analyzed in the positive ionization mode. External calibration method and the selected reaction monitoring (SRM) mode was used for quantification of all pesticides.

RESULTS AND DISCUSSION

The values of the specific surface area obtained by the dynamic method (Table I) showed an increase in the specific surface area on activation. It could be noted that specific surface area of activated CM samples depended on both amount of KOH amount and activation temperature. The increase in the KOH amount together with activation at $700\text{ }^{\circ}\text{C}$ led to the development of a specific surface. During the activation process, the decomposition of KOH was followed by a gasification process under high temperature:



Stronger activation, *i.e.*, increased ratio of KOH, opened up the porous structure and increased S_{BET} .²⁶ The specific surface area of both CM samples increased on activation at $900\text{ }^{\circ}\text{C}$ using two ratios of hydroxide. However, further increasing the amount of the activating agent decreased the specific surface area, probably due to enhanced gasification process. Therefore, an over-gasification might have occurred with the detrimental effect of reducing the surface area, especially the micropore surface area.²⁷ This phenomenon was also observed by Laine and Calafat.²⁸ The highest values of specific surface area were obtained for the samples carbonized at $700\text{ }^{\circ}\text{C}$ and activated at $900\text{ }^{\circ}\text{C}$.

TABLE I. The amount of pesticides adsorbed on the CM samples ($q / \mu\text{g g}^{-1}$)

Sample	Spec. surf. area, $\text{m}^2 \text{g}^{-1}$	Acetamiprid	Dimethoate	Nicosulfuron	Carbofuran	Atrazine
CM7	4.17	11.2	0.00	17.8	1.96	12.0
CM1	6.42	14.9	2.90	2.30	9.19	15.0
CM717	1.44	9.60	7.58	11.1	22.8	5.59
CM727	321	51.4	36.2	18.6	52.6	41.6
CM747	324	38.5	18.6	12.4	35.0	24.9
CM719	388	47.8	48.0	47.7	47.9	48.0
CM729	714	44.6	44.9	44.6	44.8	44.8
CM749	609	44.9	44.9	44.9	44.9	44.7
CM117	93.6	39.0	26.3	13.1	43.7	30.1
CM127	110	28.5	46.5	8.05	63.6	21.0
CM147	133	28.5	22.7	5.50	47.6	16.3
CM119	105	44.6	44.4	43.7	44.7	44.3
CM129	616	66.6	62.0	58.2	68.2	64.7
CM149	59.2	41.2	43.7	26.2	75.0	27.3

The concentration of the pesticides remaining in the aqueous solutions after adsorption on the CM samples was determined by the HPLC–MS/MS method. From the obtained MS² spectra of the pesticides (Fig. 3), the most abundant fragment ions were selected. The selected reaction monitoring (SRM) mode was used for quantification of all pesticides. The amounts of pesticides adsorbed on CM samples are presented in Table I. The CM samples activated at 900 °C had better adsorption properties toward the examined pesticides. Since the amounts of pesticides adsorbed were not proportional to the values of specific surface area, it could be assumed that the specific surface area is not a key factor in the adsorption of pesticides.

The porous texture of CM samples with best adsorption properties (CM119, CM129, CM719 and CM729) was determined by physical adsorption of N₂ at –196 °C. The nitrogen adsorption isotherms of selected CM samples are presented in Fig. 4. According to the IUPAC classification,²⁹ the isotherms are of type I, which are associated with microporous materials. The pore size distributions, shown in Fig. 5, confirm that examined samples were microporous, with most of the pore having a radius smaller than 2 nm. Activation with the higher amount of hydroxide slightly increased the amount of mesopores.

The specific surface areas calculated by the BET equation (S_{BET}), micropore and mesopore area, micropore volume and average pore radius are listed in Table II. The S_{BET} values cover a wide range 172–1144 $\text{m}^2 \text{g}^{-1}$ and follow the same trend as the values of the specific surface areas obtained by the dynamic method. However, the values of the specific surface area of selected CM samples obtained by dynamic method and the McBain method show some discrepancies. These discrepancies are even more pronounced with increasing S_{BET} and in microporo-

sity. The reasons for these discrepancies lie in the employed experimental conditions. In the case of microporous materials, it is essential to estimate the experimental conditions for the achievement of equilibrium N_2 adsorption, due to the slow nitrogen adsorption within the micropores. The experimental conditions used in the McBain method enabled equilibrium adsorption of N_2 , while in the case of the fast dynamic method, equilibrium nitrogen adsorption was not achieved. Consequently, the dynamic method did not give complete surface coverage and results obtained by this method are lower than those obtained by the McBain method.

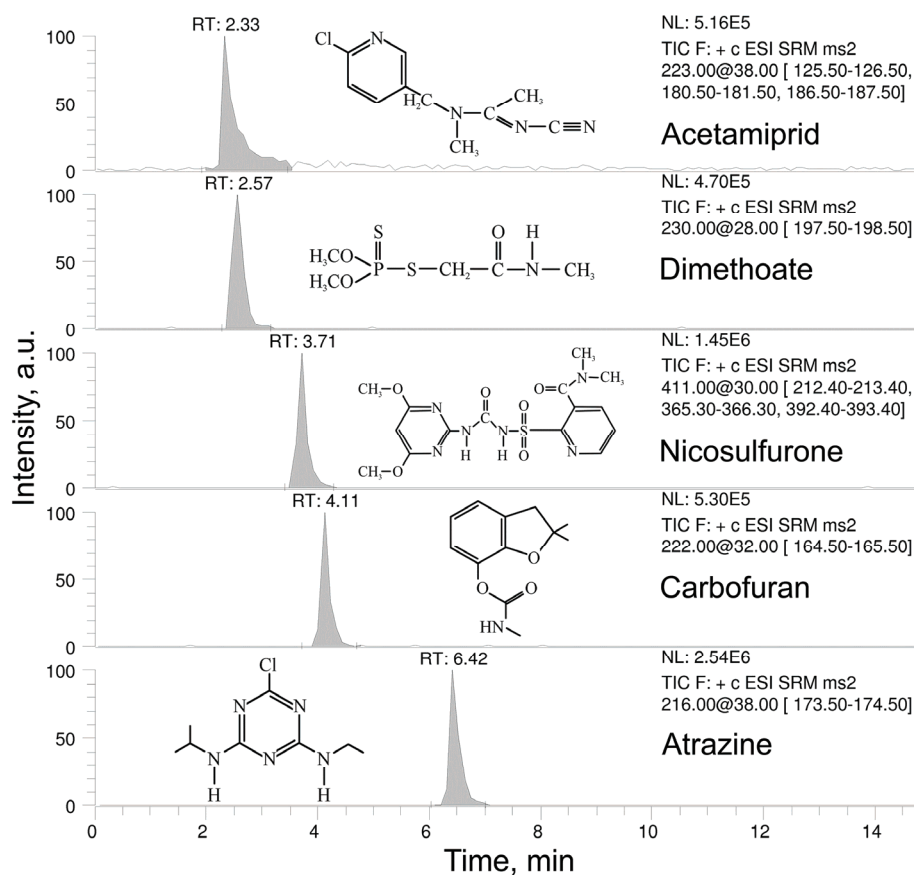


Fig. 3. HPLC Chromatogram of aqueous solutions of the pesticides.

TPD provides quantitative information on the total number of surface oxygen groups. Surface oxygen complexes on carbon materials decompose upon heating by releasing CO and CO_2 . Thus, the TPD peaks of CO and CO_2 at different temperatures correspond to specific oxygen groups. The decomposition temperature is related to the bond strength of specific oxygen-containing groups.

Thus, the position of the peak maximum at a defined temperature corresponds to a specific oxygen complex at the surface. For example, CO₂ is released by decomposition of carboxylic groups at 373–673 K,^{30–32} or lactone groups at 463–923 K.^{30,33} Both CO and CO₂ peaks originate from the decomposition of carboxylic anhydrides in the temperature range 623–900 K.^{30,31} Phenols, ethers, carbonyls and quinones give rise to CO at 973–1253 K.^{32,34,35} The quantities of CO and CO₂ released during the TPD experiments correspond to the total amount of surface oxygen groups.

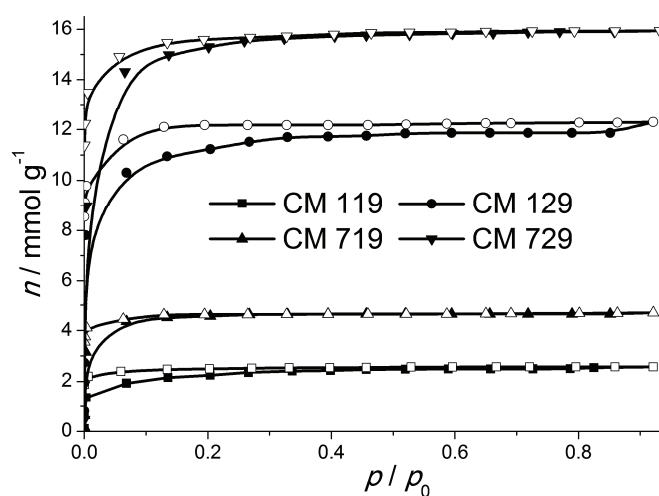


Fig. 4. Nitrogen adsorption isotherms, the amount of N₂ adsorbed as function of the relative pressure for CM samples. Solid symbols, adsorption; open symbols, desorption.

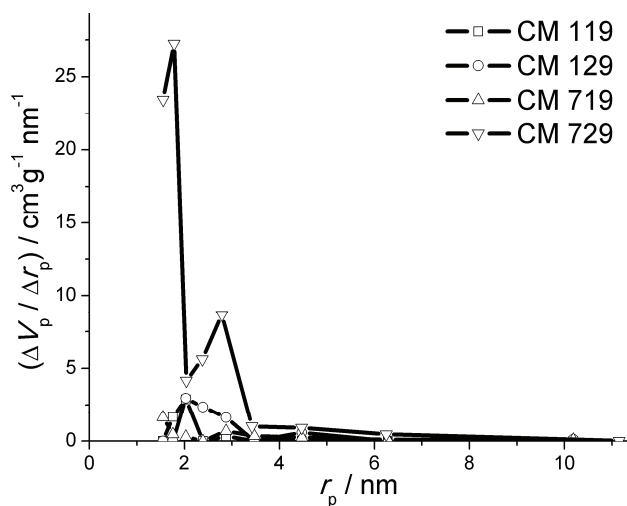


Fig. 5. Pore size distribution for the CM samples.

TABLE II. Porous properties of the CM samples

Sample	$S_{\text{BET}} / \text{m}^2 \text{g}^{-1}$	$S_{\text{micro}} / \text{m}^2 \text{g}^{-1}$	$S_{\text{meso}} / \text{m}^2 \text{g}^{-1}$	$V_{\text{micro}} / \text{cm}^3 \text{g}^{-1}$	r_p / nm
CM1	6.42	—	—	—	—
CM119	172	168	4	0.084	1.54
CM129	843	823	20	0.396	1.78
CM719	398	396	2	0.160	2.03
CM729	1144	1133	11	0.540	2.03

TPD profiles of CO and CO₂ evolution for all CM samples are shown in Fig. 6. The TPD profiles of all the tested activated CM samples showed intensive peaks at relatively high temperatures (from 650 to 780 °C). In addition, the CO desorption profiles had a maximum at the temperature which coincides with the maximum in CO₂ desorption profile, which indicates the existence of anhydride groups.³⁶ The existence of these peaks was not observed in the TPD profiles of

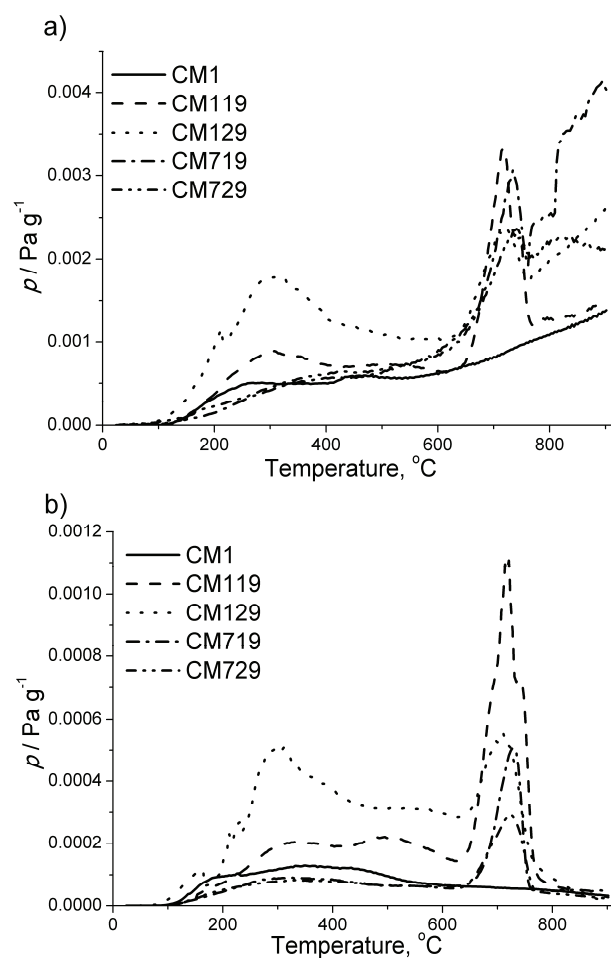


Fig. 6. TPD spectra of the CM samples. a) CO and b) CO₂ desorption profiles.

CM1.³⁰ Therefore, the presence of a large number of anhydride groups on the surface of the activated CM samples is probably the consequence of the KOH activation process. The appearance of a desorption peak at a low temperature (around 300 °C) in the CO profiles of all samples may be due to thermal decomposition of carbonyl groups in α -substituted ketones and aldehydes.³⁷ The CO₂ desorption profile (Fig. 6b) for sample CM129 showed an intensive TPD peak at around 300 °C related to the presence of carboxylic groups. For samples CM1 and CM119, the TPD peak at 300 °C was less intensive but also present, while for the CM samples carbonized at 700 °C (CM719 and CM729), a peak at this temperature was not observed.

The amounts of CO and CO₂ released from the surface of CM samples were obtained by integration of corresponding TPD curves (Table III). For the CM samples carbonized at 1000 °C, the increased amount of activating agent enhanced the number of surface oxygen groups. The highest number of surface oxygen groups was observed for the CM129 sample. On the other hand, for the CM samples carbonized at 700 °C, the increased amount of KOH decreased the number of surface oxygen groups. Comparing the results of the specific surface area and TPD, no proportionality between these results was found. Therefore, it could be concluded that the development of porosity and specific surface area during the activation process was not accompanied with the formation of surface oxygen complexes.

TABLE III. Amounts of CO (Q_{CO}) and CO₂ (Q_{CO_2}) evolving from the surface oxygen groups of the CM samples

Sample	$Q_{CO} / \text{mmol g}^{-1}$	$Q_{CO_2} / \text{mmol g}^{-1}$	$Q_{CO} + Q_{CO_2} / \text{mmol g}^{-1}$
CM1	1.404	0.297	1.701
CM119	2.068	0.772	2.840
CM129	3.103	1.031	4.134
CM719	2.637	0.335	2.972
CM729	2.173	0.283	2.456

The amount of pesticides adsorbed on the CM samples after a 2-h adsorption period is presented in Fig. 7. The adsorption main force was expected to be the dispersion force between the π electrons in the pesticide structure and the π electrons on the surface of the carbon material.¹² The presence of aromatic rings in pesticide structure increases the possibility of such interactions due to delocalized π electrons over the ring. Moreover, a branched substituent on the aromatic ring increased the level of pesticide adsorption. The obtained results showed that all the activated CM samples had good adsorption properties toward the selected pesticides compared to the CM1 sample. In addition, there was no strong adsorption competition between examined pesticides on the activated CM surfaces. The amounts of pesticides adsorbed on the samples CM119, CM719 and

CM729 were rather similar. According to the TPD results, these samples had similar total amounts of surface oxygen groups and despite of the differences in the specific surface area, they adsorb similar amounts of pesticides. It could be noted that the adsorption capability of these samples follows the same trend as that of the total number of surface oxygen groups. The most pronounced adsorption capability was observed for the sample CM129 with the highest number of surface oxygen groups. According to a suggested mechanism,¹² the specific surface area should have a crucial influence on pesticide adsorption. In the case of pesticide adsorption on activated carbon monolith surface, the specific surface area seems to play a secondary role, which implies that this mechanism cannot be applied for the pesticide adsorption on a carbon monolith surface.

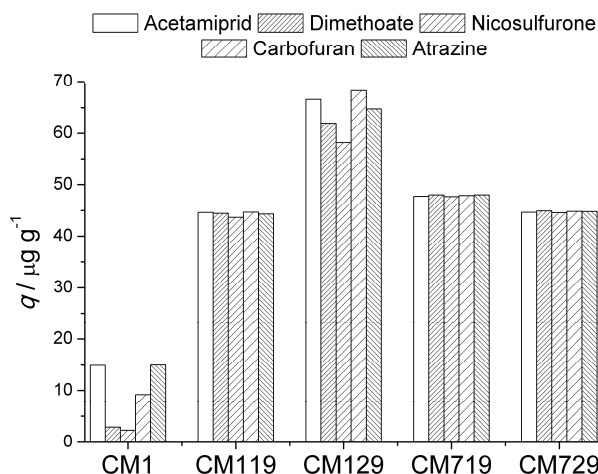


Fig. 7. Amount of pesticides adsorbed on the surface of the CM samples.

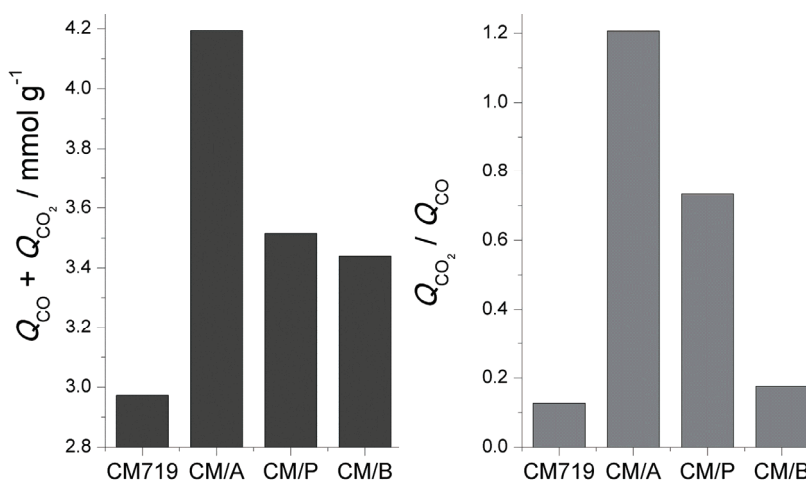
In order to examine the role of surface oxygen groups in pesticide adsorption on carbon monolith surface, sample CM719 was functionalized in a way to change surface chemistry. The nature and number of surface oxygen groups were changed by chemical treatment with different reagents. Specific surface area values for modified CM samples are presented in Table IV. It could be inferred from these results that CM modification results in almost negligible alterations in specific surface area values (less than 10 %). Based on these results, it could be concluded that the porous features of the CM were not greatly altered by chemical treatment.

According to the $\text{pH}_{\text{slurry}}$ values (Table IV), it can be noted that samples CM719 and CM/B exhibited basic character, while the oxidized samples CM/A and CM/P became more acidic, showing that the majority of the created functionalities were acidic in nature.

TABLE IV. Values of the specific surface area and $\text{pH}_{\text{slurry}}$ value for the chemically modified CM samples

Sample	$S_{\text{BET}} / \text{m}^2 \text{g}^{-1}$	$\text{pH}_{\text{slurry}}$
CM719	398	9.1
CM7-A	380	4.3
CM7-P	362	5.0
CM7-B	385	9.3

The nature of the functionalities created on the carbon surface after the chemical treatment with HNO_3 , KOH and H_2O_2 was studied by TPD method. The influence of chemical treatment on the surface oxygen groups was examined through the total amount of surface oxygen groups ($Q_{\text{CO}} + Q_{\text{CO}_2}$) and the ratio of evolved CO_2 and CO ($Q_{\text{CO}_2}/Q_{\text{CO}}$) (Fig. 8). The TPD results showed that chemical treatment enlarged total number of surface groups, especially for the sample treated with HNO_3 (sample CM/A). Treatments with HNO_3 and H_2O_2 increased surface oxidation, which resulted in the evolution of the large amounts of CO_2 . These results are consistent with the $\text{pH}_{\text{slurry}}$ results and indicate that acidic groups, such as carboxyl and lactone, which are CO_2 evolving groups, were additionally formed in the HNO_3 and H_2O_2 treatments. Although KOH treatment increased the total amount of surface groups, the $Q_{\text{CO}_2}/Q_{\text{CO}}$ ratio stayed almost unchanged, compared to the unmodified sample, which is in agreement with the $\text{pH}_{\text{slurry}}$ results.

Fig. 8. Total amount of the surface oxygen groups ($Q_{\text{CO}} + Q_{\text{CO}_2}$) and $Q_{\text{CO}_2}/Q_{\text{CO}}$ ratio for the CM samples.

According to the results obtained for the chemically modified samples, it is possible to modify the surface functionality of an activated carbon monolith without changing considerably the porous texture. In this way, a proper under-

standing of the role of the functionality of an activated carbon surface in the retention of pesticides from aqueous medium at low concentration could be acquired.

As the structure of pesticides plays an important role in adsorption, two pesticides, dimethoate and carbofuran, with different chemical structure characteristics were chosen for an examination of the adsorption properties of the chemically modified CM samples. The amounts of pesticides adsorbed on the modified CM samples are presented in Fig. 9.

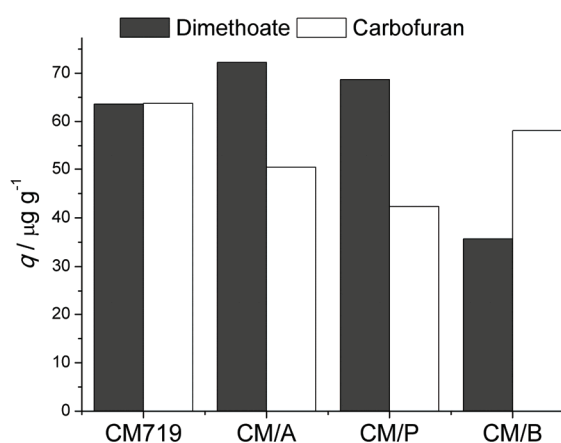


Fig. 9. Amount of dimethoate and carbofuran adsorbed on the surface of the chemically treated CM samples.

It could be seen that chemical treatment affected the adsorption capacity of the examined CM samples. The efficiency of carbofuran adsorption decrease after chemical modification, which was the most pronounced for the oxidized samples. Due to the aromatic structure of carbofuran, dispersion forces between the π electron density of the graphene layers on the CM and the aromatic ring of the adsorbate could be expected. The decrease in the adsorption rate observed after oxidation was most probably due to an alteration of the π electronic density on the carbon surface because of its functionalization. The majority of the surface groups have electron-acceptor character. Functionalization of the carbon monolith withdraws π electrons from the graphene layers, and then the contribution of dispersive interactions to adsorption is reduced. Sample CM/B showed more pronounced adsorption efficiency toward carbofuran, compared to the oxidized samples. Although CM/B had considerable number of surface oxygen groups, it displayed pronounced basic character. One of the reasons for the basic behavior of the carbon surfaces could be the π basicity of the exposed graphene layers.³⁸ Therefore, the good adsorptive capacity of CM/B toward carbofuran was probably the consequence of the increased π density and dispersive interactions.

On the other hand, the adsorption of dimethoate is not driven by the mentioned π - π interactions, due to the absence of an aromatic ring. The obtained results showed that the adsorption capacity increased after oxidation (samples CM/A and CM/P), following the same trend as the Q_{CO_2}/Q_{CO} ratio. With respect to the pH_{slurry} values and increased Q_{CO_2}/Q_{CO} ratios obtained for the oxidized samples, it could be concluded that CO_2 evolving groups play an important role in the adsorption of dimethoate.

CONCLUSIONS

In this study, microporous activated carbon monolith samples were produced by changing the parameters of carbonization and activation. Larger specific surface areas were obtained by using higher amounts of the activating agent for samples obtained at carbonization temperatures of 700 and 1000 °C. TPD analysis showed the presence of anhydride groups on all activated CM samples and carboxylic groups on CM samples carbonized at 1000 °C. The possibility of using the produced materials for pesticide removal was also tested. Although, all the tested activated CM samples had good adsorption properties, the most pronounced adsorption capability was observed for the sample CM129, which contained higher numbers of surface oxygen groups. From the obtained results, it could be concluded that the specific surface area is not a crucial factor for pesticide adsorption on the surface of CM. On the other hand, the nature and the number of surface oxygen groups show a dominant effect on pesticide adsorption. Additional functionalization of the CM surface showed that π - π interactions were the main force for the adsorption of pesticides with aromatic structure, while acidic groups play an important role in adsorption of pesticides without aromatic ring in their chemical structure.

Acknowledgments. The authors wish to thank the Ministry of Education, Science and Technological Development of the Republic of Serbia for financial support through the projects Basic Research No. 172007 and Physics and Chemistry with Ion Beams (III) No. 45006.

ИЗВОД

УТИЦАЈ ПАРАМЕТАРА ДОБИЈАЊА КАРБОН МОНОЛИТА НА АДОРПЦИЈУ ПЕСТИЦИДА

МАРИЈА ВУКЧЕВИЋ¹, АНА КАЛИЈАДИС², БИЉАНА БАБИЋ³, ЗОРАН ЛАУШЕВИЋ² и МИЛА ЛАУШЕВИЋ¹

¹Технолошко-маталуршки факултет, Универзитет у Београду, Карнегијева 4, 11001 Београд,
²Лабораторија за физику, Институт за нуклеарне науке Винча, Универзитет у Београду, Мике
Птеровића Аласа 12-14, 11001 Београд и ³Лабораторија за материјале, Институт за нуклеарне
науке Винча, Универзитет у Београду, Мике Птеровића Аласа 12-14, 11001 Београд

У овом раду је испитиван капацитет узорака карбон монолита за адсорпцију пестицида, као и механизам интеракције пестицида са површином угљеничног материјала. Различити узорци карбон монолита добијени су варирањем параметара карбонизације и активације. У циљу испитивања улоге површинских кисеоничних група у адсорпцији пестицида извршена је функционализација површине третирањем са HNO_3 , H_2O_2 и

КОН. Добијени узорци окарактерисани су одређивањем специфичне површине и расподеле пора, као и методом температурно-програмиране десорпције. За испитивање адсорпције пестицида из водених раствора коришћена је смеша пет пестицида који падају различитим хемијским групама (ацетамиприд, диметоат, никосулфурон, карбофуран и атразин). Приказани резултати указују на то да повећање температуре карбонизације, као и удела активационог агенса, омогућавају добијање микропорозног карбон монолита са већим садржајем површинских кисеоничних група. Утврђено је да површинске кисеоничне групе имају доминантан утицај на адсорпционе карактеристике активираних узорка. Добијени резултати након функционализације површине карбон монолита показују да π - π интеракције представљају главну покретачку силу за адсорпцију пестицида са ароматичном структуром, док киселе површинске групе имају водећу улогу у адсорпцији алифатичних пестицида.

(Примљено 27. децембра 2012, ревидирано 14. јануара 2013)

REFERENCES

1. L. Luo, D. Ramirez, M. J. Rood, G. Grevillot, K. J. Hay, D. L. Thurston, *Carbon* **44** (2006) 2715
2. F. D. Yu, L. Luo, G. Grevillot, *Chem. Eng. Process.* **46** (2007) 70
3. J. M. Gatica, J. M. Rodríguez-Izquierdo, D. Sánchez, T. Chafik, S. Harti, H. Zaitan, H. Vidal, *C. R. Chimie* **9** (2006) 1215
4. A. F. Pérez-Cadenas, F. Kapteijn, J. A. Moulijn, F. J. Maldonado-Hódar, F. Carrasco-Marín, C. Moreno-Castilla, *Carbon* **44** (2006) 2463
5. J. L. Williams Monolith, *Catal. Today* **69** (2001) 3
6. K. M. de Lathouder, D. Lozano-Castelló, A. Linares-Solano, F. Kapteijn, J. A. Moulijn, *Carbon* **44** (2006) 3053
7. M. Vukčević, A. Kalijadis, S. Dimitrijević-Branković, Z. Laušević, M. Laušević, *Sci. Technol. Adv. Mater.* **9** (2008) 015006
8. Y. L. Wang, Y. Z. Wan, X. H. Dong, G. X. Cheng, H. M. Tao, T. Y. Wen, *Carbon* **36** (1998) 1567
9. M. Vukčević, A. Kalijadis, Z. Jovanović, Z. Laušević, M. Laušević, *Acta Phys. Pol., A* **120** (2011) 284
10. N. Dujaković, S. Grujić, M. Radišić, T. Vasiljević, M. Laušević, *Anal. Chim. Acta* **678** (2010) 63
11. Q. Zhou, J. Xiao, Y. Ding, *Anal. Chim. Acta* **602** (2007) 223
12. E. Ayranci, N. Hoda, *Chemosphere* **60** (2005) 1600
13. B. H. Hameed, J. M. Salman, A. L. Ahmad, *J. Hazard. Mater.* **163** (2009) 121
14. N. Daneshvar, S. Aber, A. Khani, A. R. Khataee, *J. Hazard. Mater.* **144** (2007) 47
15. C. Palaekani, V. L. Snoeyink, *Carbon* **38** (2000) 1423
16. E. Ayranci, N. J. Hoda, *J. Hazard. Mater.* **112** (2004) 163
17. E. Ayranci, N. Hoda, *Chemosphere* **57** (2004) 755
18. E. Yagmur, M. Ozmak., Z. Aktas, *Fuel* **87** (2008) 3278
19. L. Chunlan, X. Shaoping, G. Yixiong, L. Shuqin, L. Changhou, *Carbon* **43** (2005) 2295
20. D. Lozano-Castello, M. V. Lillo-Rodenas, D. Cazorla-Amoros, A. Linares-Solano, *Carbon* **39** (2001) 741
21. M. A. Lillo-Ródenas, D. Cazorla-Amorós, A. Linares-Solano, *Carbon* **41** (2003) 267
22. A. H. Basta, V. Fierro, H. El-Saied, A. Celzard, *Bioresour. Technol.* **100** (2009) 3941

23. E. P. Barret, L. G. Joyner, P. P. Halenda, *J. Am. Chem. Soc.* **73** (1951) 373
24. K. Kaneko, C. Ishii, H. Kanoh, Y. Hanzawa, N. Setoyama, T. Suzuki, *Adv. Colloid Interface Sci.* **76–77** (1998) 295
25. M. Radišić, S. Grujić, T. Vasiljević, M. Laušević, *Food Chem.* **113** (2009) 712
26. M. J. B. Evans, E. Halliop, J. A. F. MacDonald, *Carbon* **37** (1999) 269
27. J. Guo, A. C. Lua, *Micropor. Mesopor. Mater.* **32** (1999) 111
28. J. Laine, A. Calafat, *Carbon* **29** (1991) 949
29. K. S. W. Sing, D. H. Everett, R. A. W. Haul, L. Moscou, R. A. Pierotti, J. Rouquérol, T. Siemieniowska, *Pure Appl. Chem.* **57** (1985) 603
30. A. Kalijadis, M. Vukčević, Z. Jovanović, Z. Laušević, M. Laušević, *J. Serb. Chem. Soc.* **76** (2011) 757
31. Y. Otake, R. G. Jenkins, *Carbon* **31** (1993) 109
32. U. Zielke, K. J. Hüttinger, W. P. Hoffman, *Carbon* **34** (1996) 983
33. B. Marchon, J. Carrazza, H. Heinemann, G. A. Somorjai, *Carbon* **26** (1988) 507
34. D. M. Nevskaja, A. Santianes, V. Muñoz, A. Guerrero-Ruiz, *Carbon* **37** (1999) 1065
35. A. A. Perić-Grujić, O. M. Nešković, M. V. Veljković, M. D. Laušević, Z. V. Laušević, *J. Serb. Chem. Soc.* **67** (2002) 761
36. M. Domingo-Garcia, F. J. Lopez Garzon, M. J. Perez-Mendoza, *J. Colloid Interface Sci.* **248** (2002) 116
37. G. S. Szymański, Z. Karpiński, S. Biniak, A. Świątkowski, *Carbon* **40** (2002) 2627
38. H. P. Boehm, *Carbon* **40** (2002) 145.